# CENTER FOR COMPOSITE MATERIALS AND STRUCTURES

## An Infiltration/Cure Model for Manufacture of Fabric Composites by the Resin Infusion Process

Mark H. Weideman
Alfred C. Loos
H. Benson Dexter
Gregory H. Hasko

Virginia Tech

VIRGINIA POLYTECHNIC INSTITUTE
AND STATE UNIVERSITY

BLACKSBURG , VIRGINIA
24061

February 1992

College of Engineering
Virginia Polytechnic Institute and State University
Blacksburg, Virginia 24061

February 1992

VPI-E-92-05
CCMS-92-05

# An Infiltration/Cure Model for Manufacture of Fabric Composites by the Resin Infusion Process

Mark H. Weideman[1]
Alfred C. Loos[2]
H. Benson Dexter[3]
Gregory H. Hasko[4]

Department of Engineering Science and Mechanics

NASA Grant NAG-1-343

Interim Report 89

The NASA-Virginia Tech Composites Program

Prepared for:       Applied Materials Branch
                    National Aeronautics and Space Administration
                    Langley Research Center
                    Hampton, Virginia 23665-5225

[1] Graduate Research Assistant, Department of Engineering Science and Mechanics,
Virginia Polytechnic Institute and State University

[2] Associate Professor, Department of Engineering Science and Mechanics,
Virginia Polytechnic Institute and State University

[3] Senior Materials Research Engineer, Applied Materials Branch,
NASA Langley Research Center

[4] Principal Engineer, Lockheed Engineering and Sciences, Co.,
Langley Program Office

# AN INFILTRATION/CURE MODEL FOR MANUFACTURE OF FABRIC COMPOSITES BY THE RESIN INFUSION PROCESS

## (ABSTRACT)

A one-dimensional infiltration/cure model was developed to simulate fabrication of advanced textile composites by the resin film infusion process. The simulation model relates the applied temperature and pressure processing cycles, along with the experimentally measured compaction and permeability characteristics of the fabric preforms, to the temperature distribution, the resin degree of cure and viscosity, and the infiltration flow front position as a function of time. The model also predicts the final panel thickness, fiber volume fraction, and resin mass for full saturation as a function of compaction pressure. The infiltration model is based on D'arcy's law for flow through porous media.

Composite panels were fabricated using the RTM film infusion technique from knitted, knitted/stitched, and 2-D woven carbon preforms and Hercules 3501-6 resin. Prior to fabrication, the deflection and permeability of the preforms were measured as a function of compaction pressure. Measurements of the temperature distribution, the resin viscosity and degree of cure, and the infiltration flow front position were compared with the RTM simulation model results. The model predictions were within 12% of the experimental results.

Fabric composites were fabricated at different compaction pressures and temperature cycles to determine the effects of the processing on the properties. The composites were C-scanned and micrographed to determine the quality of each panel. Composite panels fabricated using different temperature cycles to the same state of cure and similar compaction pressures were found to have similar compressive and shear properties.

Advanced cure cycles, developed from the RTM simulation model, were utilized to reduce the total cure cycle times by a factor of 3 and the total infiltration times by a factor of 2.

# Acknowledgements

# Table of Contents

# List of Figures

# List of Tables

# 1.0 Introduction

Advanced composites, consisting of thermoset or thermoplastic resins reinforced with graphite, aramid, or Kevlar fibers, were initially developed by the aerospace industry for the production of structurally efficient lightweight materials. At the present time, advanced composites are commonly fabricated from "prepregs" where the reinforcing fibers are pre-impregnated with resin in a separate manufacturing step. The prepregs are then cut to a desired shape and assembled into a desired stacking sequence. Finally, the uncured composite layup is placed in an autoclave or hot press for consolidation and cure.

Composite structures fabricated from prepregs are characterized by low impact strength and interlaminar shear properties. Furthermore, prepreg layup is a labor intensive process which greatly increases the manufacturing cost. Textile preforms with through-the-thickness reinforcements can be manufactured near-net shape and economically using automated textile technologies. Textile composites offer the advantages over prepreg tape layups of reduced manufacturing cost and improved damage tolerance.

Resin Transfer Molding (RTM) is an emerging one-step fabrication process by which a dry textile preform is impregnated with a matrix resin and cured to form the final composite part. During the infiltration stage, a low viscosity thermoset resin is injected into a mold containing a dry fabric preform. After the fabric preform has been fully saturated, the cure stage is initiated, with the mold and the preform being heated to the cure temperature of the resin. Finally, when the resin is fully cured, the mold is cooled to room temperature and the composite part is removed. Both the fabrication of the fabric preform and the injection of the resin are processes which may be fully automated allowing for a major cost savings over traditional hand layup techniques. Also, by using dry fabric preforms and neat resins to produce a composite part in a one-step infiltration and cure process, the need for separate prepreg manufacturing is eliminated.

RTM of advanced composites can be achieved by either pressure injection, vacuum injection, or resin film infusion techniques. The pressure injection technique utilizes two-part low viscosity resin systems under high injection pressures to saturate dry

fabric preforms and push out entrapped air. Typically, a fiberglass fabric mat, with a low resistance to flow, will be injected with resin from a single inlet port. The resin is then transferred in-plane throughout the fabric preform. A vacuum can be applied to the mold to help in the removal of entrapped air from the preform prior to resin injection.

The vacuum injection technique utilizes a vacuum to pull a low viscosity resin into a dry fabric preform enclosed in a vacuum bag layup. Resin is injected through multiple vertical or in-plane injection ports and pulled through the preform to a vacuum source until the preform is fully saturated.

The resin film infusion technique was developed to transfer hot melt resins into advanced carbon fabric preforms. Initially a degassed resin film is placed beneath a dry fabric preform and the assembly is inserted into a mold. The layup is then vacuum bagged and a full vacuum is applied to remove entrapped air. Mechanical pressure, from the vacuum bag or an external source, is then applied to the layup to compact the preform to a desired thickness and force the resin into the preform by through-the-thickness infiltration. An elevated temperature cure cycle is used to reduce the resin viscosity for infiltration and to accelerate the resin cure reactions. After the preform has been fully saturated, the resin is fully cured. The part is then removed from the mold after being cooled to room temperature. The film infusion technique was chosen for this study based on the versatility of the process and the ease of manufacture.

The large number of material properties and processing parameters that must be specified and controlled during the RTM film infusion process make trial-and-error procedures to determine the proper processing cycle extremely inefficient. Analytical models are clearly a superior alternative for determination of optimum processing cycles. The overall objective of this investigation was to develop and verify an analytical model to simulate the infiltration and cure of advanced textile preforms by the RTM film infusion technique. Specific objectives include:

1) Characterize several different types of fabric preforms to determine the influence

of applied compaction pressure on the fiber volume fraction, the porosity, and the through-the-thickness permeability.

2) Develop a nonisothermal infiltration/cure model to simulate the RTM film infusion technique based on the resin and the fabric preform characteristics and the applied boundary conditions.

3) Develop and utilize a simple one-step RTM film infusion technique to manufacture advanced textile composites.

4) Compare the RTM simulation model results with experimental results.

5) Examine the effect of applied temperature and pressure cure cycles on the rate of resin infusion and the final part quality.

6) Evaluate composites fabricated with the RTM film infusion technique through nondestructive evaluation and mechanical testing.

The initial chapters of this study will incorporate the development of a RTM simulation model to simulate nonisothermal infiltration and cure of an advanced carbon fiber preform with a hot melt resin system. Chapter 2 will present and develop theories which govern the RTM film infusion process. Chapter 3 will present the development of the one-dimensional finite element method (FEM) formulation for the RTM simulation model and describe the FORTRAN program written to simulate the process.

Several fabric preform material systems are then fully characterized to determine the compaction/porosity and permeability behavior. Chapter 4 describes the test methods utilized to characterize the compaction/porosity and through-the-thickness permeability behavior of advanced carbon fabric preforms. The methods utilized to fabricate and evaluate the panels are also presented. Chapter 5 presents the evaluation of the Hexcel Hi-Tech multiaxial warp knit fabric preforms, including the compaction and permeability behavior of the preforms prior to fabrication, and the physical properties of panels fabricated with Hercules 3501-6 resin. Chapter 6 presents a similar evaluation of TTI IM7/8HS fabric preforms. Chapter 7 presents conclusions developed from the RTM simulation model, the preform characterizations, and the fabrication experiments. Possible

future objectives are also presented. The appendices include a detailed description of the RTM film infusion technique and data for the RTM simulation model. The processing conditions and physical properties of fabricated panels are presented in tabular format.

# 2.0 RTM Simulation Model Theory

One of the major goals in the composite industry is to reduce the cost of part fabrication while maintaining high quality and good mechanical performance. The Resin Transfer Molding (RTM) film infusion technique is a simple cost-effective process for one-step infiltration and cure of advanced composites allowing for greater simplicity and shorter cure cycles when compared to more traditional fabrication methods. By gaining a full understanding of the RTM film infusion technique, the processing engineer will be able to fabricate void free, fully infiltrated and cured textile composites. The goal of this chapter is to describe the theories which govern the infiltration and cure of textile composites fabricated with the RTM film infusion technique.

In the RTM film infusion process, a degassed hot-melt thermoset resin film is placed beneath the dry fabric preform and the assembly is placed onto the bottom plate of a matched metal mold (see Fig. 2.0.1). The sides of the mold are tightened against the bottom plate and the layup. A special sealing mechanism is placed in the gap between the mold sides and the mold plunger to allow air to be removed from the preform prior to resin infiltration. (After the preform has been fully saturated, the seal prevents resin from exiting the mold.) The entire layup is then placed into a vacuum bag and a full vacuum is applied to remove entrapped air from the preform. A single-step, elevated pressure is applied to the layup and held constant throughout the entire process. The pressure compacts the fabric preform to a desired fiber volume fraction and forces the resin into the preform. The layup is heated according to a prescribed temperature cycle which reduces the resin viscosity, allowing for infusion and fiber wet out, and cures the resin once the preform has been fully saturated.

A model was developed which can be used to simulate the fabrication of textile composites using the RTM film infusion technique. The model simulates nonisothermal infiltration of a hot-melt resin into a dry carbon fiber preform and cure of the resin saturated preform. The model is composed of the following sub-models:

**Heat and Pressure**

Vacuum Sealant
(Sealing Mechanism)

Steel Plunger

Mold Side

Vacuum Bag

Resin Panel

Fabric Preform

Mold Bottom Plate

Support Plate

**Heat and Pressure**
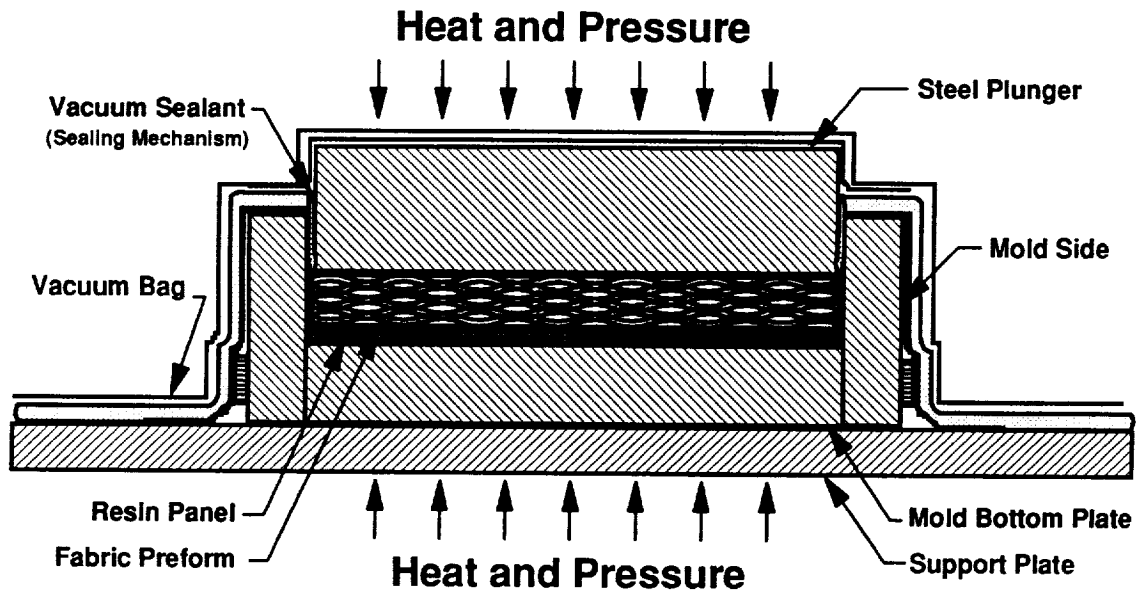
*Figure 2.0.1  Schematic of RTM film infusion layup assembly.*

1) Fabric Preform Compaction/Porosity Sub-Model

2) Transient Heat Transfer Sub-Model

3) Resin Cure Kinetics/Viscosity Sub-Model

4) Flow Sub-Model

In this chapter, each of the sub-models will be described separately.

## 2.1 Fabric Preform Compaction/Porosity Sub-Model

At the beginning of the fabrication process, pressure is applied to compact the dry fabric preform to the desired thickness and fiber volume fraction. The compaction pressure is usually held constant during resin infiltration and cure. The initial resin volume must fully saturate the compacted preform. Since there is no resin bleed, excess resin is not required. If the resin volume is too low, the fabric preform will have dry regions with a high void content. If the resin volume is too high, the fabric preform will have a nonuniform resin and fiber distribution, the panel thickness will be higher than desired, and the fiber volume fraction will be lower than desired. Therefore, knowledge of the effect of applied compaction pressure is essential to the fabrication of high quality panels.

When a compaction pressure is applied to a multiple ply dry fabric preform, the fiber bed will deflect to form a new orientation. On the microscopic level, individual fibers will deflect and come into contact with adjacent fibers within the filament tows. As the number of fiber contact points increases, the stiffness of the fiber bed also increases until the fabric preform is able to support the applied pressure. On the macroscopic level, individual plies will adjust to interlock with adjacent plies, forming an orientation which will support the applied compaction pressure. Dry compaction studies conducted by Claus and Loos [1] have indicated that the deflection behavior of 2-D woven carbon fabric preforms varies nonlinearly with the applied compaction pressure and can be determined through empirical methods. A similar approach is utilized in this investigation to

determine the compaction behavior of 2-D woven, knitted, and knitted/stitched carbon fabric preforms. Initially, a fabric preform is subjected to transverse compaction pressures ranging from 0 to 1400 kPa, and the resulting deflection of the fabric preform is measured. The experiments are conducted at slow and fast loading rates to determine the effect of loading rate upon the deflection characteristics of the fabric preform. The experimental results are reduced and fitted to the following 4th order least-squares polynomial equation:

$$d_{fp} = \sum_{i=0}^{4} a_i (\ln(P_{comp}))^i \qquad (2.1.1)$$

where $P_{comp}$ is the applied compaction pressure, $a_i$ are the compaction model coefficients, and $d_{fp}$ is deflection of the fabric preform. Equation 2.1.1 is utilized to represent the deflection characteristics of a single layer of fabric. Fabric preforms composed of individual plies stitched or knitted together, were characterized as a single layer of material.

The corresponding thickness of the fabric preform, $t_{fp}$, under a transverse compaction pressure, can then be determined from the relationship,

$$t_{fp} = n(t_{un} - d_{fp}) \qquad (2.1.2)$$

where $t_{un}$ is the initial uncompacted thickness of a single fabric preform layer and n is the number of individual fabric preform layers.

Compaction experiments have been conducted to load and unload fabric preform test samples for a number of cycles. Results of these experiments have shown that cyclic loading will reduce the stiffness of the test samples, leading to higher preform deflections. However, the acquired deformation is not permanent and the test samples recover a significant portion of the original stiffness when allowed to relax over time. For this particular study, Eq. 2.1.1 was utilized to model the initial deflection behavior of an uncompacted fabric preform.

In addition to the dry compaction experiments, fabric preforms fully saturated with

water were compacted under similar conditions to determine the compaction or consolidation behavior of a saturated preform. Equation 2.1.1 was then utilized to reduce the wet compaction experimental results. The wet compaction characterization is used in the simulation model to predict the deflection of a fabric preform when additional pressure is applied after the preform has been fully saturated. If additional compaction pressures are applied to a fully saturated fabric preform, the fluid within the fabric preform will support a sizable fraction of the pressure, increasing the stiffness of the fabric preform. The compaction pressure versus deflection behavior will depend on how the fluid is allowed to escape from the preform during compaction. If the fluid is prevented from escaping a saturated preform, the preform will be incompressible and consolidation cannot take place. If the fluid is allowed to escape from the preform and the compaction rate is very slow, the compaction behavior of the wet preform will resemble the compaction behavior of a dry preform.

## 2.1.1 Fiber Volume Fraction/Porosity/Resin Mass

After the fabric preform thickness has been modeled as a function of applied compaction pressure, the corresponding fiber volume fraction, porosity, and required resin mass to fully saturate the preform can be calculated. The macroscopic fiber volume fraction of a fabric preform is defined as the ratio of the solid fiber volume to the total fabric preform volume. A relationship was derived to model the fiber volume fraction of a fabric preform as a function of the fabric preform thickness using the method of Gauvin et al. [2].

The solid fiber volume of the fabric preform, $V_f$ , is determined from the following relationship,

$$V_f = \sum_{i=1}^{N} \frac{(M_f)_i}{(\rho_f)_i} \tag{2.1.3}$$

10

where $(M_f)_i$ is the mass of a particular fiber type within the fabric preform, $(\rho_f)_i$ is the corresponding fiber density, and N is the number of materials. Fabric preforms are frequently composed of both primary structural fibers and secondary binding fibers.

The total fabric preform volume, $V_{fp}$, which contains both the solid fiber volume and the pore volume, can be written as,

$$V_{fp} = A_{xy} t_{fp} \qquad (2.1.4)$$

where $A_{xy}$ is the surface area of the fabric preform, and $t_{fp}$ is the thickness of the fabric preform obtained from Eq. 2.1.2.

Dividing Eq. 2.1.3 by Eq. 2.1.4 and introducing the following expression for the areal weight, $\zeta_i$, of a particular fiber type within the fabric preform

$$\zeta_i = \frac{(M_f)_i}{A_{xy}} \qquad (2.1.5)$$

results in the final equation for the fiber volume fraction of the fabric preform. For "n" layers of fabric the fiber volume fraction, $v_f$, can be written as,

$$v_f = \frac{V_f}{V_{fp}} = \frac{n}{t_{fp}} \sum_{i-1}^{N} \frac{\zeta_i}{(\rho_f)_i} \qquad (2.1.6)$$

The previous equation assumes that the fabric preform is composed of planar plies containing uniformly distributed tows. If gaps exist between the fabric tows, a variation in the local fiber volume fraction will occur.

The porosity of the fabric preform is defined as the ratio of the total volume of open pores to the total volume of the fabric preform. The porosity, $\phi$, may also be defined as the resin volume faction, $v_r$, of a fully saturated fabric preform and can simply be written as,

$$\phi = v_r = 1 - v_f \qquad (2.1.7)$$

**RTM Simulation Model Theory**

Once the resin volume fraction is known, the corresponding resin mass required for the complete saturation of the fabric preform may be determined from the following equation:

$$M_r = v_r A_{xy} t_{fp} \rho_r$$

(2.1.8)

where $M_r$ is the resin mass, and $\rho_r$ is the density of the resin. Equation 2.1.8 assumes that the entire pore volume of the fabric preform is completely saturated with resin after infusion.

By utilizing Eqs. 2.1.1 and 2.1.2, the fabricator is able to determine the final thickness of a fabric preform subjected to an applied compaction pressure during processing. Eqs. 2.1.6, 2.1.7, and 2.1.8 are then utilized to determine the respective fiber volume fraction, porosity, and required resin mass for full preform saturation.

After a fabric preform has been fully characterized, the RTM film infusion technique is used to fabricate textile composites at different compaction pressures. Measurements are made on the panels to determine the thickness, fiber volume fraction, and resin mass.

## 2.2 Transient Heat Transfer Sub-Model

The success or failure of the RTM film infusion technique greatly depends upon the applied temperature cure cycle which affects the rate of infiltration and the total time required for full cure. The RTM layup is initially heated to reduce the viscosity of the resin which allows for resin infiltration of the fabric preform. Once the preform has been fully saturated, additional heat is applied to cure the resin. When the proper cure cycle is utilized, the fabricator is able to produce fully infiltrated and cured textile composites with good mechanical properties.

In this section a one-dimensional transient heat transfer sub-model is developed which can be used to determine the temperature distribution in the fabric preform during infiltration and cure. The sub-model will be developed to simulate the three distinct phases of the process: initial heating of the layup prior to infiltration, resin infiltration of

the fabric preform, and final curing of the fully saturated preform. The initial and boundary conditions for the process will then be described.

## 2.2.1 One-Dimensional Analysis

The following assumptions are made in the development of the heat transfer sub-model of the RTM film infusion process.

1) The primary mechanism of heat transfer to the layup is by conduction from the platen surfaces of a hot press.

2) Conduction is the dominant form of thermal transport through the thickness of the layup. Convective losses from the insulated sides of the mold and temperature variations in the horizontal plane of the panel are negligible.

3) The thicknesses of the layup materials remain uniform during the entire process. The thicknesses of the fabric preform, the resin film, and the saturated preform region are a function of the infiltration flow front position.

4) The resin begins to cure and heat is generated from exothermic chemical reactions at the beginning of the process. The resin may have an initial degree of cure.

5) The properties of the layup materials, the dry fabric preform, and the resin film are assumed to remain constant during the entire process.

The majority of the material layers within the layup (Fig. 2.0.1), including the unsaturated fabric preform, do not produce heat from exothermic chemical reactions during the cure cycle. Hence, the temperature distributions in these layers can be determined using the one-dimensional form of the transient heat conduction equation given by Chapman [3] as,

$$\rho_n C_n \frac{\partial T_n}{\partial t} - K_{T_n} \frac{\partial^2 T_n}{\partial z^2} \tag{2.2.1}$$

**RTM Simulation Model Theory**

where $\rho$ is the material density, C is the specific heat, T is the temperature, $K_T$ is the thermal conductivity, and z is the spatial coordinate, (defined in Section 2.2.2). The subscript n refers to any one of the following layup materials: vacuum bag layers, fiberglass plies, mold plunger, porous Teflon coated fiberglass release film, nonporous release film, mold bottom plate, fabric preform, or the support plate.

For the resin film and saturated preform region, the transient heat conduction equation, which includes a term for heat generation due to exothermic chemical reactions, is given by Loos and Springer [4] as,

$$\rho_n C_n \frac{\partial T_n}{\partial t} - K_{T_n} \frac{\partial^2 T_n}{\partial z^2} + \rho_n \dot{H}_n \qquad (2.2.2)$$

where $\dot{H}$ is the rate of heat generated by chemical reactions. The subscript n refers to either the resin panel or the saturated preform.

Before Eqs. 2.2.1 - 2.2.2 can be utilized to model the temperature distribution within the layup, the layup geometry must be defined and the initial and boundary conditions must be specified.

## 2.2.2 Layup Geometry

The RTM film infusion technique was subdivided into three distinct phases for modeling the transient heat transfer. The first phase, models initial heating of the layup prior to resin infusion of the dry preform. The layup geometry is presented on Fig. 2.2.1. As the resin begins to infiltrate the fabric preform, a saturated fabric preform region is created. The resulting layup geometry is presented on Fig. 2.2.2. Finally, after the preform has been fully saturated, the dry fabric preform and the resin film layers no longer appear in the layup. The geometry for final cure after complete saturation is shown in Fig 2.2.3. The thickness of the saturated fabric preform will be equivalent to the initial thickness of the fabric preform if no additional pressure is applied during the infiltration.
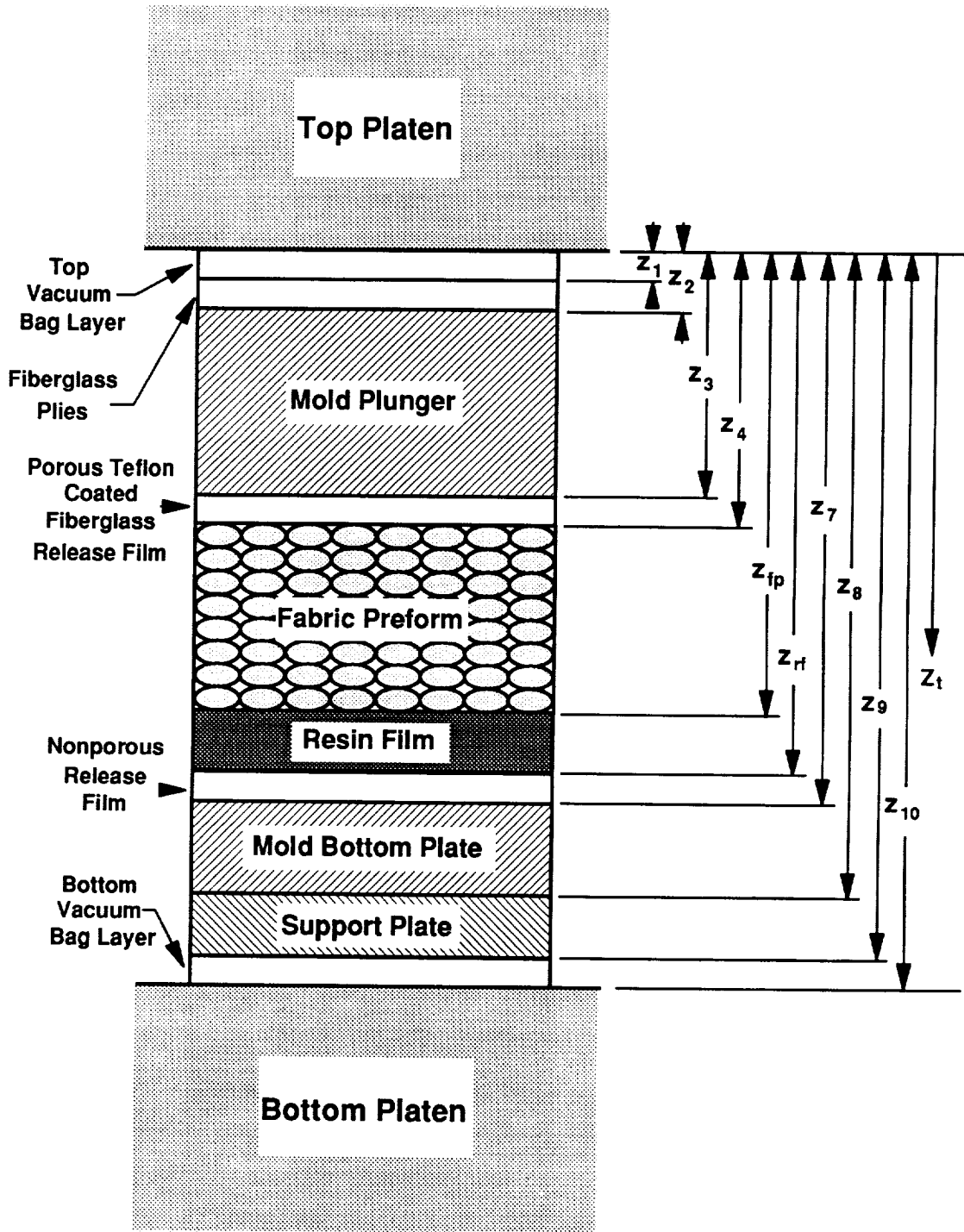
Figure 2.2.1 Schematic of thermal sub-model layup geometry
for the pre-infiltration phase.
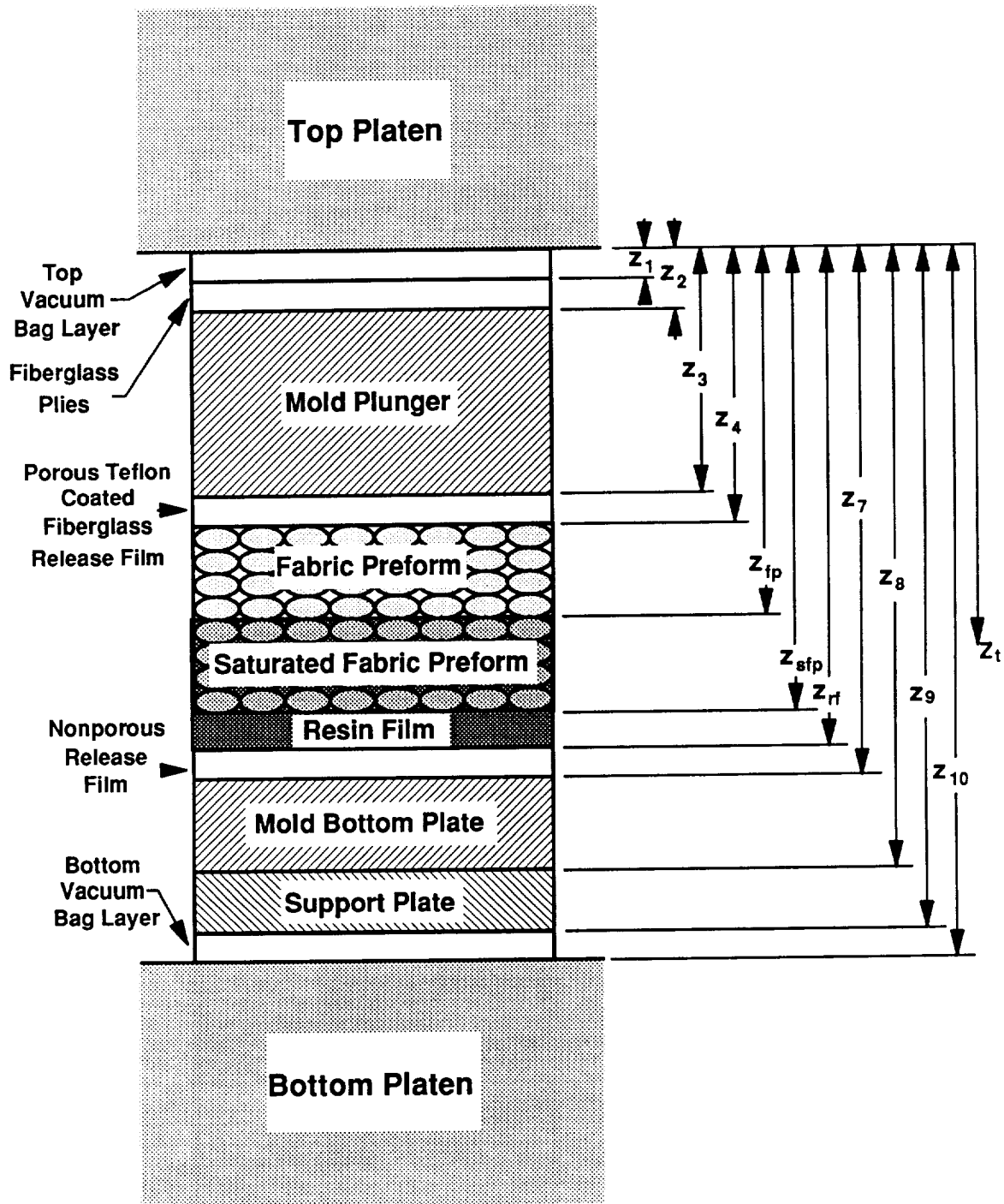
*Figure 2.2.2 Schematic of thermal sub-model layup geometry for the infiltration phase.*
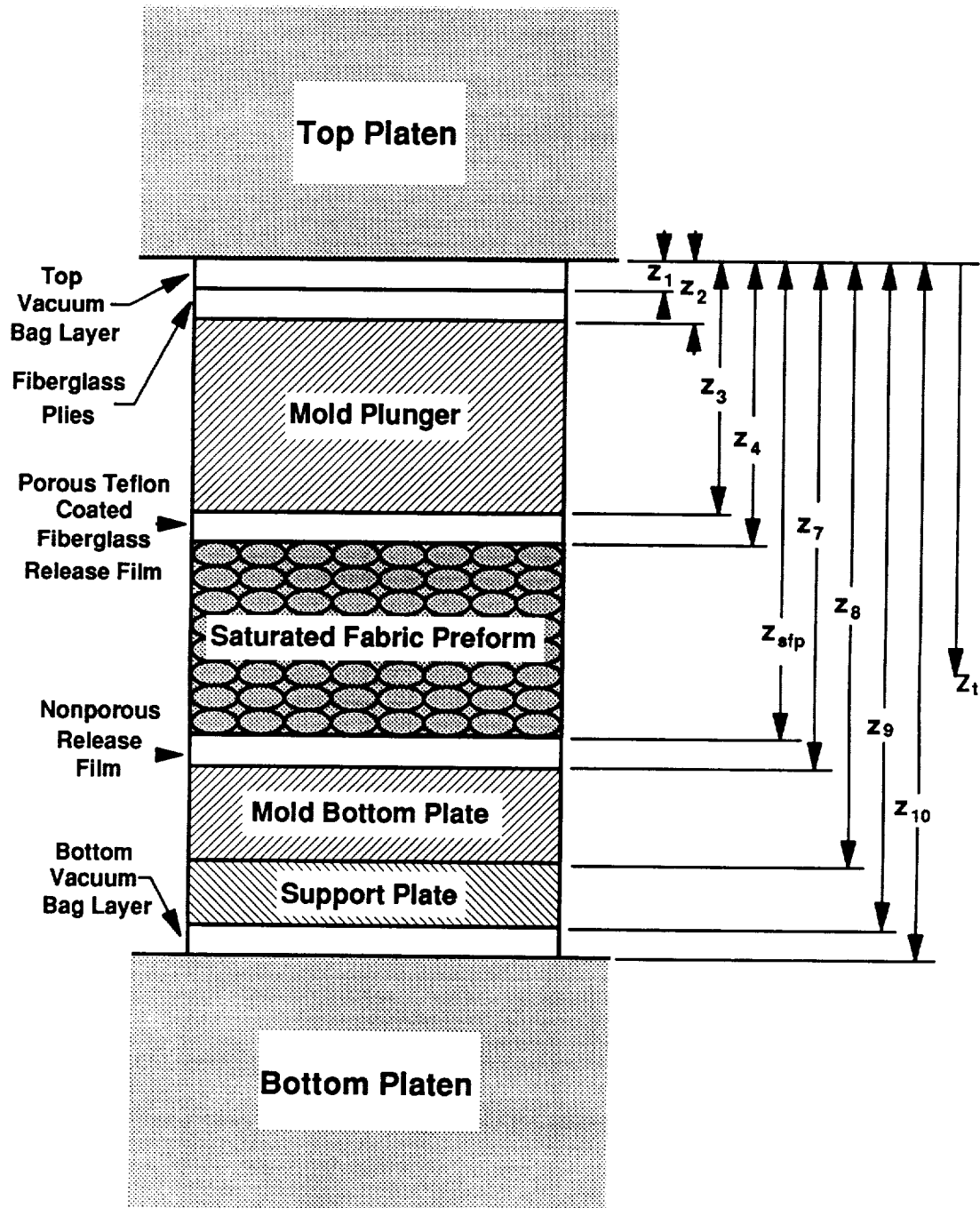
*Figure 2.2.3 Schematic of thermal sub-model layup geometry for the cure phase.*

## 2.2.3 Initial and Boundary Conditions

The initial temperature distributions in the RTM layup must be specified prior to the start of the temperature cure cycle (t<0). The initial temperature distribution for the layup geometry (Fig. 2.2.1) is specified as follows

$$T_n(z,0) - T_n^i(z), \quad t<0, \quad n-1,N \qquad (2.2.3)$$

where $T_n^i(z)$ are the initial temperatures of the respective material layers and N is the total number of distinct material layers within the layup.

Solution of Eqs. 2.2.1 and 2.2.2 requires the specification of the boundary temperatures and the mechanisms of heat transfer between the material layer interfaces. Boundary conditions for the RTM layup can be written as

$$T(0,t) - T_{TP}(t) \qquad (2.2.4)$$

for the top platen (z=0, Fig. 2.2.1) and

$$T(z_{10},t) - T_{BP}(t) \qquad (2.2.5)$$

for the bottom platen (z=$z_{10}$, Fig. 2.2.1).

## 2.2.4 Thermal Constants of the Layup Materials

The thermal conductivity, specific heat, and density of the RTM layup materials are presented in Appendix A.3. The saturated fabric preform and the dry preform thermal properties were modified to account for the presence of resin and air, respectively.

The thermal properties of the saturated fabric preform layer depend upon the fiber and the resin thermal properties. The density of saturated fabric preform layer, $\rho_{sfp}$, is determined from a "rule of mixture approach" as given by Loos and Springer [4] as,

$$\rho_{sfp} = \rho_f + (\rho_r - \rho_f)v_r \qquad (2.2.6)$$

while the specific heat of the saturated preform is written as,

$$C_{sfp} = C_f + (C_r - C_f)\frac{\rho_r}{\rho_{sfp}}v_r \qquad (2.2.7)$$

where C the specific heat and $\rho$ is the density. Subscripts r, f, and spf refer to the resin, the fiber, and the saturated fabric preform layer, respectively.

The heat of reaction within the saturated fabric preform layer, $H_{sfp}$, is given by the following relationship,

$$H_{sfp} = \frac{\rho_r}{\rho_{sfp}}v_r H_r \qquad (2.2.8)$$

where $H_r$ is the heat of reaction of the resin.

Finally, the thermal conductivity in the through-the-thickness direction (z-direction) of the saturated fabric preform layer, $K_{Tsp}$, is given by Springer and Tsai [5] to be

$$K_{T_{sfp}} = (1 - 2\sqrt{\frac{v_f}{\pi}})K_{T_r} + \frac{K_{T_r}}{B_f}[\pi - \frac{4}{\sqrt{1 - \frac{B_f^2 v_f}{\pi}}}\tan^{-1}(\frac{\sqrt{1 - \frac{B_f^2 v_f}{\pi}}}{1 + B_f\sqrt{\frac{v_f}{\pi}}})]$$

$$(2.2.9)$$

and $B_f$ is defined as,

$$B_f = 2(\frac{K_{T_r}}{K_{T_f}} - 1) \qquad (2.2.10)$$

where $K_{Tr}$ and $K_{Tf}$ are the thermal conductivities of the resin and fiber, respectively.

The density of the dry fabric preform layer, $\rho_{fp}$, is determined from the following relationship

$$\rho_{fp} = v_f \rho_f \qquad (2.2.11)$$

where the subscript fp refers to the dry fabric preform.

The specific heat of the dry fabric preform, $C_{fp}$, is written as,

$$C_{fp} = C_f \qquad (2.2.12)$$

Finally, the thermal conductivity of the dry fabric preform, $K_{Tfp}$, was derived as,

$$K_{T_{fp}} = v_f K_{T_f} \qquad (2.2.13)$$

## 2.3 Resin Cure Kinetics/Viscosity Sub-Model

The RTM film infusion process utilizes a fully degassed hot-melt resin system with a high initial viscosity. During infiltration, the cure temperature must be selected so that the viscosity of the resin becomes low enough to allow for wet out of the fiber bundles and complete saturation of the fabric preform. After the infiltration phase is complete, the resin should gel in the shortest amount of time. The thermoset resin system must be modeled to determine the degree of resin cure, the rate of heat generation, and the viscosity for a specified cure cycle. An empirical approach will be used to determine the reaction kinetics and viscosity for a thermoset epoxy resin system during cure.

The degree of cure of a thermoset resin is a relative measure of the degree of cross-linking. As the chemical cross-linking process progresses within the resin, thermal energy is liberated. If the rate of heat generation during cure is assumed to be proportional to the rate of cure reaction, the degree of resin cure, $\alpha(t)$, at any time t may be determined from

the following relationship,

$$\alpha(t) = \frac{H(t)_r}{H_T} \qquad (2.3.1)$$

where $H(t)_r$ is the amount of heat generated from the beginning of the reaction to an intermediate time t, and $H_T$ is the total heat generated during cure. The degree of cure can range from 0 (completely uncured resin) to 1 (fully cured resin), at which the crosslinking and the corresponding release of thermal energy will cease.

Differentiating Eq. 2.3.1 with respect to time and rearranging results in an expression for the rate of thermal energy production at any time t

$$\dot{H}(t)_r = \frac{\partial \alpha(t)}{\partial t} H_T \qquad (2.3.2)$$

where $\frac{\partial \alpha(t)}{\partial t}$ is the reaction or cure rate. The cure rate is dependent upon both the degree of resin cure and the temperature. The cure rate and total heat generated during cure are measured from isothermal or dynamic differential scanning calorimetry experiments (DSC). The data are then fit to a mathematical model relating the cure rate to the degree of cure and temperature.

If the diffusion of chemical species is neglected, the degree of cure of the resin is then determined at any time t by integrating the expression for cure rate with respect to time.

$$\alpha(t) = \int_0^t \frac{\partial \alpha(t)}{\partial t} dt \qquad (2.3.3)$$

The viscosity of a thermoset resin is usually determined from isothermal or dynamic rheometry experiments. If a thermoset resin is assumed to have a Newtonian behavior at low stages of cure, the viscosity, $\mu$, will be independent of shear rate and dependent upon the temperature and degree of resin cure.

$$\mu - f(T,\alpha) \tag{2.3.4}$$

When the degree of resin cure reaches between 0.5 to 0.7, the resin viscosity will begin to increase significantly and the resin will begin to harden (viscosity > 1000 Pa.s). At this point the resin has reached a state of gelation. The time at which the resin viscosity is low enough to allow for flow to occur (viscosity < 1000 Pa.s) is commonly referred to as the flow window.

Hercules 3501-6 is a B-staged hot melt thermoset resin system commonly used for prepregging and autoclave fabrication techniques. The resin was chosen for its physical properties, which have been extensively characterized [6-8]. A kinetics model recently developed by Chiou and Letton [8] was chosen for this study based on an excellent agreement between the model and experimental dynamic kinetic/viscosity data. The kinetics and viscosity model for Hercules 3501-6 resin is presented in Appendix A.2.

## 2.4 Flow Sub-Model

Knowledge of the fluid transport mechanisms which govern the infiltration of a hot melt resin system into a dry carbon fabric preform is essential for the efficient and successful fabrication of a textile composite with the RTM film infusion technique. Process variables, which include the applied infiltration pressure, the resin viscosity, the injection port geometry, and the fabric preform permeability will greatly affect when infiltration begins, the rate of infiltration, and the total time required for complete preform saturation.

In this section, the governing equations for viscous fluid transport into an anisotropic, homogeneous, porous fiber bed will be discussed. Equations will be presented to characterize the through-the-thickness permeability of a fabric preform as a function of porosity. A one-dimensional, flow sub-model will then be developed to simulate through-the-thickness resin infiltration into a fabric preform. Finally, the initial and boundary conditions will be described.

**RTM Simulation Model Theory**

## 2.4.1 Governing Equations

During the RTM film infusion process, a through-the-thickness pressure gradient is applied to the layup to force the resin into the preform by through-the-thickness infiltration (see Fig. 2.0.1). Resin flow is infused into the fabric preform from an uniform source across the entire lower surface. If the sides of the preform are sealed to prevent leakage and the resin flow front is uniform, the in-plane pressure gradients and fluid velocities are negligible in comparison to the through-the-thickness pressure gradient and velocity. Hence, the infusion process can be modeled as being one-dimensional.

D'arcy's law was utilized as the governing equation to model the transport of a reactive resin into a porous fabric preform, based on the approaches developed by Claus and Loos [1], Coulter and Guceri [9], Young et al.[10], Milovich and Nelson [11], Um and Lee [12], and Gutowski and Cai [13]. A one-dimensional form of D'arcy's law for through-the-thickness fluid flow equates the superficial flow velocity, $q_z$, to the applied infiltration pressure gradient, $\dfrac{\partial P}{\partial z^*}$, the viscosity of the fluid, $\mu$, and the permeability of the medium, $K_{Pz}$, as follows

$$q_z - v_z \phi = -\frac{K_{P_z}}{\mu} \frac{\partial P}{\partial z^*} \qquad (2.4.1)$$

where $\phi$ is the porosity, $v_z$ is the nominal flow velocity, and $z^*$ is the spatial coordinate of the flow front, (defined in Section 3.2).

For D'arcy's law to be valid the following precepts must hold,

1) The resin transfer process must be quasi-static and the material system must behave as a continuum.

2) D'arcy's law in its present form is valid only for Newtonian fluids (thermoset resins are generally classified as being Newtonian fluids).

3) The vertical distance traveled by the resin through the porous medium is small

enough for gravitational effects to be negligible in comparison to the applied infiltration pressure.

4) The viscous forces dominate over inertial forces and the flow is in the laminar regime [14].

5) The effect of surface tension between the resin and the fabric preform is negligible.

D'arcy's law is a valid governing equation for single-phase flow through anisotropic homogeneous porous media. The law was successfully utilized for the through-the-thickness flow characterization of fully saturated fabric preforms (Sections 5.3 and 6.3). During resin infiltration into a dry fabric preform (unsaturated porous medium) capillary effects may be important [15]. The capillary pressure, $P_{cp}$ at the resin flow front was defined by Williams et al. [16] as,

$$P_{cp} = \frac{\sigma \cos\theta}{m} \qquad (2.4.2)$$

where $\theta$ is the contact angle of the resin/fiber bed interface, $\sigma$ is the surface tension of the resin, and m is the hydraulic radius which is defined as the ratio of total cross-sectional area normal to the flow path over the perimeter presented to the flow.

For flow in aligned fiber beds parallel to the fibers, m is given as [16],

$$m_{\parallel} = \frac{d_f}{4} \frac{\phi}{(1-\phi)} \qquad (2.4.3)$$

where $d_f$ is the fiber diameter and $\phi$ is the fabric preform porosity.

Ahn and Seferis [17] reported that m is dependent on the fiber bed orientation, preform weave style, and the fiber bed porosity, and modified Eq. 2.4.3 for flow in fiber preforms perpendicular to the fibers as follows

$$m_{\perp} = \frac{d_f}{F} \frac{\phi}{(1-\phi)} \qquad (2.4.4)$$

**RTM Simulation Model Theory**

where F is a form factor for a particular fiber preform geometry.

## 2.4.2 Permeability/Porosity Characterization

The through-the-thickness permeability of advanced carbon fabric preforms has been found to be dependent on fabric preform porosity, $\phi$, by a number of investigators [18-22]. Several models have been utilized to establish a relationship between the measured through-the-thickness permeability and the corresponding fabric preform porosity.

The Kozeny-Carman relationship [18], derived from the Navier-Stokes equation for the flow through a collection of parallel stream tubes, was utilized for the characterization of fabric preforms which contained fiber tows parallel and perpendicular to the flow path. The Kozeny-Carman relationship for through-the-thickness fluid flow through packed fibers is written as,

$$(2.4.5) \qquad \frac{K_{P_z}}{d_f^2} = \frac{1}{\kappa_z} \left( \frac{\phi^3}{(1 - \phi)^2} \right)$$

where $\kappa_z$ is the Kozeny-Carman constant. $\kappa_z$ was empirically derived for the fabric preforms investigated.

An approach derived by Gebart [19] was utilized to model the through-the-thickness permeability as a function of the fiber bed porosity and packing arrangements for fabric preforms which solely contained aligned fibers perpendicular to the flow path. The model assumes that the resistance to flow within the fabric preform is due to the pressure drop across the gaps between individual fibers. If the fabric preform is composed of aligned quadrilaterally packed fibers, an analytical relationship between the through-the-thickness permeability and the preform porosity is written as,

$$\frac{K_{P_z}}{\frac{1}{4}d_f^2} = \frac{16}{9\pi\sqrt{2}} \left( \sqrt{\frac{(1 - \phi_{min})}{(1 - \phi)}} \right)^{\frac{5}{2}} \qquad (2.4.6)$$

25

If the fiber bed packing is hexagonal, the permeability/porosity relationship is written as,

$$\frac{K_{P_z}}{\frac{1}{4}d_f^2} = \frac{16}{9\pi\sqrt{6}} \left( \sqrt{\frac{(1 - \phi_{min})}{(1 - \phi)}} \right)^{\frac{5}{2}} \qquad (2.4.7)$$

where $\phi_{min}$ is the minimum fiber bed porosity for the respective fiber bed packing arrangements. $\phi_{min}$ for quadrilateral and hexagonal fiber bed packing arrangements are 0.215 and 0.093, respectively.

Since most fiber preforms do not contain perfect quadrilateral or hexagonal packing arrangements, a form of Eqs. 2.4.6-2.4.7 was derived to model the experimentally measured through-the-thickness permeability as a function of porosity,

$$\frac{K_{P_z}}{\frac{1}{4}d_f^2} = S \left( \sqrt{\frac{(1 - \phi_{min})}{(1 - \phi)}} \right)^{\frac{5}{2}} \qquad (2.4.8)$$

where $S$ and $\phi_{min}$ are empirically derived constants.

Depending upon the composition of the fabric preforms, either Eq. 2.4.5 or 2.4.8 was utilized to relate the through-the-thickness permeability to the porosity, for use in the RTM simulation model.

## 2.4.3 One-Dimensional Analysis

A one-dimensional, nonisothermal flow sub-model was developed to simulate the through-the-thickness infusion of a resin into a porous fabric preform. In the development of the flow sub-model the following assumptions are made:

1) Darcy's law and supporting precepts (Section 2.4.1) govern the infiltration of resin into an anisotropic, homogeneous, porous fabric preform.

RTM Simulation Model Theory

2) The infiltration fluid (resin) is incompressible.

3) Resin is transferred into the dry fabric preform by the application of a single compaction pressure applied at the beginning of infiltration and maintained during infiltration. No additional consolidation pressure is applied during the resin infiltration phase.

4) Through-the-thickness fluid flow dominates the RTM film infusion process for the techniques utilized.

5) The resin flow front is uniform. Leakage along the outer edges of the fabric preform is negligible.

Using an approach similar to Claus and Loos [1], the equation of continuity combined with D'arcy's law results in an equation for the pressure distribution through-the-thickness of the advancing flow front at any time during the infiltration phase. The continuity equation for one-dimensional, incompressible, flow through the thickness of the fabric preform is written as,

$$\frac{\partial q_z}{\partial z^*} = 0 \tag{2.4.9}$$

where $q_z$ is the superficial flow velocity.

Substituting Eq. 2.4.1 into Eq. 2.4.9, results in an equation for the pressure distribution through the thickness of the saturated preform.

$$\frac{\partial \left( -\dfrac{K_{P_z}}{\mu} \dfrac{\partial P}{\partial z^*} \right)}{\partial z^*} = 0 \tag{2.4.10}$$

The presence of flow sources or sinks within the flow field is neglected, while the pressure distribution within the resin film region is assumed to be homogeneous and equal to the applied compaction pressures.

Once Eq. 2.4.10 has been solved to determine the pressure distribution within the flow front, the pressure gradient at the tip of the flow front is utilized along with the

**RTM Simulation Model Theory**

viscosity of the resin, and the through-the-thickness permeability of the fabric preform (Section 2.4.2) to determine the advancement of the flow front with Eq. 2.4.1. The model geometry for the flow sub-model is presented in Section 3.2.

## 2.4.4 Initial and Boundary Conditions

During the infiltration phase, the resin flow front region is defined as the saturated fabric preform region, $z_{sfp}$, which lies between the dry fabric preform and the resin film, (see Fig. 2.2.2).

For any time t, the pressure boundary condition at the bottom of the saturated fabric preform ($z=z_{sfp}$, Fig. 2.2.2), $P_{ap}$, is defined as,

$$P_{ap} = P_{comp} + P_{atm} \tag{2.4.11}$$

where $P_{comp}$ is the applied compaction pressure and $P_{atm}$ is the atmospheric pressure (absolute).

The pressure boundary condition at the resin flow front/dry fabric preform interface ($z=z_{fp}$, Fig. 2.2.2), $P_{rff}$, is given by Gutowski and Cai [13] as,

$$P_{rff} = P_{vac} - P_{cp} \tag{2.4.12}$$

where $P_{cp}$ is the capillary pressure defined by Eq. 2.4.2 and $P_{vac}$ is the vacuum bag pressure.

# 3.0 RTM Simulation Model

The finite element method (FEM) was used to model the heat transfer and resin infiltration during the fabrication of a textile composite using the RTM film infusion technique. A transient one-dimensional FEM heat transfer model was developed to determine the temperature distribution within the RTM layup during the pre-infiltration phase, the infiltration phase, and the cure phase. A one-dimensional model, based on D'arcy's law for flow through porous media, was used to predict through-the-thickness resin infiltration into the fabric preform. The RTM simulation model is used to predict the position of the infiltration flow front, the resin degree of cure and viscosity, and the temperature distribution within the preform during processing.

In this chapter, a transient one-dimensional FEM heat transfer model will be presented followed by a one-dimensional FEM flow model. Finally, computer software which encompasses both models along with the material layer characteristics will be presented.

## 3.1 FEM Heat Transfer Model

The temperature distribution in the RTM layup (see Fig. 2.2.1-2.2.3) is determined using the transient FEM heat transfer model. The layup is subjected to applied temperature boundary conditions on the top ($z = 0$) and bottom ($z=z_{10}$) faces of the vacuum bag layers. The analysis is one-dimensional and considers temperature variations in the z-direction only. Hence, temperature variations in the plane of the layup are neglected. The thickness of the layup is subdivided into one-dimensional elements that contain a finite number of nodal points at which the thermal behavior of the materials may be analyzed. An approach derived from Cook [23] was used to develop the one-dimensional transient FEM heat transfer model.

The governing equation for one-dimensional (z-direction) transient heat transfer in the resin film and the saturated fabric preform layers (see Fig. 2.2.2) is written as,

$$K_{T_n} \frac{\partial^2 T}{\partial z^2} - \rho_n C_n \frac{\partial T}{\partial t} - \rho_n \dot{H}_n \qquad (3.1.1)$$

where $K_T$ is the thermal conductivity, C is the specific heat, $\rho$ is the density, $\dot{H}$ is the rate of heat generated due to exothermic chemical reactions, and the subscript "n" refers to the material layer.

The governing equation for heat transfer in the layers of the RTM layup that do not contain resin is written as,

$$K_{T_n} \frac{\partial^2 T}{\partial z^2} - \rho_n C_n \frac{\partial T}{\partial t} \qquad (3.1.2)$$

where the constants have been previously defined.

The spatial domains of Eqs. 3.1.1 and 3.1.2 for the three phases of the RTM process (pre-infiltration, infiltration, and cure) have been presented in Section 2.2.2. The initial and boundary conditions were presented in Section 2.2.4.

The functional of Eq. 3.1.1 , $\Pi_{RT}$, based upon the principle of minimal potential energy, is written as,

$$\Pi_{RT} - \frac{1}{2} \int (\frac{\partial T}{\partial z} K_{T_n} \frac{\partial T}{\partial z} + 2\rho_n C_n T \frac{\partial T}{\partial t} - 2\rho_n \dot{H}_n T) dz \qquad (3.1.3)$$

and the functional of Eq. 3.1.2, $\Pi_{NRT}$ is written as,

$$\Pi_{NRT} - \frac{1}{2} \int (\frac{\partial T}{\partial z} K_{T_n} \frac{\partial T}{\partial z} + 2\rho_n C_n T \frac{\partial T}{\partial t}) dz \qquad (3.1.4)$$

where T is the spatial field temperature (T(z)) of an individual element in the RTM layup.

At every instant of time, the temperature distribution in the resin film and the saturated fabric preform must satisfy the following equation.

$$\frac{\partial \Pi_{RT}}{\partial T} - 0 \qquad (3.1.5)$$

**RTM Simulation Model**

The temperature distribution in the remaining non resin layers of the RTM layup must satisfy the following equation.

$$\frac{\partial \Pi_{NRT}}{\partial T} = 0 \qquad (3.1.6)$$

## 3.1.1 Finite Element Formulation

The spatial field temperatures, $T(z)$, of an individual element can be represented as the product of local nodal temperatures, $\{T_e\}$, and the shape functions $[N_T]$. Likewise the heat sources $\rho_n \dot{H}_n(z)$ of an individual element can be represented as the product of the local nodal heat sources, $\{\rho_n \dot{H}_n\}_e$, and the shape functions, $[N_{\rho \dot{H}}]$, (for this study, $[N_{\rho \dot{H}}] = [N_T]$). The spatial variables are rewritten as,

$$T(z) = [N_T]\{T_e\}$$

$$\frac{\partial T(z)}{\partial z} = \frac{\partial [N_T]}{\partial z}\{T_e\} \qquad (3.1.7)$$

$$\rho_n \dot{H}_n(z) = [N_{\rho \dot{H}}]\{(\rho_n \dot{H}_n)_e\}$$

Lagrange quadratic interpolation functions [24], are used in the FEM formulation to write the functionals of Eqs. 3.1.3 and 3.1.4 in terms of the local nodal variables. The relationship between the local nodes and the corresponding shape functions are presented on Fig. 3.1.1, where $h_e$ is the height of an individual element.

After substituting the nodal relationships in Eq. 3.1.7 into Eqs. 3.1.3 and 3.1.4, the following relationships were derived:

Conductivity Matrix,

$$[K_T]_e = \int_z \left(\frac{\partial [N_T]^T}{\partial z} K_{T_n} \frac{\partial [N_T]}{\partial z}\right) dz$$

**Quadratic (3-Node) 1-D Element**

1 (L = -1)

2 (L = 0) $h_e$

L

3 (L = 1)
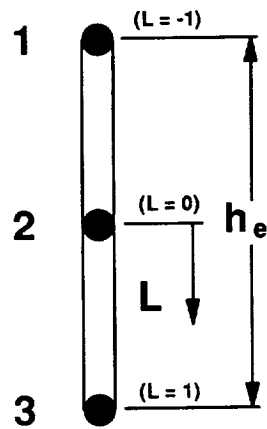
$[N_i]_{i=1,3}$

$N_1 = -L\dfrac{(1-L)}{2}$

$N_2 = (1+L)(1-L)$

$N_3 = L\dfrac{(1+L)}{2}$

**Lagrange Quadratic Interpolation Functions**

$\dfrac{\partial[N_i]}{\partial L}_{i=1,3}$

$\dfrac{\partial N_1}{\partial L} = -\dfrac{(1-2L)}{2}$

$\dfrac{\partial N_2}{\partial L} = -2L$

$\dfrac{\partial N_3}{\partial L} = \dfrac{(1+2L)}{2}$

$$[K_T]_e = \frac{K_{T_a}}{h_e}\begin{bmatrix} 2.3 & -2.6 & 0.3 \\ -2.6 & 5.6 & -2.6 \\ 0.3 & -2.6 & 2.3 \end{bmatrix}$$

**Thermal Conductivity Matrix**

$$[C_T]_e = \frac{\rho_n C_n h_e}{10}\begin{bmatrix} 1.3 & 2.6 & -0.3 \\ 0.6 & 5.3 & 0.6 \\ -0.3 & 0.7 & 1.3 \end{bmatrix}$$

**Specific Heat Matrix**

$$\{r_{\rho\dot{H}}\}_e = \frac{h_e}{10}\begin{bmatrix} 1.3 & 2.6 & -0.3 \\ 0.6 & 5.3 & 0.6 \\ -0.3 & 0.7 & 1.3 \end{bmatrix}\begin{Bmatrix} (\rho_n\dot{H}_n)_1 \\ (\rho_n\dot{H}_n)_2 \\ (\rho_n\dot{H}_n)_3 \end{Bmatrix}$$

**Heat Source Vector**

*Figure 3.1.1. Lagrange quadratic interpolation functions, thermal conductivity matrix, specific heat matrix, and heat source vector for the FEM heat transfer model.*

**RTM Simulation Model**

Specific Heat Matrix,

$$[C_T]_e - \int_z (\rho_n C_n [N_T]^T [N_T]) dz \qquad (3.1.8)$$

Heat Source Vector,

$$\{r_{\rho\dot{H}}\}_e - \int_z ([N_T]^T [N_{\rho\dot{H}}]) dz \{\rho_n \dot{H}_n\}_e$$

The relationships in Eq. 3.1.8 are numerically integrated to give $[K_T]_e$, $[C_T]_e$, and $\{r_{\rho\dot{H}}\}_e$, and are shown in Fig. 3.1.1.

For an element located within either the resin film or the saturated fabric preform layer, the functional $\Pi_{RT}$ (Eq. 3.1.3) can be written in terms of the relationships defined in Eq. 3.1.8

$$\Pi_{RT_e} - \frac{1}{2}\{T_e\}^T[K_T]_e\{T_e\} + \{T_e\}^T([C_T]_e \frac{\partial\{T_e\}}{\partial t} - \{r_{\rho\dot{H}}\}_e) \qquad (3.1.9)$$

and the corresponding functional $\Pi_{NRT}$ (Eq. 3.1.4) for an element located within the remaining non resin layers of the layup is written as,

$$\Pi_{NRT_e} - \frac{1}{2}\{T_e\}^T[K_T]_e\{T_e\} + \{T_e\}^T[C_T]_e \frac{\partial\{T_e\}}{\partial t} \qquad (3.1.10)$$

The local potential energy contributions from individual elements are assembled to obtain the global potential energy of the entire layup. The assembly of the element variables in individual material layers is written as,

$$\{T\} - \sum_{e-1}^{N} \{T_e\} \qquad [C_T] - \sum_{e-1}^{N} [C_T]_e$$

$$[K_T] - \sum_{e-1}^{N} [K_T]_e \qquad \{R_{\rho\dot{H}}\} - \sum_{e-1}^{N} \{r_{\rho\dot{H}}\}_e \qquad (3.1.11)$$

where N is the total number of elements located in a particular material layer. The element variables of individual material layers are then assembled using the layer sequence presented in Section 2.2.2.

Based upon the relationships in Eq. 3.1.11, the global functional, $\Pi_T$ ,of the entire layup may be written as,

$$\Pi_T - \frac{1}{2}\{T\}^T[K_T]\{T\} + \{T\}^T([C_T]\frac{\partial\{T\}}{\partial t} - \{R_{p\ddot{H}}\}) \tag{3.1.12}$$

The contribution to $\{R_{p\ddot{H}}\}$ comes only from the resin film and saturated fabric preform layers.

Temperatures must vary within the RTM layup in such a way that $\frac{\partial\Pi_T}{\partial T} = 0$, which represents the state of minimum potential energy due to temperature variations within the element field.

Taking $\frac{\partial\Pi_T}{\partial T} = 0$, the final equation for one-dimensional, transient heat transfer in the entire RTM layup is written as,

$$\frac{\partial\Pi_T}{\partial T} - 0 - [K_T]\{T\} + [C_T]\frac{\partial\{T\}}{\partial t} - \{R_{p\ddot{H}}\} \tag{3.1.13}$$

## 3.1.2 Transient Thermal Problem Solution

A finite difference scheme is used to solve for the temperatures in Eq. 3.1.13. The following relationship can be utilized to solve for the temperatures at time t + $\Delta$t from the temperatures at time t [23].

$$\{T\}_{t+\Delta t} - \{T\}_t + [(1 - \Theta)\frac{\partial\{T\}_t}{\partial t} + \Theta\frac{\partial\{T\}_{t+\Delta t}}{\partial t}]\Delta t \tag{3.1.14}$$

where $\Theta$ can range from 0 to 1. For this study a $\Theta$ value of .878 [25] was used for stable, accurate solutions.

After algebraic manipulations involving Eqs. 3.1.14 and 3.1.13, the time derivatives of temperature are eliminated, and the following equation can be solved for the temperature distribution in the RTM layup.

$$(\frac{1}{\Delta t}[C_T]) + \Theta[K_T]\}\{T\}_{t+\Delta t} - (\frac{1}{\Delta t}[C_T] - (1-\Theta)[K_T])\{T\}_t$$

$$+ (1-\Theta)\{R_{\rho\dot{H}}\}_t + \Theta\{R_{\rho\dot{H}}\}_{t+\Delta t}$$

(3.1.15)

## 3.2 FEM Flow Model

A one-dimensional FEM flow model was developed to determine the through-the-thickness resin pressure distribution in the saturated fabric preform ($z_{fp}<z<z_{rfp}$, Fig. 2.2.2) during the infiltration phase. The FEM flow model relates the resin pressures within the saturated fabric preform to the applied boundary pressures in a manner similar to that developed by Claus and Loos [1].

The governing equation for the through-the-thickness pressure distribution of the infiltration region was derived in Chapter 2 by the substitution of D'arcy's law into the equation of continuity (Eq. 2.4.10),

$$\frac{\partial(-\frac{K_{P_z}}{\mu}\frac{\partial P}{\partial z^*})}{\partial z^*} - 0$$

(3.2.1)

where $K_{P_z}$ is the through-the-thickness permeability, $\mu$ is the resin viscosity, and $\dfrac{\partial P}{\partial z^*}$ is the resin pressure gradient.

In the flow analysis, the resin film and dry fabric preform regions of the RTM layup ($z_{fp} < z^* < z_{rf}$, Fig. 2.2.2) define the boundaries of the spatial domain shown in Fig. 3.2.1. The boundary conditions, presented in Section 2.4.4, are the prescribed pressures at the resin film/saturated fabric preform and the saturated fabric preform/dry fabric preform interfaces.

The functional, $\Pi_P$, of Eq. 3.2.1, using the principle of minimum potential energy is written as,

$$\Pi_P = \frac{1}{2}\int_{z^*} \left( \frac{\partial P}{\partial z^*} \frac{K_{P_z}}{\mu} \frac{\partial P}{\partial z^*} \right) dz^* \tag{3.2.2}$$

At any instant of time, the pressure distribution in the saturated preform must satisfy the following equation.

$$\frac{\partial \Pi_P}{\partial P} = 0 \tag{3.2.3}$$

## 3.2.1 Finite Element Formulation

Through-the-thickness spatial field pressures, $P(z^*)$, are related to the local nodal pressures, $\{P_e\}$, of an individual element within the saturated fabric preform through the use of shape functions $\{N_P\}$. The nodal relationships are written as,

$$P(z^*) = [N_P]\{P_e\}$$
$$\frac{\partial P(z^*)}{\partial z^*} = \frac{\partial [N_P]}{\partial z^*}\{P_e\} \tag{3.2.4}$$

**RTM Simulation Model**

Porous Flow Problem Geometry



Quadratic (3-Node) 1-D Element

$$N_1 = -L\frac{(1-L)}{2}$$

$$N_2 = (1+L)(1-L)$$

$$N_3 = L\frac{(1+L)}{2}$$

$$[N_i]_{i-1,3}$$

$$\frac{\partial[N_i]}{\partial L}_{i-1,3}$$

$$\frac{\partial N_1}{\partial L} = -\frac{(1-2L)}{2}$$

$$\frac{\partial N_2}{\partial L} = -2L$$

$$\frac{\partial N_3}{\partial L} = \frac{(1+2L)}{2}$$

Lagrange Quadratic Interpolation Functions
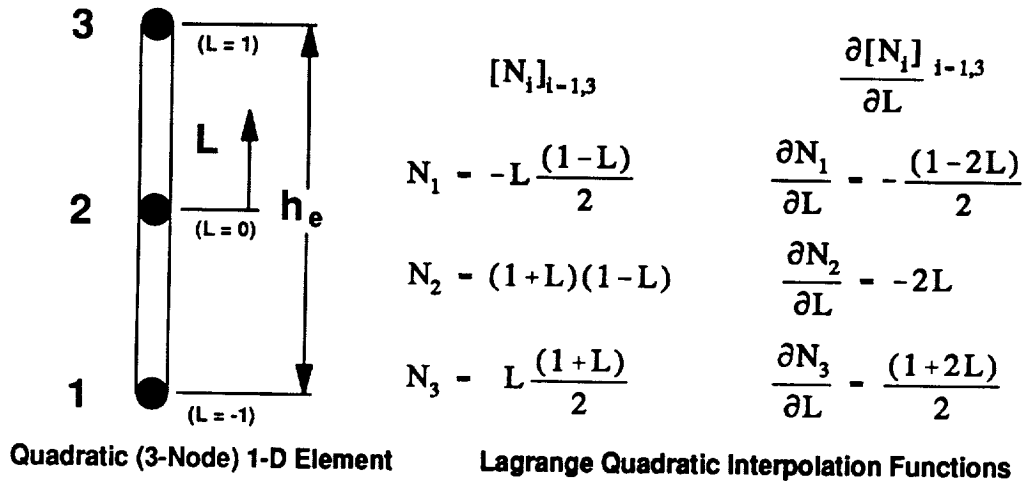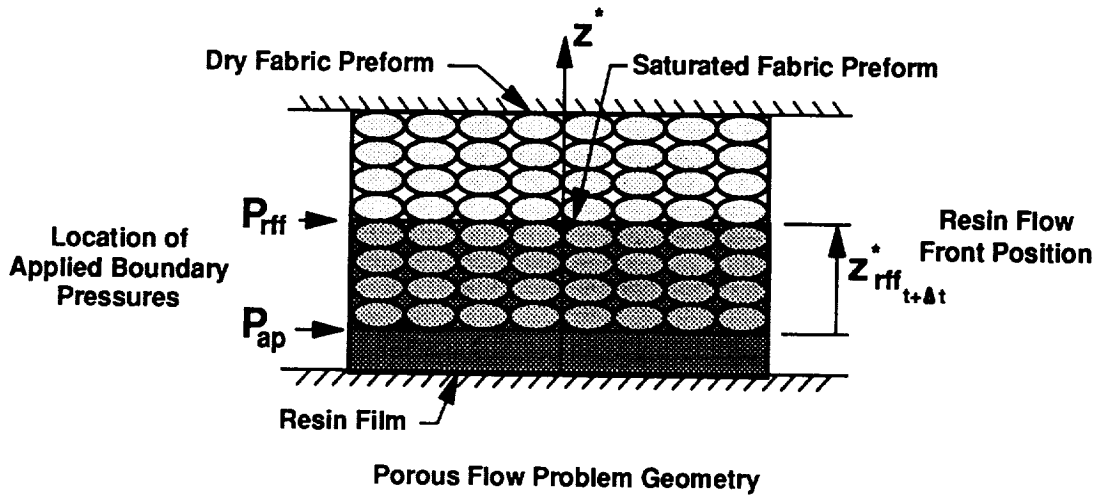
$$[K_P]_e = \frac{K_{P_z}}{\mu h_e} \begin{bmatrix} 2.3 & -2.6 & 0.3 \\ -2.6 & 5.6 & -2.6 \\ 0.3 & -2.6 & 2.3 \end{bmatrix}$$

Porous Flow Matrix

Figure 3.2.1.    Problem geometry, Lagrange quadratic interpolation functions, and porous flow matrix for the FEM flow model.

RTM Simulation Model

Lagrange quadratic interpolation functions (identical to the interpolation functions used for the transient FEM heat transfer model) are used to write the functional in Eq. 3.2.2 in terms of local nodal values.

After substituting the nodal relationships in Eq. 3.2.4 into Eq. 3.2.2, the following relationship was derived.

Porous Flow Matrix

$$[K_P]_e - \int_{z^*} (\frac{\partial [N_P]^T}{\partial z^*} \frac{K_{P_z}}{\mu} \frac{\partial [N_P]}{\partial z^*}) dz^* \tag{3.2.5}$$

which is numerically integrated and shown at the bottom of Fig. 3.2.1.

For an element located in the saturated fabric preform, the functional in Eq. 3.2.2 can be written in terms of the relationship defined in Eq. 3.2.5.

$$\Pi_{P_e} - \frac{1}{2} \{P_e\}^T [K_P]_e \{P_e\} \tag{3.2.6}$$

The local functionals of individual elements are assembled into a global functional for the entire saturated fabric preform through the use of the following relationships

$$\{P\} - \sum_{e-1}^{N} \{P_e\} \quad [K_P] - \sum_{e-1}^{N} [K_P]_e \tag{3.2.7}$$

where N is the total number of elements in the saturated fabric preform.

The global functional for the resin pressure distribution in the saturated fabric preform is then written as,

$$\Pi_P - \frac{1}{2} \{P\}^T [K_P] \{P\} \tag{3.2.8}$$

**RTM Simulation Model**

The resin pressure distribution within the saturated fabric preform must vary in such a way that $\dfrac{\partial \Pi_P}{\partial P} = 0$, which represents the state of minimum potential energy due to pressure variations within the element field.

The resulting relationship for the resin pressure distribution in the saturated fabric preform is written as,

$$\frac{\partial \Pi_P}{\partial P} = 0 = [K_P]\{P\} \tag{3.2.9}$$

Pressures at the resin film/saturated fabric preform and the saturated fabric preform/ dry fabric preform interfaces are substituted into Eq. 3.2.9 as boundary conditions to solve for the resin pressure distribution in the saturated fabric preform during the infiltration phase.

## 3.3 Flow Front Advancement

The movement of the resin flow front into the dry fabric preform is governed by D'arcy's law. At any instant of time, the superficial velocity, $q_z$, can be written as

$$q_z = v_z \phi = -\frac{K_{P_z}}{\mu}\frac{\partial P}{\partial z^*} \tag{3.3.1}$$

where $K_{P_z}$ is the through-the-thickness permeability of the fiber bed, $\mu$ is the resin viscosity, $\phi$ is the porosity of the fabric preform, $v_z$ is the nominal resin velocity, and $\dfrac{\partial P}{\partial z^*}$ is the resin pressure gradient.

For a small finite time step, $\Delta t$, the nominal velocity of the advancing resin flow front at time $t+\Delta t$ can be written as,

$$v_{z_{t+\Delta t}} = \frac{\Delta z^*_{t+\Delta t}}{\Delta t} \tag{3.3.2}$$

**RTM Simulation Model**

where $\Delta z^{*}_{t+\Delta t}$ is the advancement of the resin flow front at time $t+\Delta t$.

The pressure gradient, $\dfrac{\partial P_t}{\partial z^{*}}$ , at the resin flow front (top of the saturated fabric preform) is obtained from the resin pressure distribution in the saturated fabric preform, determined by the FEM flow model (Section 3.2). The pressure gradient is obtained from the following relationship [24],

$$\frac{\partial P_t}{\partial z^{*}} = \frac{2}{h_e} \sum_{i=1}^{3} P_i \frac{\partial N_i}{\partial L} \qquad (3.3.3)$$

where $P_i$ are the local nodal pressures, and $\dfrac{\partial N_i}{\partial L}$ are the local derivatives of the Lagrange interpolation functions (presented on Fig. 3.2.1) of the top element.

Substituting Eqs. 3.3.2 and 3.3.3 into Eq. 3.3.1 and solving for the advancement of the resin flow front, $\Delta z^{*}_{t+\Delta t}$, at time $t+\Delta t$, results in the following relationship

$$\Delta z^{*}_{t+\Delta t} = \frac{-2 K_{P_z} \Delta t}{\phi \mu h_e} \left( \sum_{i=1}^{3} P_i \frac{\partial N_i}{\partial_L} \right) \qquad (3.3.4)$$

At the start of the simulation ($t=0$), a single quadratic element (assumed thickness $\Delta z^{*}_{t}$ $=h_e$) is used to represent the saturated fabric preform layer. The resin pressure distribution is then calculated and the flow front advancement, $\Delta z^{*}_{t+\Delta t}$, at time $t=t+\Delta t$ is calculated from Eq. 3.3.4. The value of $\Delta z^{*}_{t+\Delta t}$ is used as a new estimate of the element thickness $h_e$ and a new estimate of the resin pressure distribution in the resin flow front is calculated. $\Delta z^{*}_{t+\Delta t}$ is then recalculated from Eq. 3.3.4. The iteration scheme is repeated three times.

For time steps, $t>0$, a new quadratic element of thickness $h_e = \Delta z^{*}_{t}$ is added to the finite element mesh of the saturated preform. The value, $\Delta z^{*}_{t}$, which represents the resin flow front advancement at time $t$, is used as an initial estimate of the flow front advancement at time $t+\Delta t$. An identical iteration scheme as discussed in the preceding paragraph is

**RTM Simulation Model**
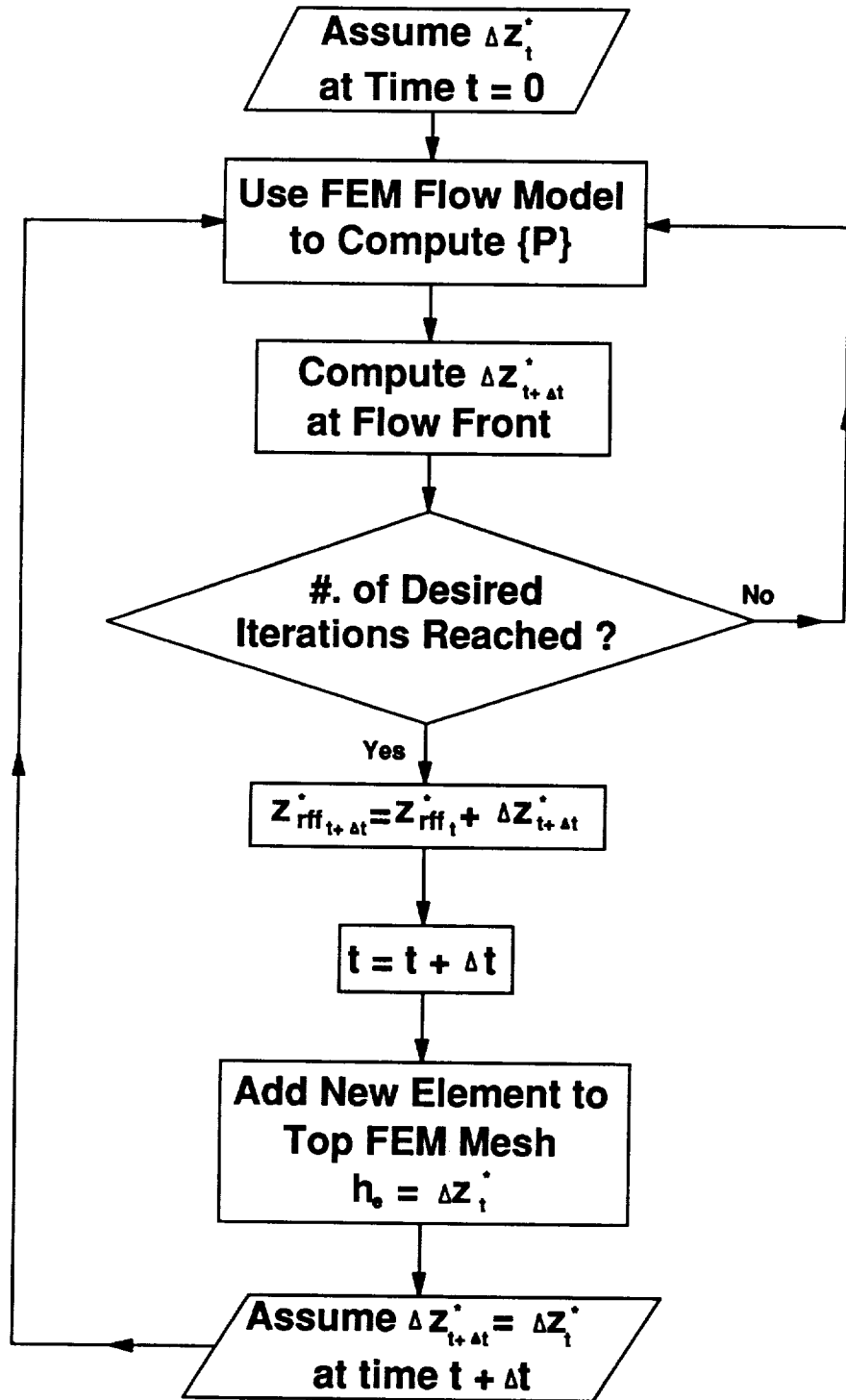
*Figure 3.3.1. Schematic of flow front position iteration procedure.*

used to calculate $\Delta z^*_{t+\Delta t}$. A flow chart of the iteration process is presented on Fig. 3.3.1.

The position of the resin flow front, $z^*_{rff}$, at time $t+\Delta t$ is determined from the following relationship,

$$z^*_{rff_{t+\Delta t}} = z^*_{rff_t} + \Delta z^*_{t+\Delta t} \qquad (3.3.5)$$

and the normalized infiltration flow front position, $D_{rff}$, at time $t+\Delta t$ is given as,

$$D_{rff_{t+\Delta t}} = \frac{z^*_{rff_{t+\Delta t}}}{t_{fp_{t=0}}} \qquad (3.3.6)$$

where $t_{fp}$ is the initial compacted thickness of the fabric preform (Eq. 2.1.2).

## 3.4 Mesh Regeneration for the FEM Heat Transfer Model

During the pre-infiltration phase, the mesh geometry remains fixed. Each material layer in the RTM layup is represented by primary elements of equal height and a single boundary element located at the material layer interface, (see top of Fig. 3.4.1). The total height of the primary elements and the boundary element is equal to the thickness of the material layer. The dry fabric preform, the saturated fabric preform, and the resin film, contain very fine finite element meshes with primary elements of equal length ($h_e = 0.1$ mm).

When the height of the infiltration flow front, $z^*_{rff}$, is equal to the height of a dry fabric preform primary element used in the transient FEM heat transfer model, the infiltration phase is initiated. The saturated fabric preform layer is then included into the model geometry, (see Fig. 2.2.2). The element mesh for the heat transfer model is generated from the top platen down to the bottom platen while the element mesh for the flow model is generated from the bottom of the saturated fabric preform/resin film interface up to the resin flow front.

The spatial coordinate and thickness of the dry fabric preform, $z_{fp}$, decreases as the

**RTM Simulation Model**
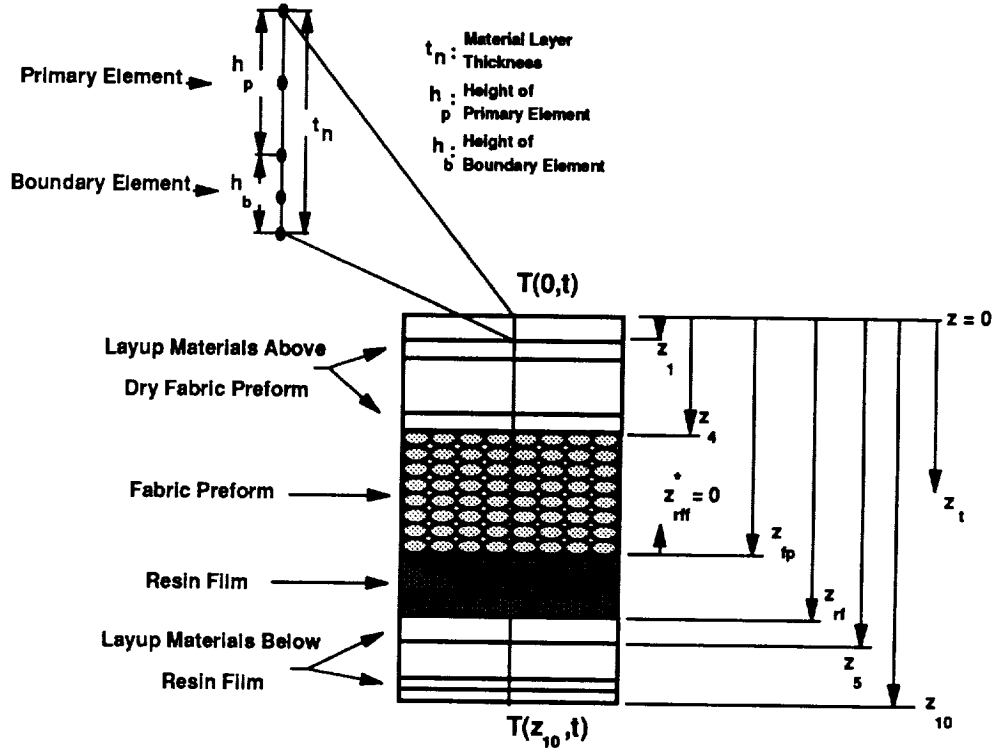
**Pre-Infiltration Phase (t=0)**
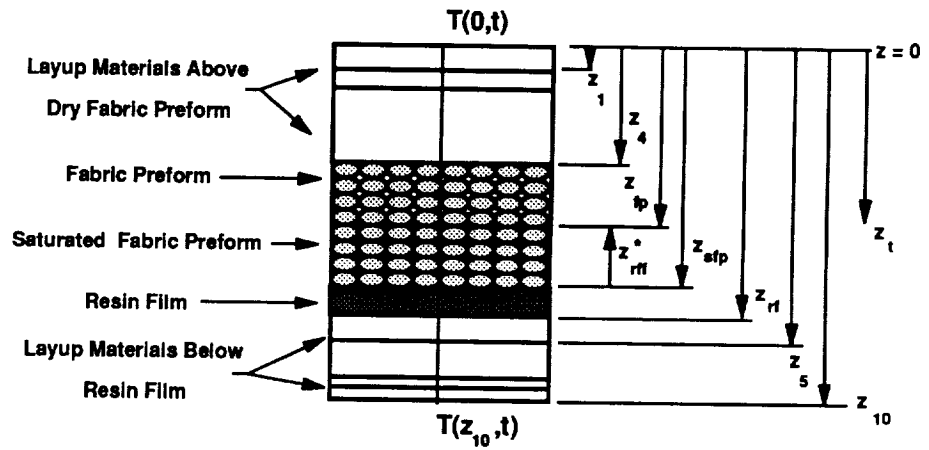


**Infiltration Phase (t=t+Δt)**

*Figure 3.4.1  Transient FEM heat transfer mesh geometry during the pre-infiltration phase and the infiltration phase*

**RTM Simulation Model**

43

resin flow front advances, (see bottom of Fig 3.4.1). The spatial coordinate of the fabric preform, at time t+Δt, is determined from the following relationship,

$$z_{fp_{t+\Delta t}} = z_{fp_{t=0}} - z^{*}_{rff_{t+\Delta t}}$$

(3.4.1)

where $z^{*}_{rff}$ is the position of the resin flow front (measured from the bottom of the preform) at time t+Δt.

If no additional compaction pressures are applied during the infiltration phase, the spatial coordinate of the saturated fabric preform, $z_{sfp}$, at time t+Δt is equal to the initial spatial coordinate of the dry fabric preform, $z_{fp}$, at time t=0, (see Fig. 2.2.2). The thickness of the saturated preform is equal to $z^{*}_{rff}$ at time t+Δt.

As the resin is infused into the dry fabric preform, the thickness of the resin film will decrease by a proportional amount, and the spatial coordinates of the material layers beneath the resin film will change. The spatial coordinate of the resin film and the material layers beneath the resin film at time t+Δt are given as,

$$z_{n_{t+\Delta t}} = z_{n_{t=0}} - \phi z^{*}_{rff_{t+\Delta t}}$$

(3.4.2)

where $\phi$ is the fabric preform porosity and the subscript n refers to the resin film or a material layer beneath the resin film.

A new FEM mesh is generated at time t+Δt to reflect the new spatial coordinates of the material layers. Depending upon the magnitude of the change in the flow front position at time t+Δt, $\Delta z^{*}_{t+\Delta t}$, either the height of the boundary elements in the fabric preform and the resin film will be decreased, or elements (primary or boundary) will be eliminated from the fabric preform and resin film layers. If elements are removed, a new boundary element is created from a primary element at the lower surface of the fabric preform and resin film layers. The dry fabric preform region infiltrated at time t+Δt becomes part of the saturated fabric preform layer. The physical properties of the resin at the flow front (degree of cure and viscosity) at time t are transferred to the new flow

**RTM Simulation Model**

front position at time t+Δt.

The former node positions at time t are referenced to the new node positions at time t+Δt, to calculate the temperatures at time t+Δt from Eq. 3.1.15. The nodal temperatures in the dry fabric preform region, infiltrated at time t+Δt, are used as the node temperatures in the new saturated fabric preform region. The spatial coordinates of the nodes in the material layers beneath the resin film are decreased and the global numeric reference to the nodes is updated to reflect the loss of nodes from the resin film.

The FEM heat transfer model and the resin cure kinetics/viscosity model (Section 2.2) are used to determine the resin viscosity as a function of time at the nodes in the saturated fabric preform FEM heat transfer mesh. The node viscosities are then translated over to the FEM flow model node locations (See Fig. 3.4.2). The node viscosity in the heat transfer mesh with the closest corresponding position to the middle node of a flow model element is used as the element viscosity for the determination of the pressure distribution from Eq. 3.2.8. Since both the flow mesh and the heat transfer meshes are very fine, negligible error is incurred by any possible spatial mismatch.

After the fabric preform has become fully saturated, the position of the resin flow front, $z^*_{rff}$, should be at the porous Teflon coated fiberglass release film/saturated fabric preform interface (see Fig. 2.2.3). All of the elements of the resin film have been eliminated and all of the elements in the dry fabric preform have been converted into saturated fabric preform elements. The resin film and dry fabric preform layers are effectively eliminated from the transient FEM heat transfer model. The FEM flow model is halted. The transient FEM heat transfer model is then used in the cure phase to determine resin state of cure and viscosity and the temperature distribution within layup as a function of time.
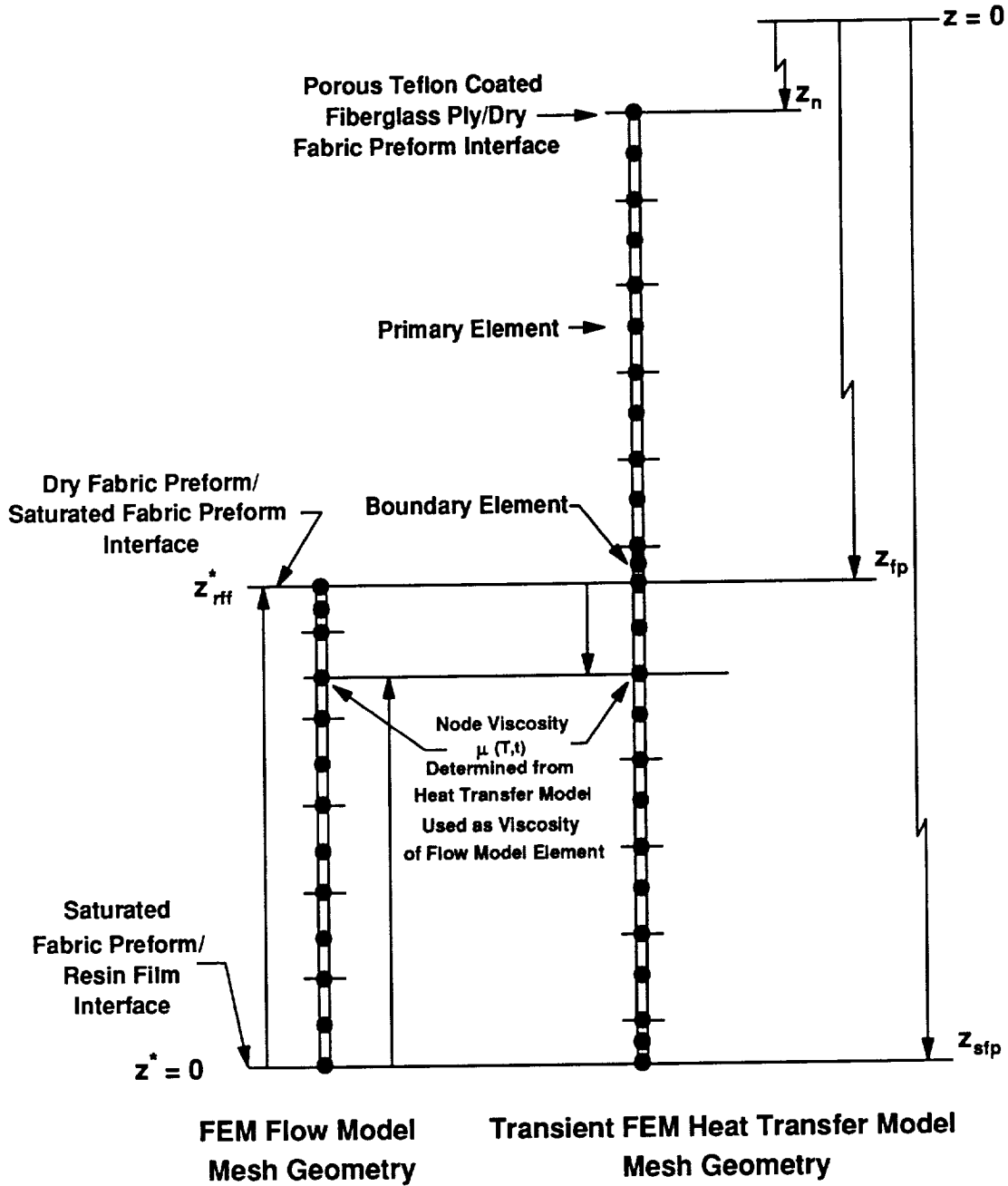
*Figure 3.4.2  Schematic of FEM heat transfer/flow model mesh interrelationship.*

## 3.5 RTM Simulation Model Software

A FORTRAN software program was developed to simulate fabrication of an advanced textile composite panel with the RTM film infusion technique. The software is based upon the transient heat transfer and FEM flow models presented in Sections 3.1 and 3.2, respectively. The user inputs the fabric and resin used for the fabrication of the panel, and prescribes an applied heat and pressure cycle to the RTM layup. The model outputs the final panel thickness, fiber volume fraction, and resin mass, along with the position of the infiltration front, the temperature distribution within the layup, and the resin degree of cure and viscosity as a function of time. A flow chart of the RTM simulation model is presented in figure 3.5.1.

The RTM simulation model utilizes the following data in SI units as fixed input:

1) Fabric Characteristics
   a) Dry/Wet compaction coefficients
   b) Through-the-thickness permeability coefficients
   c) Thermal coefficients (thermal conductivity, specific heat, etc.)
   d) Physical characteristics (areal weight, density, etc.)
   e) Number of primary finite elements per meter for the transient FEM heat transfer model

2) Resin Characteristics
   a) Thermal coefficients (thermal conductivity, specific heat, etc.)
   b) Physical characteristics (areal weight, density, etc.)
   c) Kinetics model coefficients
   d) Viscosity model coefficients
   e) Number of primary finite elements per meter for the transient FEM heat transfer model

3) Layup material characteristics
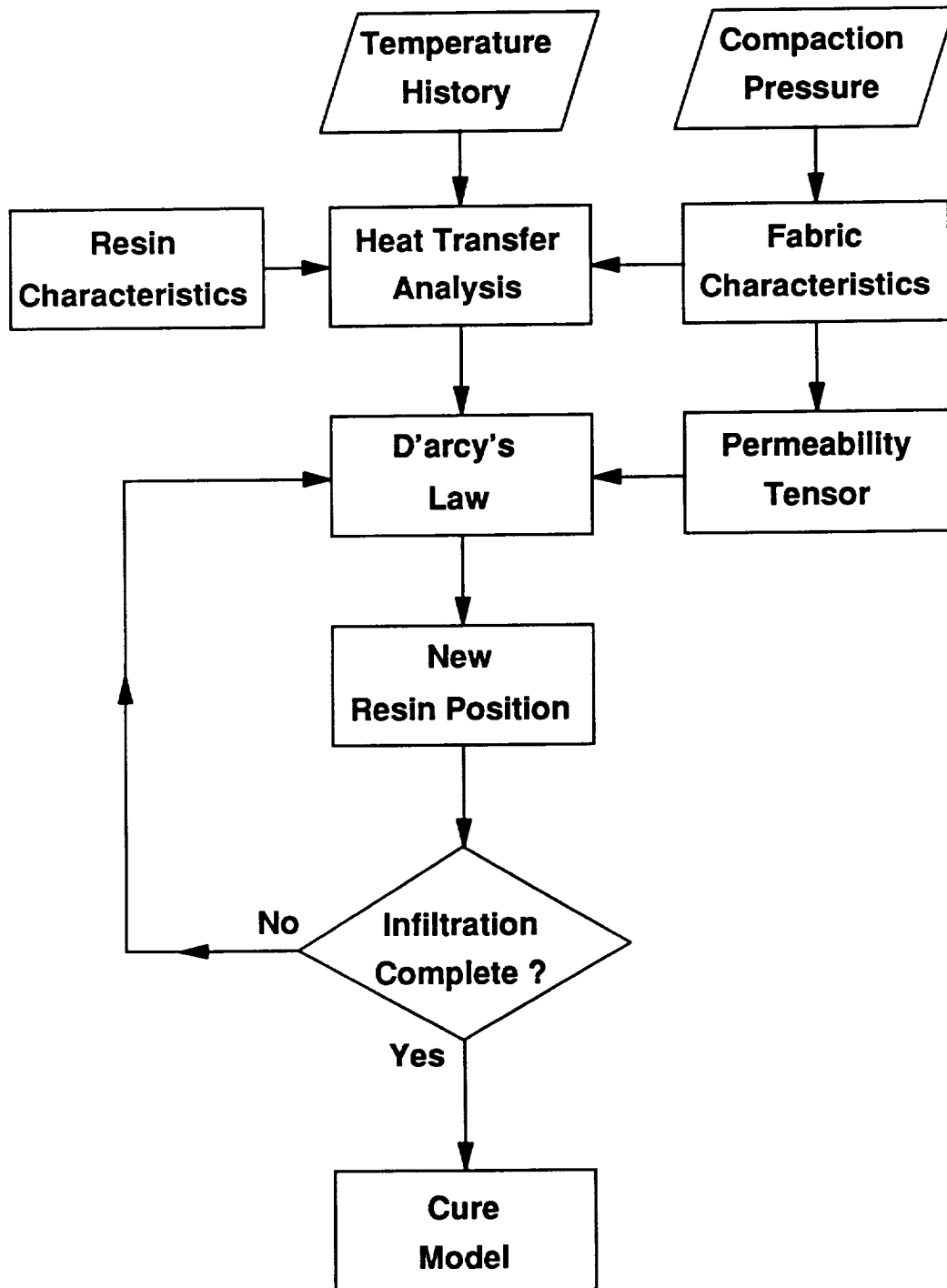
*Figure 3.5.1. Schematic of RTM simulation model.*

a) Thermal coefficients (thermal conductivity, specific heat, etc.)

b) Physical characteristics (areal weight, density, etc.)

c) Number of primary finite elements per meter for the transient FEM heat transfer model

The user directly inputs the following information:

1) Title of simulation

2) Fabric preform and compaction model to be used

3) Resin system to be used

4) Initial degree of cure of the resin film

5) Planar dimensions of the fabric preform

6) Layup stacking sequence

7) Applied temperature history at the boundaries of the layup

8) Applied pressure history on the layup

9) Temperature survey location

The RTM simulation model outputs the following information:

1) Input data

2) Final thickness, fiber volume fraction and resin film mass and thickness as a function of the applied pressure history

3) Temperature, degree of cure, viscosity of resin flow front and resin flow front position as a function of time

4) The temperature, and the resin degree of cure and viscosity (if appropriate) as a function of time at selected positions within the layup

# 4.0 Experimental Test Methods

The goal of this chapter is to present the experimental procedures used to characterize the compaction and flow characteristics of fabric preforms and the physical and mechanical characteristics of textile composites. A reliable cost effective fabrication technique for RTM film infusion technique will also be presented.

Typically, a fabric preform will have an unique compaction and permeability behavior depending on tow size, fiber orientation, weave type, and type of through-the-thickness reinforcement in the form of stitching. Two experimental studies were used to characterize the fiber preforms. Initially, an experimental study was conducted on fabric preforms to determine the dry and wet compaction behavior. A prescribed loading rate was applied to a fabric preform test sample and the resulting deflection was recorded. Empirical relationships were developed to describe the preform thickness, fiber volume fraction, porosity, and resin mass required for full saturation as a function of the applied compaction pressure. A second series of experiments were conducted to determine the through-the-thickness permeability as a function of the fabric preform compaction.

Textile composite panels were fabricated using different temperature and pressure processing cycles. In-situ measurements obtained during fabrication were compared with results obtained from the initial characterization experiments and the RTM simulation model. During the fabrication process, the infiltration front position was recorded as a function of time and compared with results obtained from the simulation model. The final laminate thickness, fiber volume fraction, and resin mass were measured and compared with model results.

Panels fabricated using the RTM film infusion technique were analyzed to determine the final quality and to compare the mechanical strengths with similar panels fabricated from prepreg materials. Non-destructive evaluation (NDE) was used to check for the presence of macroporosity and to observe the resin distribution within the panels, while micrographs were taken to determine if the panels contained microporosity.

## 4.1 Fabric Preform Material Systems

The fabric preforms utilized for the present study were composed of either Hercules AS4 or IM7 graphite fibers. The AS4 fibers have moderate strength and modulus properties and the IM7 fibers have high strength and modulus properties, (see Table 4.1.1). The surfaces of both fiber types were treated with a sizing agent by the manufacturer and assembled into filament tows which were then woven together to form multi-directional fabric preforms, or knitted together into individual unidirectional plies for a particular layup orientation.

Advanced fabric preforms, supplied by Hexcel Hi-Tech, were examined to determine the effect of through-the-thickness stitching on the processing behavior of textile preforms. Hexcel quasi-isotropic $(+45°/0°/-45°/90°)_{2s}$ fabric preforms, consisting of individual unidirectional plies of AS4 6k filament tows knitted together with a 70 denier polyester knitting yarn [27], were examined in both stitched and unstitched configurations (see Fig. 4.1.1). The knitting yarns had a pitch of 3.54 stitches/cm and were spaced 0.42 cm apart. The stitched preforms utilized a Toray T-900-1000-50 carbon stitching yarn to lock together individual plies. Stitching yarns had a pitch of 3.15 stitches/cm and were spaced 0.635 cm apart in rows aligned with the 0° and 90° fiber orientations of the preform.

An eight harness satin-weave, manufactured by Textile Technologies Incorporated (TTI), was examined to characterize compaction and permeability behavior of two-dimensional woven fabric preforms. Individual plies were composed of IM7 fibers arranged in 6k tows woven in a 0°/90° orientation. Individual plies and multiple ply preforms contained an equal number of tows in the warp (0°) and fill (90°) direction. Single Kevlar tows were interspaced at 4 cm apart along the warp and fill directions to help determine the orientation of the carbon fiber tows.

*Tabel 4.1.1. AS4 and IM7 physical properties [26].*

| Fiber | Density*$10^6$ (g/m$^3$) | Filament Diameter*$10^{-6}$ (m) | Tensile Strength (MPa) | Tensile Modulus (GPa) |
|---|---|---|---|---|
| IM7 | 1.78 | 5 | 5,343 | 276 |
| AS4 | 1.80 | 8 | 3,999 | 214 |

**Experimental Test Methods**
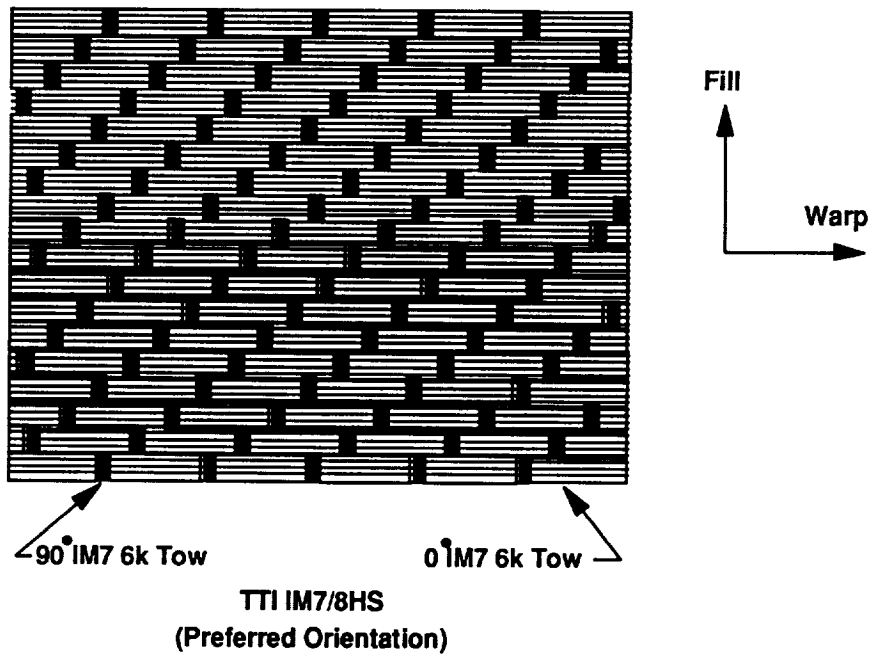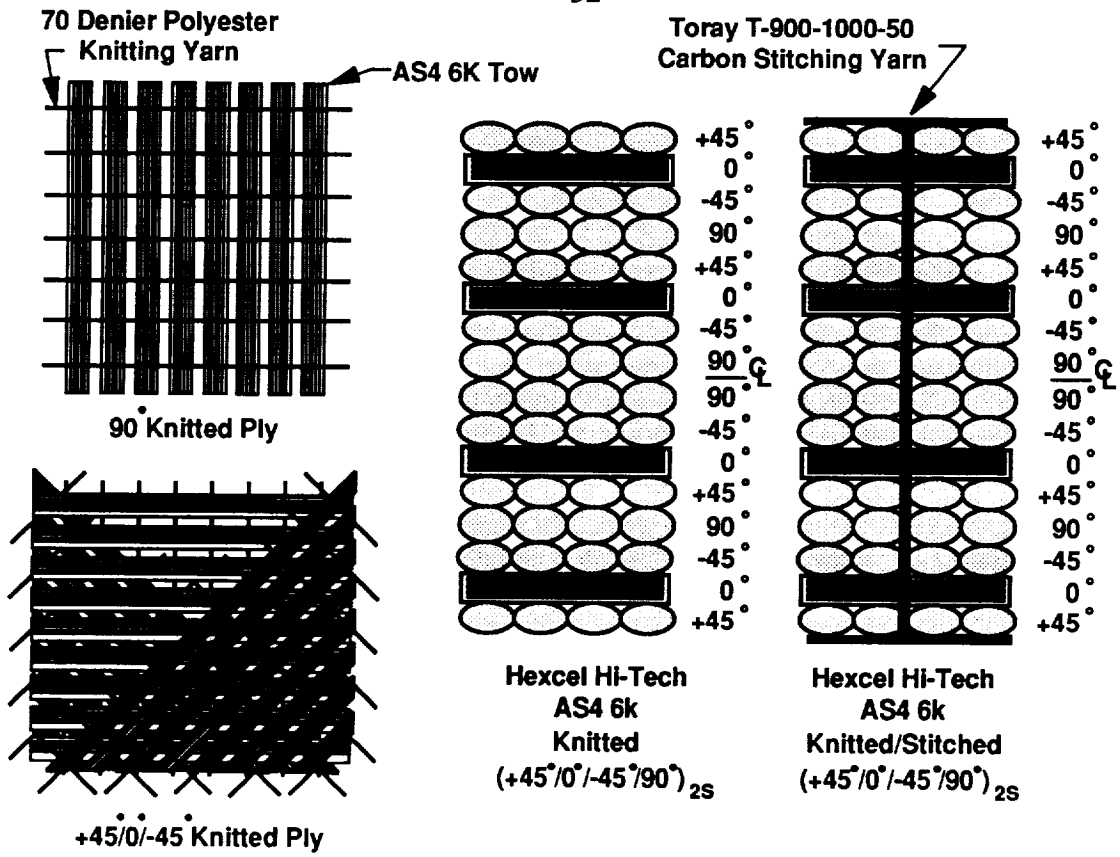
Figure 4.1.1. Schematic of Hexcel Hi-Tech multiaxial warp knit and
TTI IM7/8HS fabric preforms.

## 4.2 Test Fixtures

Through-the-thickness permeability and dry and wet compaction characterization studies were conducted using a specially designed test fixture. A small stainless steel fixture was designed and fabricated to determine the compaction and flow characteristics of advanced carbon fabric preforms (Fig. 4.2.1). The fixture test section was designed to characterize small fabric preform test samples 51 mm long by 51 mm wide and up to 90 mm thick. The upper and lower matching plungers of the test section were aligned by control rods that were mounted in the central body. Porous or nonporous compaction plates attached to the surface of each plunger constituted the upper and lower surfaces of the test section. Each plunger contained a single pipe fitting for connection to an external fluid line and a fluid staging chamber to reduce the vorticity of the fluid prior to entrance into the fixture test section. A special rod assembly was fitted to each plunger to allow the test fixture to be attached to the radial grip of an Instron 1321 test machine.

For the through-the-thickness permeability and wet compaction experiments, the upper and lower plungers were fitted with porous plates and connected to external fluid lines. O-rings (3 mm dia.) coated with vacuum grease were inserted into small groves circumnavigating the outer edges of the top and bottom porous plates. The O-rings formed a high pressure seal between the plungers and the cavity. The lower plunger (connected to rod assembly) was inserted into the cavity and bolted to the central body. The upper plunger was then inserted into the cavity to form the upper half of the test section and was free to move vertically along the control rods. The alignment rods ensured that the plates of both plungers remained parallel during displacement of the upper plunger. Hence, the test samples compacted by the plungers had uniform thicknesses and porosities across the entire test section. The dry compaction experiments utilized nonporous plates in place of the porous plates on both plungers.

A steel flat plate mold assembly (Fig. 4.2.2) was used to fabricate advanced textile composite panels. The cavity consists of a flat plate with side pieces that were attached with bolts. The side pieces guided the movement of the plunger during insertion and

Experimental Test Methods
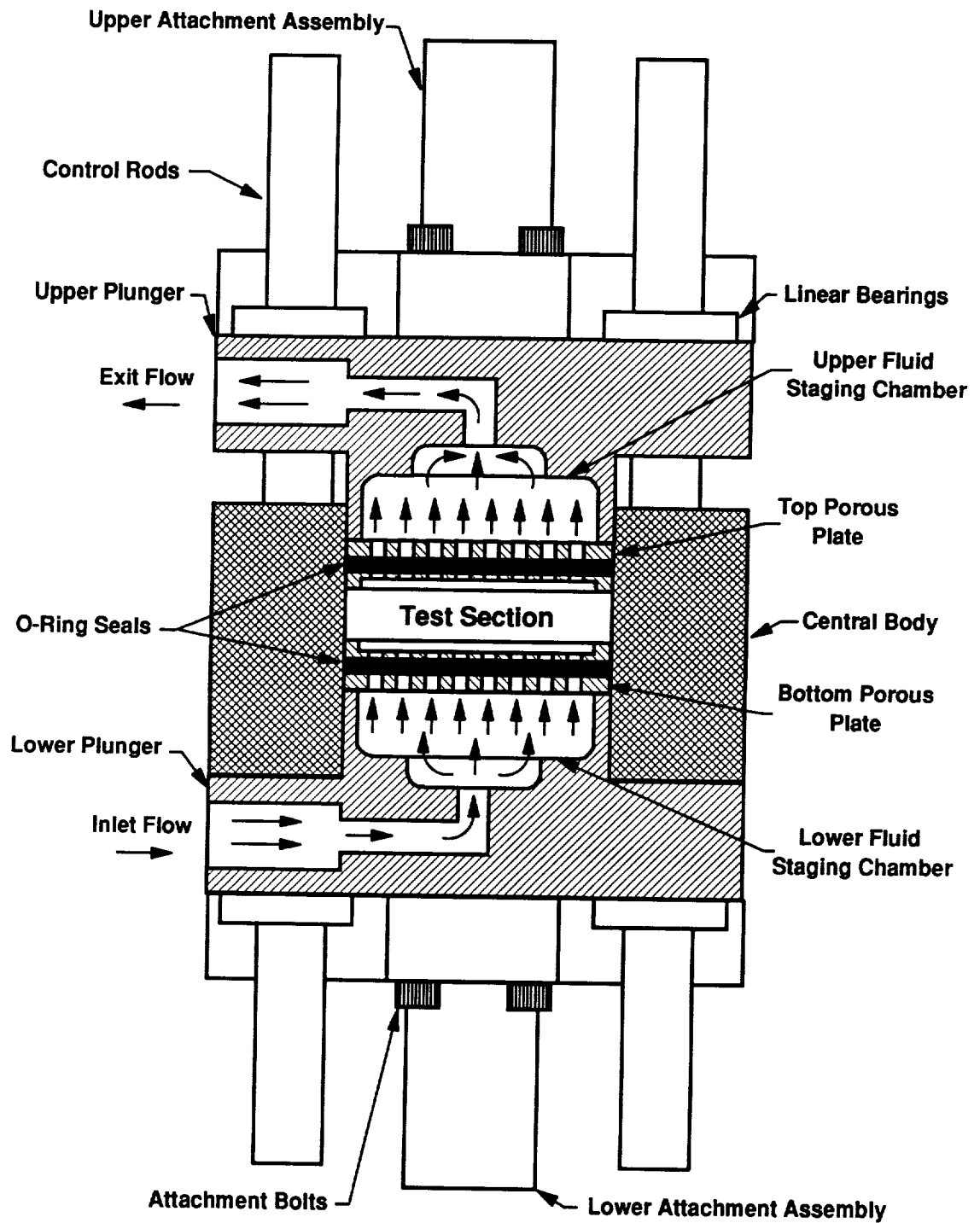
Figure 4.2.1   Schematic of through-the-thickness permeability and dry/wet compaction test fixture.
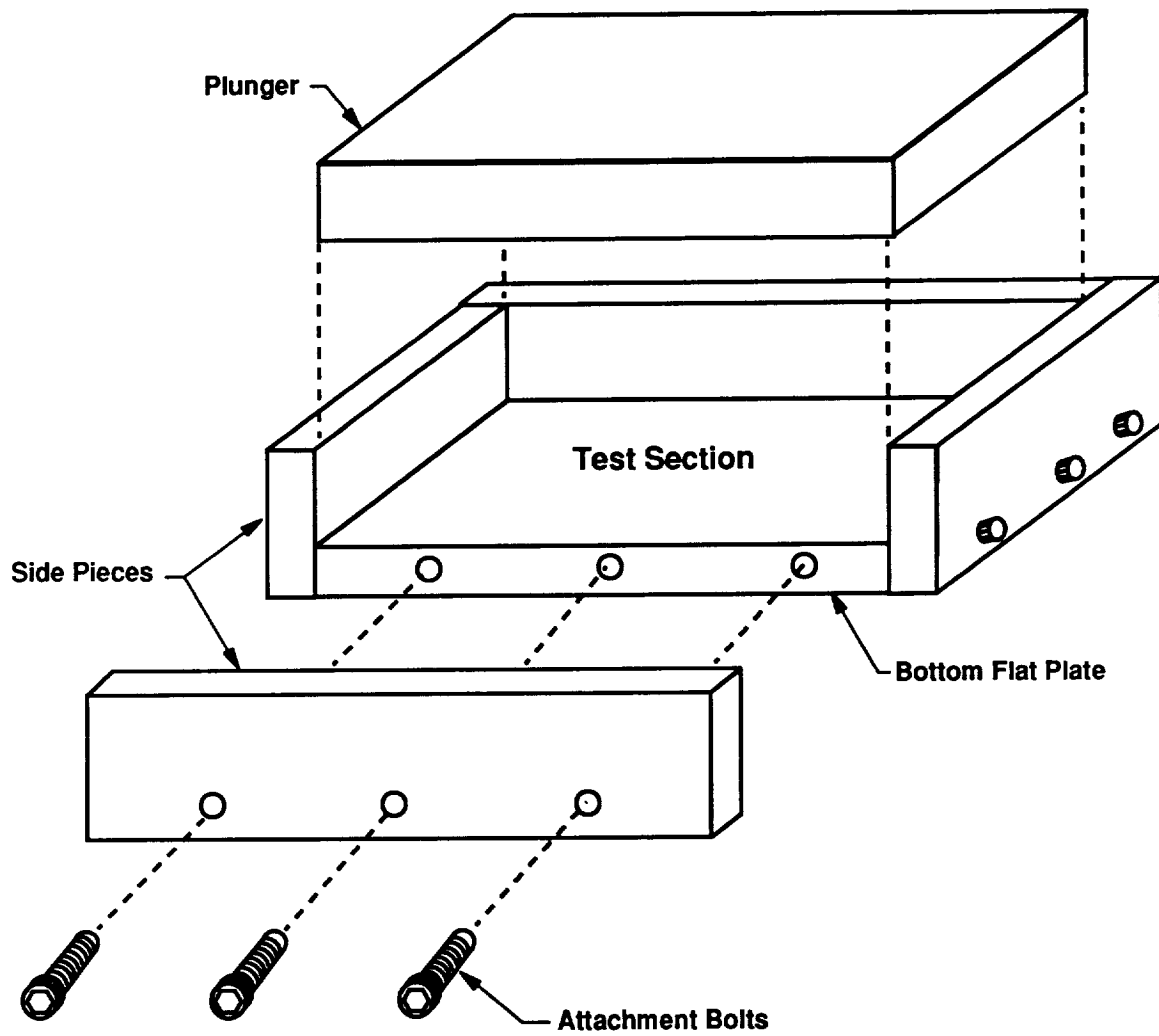
*Figure 4.2.2. Schematic of flat plate mold utilized for the fabrication of composite panels with the RTM film infusion technique.*

**Experimental Test Methods**

prevented fiber slippage when transverse compaction loads were applied. The mold had a 152 mm by 152 mm by 10 mm test section.

## 4.3 Test Sample Preparation Procedure

Fabric preform test samples for the compaction and permeability experiments were carefully cut to the dimensions of the test cavity to help prevent tow breakage and misalignment. Initially, the fabric preforms were placed onto a sheet of plastic release film taped to the top of a cutting table. The fabric preforms were then adjusted until the $0°$ and $90°$ tows and/or plies were perpendicular. The outer perimeter of the fabric preform was then taped to the table and a second piece of plastic release film was placed on top of the preform and secured to the table to help reduce the loss of fibers from the preform during cutting.

Composite pattern plates, with dimensions identical to the respective flat plate mold and permeability fixture test section, were utilized to properly size the fabric preform samples. The cutting patterns were oriented to have the longitudinal sides perpendicular to the $0°$ fiber orientation of the preform. A slight hand pressure was applied to the mold pattern (to keep the fabric from slipping), and the fabric was carefully cut around the edges of the pattern with a razor knife. The test samples were then removed from the remaining fabric preform.

Dry compaction specimens were cut from dry fabric preforms and the uncompacted initial thickness and surface dimensions were measured with Sylvac electronic calipers. The test samples were then weighed and the corresponding areal weight was calculated from Eq. 2.1.5. The test samples were then stored in sealed polyethylene bags to prevent contamination.

The wet compaction and permeability samples were cut from fabric preforms presaturated with tap water and sealed in polyethylene bags to prevent moisture evaporation (wet samples were measured but not weighed). The samples were wetted to prevent fiber misalignment during cutting and to help remove entrapped air.

## 4.4 Dry/Wet Compaction Procedure

The permeability/compaction test fixture, with nonporous plates attached to the surfaces of the upper and lower plungers, was initially loaded in compression to determine the deflection behavior of the test section as a function of the applied load. The test section was subjected to transverse compaction loads ranging from 0 to 3550 N from a Instron 1321 multi-axial hydraulic testing machine. The lower grip/actuator of the test machine was attached to a Linear Voltage Displacement Transducer (LVDT) to measure the transverse deflection, while the upper grip was connected to a 20 kip load cell which measured the applied compaction loads. The load and displacement readings from the Instron test machine were collected using an IBMpc controlled data acquisition system.

The deflection behavior of the test fixture was measured using the following procedure. The test fixture was assembled with the surfaces of the upper and lower plungers touching and attached to the lower grip of the Instron test machine. The lower grip/actuator was raised to place the upper attachment assembly rod of the test fixture into the upper grip. The LVDT was zeroed and the data acquisition was started. A function generator was then utilized to raise the lower actuator at a rate of 0.02 mm/min and load the test fixture. When a load of 3550 N was reached, the displacement was reversed, and the test fixture was unloaded. After repeating the experiment three times, the data acquisition was halted and the test fixture was removed from the test machine. Identical experiments were performed to measure the deflection of the test fixture fitted with the porous plates in place of the nonporous plates.

After the test fixture deflection was measured, the compaction of the preforms was measured. A fabric preform test sample was removed from the polyethylene bag, thoroughly cleaned, and inserted into the test fixture. (Single ply fabrics were assembled into a fabric preform with a desired lay-up orientation prior to insertion into the test section.) The upper plunger was then inserted into the vertical cavity until contact with the top of the fabric preform was achieved and the top plunger was supported by the fabric preform.

The lower attachment rod of the fixture was secured to the lower grip of the Instron test machine and the actuator was raised to place the upper attachment rod into the upper grip, (Fig. 4.4.1). The displacement transducer was zeroed and the data acquisition system was started. The fixture and the fabric preform test sample were compacted at either a fast (0.2 mm/min ) or a slow (0.02 mm/min) displacement rate until a compaction load of 3550 N was reached. When the maximum compaction load was obtained, the data acquisition was halted, and the fixture was unloaded. Upon completion of the compaction experiments, the test fixture was removed form the test machine grips and the test sample was removed from the test fixture.

An identical procedure was utilized to characterize the wet compaction behavior of the fabric preforms. Wet fabric preform test samples, fully saturated with water, were compacted from 0 to 3550 N at a fast (2 mm/min) displacement rate. Porous plates, mounted on the upper and lower plungers, allowed for the unrestricted transfer of excess fluid from the preforms during compaction.

## 4.4.1 Dry/Wet Compaction Analysis

Load and deflection data obtained from the compaction experiments were fit to 4th order least squares polynomials. The weight of the upper plunger was added to the applied compaction load from the test machine to give the total applied compaction load. The applied compaction pressure was calculated using the following expression

$$P_{comp} = \frac{F_{comp} + F_{upl}}{A_{xy}} \qquad (4.4.1)$$

where $P_{comp}$ is the total applied compaction pressure to the fixture test section, $F_{comp}$ is the applied compaction load from the test machine, $F_{upl}$ is the weight of the upper plunger, and $A_{xy}$ is the cross sectional area of the test section.

The deflection data obtained from the empty test fixture compaction experiments were fit with the following 4th order least squares nonlinear polynomial,
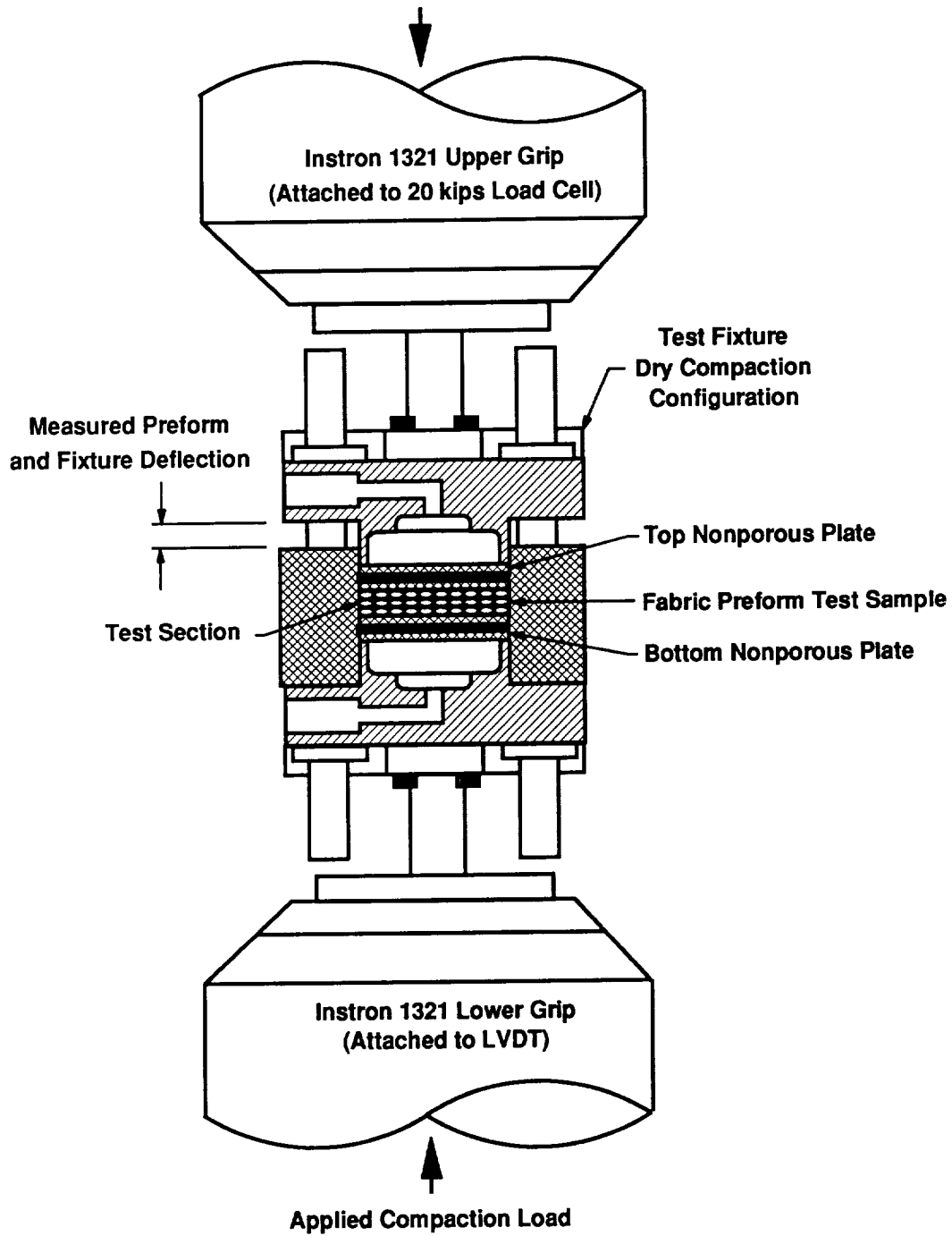
*Figure 4.4.1.* Schematic of dry compaction experimental apparatus.

$$d_{fix} - \sum_{i=0}^{4} a_{i_{fix}} (\ln(P_{comp}))^i \qquad (4.4.2)$$

and deflection data obtained from the fabric preform compaction experiments were fitted to an similar relationship written as

$$d_{fab} - \sum_{i=0}^{4} a_{i_{fab}} (\ln(P_{comp}))^i \qquad (4.4.3)$$

where $a_i$ are the compaction model coefficients, d is the deflection, and the subscripts fix and fab refer to the test fixture and fabric preform, respectively.

The fixture deflection was subtracted from the total measured deflection obtained from the fabric preform compaction experiments to give the resulting net deflection for the fabric preform

$$d_{fp} - d_{fab} - d_{fix} - \sum_{i=0}^{4} (a_{i_{fab}} - a_{i_{fix}})(\ln(P_{comp}))^i - \sum_{i=0}^{4} a_i (\ln(P_{comp}))^i \qquad (4.4.4)$$

where the subscript fp refers to the fabric preform alone.

Equations 4.4.1-4.4.4 where utilized to characterize the compaction behavior of both the dry and wet fabric preform test samples. Equation 2.1.2 was then utilized to model the fabric preform thickness as a function of applied compaction pressure. The fiber volume fraction, porosity, and resin mass required for full saturation, were then determined from Eq. 2.1.6, Eq. 2.1.7, and Eq. 2.1.8, respectively.

## 4.5 Permeability Characterization Procedure

Flow experiments were initially conducted with an empty test section (no fabric preform) of the test fixture configured for the through-the-thickness permeability experiments (see Fig. 4.2.1) to measure the pressure drop within the fixture as a function of the flow rate.

The test fixture was secured to the lower actuator of the Instron test machine and the

upper and lower plungers were connected to the external fluid transfer lines. The lower actuator of the Instron was raised to provide a gap of 1 mm between the top and bottom porous plates. Tap water at room temperature was transferred from a wall outlet to a Matheson Co., Inc. bubble type flowmeter which was used to control and measure the rate of flow entering the permeability fixture. The flowmeter was calibrated prior to the flow experiments using a graduated cylinder and a digital stop watch. Marshalltown dial pressure gauges, ranging from 0 to 2.5 kPa were utilized to measure the inlet and exit port pressures.

A steady-state flow rate was set through the fixture test section and the resulting pressure drop across the empty test section was recorded. A total of 6 different flow rates ranging from 2 cc/min to 20 cc/min were applied. The flow experiments were repeated using several different gap heights ranging from 1 mm to 16 mm.

After the empty test section pressure loss was measured, fabric preforms were characterized to determine the through-the-thickness permeability as a function of porosity. A presaturated fabric preform test sample (Section 4.3) was removed from the protective bag, thoroughly cleaned with water, and placed into the test section. The test sample was then presaturated with water to remove any entrapped air which may affect experimental results. Care was taken to ensure that a uniform tight fit was achieved between the edges of the test sample and the inner walls of the test section.

The fixture was loaded into the test machine and secured to the lower actuator (Fig. 4.5.1). The actuator was raised to attach the fixture to the upper grip and the inlet and exit fluid lines were connected to the inlet and exit ports of the fixture. The lower actuator was raised until the separation distance between the upper and lower porous plates was equal to the measured uncompacted fabric preform thickness. Finally, the LVDT was zeroed.

The fabric preform test sample in the test section was then compacted to a desired thickness. The thickness of the test sample was determined by subtracting the deflection of the test sample measured by using the LVDT (at a particular compaction pressure) from the initial uncompacted thickness. A second measurement of the test sample
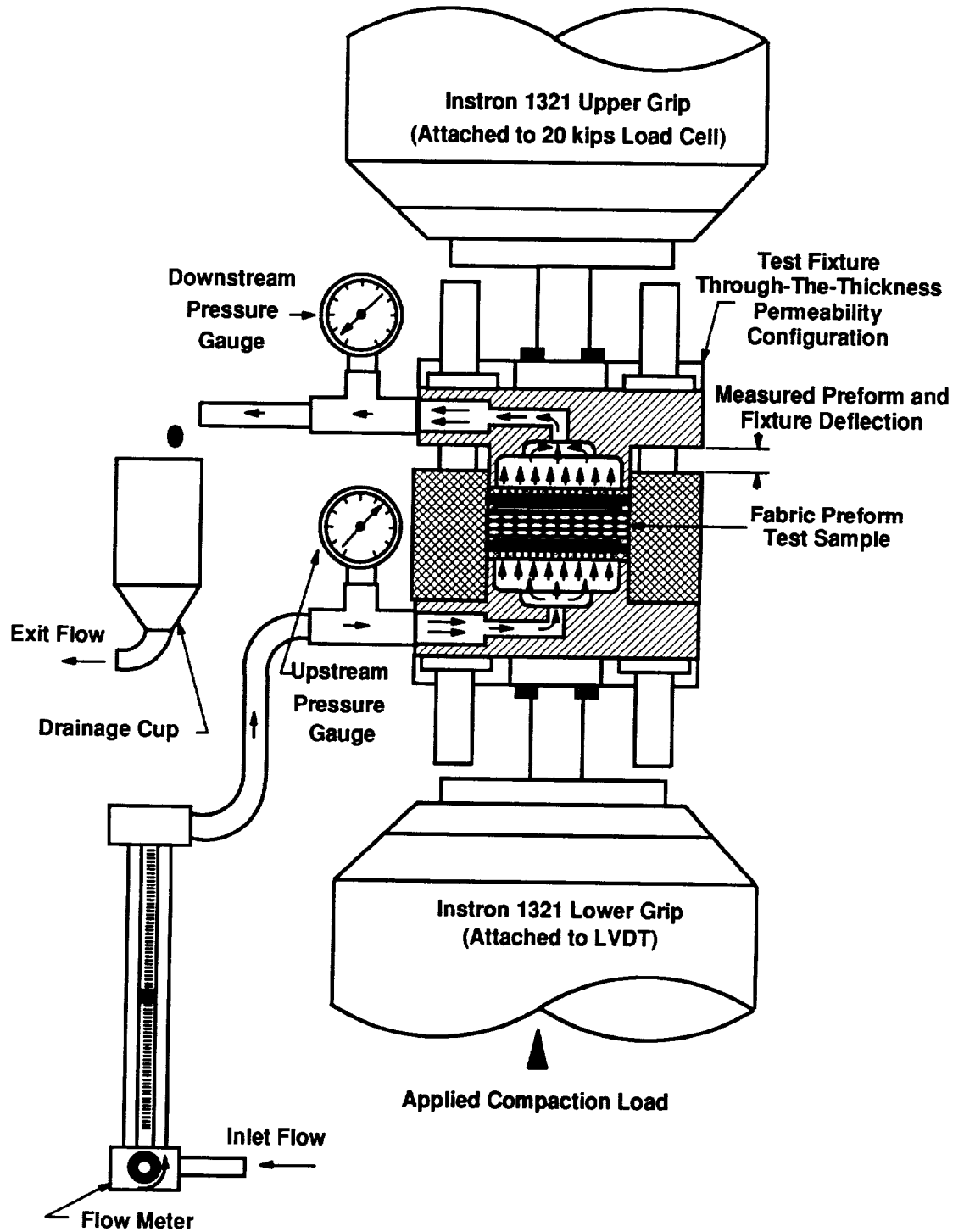
Figure 4.5.1.  Schematic of through-the-thickness permeability
experimental apparatus.

thickness was obtained by measuring the separation distance between the upper plunger and the central body (see Fig. 4.5.1) of the test fixture with electronic calipers. The compaction load applied to the test sample was recorded from the upper load cell of the Instron test machine. A steady-state flow rate was established through the test section and the resulting pressure differential across the test sample was measured using dial pressure gauges. A Marshalltown 0 to 2.5 kPa dial pressure gauge was used at the exit while either a 0 to 25.8 kPa or a 0 to 69 kPa Marshalltown dial pressure gauge was used at the inlet. All pressure gauges were ANSI standard 3% accurate. At each fabric preform thickness and compaction load, 6 to 8 different flow rates (2 cc/min to 20 cc/min) were established and the pressure differential across the fabric preform was measured. Overall, 8 permeability/porosity data sets were obtained from each test sample. One to two test samples of each type of fabric preform were examined.

## 4.5.1 Permeability Characterization Analysis

Results from the permeability experiments were used to relate the fabric preform permeability to the porosity.

The flow meters were calibrated to measure the volumetric flow rate, $Q_z$, as a function of the flow meter setting, s. The data were fit to a 5th order least squares polynomial written as,

$$Q_z = \sum_{i=0}^{5} b_i s^i \tag{4.5.1}$$

where $b_i$ represent the least squares coefficients.

The through-the-thickness pressure drop, $\Delta P_{fix}$, of the empty permeability fixture test section was measured as a function of the flow rate. The effect of gap height was found to be insignificant. The results were fit to a 6th order least-squares polynomial written as,

$$\Delta P(Q_z)_{fix} = (P(Q_z)_{up} - P(Q_z)_{down})_{fix} = \sum_{i=0}^{6} dp_i Q_z^i \tag{4.5.2}$$

where dp$_i$ are the least squares coefficients and the subscripts up and down refer to the location at which the fluid pressure measurements were taken.

The through-the-thickness pressure drop across the fabric preform test samples, $\Delta P(Q_z)_{fp}$, was calculated using the following expression.

$$\Delta P(Q_z)_{fp} - (P(Q_z)_{up} - P(Q_z)_{down})_{fab} - \Delta P(Q_z)_{fix} \qquad (4.5.3)$$

The through-the-thickness pressure differentials and flow rates were utilized in D'arcy's law to determine the permeability constant, $K_{Pz}$. The volumetric flow rate, $Q_z$, was plotted as a function of the pressure gradient, $\dfrac{\Delta P(Q_z)_{fp}}{t_{fp}}$, and the slope, $C_z$, was measured from a linear least-squares curve fit to the data. The permeability constant was then determined from the following relationship:

$$K_{P_z} - \frac{C_z \mu}{A_{xy}} \qquad (4.5.4)$$

where $\mu$ is the viscosity of the test fluid (tap water).

The measured thickness (corrected for the deflection of the test fixture) at which the permeability, $K_{Pz}$, was obtained was substituted into Eq. 2.1.6. to determine the fiber volume fraction. Equation 2.1.7 was then utilized to determine the corresponding porosity.

The Kozeny-Carman relationship (Eq. 2.4.5) or the modified Gebart relationship (Eq. 2.4.8) was then utilized to model the through-the-thickness permeability as a function of the fabric preform porosity.

## 4.6 RTM Panel Fabrication Technique

A one-step RTM film infusion technique was developed to successfully fabricate advanced textile composite panels. The technique uses advanced cure cycles generated from the RTM simulation model and single-step pressure applications. The processing

steps for the fabrication of a panel composed of a 16 ply TTI IM7/8HS fabric preform and Hercules 3501-6 resin are described in detail in Appendix A.1.

One major advantage of the RTM film infusion technique involves the use of a single applied pressure to infuse the resin into the preform and provide resin pressure for the remainder of the cure cycle. By consolidating the fabric preform at the beginning of fabrication, the entire process is greatly simplified, and the simulation model needs to describe only the infiltration and cure of the panel. Shorter cure cycles were also achieved by allowing the resin to quickly gel once infusion is complete. Using this premise, advanced cure cycles developed using the RTM simulation model (Chapter 3) were utilized to successfully fabricate advanced textile composite panels with significantly shorter processing cycles.

Single ramp and hold cycles with heating rates ranging from 3 °C/min to 7 °C/min and total cure cycle times (not including cool down) ranging from 90 to 150 minutes (as opposed to the 230 minute manufacturer's cure cycle) were developed and utilized (see Table 4.6.1). The manufacturer's cure cycle (230 minutes) contains an initial temperature hold of 60 minutes at 117 °C to help degas the resin during processing. The model generated rapid cure cycle (150 min) was developed to eliminate the intermediate hold while using the same heating rates and final cure temperature (177 °C). The model generated advanced cure cycle (100 min) utilizes a high heating rate (7.5 °C/min) and cure temperature (190 °C) to significantly decrease the overall processing time. Finally, the model generated instantaneous cure cycle (90 min) utilizes preheated platens (117 °C) and a moderate heating rate (4 °C/min) to the final cure temperature (177 °C) to help decrease the processing time even further.

The one-step RTM film infusion technique was utilized to fabricate several different textile composites with the Hercules 3501-6 resin. The Hexcel preform materials were fabricated at different compaction pressures using the resin manufacturer's cure cycle and the rapid cure cycle (see Table 4.6.1). The influence of stitching upon fabrication was examined. 16 Ply TTI IM7/8HS fabric preforms were fabricated under a number of different compaction pressures using the manufacturer's recommended cure cycles and

**Experimental Test Methods**

Table 4.6.1 Cure cycles utilized for the fabrication of advanced
textile preforms with Hercules 3501-6 resin.

| Cure Cycle Step | Initial Temperature, °C | Temperature Ramp, °C/min | Duration, min |
|---|---|---|---|
| First Ramp | 27 | +3 | 30 |
| First Hold | 117 | 0 | 60 |
| Second Ramp | 117 | +3 | 20 |
| Second Hold | 177 | 0 | 120 |
| Cool Down | 177 | -3 | 50 |

**Manufacturer's Cure Cycle**

| Cure Cycle Step | Initial Temperature, °C | Temperature Ramp, °C/min | Duration, min |
|---|---|---|---|
| Ramp | 27 | +3 | 50 |
| Hold | 177 | 0 | 100 |
| Cool Down | 177 | -3 | 50 |

**Rapid Cure Cycle**

| Cure Cycle Step | Initial Temperature, °C | Temperature Ramp, °C/min | Duration, min |
|---|---|---|---|
| First Ramp | 27 | +7.5 | 20 |
| Second Ramp | 177 | +0.4 | 30 |
| Hold | 190 | 0 | 50 |
| Cool Down | 190 | -3 | 50 |

**Advanced Cure Cycle**

| Cure Cycle Step | Initial Temperature, °C | Temperature Ramp, °C/min | Duration, min |
|---|---|---|---|
| Ramp | 117 | +4 | 15 |
| Hold | 177 | 0 | 75 |
| Cool Down | 177 | -3 | 50 |

**Step Cure Cycle**

Experimental Test Methods

three different model generated cure cycles.

## 4.7 In-Situ Monitoring

Extensive in-situ monitoring was performed on all the advanced textile composite panels fabricated using the RTM film infusion technique to determine the influence of applied compaction pressure and thermal cure cycles on the rate of resin infusion and the time required for complete cure.

Applied compaction pressures (in addition to the vacuum bag compaction pressures) were measured with a calibrated pressure gauge connected to the lower hot press platen. As the resin infused into the dry fabric preform, the thickness of the resin film and the corresponding layup decreased and the lower platen was displaced upward due to the compaction load applied by the lower actuator of the hot press. A LVDT connected to the upper platen (fixed) and a digital stop watch were used to measure the displacement of the lower platen as a function of time. The resin flow front position as a function of time, $D(t)_{rff}$, was normalized using the following relationship:

$$D(t)_{rff} = \frac{|D(0)_g - D(t)_g| + D(t)_{th}}{t_{rp}}$$ (4.7.1)

where $t_{rp}$ is the initial thickness of the resin panel (measured with electronic calipers), $D(t)_g$ is the position of the lower platen at time $t>0$, $D(0)_g$ is the initial position of the lower platen at time, $t = 0$, and $D(t)_{th}$ is the thermal expansion of the layup and the platens (measured as a function of time from a previous experiment without the composite layup materials).

Thermocouples (J-type or K-type) were placed at the bottom of the resin film to measure the temperature of the resin during infusion and at the top and bottom of the fabric preform to determine the temperature distribution within the panel during cure. Frequency Dependent Electromagnetic Sensors (FDEMS)[28-30], provided by the College of William and Mary, were utilized to monitor the resin degree of cure and viscosity during fabrication and the total infiltration time.

Experimental Test Methods

# 4.8 Non-Destructive Evaluation

After the advanced textile composite panels were fabricated, the thickness and planar dimensions were measured, and the panels were weighed. The final fiber volume fraction, $v_f$ was determined from the following relationship:

$$v_f = \frac{M_{fp}}{\rho_f(h_a l_a w_a)} \tag{4.8.1}$$

where $M_{fp}$ is the initial mass of the dry fabric preform, $\rho_f$ is the fiber density, and $w_a$, $l_a$, and $h_a$ are the respective width, length, and height of the fabricated panel.

The final resin mass, $M_r$, is determined from the relationship:

$$M_r = M_p - M_{fp} \tag{4.8.2}$$

were $M_p$ is the final panel mass. The final results were compared with the RTM simulation model results.

Ultrasonic C-scans (10 MHz) were taken to determine the presence of voids and the final resin distribution of the fabricated panels.

After the panels were C-scanned, specimens were cut from the panels and used to determine the fiber volume fraction, check for the presence of voids, and evaluate the mechanical properties, (see Fig. 4.8.1). One to two specimens (2 mm by 5 mm) were removed from each panel to determine the fiber volume fraction by acid digestion techniques (ASTM D-3171). One or two micrograph specimens (10 mm by 16 mm) were taken from each panel to determine the overall quality of the panels, and detect the presence of microporosity and microcracking. Micrographs were taken at magnifications of 40X and 400X.

3.2 mm

6.4 mm
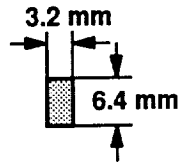
Acid Digestion Specimen

19 mm

19 mm

Micrograph Specimen

38.1 mm

44.5 mm

90°

0°

Reference Axis
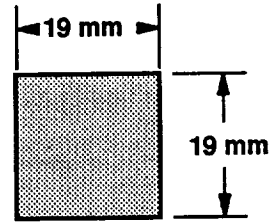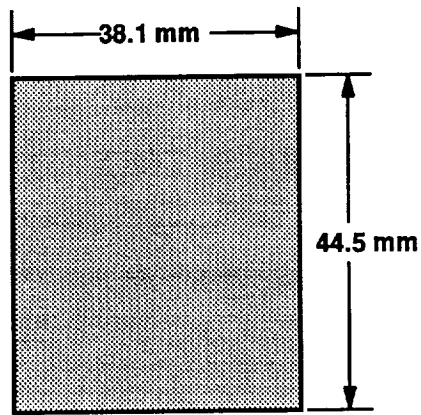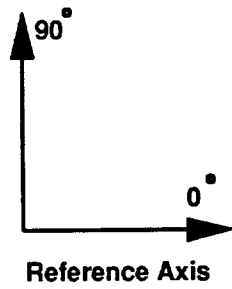
Short Block Compression Specimen

90°

R 1.3 mm

19.1 mm

76.2 mm
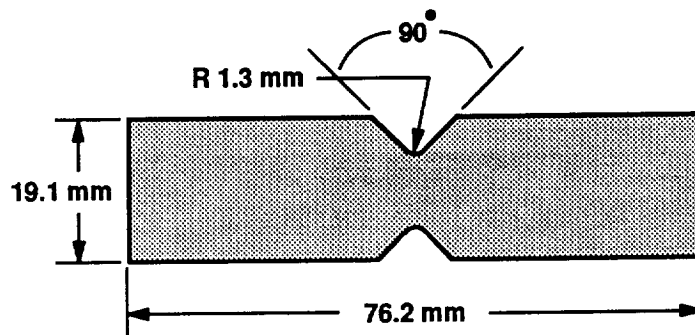
Iosipescu Shear Specimen

*Figure 4.9.1. Specimens utilized for non-destructive and
destructive evaluation studies.*

Experimental Test Methods

## 4.9 Destructive Evaluation

Short block compression (SBC) specimens (see middle of Fig. 4.8.1) were taken from each panel and tested to failure using the NASA procedure (RP-1142) [31]. Specimens were loaded in compression along either the 0° or 90° plies. Stain gauges (stacked 0°/90° with respect to the 0° plies of the specimen) were attached to both sides of the SBC specimens to measure the average longitudinal and lateral strain. A data acquisition system was then utilized to measure and record the compaction load applied to the SBC specimens and the resulting microstrain during testing. The test fixture used for the SBC experiments is shown in Fig. D.1.1, Appendix D.1, along with the equations utilized to determine the compressive strength, the ultimate longitudinal load, the Poisson's ratio at 0.2% longitudinal strain, and the Young's modulus at 0.2% longitudinal strain.

Iosipescu shear specimens (bottom of Fig. 4.8.1) were taken from each panel and tested to failure using a procedure presented in [32]. The Iosipescu shear specimens were tested with either the 0° or the 90° plies being perpendicular to the direction of the applied load, (see Fig. D.2.1). Strain rosettes (+/-45° with respect to the 0° plies) were attached to both sides of the Iosipescu shear specimens to measure the shear strain. The applied load and strain were measured and recorded with a data acquisition system. A drawing of the Iosipescu test fixture and the equations utilized to determine the shear strength and shear modulus at 0.2% shear strain are presented in Fig. D.2.1, Appendix D.2.

Both mechanical tests were utilized to determine the effects of processing variables upon matrix dominated properties. Photomicrographs (6.5X to 16X) of SBC and Iosipescu Shear failure surfaces were also taken.

# 5.0 Hexcel Hi-Tech Multiaxial Warp Knit Material Evaluation

Experiments were conducted to determine the compaction and permeability characteristics of the Hexcel Hi-Tech multiaxial warp knit fabric preforms (Section 4.1). The results were then incorporated into the RTM simulation model. Textile composite panels were fabricated with the Hexcel Hi-Tech fabric preforms and Hercules 3501-6 resin using the RTM film infusion technique. During fabrication, in-situ measurements of the temperature distribution, the resin degree of cure, and the resin viscosity were recorded as a function of time for comparison with results obtained from the RTM simulation model. Fabricated panels were C-scanned and micrographed. Test specimens obtained from the panels were mechanically tested in compression and shear.

The purpose of this chapter is to compare and contrast the physical properties of the Hexcel Hi-Tech fabric preforms, prior to and after fabrication. The accuracy and validity of the RTM simulation model predictions will also be examined.

## 5.1 Areal Weight/Initial Thickness

The average initial uncompacted thickness and areal weights of knitted and knitted/ stitched Hexcel Hi-Tech fabric preform materials are presented in Table 5.1.1. Measurements were obtained from 50.8 mm by 50.8 mm and 152.4 mm by 152.4 mm fabric preform test samples as described in Section 4.3. Three different test samples of each fabric preform were used for the measurements. The knitted/stitched test samples were found to have a lower (27%) initial thickness and a higher (5%) areal weight in comparison to the knitted test samples.

*Table 5.1.1. Areal weight and initial uncompacted thickness of Hexcel Hi-Tech multiaxial warp knit fabric preforms.*

| Hexcel Hi-Tech AS4 6k | Areal Weight, $g/m^2$ | Initial Thickness, mm |
|---|---|---|
| Knitted $(+45°/0°/-45°/90°)_{2S}$ | 6,957 | 10.54 |
| Knitted/Stitched $(+45°/0°/-45°/90°)_{2S}$ | 7,326 | 7.69 |

## 5.2 Dry/Wet Compaction

Compaction experiments were conducted to model the transverse deflection of the Hexcel Hi-Tech fabric preforms (Section 4.1) as a function of applied compaction pressure. Three test samples (50.8 mm by 50.8 mm) were cut from each of the Hexcel fabric preforms. Dry and wet test samples were individually subjected to transverse compaction loads ranging from 0 to 3550 N using either a fast deflection rate (0.2 mm/min) or a slow deflection rate (0.02 mm/min). Experimental results are presented in the following section along with a comparison of the compaction behavior of the fabric preforms.

The compaction experiments were initially conducted with the empty compaction/ permeability test fixture (Section 4.2) using the procedures presented in Section 4.4. The transverse deflection data of the test fixture as a function of applied compaction pressure (applied to the test section), are given in Appendix B.1.

The Hexcel Hi-Tech fabric preform test samples were tested in compression using the test fixture and the deflection data were fit with a least squares routine to Eq. 4.4.3. Equation 4.4.4 was then utilized to subtract out the deflection of the test fixture, resulting in a compaction model for the fabric preforms. The dry and wet compaction model coefficients obtained from Eq. 4.4.4 are presented on Table 5.2.1. The deflection of each fabric preform test sample is plotted as a function of applied compaction pressure in Fig. 5.2.1. A fast wet compaction experiment with the knitted fabric preforms was not performed due to a shortage of material.

All of the compaction results showed a nonlinear relationship between the applied pressure and the measured deflection at compaction pressures ranging from 0 to 700 kPa, while a linear relationship existed at pressures greater than 700 kPa. The knitted fabric preform test samples obtained the greatest deflection. A majority of the acquired deflection of the knitted test samples occurred when the compaction pressure was increased from 0 to 150 kPa.

The deflection of the fast dry and wet knitted/stitched test samples were lower in

Table 5.2.1  Dry/wet compaction model coefficients (Eq. 4.4.4) for
the Hexcel Hi-Tech multiaxial warp knit fabric preforms.

| Hexcel Hi-Tech AS4 6k Knitted (+45°/0°/-45°/90°)$_{2S}$ | | | | | |
|---|---|---|---|---|---|
| Compaction Model | $a_0$ (mm) | $a_1$ (mm) | $a_2$ (mm) | $a_3$ (mm) | $a_4$ (mm) |
| Slow Dry | -2.83410 | 0.14711 | 0.70999 | -0.13882 | 0.00792 |
| Fast Dry | -0.00725 | 0.61973 | 0.03279 | -0.00604 | 0.00018 |

| Hexcel Hi-Tech AS4 6k Knitted/Stitched (+45°/0°/-45°/90°)$_{2S}$ | | | | | |
|---|---|---|---|---|---|
| Compaction Model | $a_0$ (mm) | $a_1$ (mm) | $a_2$ (mm) | $a_3$ (mm) | $a_4$ (mm) |
| Slow Dry | 0.11988 | -0.07467 | -0.06564 | 0.28464 | -0.00195 |
| Fast Dry | 0.04923 | -0.03292 | 0.03036 | -0.00106 | 0.00009 |
| Fast Wet | 0.06792 | -0.01221 | -0.03141 | 0.01457 | -0.00096 |
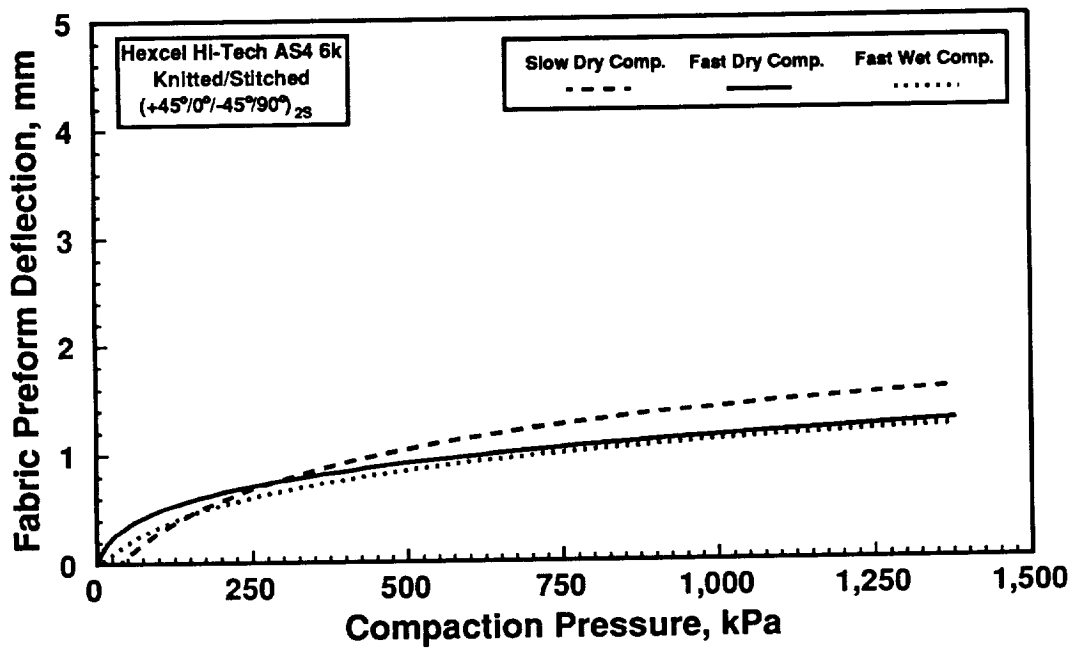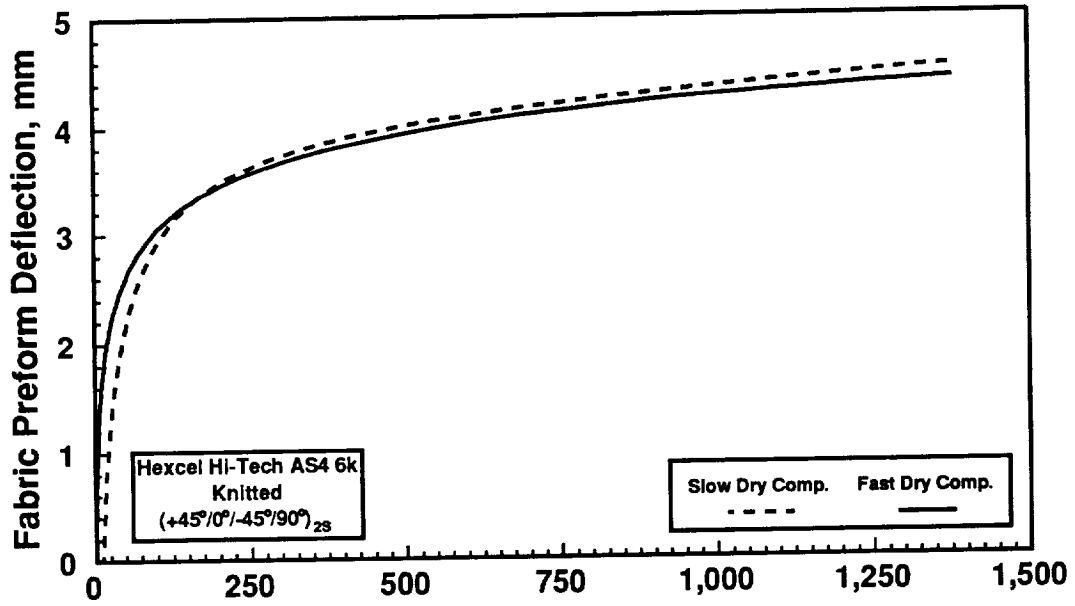
Figure 5.2.1  Wet and dry fabric preform deflections as a function of applied
compaction pressure for the Hexcel Hi-Tech multiaxial warp knit
fabric preforms.

Hexcel Hi-Tech Multiaxial Warp Knit Material Evaluation

comparison to the deflection of the slow dry knitted/stitched test sample. The fast wet knitted/stitched test sample had the lowest deflections due to the presence of an incompressible fluid (water) within the test sample during compaction. As the fully saturated test sample was compacted, excess fluid trapped within the fiber bed supported a small finite portion of the applied pressure resulting in lower measured deflections.

The application of a slow deflection rate to the dry knitted and knitted/stitched test samples resulted in the highest measured deflection at compaction pressures greater than 250 kPa (see Fig. 5.2.1). The larger deflections may be due to a time dependent relaxation of the fiber bed and fiber slippage during compaction. Over a finite time, a fabric preform under an applied compaction pressure will obtain an optimal fiber bed orientation. A significant difference in the deflection of the fast and slow knitted/stitched test samples was observed at compaction pressures greater than 350 kPa (see bottom of Fig. 5.2.1). The through-the-thickness carbon stitches were found to hinder both tow slippage and fiber realignment, affecting both the measured stiffness and the time dependent nature of the compaction models. Conversely, the knitted fabric preform test samples were allowed to freely reorient (to support the applied compaction pressure) due to a lack of vertical constraining fibers within the fiber bed. Hence, the effect of loading rate upon the measured deflection of the knitted test samples was negligible.

## 5.3 Through-The-Thickness Permeability

The Hexcel Hi-Tech Multiaxial Warp Knit fabric preforms were investigated to determine the through-the-thickness permeability as a function of porosity. The experimental techniques utilized for the permeability characterization study are presented in Section 4.5, and the data reduction techniques are presented in Section 4.5.1. Two or three test samples (50.8 mm by 50.8 mm) were obtained from each of the Hexcel fabric preforms and examined with the compaction/permeability test fixture (Section 4.2). The fabric preform test samples were characterized in a fully saturated state using tap water at room temperature (17 °C) with a viscosity of 0.001 Pa.s. The purpose of this section

is to present the through-the-thickness permeability characteristics of the Hexcel fabric preforms at porosities ranging from 0.30 to 0.55.

The test fixture, configured for the through-the-thickness permeability experiments (Section 4.5), was initially characterized to determine the through-the-thickness pressure drop through the empty test section as a function of the flow rate (results were fit to Eq. 4.5.2). The flow characterization data for the test fixture and the calibration data for the flow meter (Eq. 4.5.1) are given in Appendix B.2

The applied through-the-thickness pressure differentials measured during the fabric preform permeability experiments were initially corrected for the pressure drop due to the test fixture (Eq. 4.5.3). The measured flow rate is plotted as a function of the applied through-the-thickness pressure gradient in Fig. 5.3.1. The knitted and knitted/stitched test samples appeared to follow D'arcy's law and linear relationships were established between the flow rates and the pressure gradients for the entire porosity range. The figure indicates that the resistance to flow of the knitted and knitted/stitched preforms increases as the porosity decreases. Measurement of the slope of the flow rate verses pressure gradient curve along with Eq. 4.5.4 were used to determine the permeability.

A relationship between the through-the-thickness permeability and the fiber bed porosity was established by fitting either Eq. 2.4.5 or Eq. 2.4.8 to the data. The measured permeability constants for the Hexcel Hi-Tech fabric preforms are plotted as a function of porosity in Fig. 5.3.2.

The knitted test samples were tested in a fully unstitched and a lightly stitched configuration. Two knitted test samples were lightly stitched around the outer perimeter with a single yarn of fiberglass, to hold the individual plies together. The modified Gebart relationship (Eq. 2.4.8) provided the best model to relate the permeability constants to the preform porosities. The lightly stitched fabric preforms were found to have a minimum porosity, $\phi_{min}$, of 0.236 and the constant S was 2.37. The fully unstitched samples were found to have a minimum porosity, $\phi_{min}$, of 0.293 and the constant S was 1.966. Upon examination of the results it was concluded that both preforms contained a continuous yet irregularly packed arrangement of fibers within the fiber bed at porosities ranging from

**Hexcel Hi-Tech Multiaxial Warp Knit Material Evaluation**
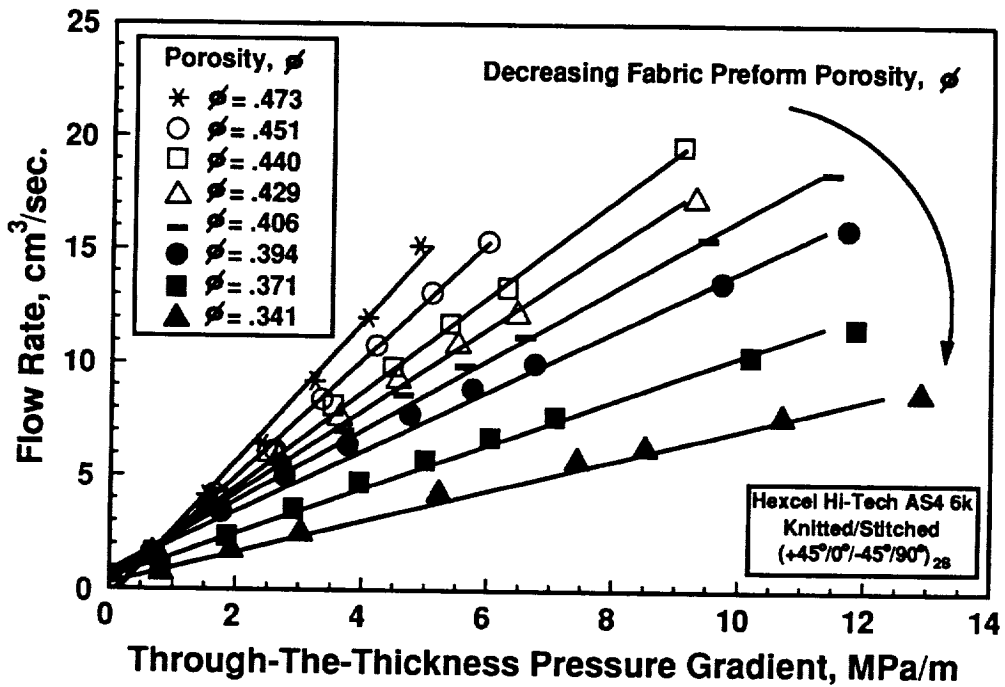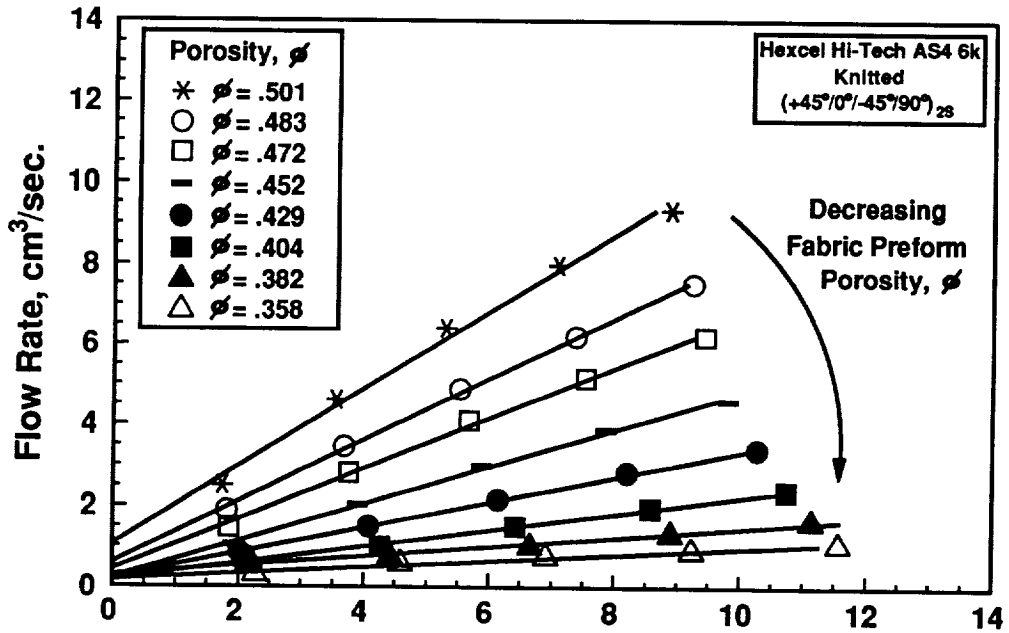
Figure 5.3.1   Flow rate as a function of the through-the-thickness pressure
gradient for the Hexcel Hi-Tech multiaxial warp knit
fabric preforms.

Hexcel Hi-Tech Multiaxial Warp Knit Material Evaluation
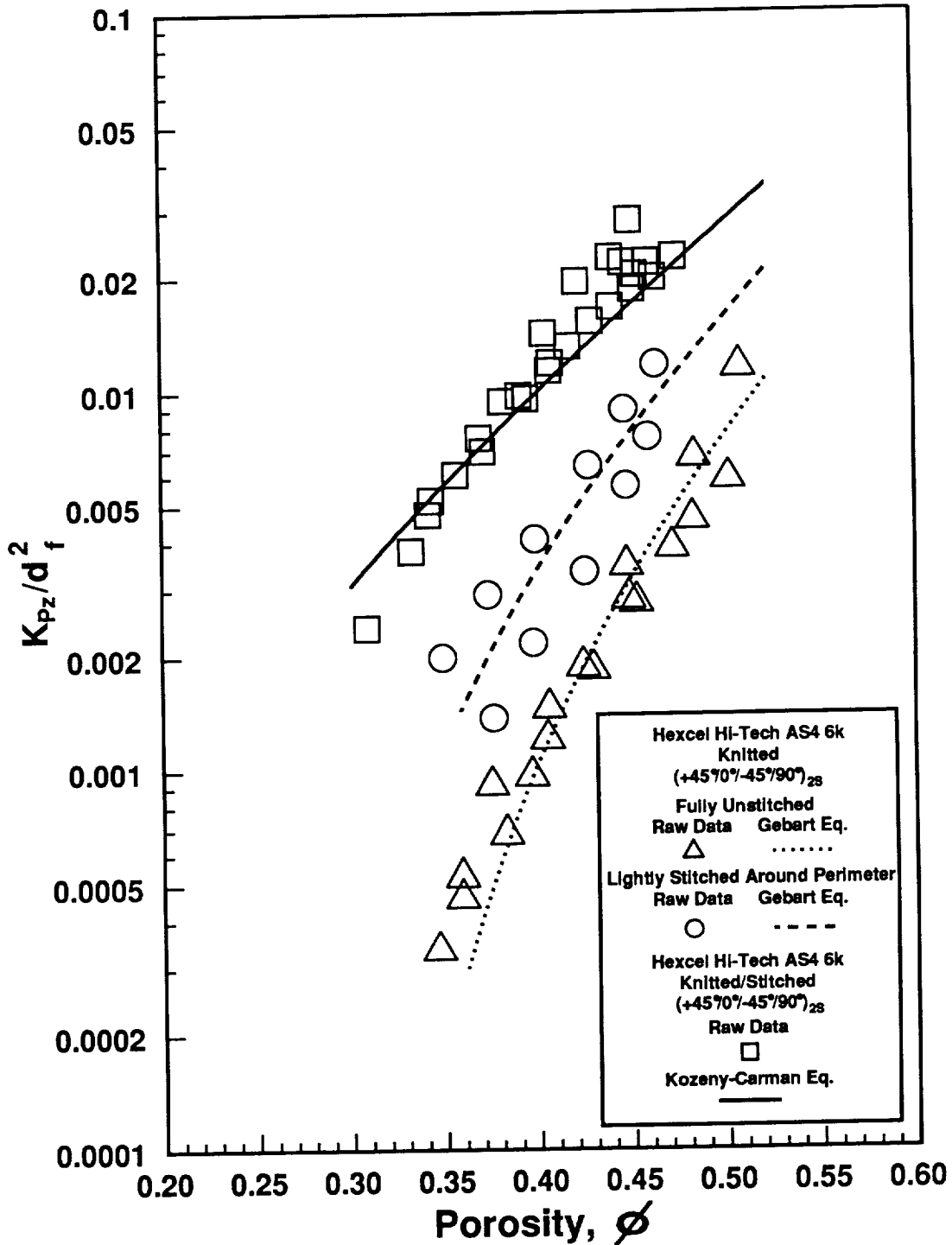
Figure 5.3.2.  $K_{pz}/d_f^2$ as a function of porosity for the
Hexcel Hi-Tech multiaxial warp knit
fabric preforms.

Hexcel Hi-Tech Multiaxial Warp Knit Material Evaluation

0.30 to 0.55. Subsequent microscopic investigations of panels fabricated with the lightly stitched preforms has confirmed this conclusion (Section 5.7). The lightly stitched and unstitched knitted preforms obeyed the Gebart relationship since the through-the-thickness flow was forced though a continuous fiber bed where gaps between individual fibers control both the flow rate and the pressure gradient within the fabric preform, (Section 4.5.1).

The knitted/stitched test samples obeyed the Kozeny-Carman relationship (Eq. 2.4.5) for the entire porosity range. The Kozeny-Carman constant was measured to be 17.94. The knitted/stitched test samples have significantly higher through-the-thickness permeabilities (lower flow resistance) than the fully unstitched knitted test samples, at similar porosities, (see Fig, 5.3.2). The through-the-thickness carbon stitches dramatically decreased the through-the-thickness flow resistance by providing low flow resistance pathways for the flow to transfer through the test sample. The Kozeny-Carman relationship, derived for flow along constricting stream tubes, was the best model for the knitted/stitched preforms.

## 5.4 Final Thickness/Fiber Volume Fraction/Resin Mass

An experimental study was conducted with the Hexcel Hi-Tech fabric preform test samples to determine the effects of compaction pressure on the final thickness, fiber volume fraction, and resin mass required for full saturation. The uncompacted thickness and areal weight (Section 5.1) along with the compaction models for the Hexcel fabric preform test samples (Section 5.2) were incorporated into the RTM simulation model to predict the final thickness (Eq. 2.1.2), fiber volume fraction (Eq. 2.1.6), and resin mass for full saturation (Eq. 2.1.8) as a function of the applied compaction pressure.

Textile composite panels were fabricated at different compaction pressures and temperature cure cycles using the RTM film infusion technique described in Appendix A.1. The final thickness, fiber volume fraction, and resin mass at full saturation were measured and calculated using the techniques described in Section 4.8 and compared to

the predictions obtained from the RTM simulation model.

The final thickness, fiber volume fraction, and resin mass of the Hexcel Hi-Tech/Hercules 3501-6 composite panels are plotted as a function of compaction pressure in Figs. 5.4.1 and 5.4.2. RTM simulation model results and the measurements obtained from fabricated panels are presented on each figure. The processing conditions for the fabricated panels are presented along with the model and experimental results in Appendix C. Due to a low supply of the knitted fabric preforms, only two panels were fabricated using the manufacturer's cure cycle (Table 4.6.1) at 347.4 kPa.

The slow dry compaction model results for the knitted and knitted/stitched fabric preforms showed the best correlation with the respective panel properties when the preforms were fabricated with a single step compaction pressure application (see Figs. 5.4.1 and 5.4.2). For the knitted panels, the measured final thickness, fiber volume fraction, and resin mass were within 0.6%, 3%, and 4% of predicted values (slow dry compaction model), respectively. The measured final thickness and fiber volume of the knitted/stitched panels were within 3.3% of predicted values and the measured resin mass was within 11% of predicted values (slow dry compaction model). The difference between the measured results and the model predictions may have resulted from an incorrect measurement of the applied processing load or an incorrect measurement of the preform stiffness (Section 5.2). Comparing both sets of results, it may be concluded that if a single-step compaction pressure is used during processing, the slow dry fabric preform compaction data can be used to successfully predict the final thickness, fiber volume fraction, and resin mass at full saturation.

The final thickness, fiber volume fraction and resin mass at full saturation, as a function of applied compaction pressure, for the slow dry compaction models of both Hexcel fabric preform test samples are presented on Fig. 5.4.3. The knitted test sample had the greatest thickness and resin mass, and the lowest fiber volume fraction at compaction pressures less than 125 kPa. At pressures greater than 125 kPa the knitted and knitted/stitched test samples have nearly identical physical properties. The thickness of the knitted test sample under a compaction pressure of 100 kPa was equal to the
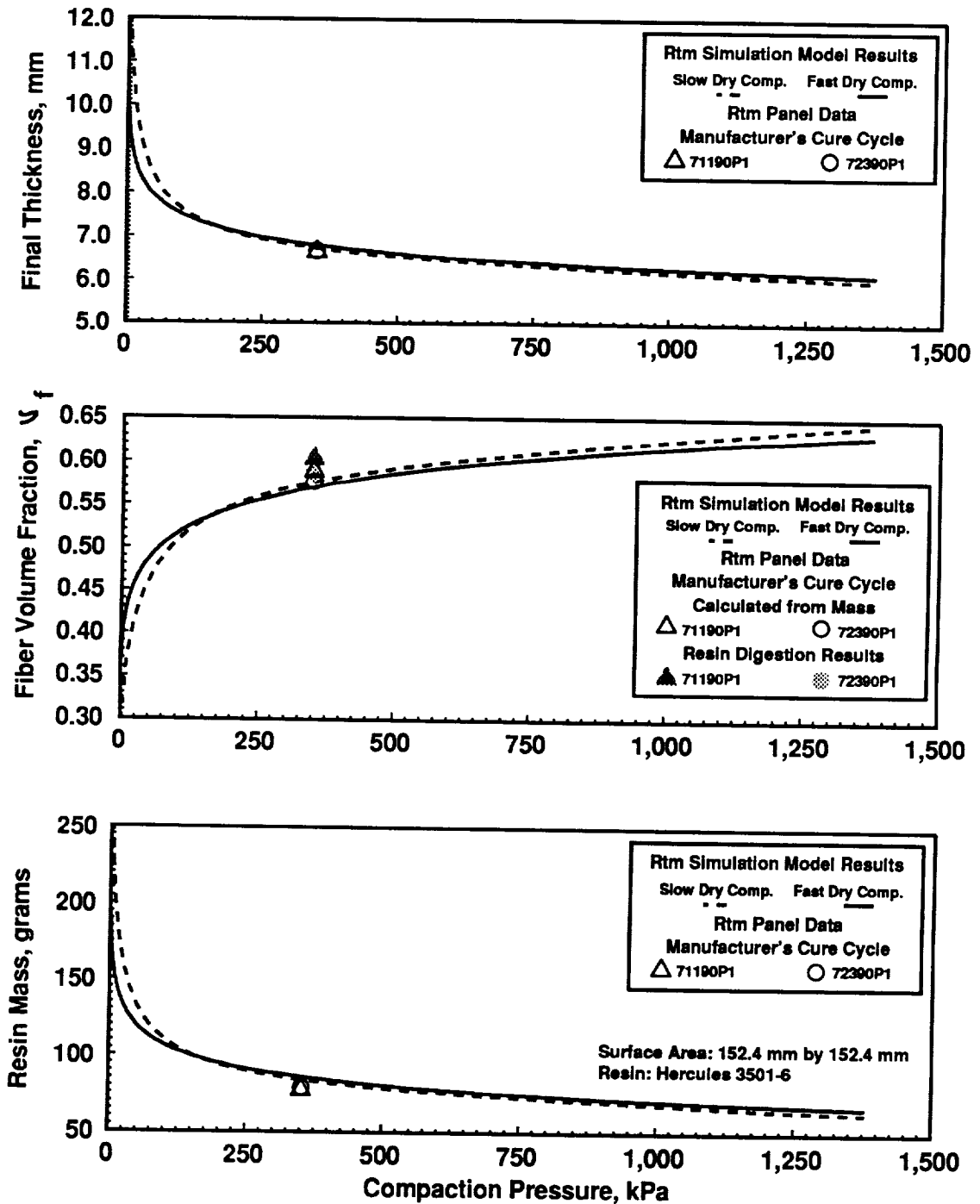
Figure 5.4.1 Final thickness, fiber volume fraction, and resin mass as a function of applied compaction pressure for the Hexcel Hi-Tech AS4 6k knitted $(+45°/0°/-45°/90°)_{2S}$/Hercules 3501-6 composite panels.

Hexcel Hi-Tech Multiaxial Warp Knit Material Evaluation

C-2
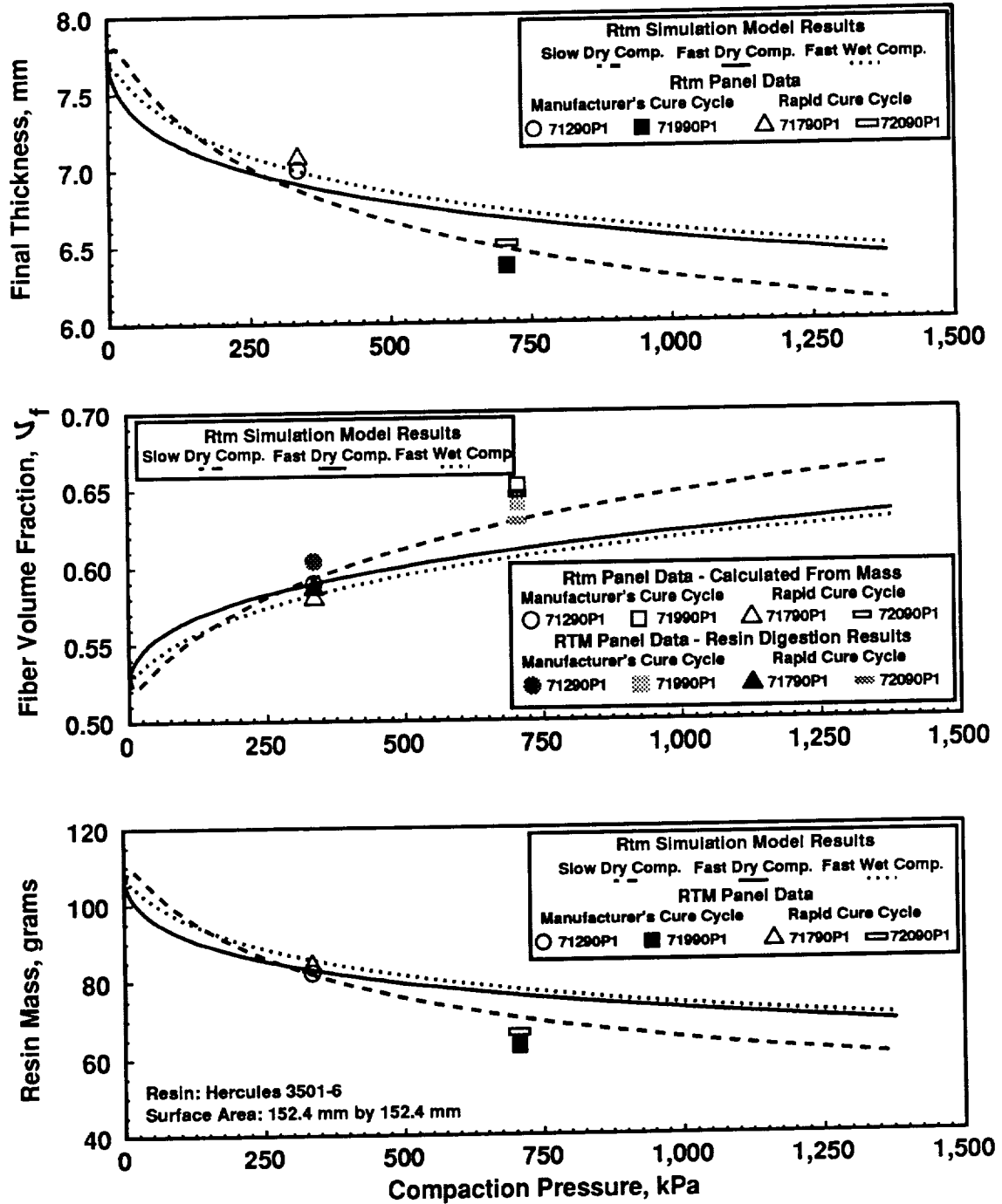
*Figure 5.4.2  Final thickness, fiber volume fraction, and resin mass as a function of applied compaction pressure for the Hexcel Hi-Tech AS4 6k knitted/stitched ($+45°/0°/-45°/90°)_{2s}$ /Hercules 3501-6 composite panels.*

**Hexcel Hi-Tech Multiaxial Warp Knit Material Evaluation**
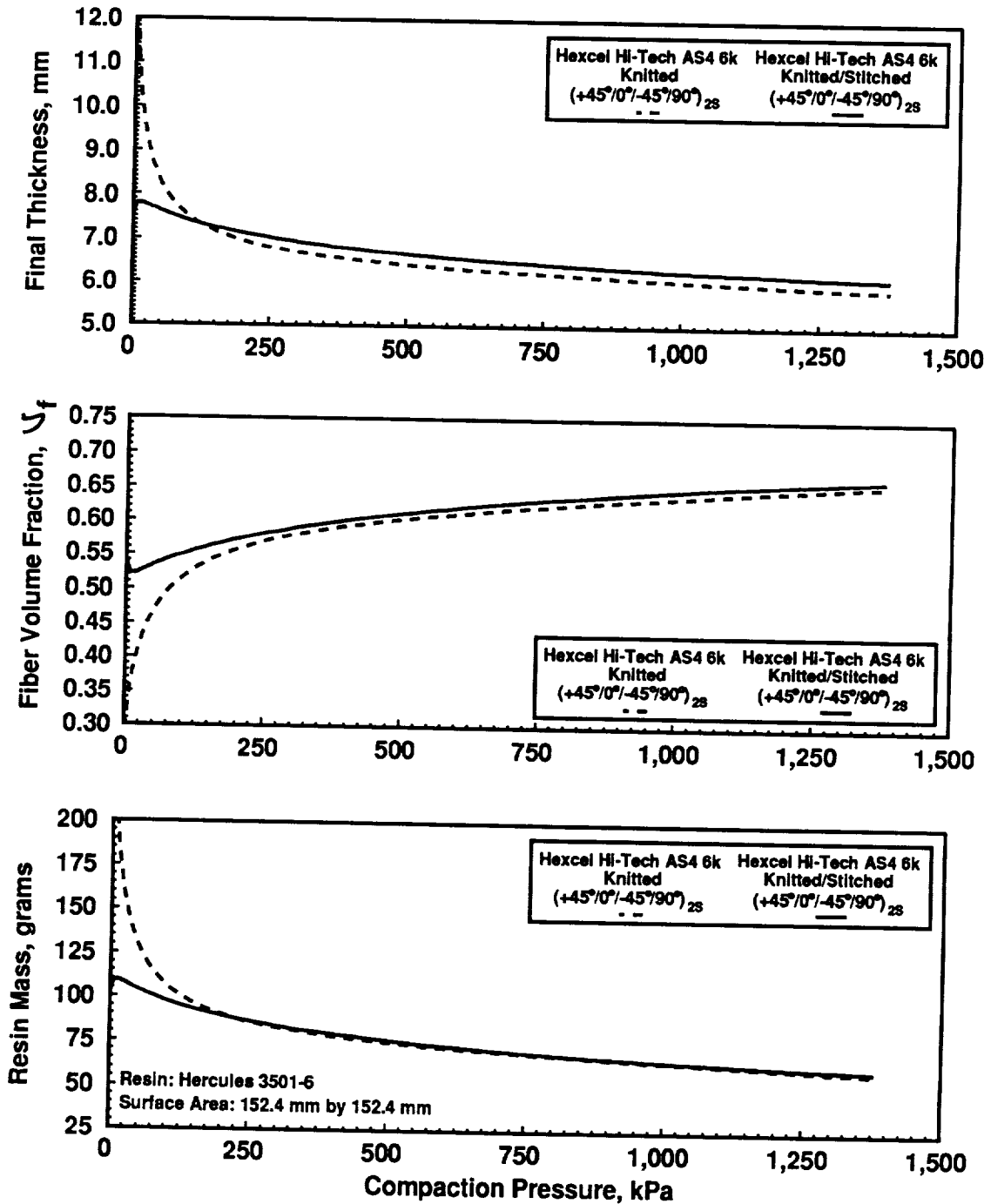
Figure 5.4.3 Comparisons of the final thickness, fiber volume fraction, and
resin mass as a function of applied compaction pressure
obtained from the Hexcel Hi-Tech multiaxial warp knit
slow dry compaction models.

Hexcel Hi-Tech Multiaxial Warp Knit Material Evaluation

uncompacted thickness of knitted/stitched test sample.

## 5.5 Temperature Simulation

The RTM simulation model was used to predict the through-the-thickness temperature distribution in the RTM layup (Section 2.2) and the resin degree of cure and viscosity as a function of time during the fabrication of a textile composite using the RTM film infusion technique. Composite panels composed of Hexcel Hi-Tech fabric preforms and Hercules 3501-6 resin were fabricated with either the manufacturer's cure cycle or a model generated rapid cure cycle (Table 4.6.1). The temperature cure cycles were used in the RTM simulation model as the temperature boundary conditions applied to the exterior faces of the RTM layup (Figs. 2.2.1-2.2.3). The RTM simulation model predictions of the resin degree of cure and viscosity are based upon the Hercules 3501-6 kinetics/viscosity model developed by Chiou and Letton [8]. During fabrication, the temperatures at the top and bottom of the composite panel were measured with either J-type or K-type thermocouples (Fig. A.1.2) and recorded as a function of time. The resin degree of cure and viscosity were measured with a frequency dependent electromagnetic sensor, (FDEMS), located at the bottom of the composite panel. The purpose of this section is to compare the RTM simulation model predictions of the temperature distribution and the resin degree of cure and viscosity with the experimental results.

The temperature distribution in the RTM layup is plotted as a function of time in Figure 5.5.1. The RTM simulation model predictions and experimental measurements are presented for Hexcel Hi-Tech knitted/stitched/Hercules 3501-6 panels fabricated with the manufacturer's cure cycle (top of Fig. 5.5.1) and the rapid cure cycle (bottom of Fig. 5.5.1). The model predictions of the temperature at the top and bottom of the composite panels were within 5 °C of the experimentally measured temperatures. The slight disagreement between the model predictions and the experimental measurements may have resulted from experimental errors incurred during the measurement of the platen temperatures which were used in the RTM simulation model as boundary conditions.

**Hexcel Hi-Tech Multiaxial Warp Knit Material Evaluation**
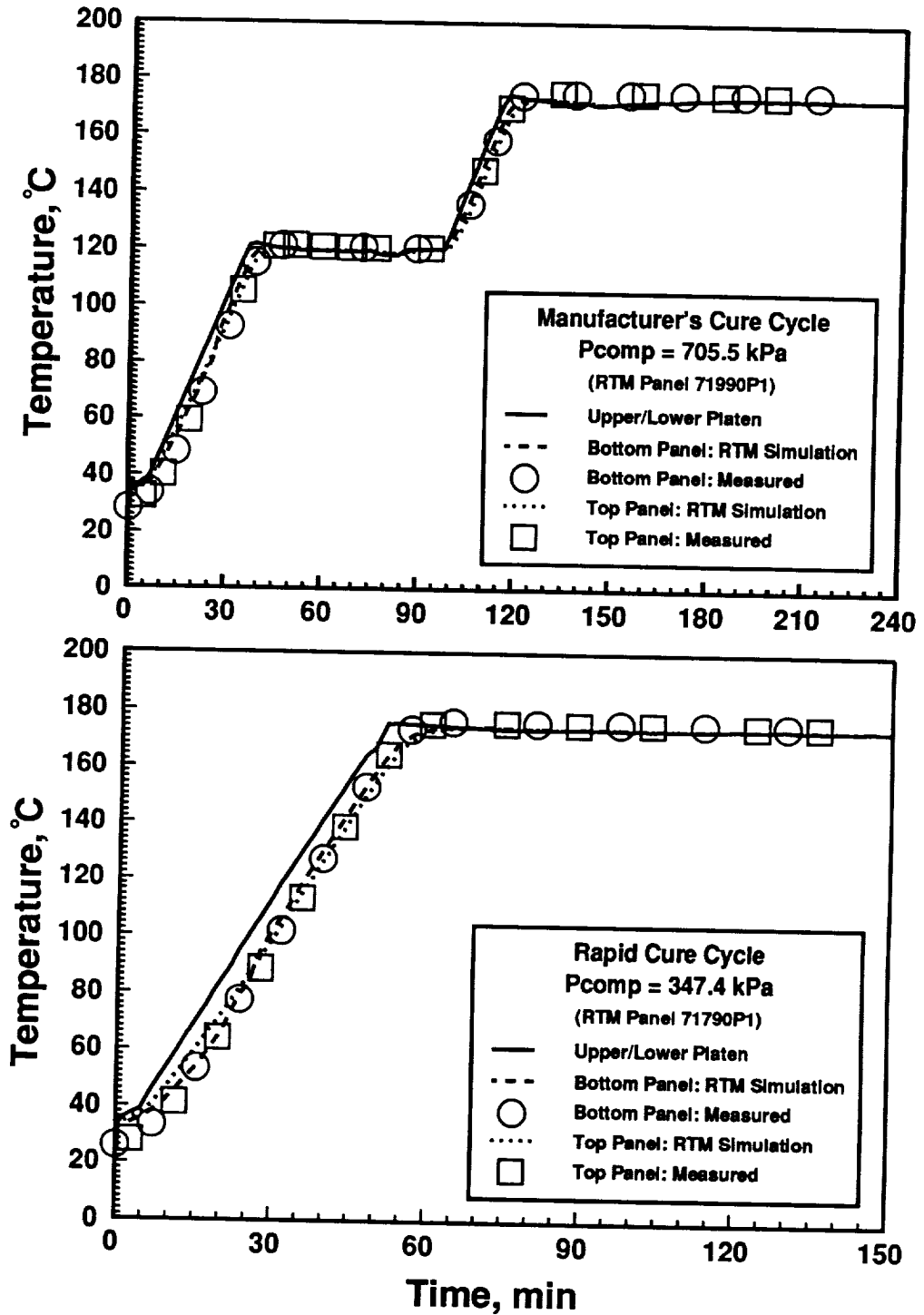
Figure 5.5.1   Temperature as a function of time at selected locations in Hexcel Hi-Tech AS4 6k knitted/stitched $(+45°/0°/-45°/90°)_{2s}$/ Hercules 3501-6 composite panels fabricated with the cure cycles shown.

Hexcel Hi-Tech Multiaxial Warp Knit Material Evaluation

The resin viscosity and degree of cure as a function of time for a Hexcel knitted/stitched panel fabricated with the manufacturer's cure cycle is presented on the top and bottom of Fig. 5.5.2, respectively. Similar plots are presented on Fig. 5.5.3 for a panel fabricated with the rapid cure cycle. The temperature at the bottom of the composite panel (FDEMS location) predicted by the RTM simulation model is presented as a function of time on each figure. Results from the manufacturer's cure cycle indicated that resin gelation (viscosity > 1000 Pa.s) occurred at 132 minutes into the cure cycle at a degree of cure of 0.50. Resin gelation was found to occur at 77 minutes into the rapid cure cycle at a degree of cure of 0.50. Both cure cycles had sufficiently long (118.5 minutes for manufacturer's cure cycle and 55.5 minutes for rapid cure cycle) flow windows (viscosity <1000 Pa.s) to allow for full infiltration of the fabric preforms prior to resin gelation.

The prediction of the resin degree of cure and viscosity by the RTM simulation model differed slightly from the FDEMS measurements. The prediction of resin gelation by the model for the manufacturer's and rapid cure cycle panels tended to precede the FDEMS measurements by 10 minutes (see Figs. 5.5.2 and 5.5.3). Also, the FDEMS tended to predict lower resin viscosities and higher states of cure as a function of time during the rapid cure cycle than were predicted by the RTM model. Differences between the model predictions and the in-situ measurements of the resin degree of cure and viscosity may have resulted from experimental error in the FDEMS calibrations or errors resulting from the simulation model prediction of the resin degree of cure and viscosity in the RTM layup.

## 5.5 Infiltration Simulation

The RTM simulation model was used to predict the infiltration front position as a function of time and the total infiltration time during the fabrication of Hexcel Hi-Tech/Hercules 3501-6 composite panels using the RTM film infusion technique. The temperature cure cycles (see Table 4.6.1) and processing pressures used for fabrication
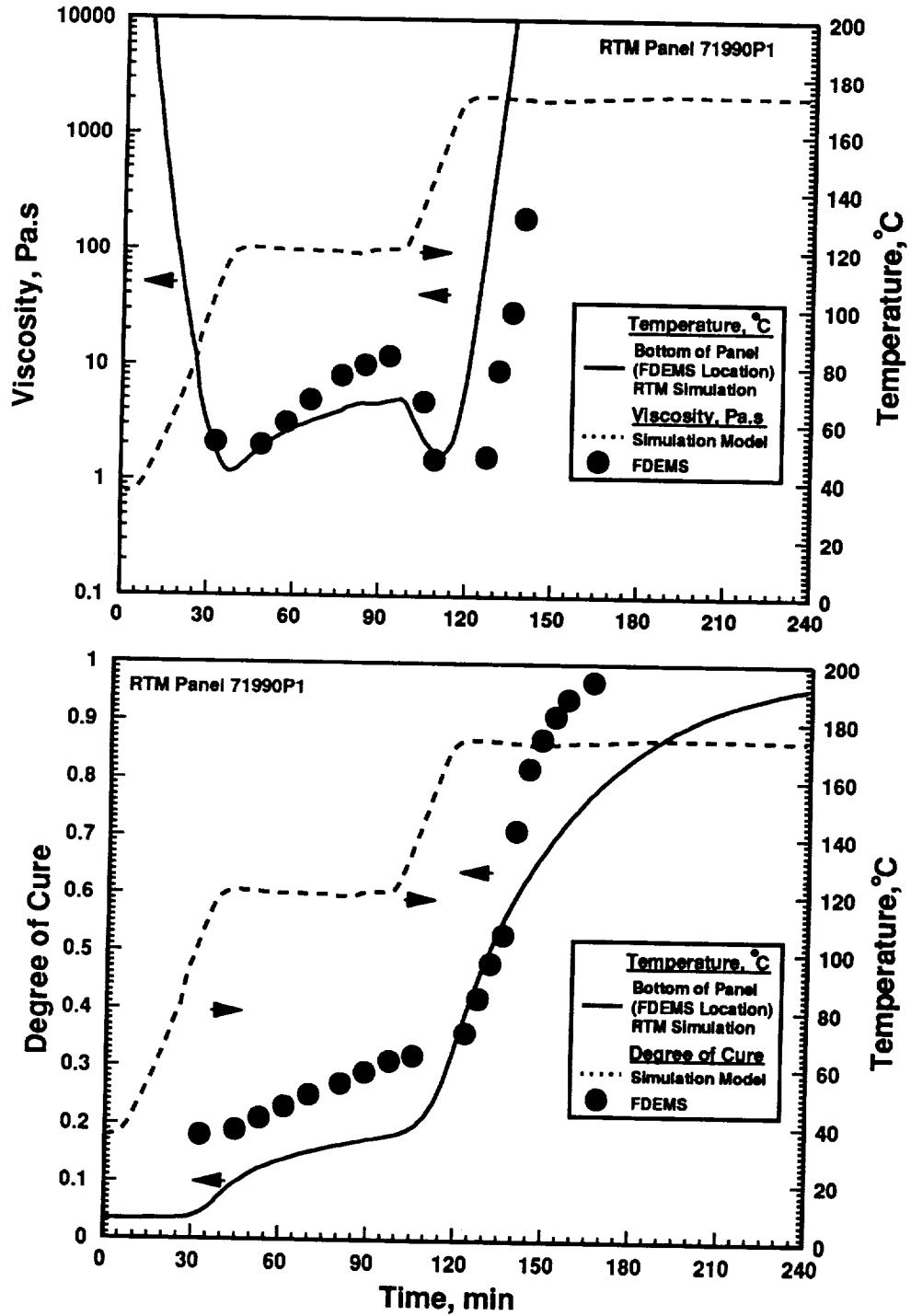
Figure 5.5.2   Resin viscosity and degree of cure as a function of time
at the bottom of a Hexcel Hi-Tech AS4 6k knitted/stitched
$(+45^\circ/0^\circ/-45^\circ/90^\circ)_{2s}$/Hercules 3501-6 composite panel
fabricated at 705.5 kPa with the manufacturer's cure cycle.

Hexcel Hi-Tech Multiaxial Warp Knit Material Evaluation
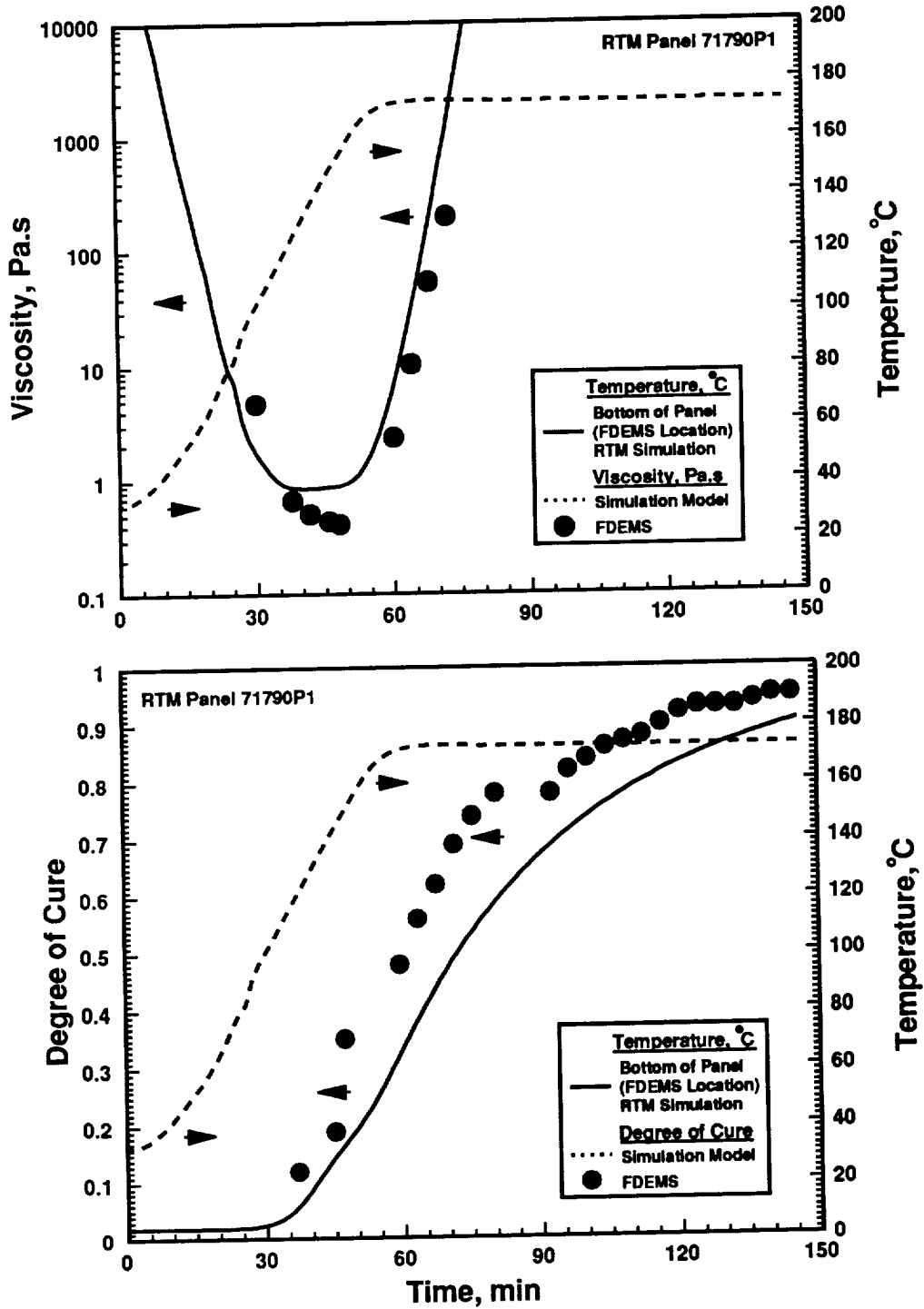
Figure 5.5.3   Resin viscosity and degree of cure as a function of time
at the bottom of a Hexcel Hi-Tech AS4 6k knitted/stitched
$(+45°/0°/-45°/90°)_{2s}$ /Hercules 3501-6 composite panel
fabricated at 347.4 kPa with the rapid cure cycle.

Hexcel Hi-Tech Multiaxial Warp Knit Material Evaluation

were incorporated into the RTM simulation model as boundary conditions, (see Section 2.2.4 and 2.4.3). The RTM simulation model predictions of the resin viscosity are based upon the Hercules 3501-6 viscosity model obtained from Chiou and Letton [8]. Experimental measurements of the infiltration front position as a function of time and the total infiltration time were obtained during fabrication using the techniques presented in Section 4.8 and 4.9. The purpose of this section is to compare the RTM simulation model predictions of the normalized infiltration position and total infiltration time with the experimental measurements. The effect of the temperature cure cycle and processing pressure on the infiltration of Hexcel fabric preforms with Hercules 3501-6 resin will also be investigated.

The normalized flow front position and resin viscosity (predicted by the RTM simulation model) for Hexcel Hi-Tech knitted panels fabricated with the manufacturer's cure cycle (Table 4.6.1) at 347.4 kPa are plotted as a function of time in Fig. 5.6.1. The RTM model simulation results were generated using the through-the-thickness permeability characterization results obtained from the lightly stitched knitted preforms (see Section 5.3). The fabrication test samples were stitched around the perimeter in an identical mannner as the knitted/lightly stitched permeability test samples. Most of the infiltration occurred when the resin viscosity was less than 30 Pa.s. The RTM model predictions of the flow front position tended to lag the measured position by 2 minutes. The difference may be attributed to errors in the measurement of the flow front position and/or the use of an incorrect permeability constant by the RTM simulation model.

The total infiltration times obtained from the in-situ measurements and the RTM simulation model for the lightly stitched knitted panels are presented in Fig. 5.6.2. The model predictions of the overall infiltration time were within 6% of experimental results.

The normalized flow front position and resin viscosity of Hexcel Hi-Tech knitted/stitched panels fabricated at 347.4 and 705.5 kPa with the manufacturer's cure cycle are presented on the top and bottom of Fig. 5.6.3, respectively. The normalized infiltration front position and resin viscosity of knitted/stitched panels fabricated at 347.4 kPa and 705.5 kPa with the rapid cure cycle (Table 4.6.1) are plotted as a function of
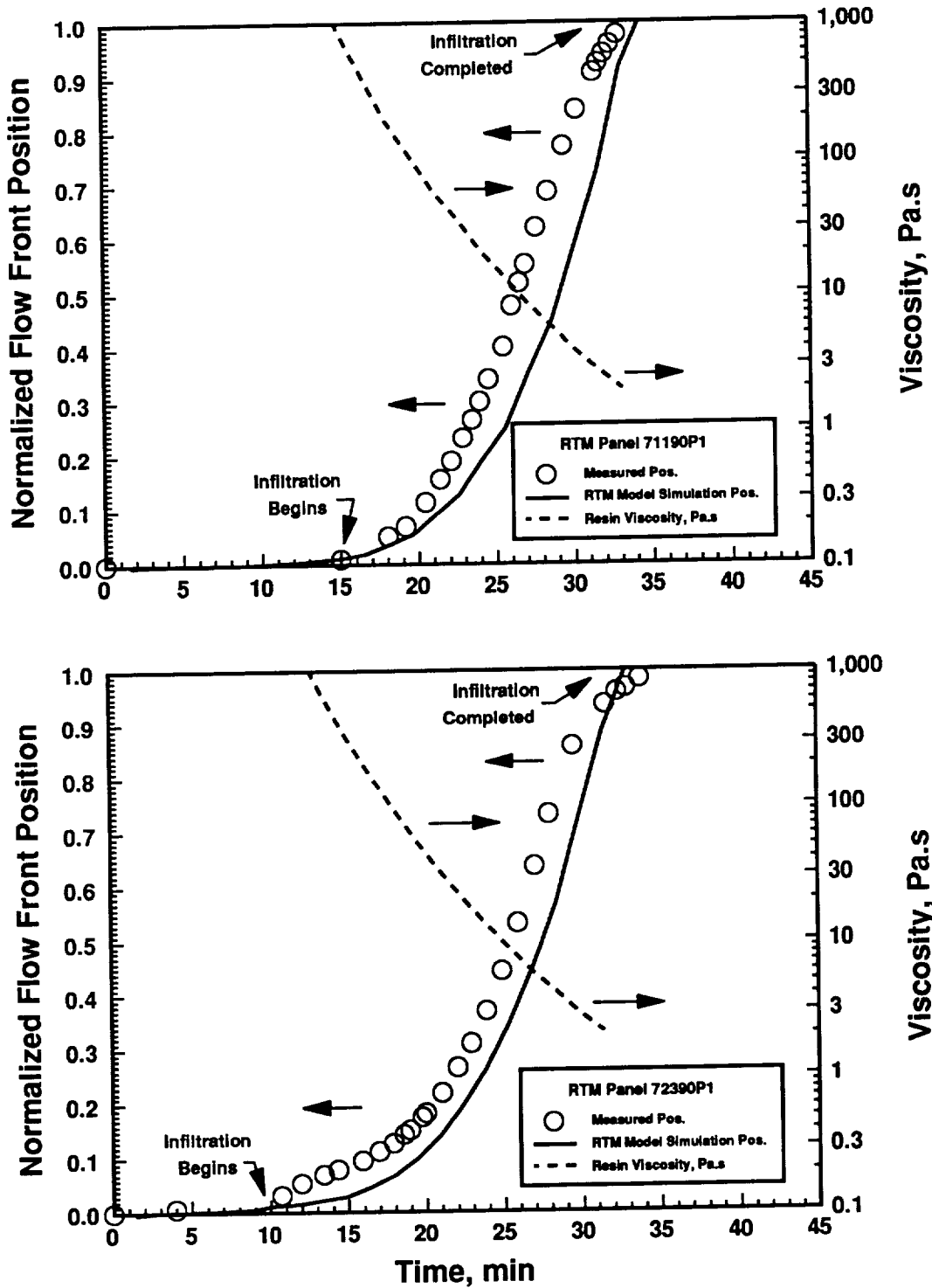
Figure 5.6.1   Normalized flow front position and resin viscosity as a function of time for Hexcel Hi-Tech AS4 6k knitted (+45°/0°/-45°/90°)$_{2s}$ / Hercules 3501-6 composite panels fabricated at 347.4 kPa with the manufacturer's cure cycle.

Hexcel Hi-Tech Multiaxial Warp Knit Material Evaluation
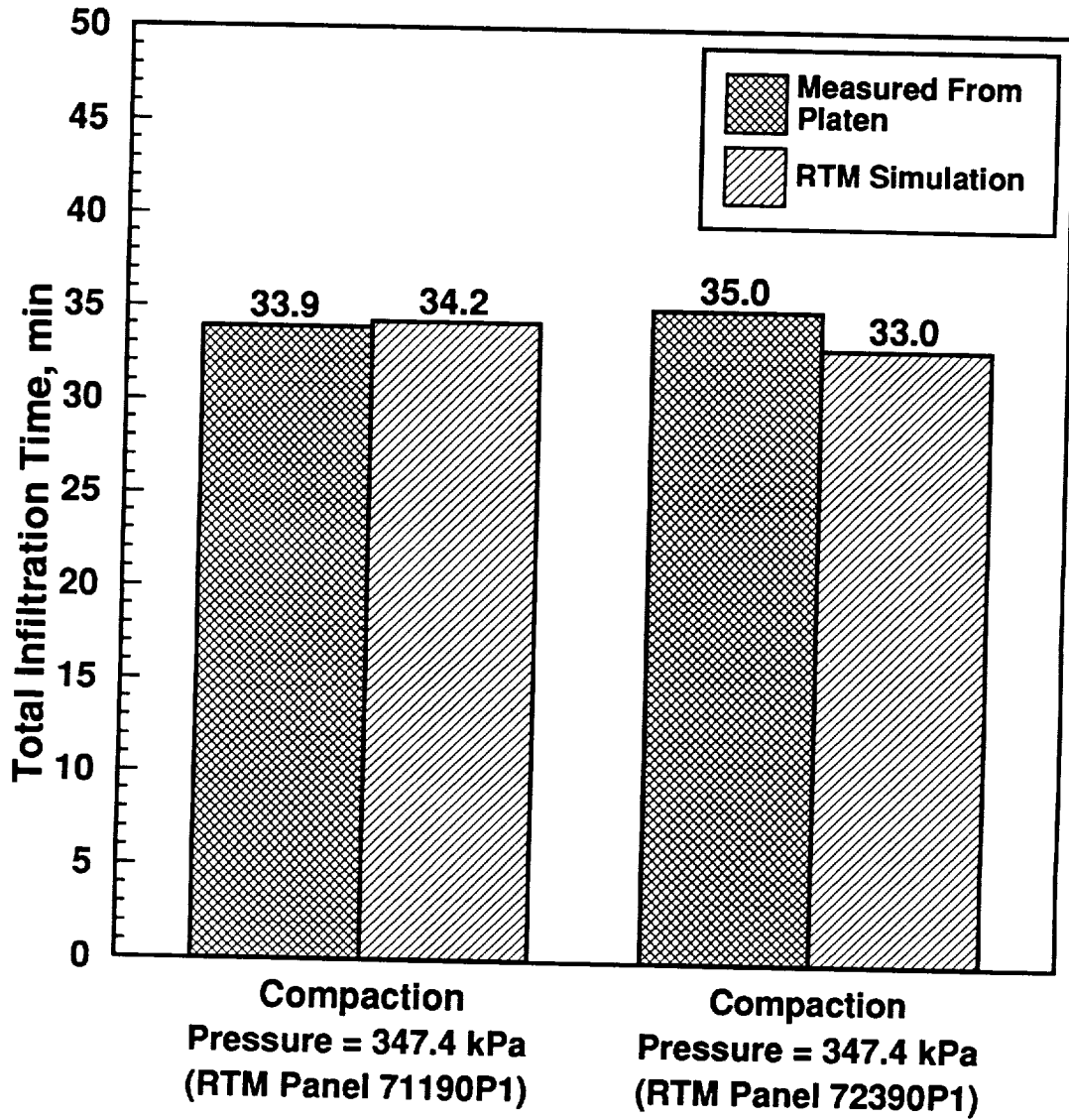
*Figure 5.6.2  Total infiltration times for Hexcel Hi-Tech AS4 6k knitted (+45°/0°/-45°/90°)$_{2s}$/Hercules 3501-6 composite panels fabricated with the manufacturer's cure cycle.*
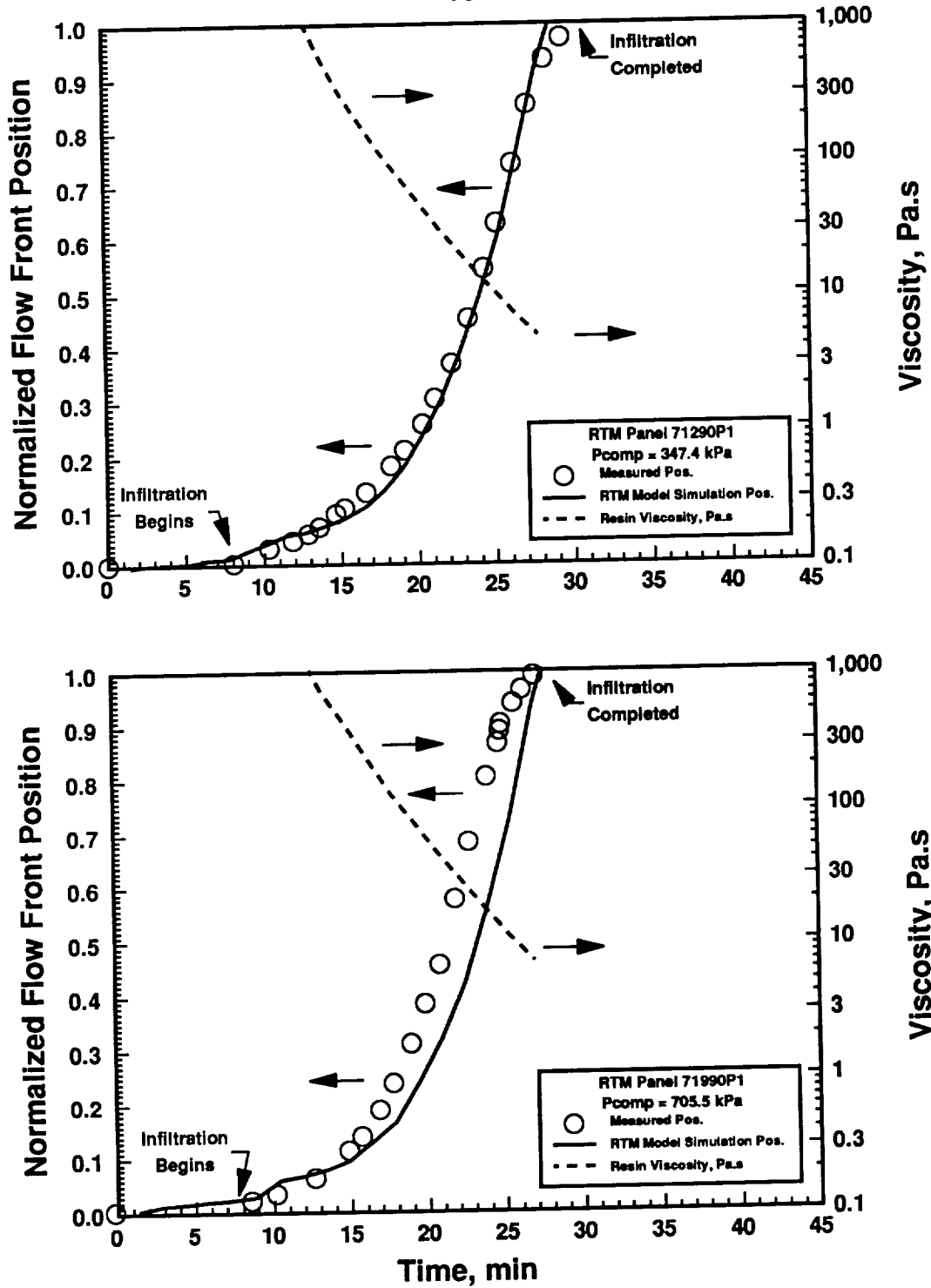
Figure 5.6.3 Normalized flow front position and resin viscosity as a function of time for Hexcel Hi-Tech AS4 6k knitted/stitched (+45°/0°/-45°/90°)$_{2s}$ / Hercules 3501-6 composite panels fabricated at different compaction pressures with the manufacturer's cure cycle.

94

time on the top and bottom of Fig. 5.6.4, respectively. As with the knitted panels, most of the infiltration occurred when the resin viscosity was less than 30 Pa.s. The model predictions of the flow front position agree with the experimental results for panels fabricated at 347.4 kPa with the manufacturer's cure cycle and at 705.5 kPa with the rapid cure cycles. It appears that the measured permeability constant is accurate due to the good correlations between the experimental and model results. The model predictions for the remaining panels tended to lag the experimental results by 2 minutes. The difference between the model predictions and the experimental results may have resulted from errors in the measurement of the flow front position.

The total infiltration times for the knitted/stitched composite panels fabricated with the manufacturer's cure cycle and the rapid cure cycle are presented as a function of applied compaction pressure on the top and bottom of Fig. 5.6.5, respectively. Infiltration times obtained from FDEMS attached to the top of the fabric preform are presented for selected panels. The RTM simulation model predictions of the total infiltration times for the knitted/stitched panels were within 12% of the experimentally measured results obtained from the platen displacement, (see Section 4.9). The RTM simulation model predictions were within 4% of FDEMS measured infiltration times.

The greater flow resistance (lower permeability) of the lightly stitched knitted fabric preforms (Fig. 5.3.2) resulted in greater infiltration times compared to the knitted/stitched preforms. At identical compaction pressures, both the manufacturer's and rapid cure cycle fabricated knitted/stitched composites had similar infiltration front verses time profiles. When the applied compaction pressure was increased from 347.4 kPa to 705.5 kPa, the total infiltration time was decreased by at least 10%. The decrease in total infiltration time may be attributed to a reduction in thickness of the preform at higher compaction pressures.
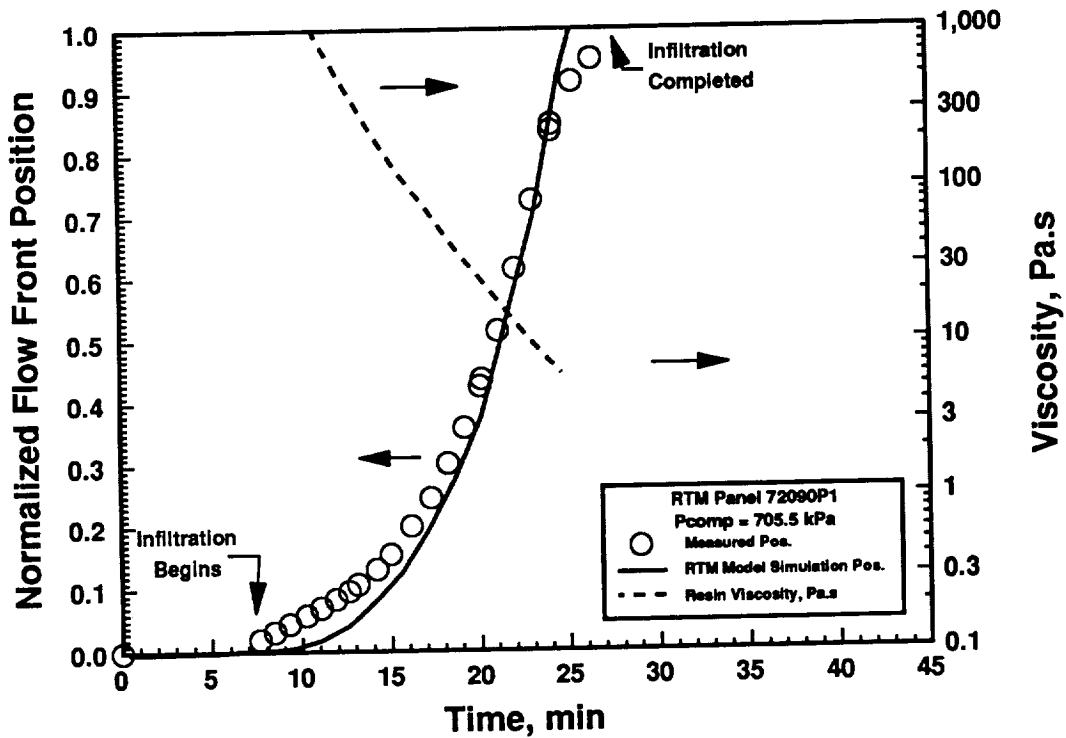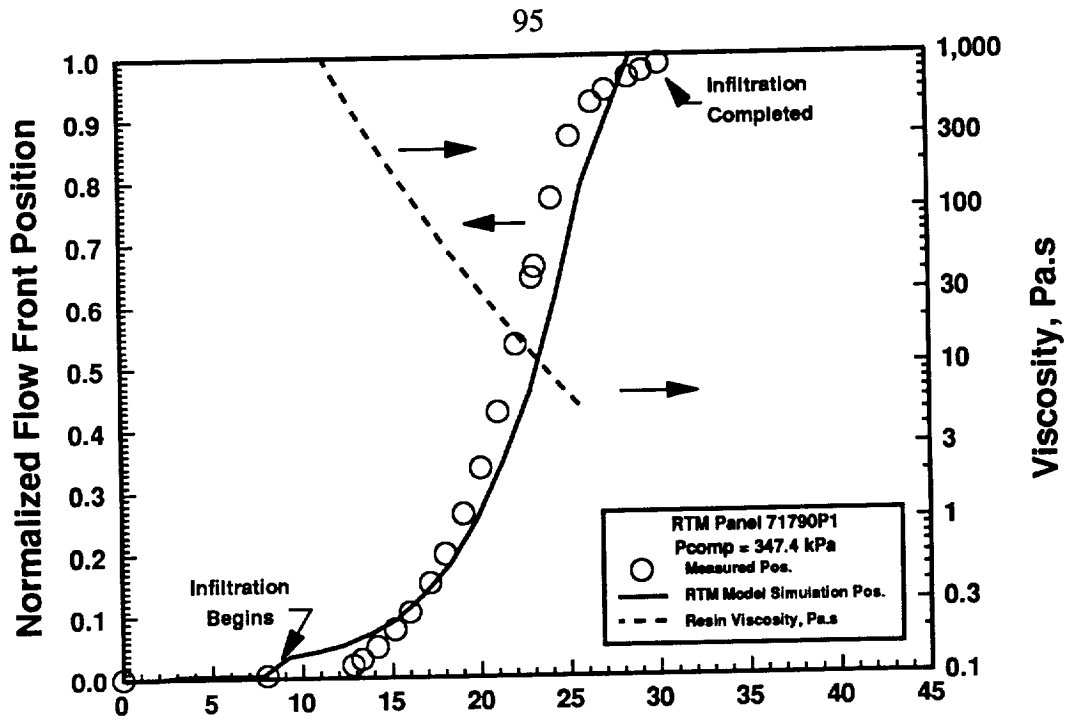
Figure 5.6.4 Normalized flow front position and resin viscosity as a function of time for Hexcel Hi-Tech AS4 6k knitted/stitched (+45°/0°/-45°/90°)$_{2s}$ / Hercules 3501-6 composite panels fabricated at different compaction pressures with the rapid cure cycle.
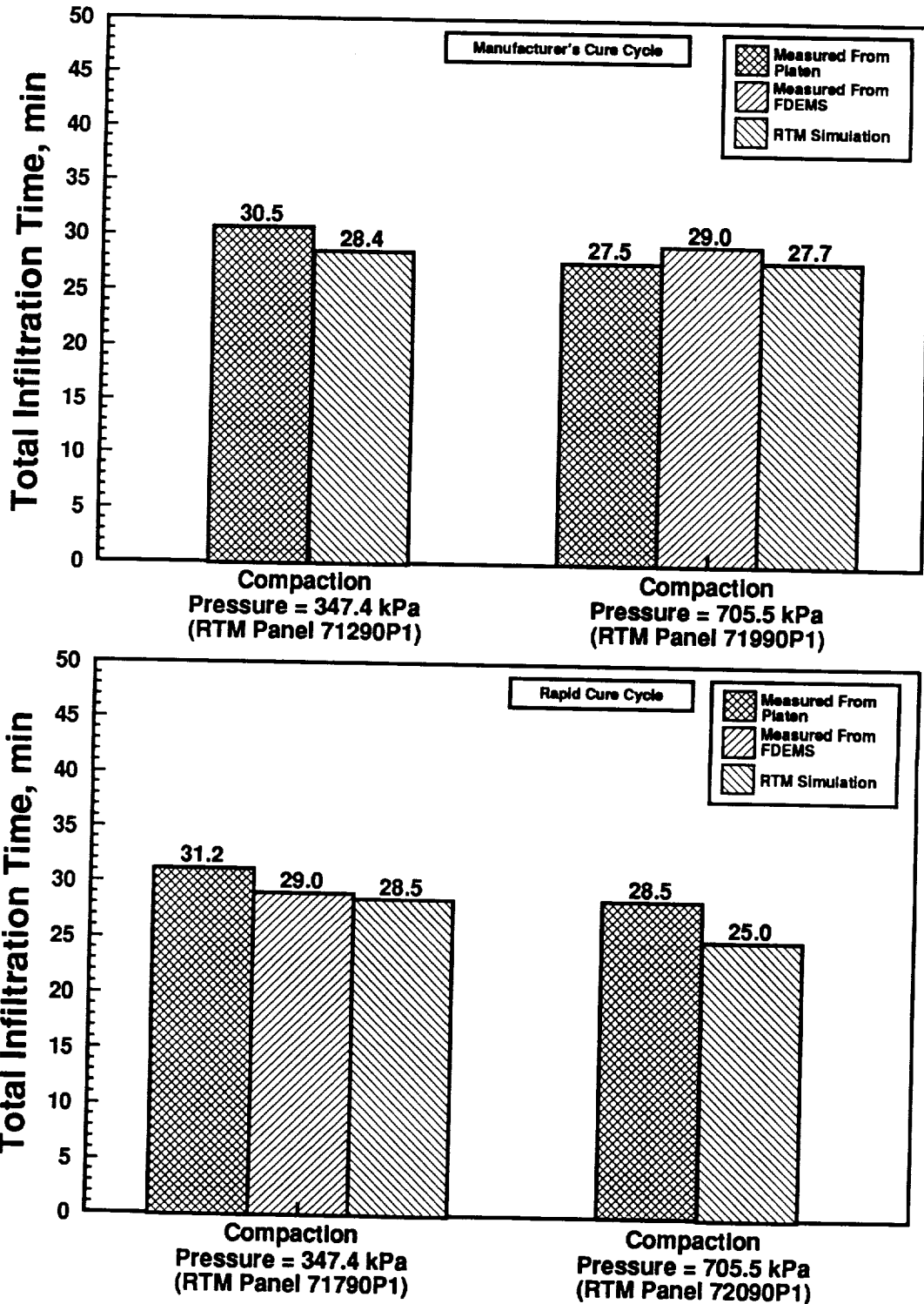
Figure 5.6.5.  Total infiltration times for Hexcel Hi-Tech AS4 6k knitted/ stitched $(+45^{\circ}/0^{\circ}/-45^{\circ}/90^{\circ})_{2s}$/Hercules 3501-6 composite panels.

Hexcel Hi-Tech Multiaxial Warp Knit Material Evaluation

# 5.7 Non-Destructive Evaluation

Non-destructive evaluation was used to evaluate the effect of different processing cycles on the quality of Hexcel Hi-Tech/Hercules 3501-6 panels. C-scans (10 MHz) were obtained from each panel to evaluate the overall quality. Cross-sectional photomicrographs (40X) of specimens (taken from each panel) were used to detect the presence of macroporosity, microcracks, and nonuniform resin distribution. Local photomicrographs (400X) were taken to observe the fiber packing arrangements of individual tows and to detect the presence of microporosity. Results are presented in this section for selected panels.

Cross-sectional photomicrographs (40X) of the Hexcel Hi-Tech knitted panels processed at 347.4 kPa with the manufacturer's cure cycle are presented in Fig. 5.7.1. Individual ply orientations are presented next to each photomicrograph. Both photomicrographs show microcracking and layer waviness. However, no macroporosity was detectable. Resin rich areas were evident at the intersections of individual fiber tows separated by the knitting.

An ultrasonic C-scan (with signal response scale), a mechanical test specimen cutting diagram, and a local photomicrograph (400X) are shown in Fig. 5.7.2 for a knitted panel processed at 347.4 kPa with the manufacturer's cure cycle. A high signal response (white area) corresponds to a void free region. The ply orientation and scale are presented next to the corresponding figures. The C-scans revealed a high level of porosity at the FDEMS location at the lower left edge of the panel. The packing arrangement of individual fibers tended to be random and no microporosity was detected, (see bottom of Fig. 5.7.2).

Cross-sectional photomicrographs (40X) of Hexcel Hi-Tech knitted/stitched panels processed at 347.4 kPa with the manufacturer's cure cycle and at 705.5 kPa with the rapid cure cycle are presented on the top and bottom of Fig. 5.7.3, respectively. Extensive microcracks are visible in the individual plies and resin rich areas surrounding the stitching. A small amount of macroporosity is visible in photomicrograph of the panel processed at 347.4 kPa (top of Fig. 5.7.3). The individual plies of the knitted/stitched

**Ply Orientation**

0 °

-45°

90 °

90 °

-45°

0 °
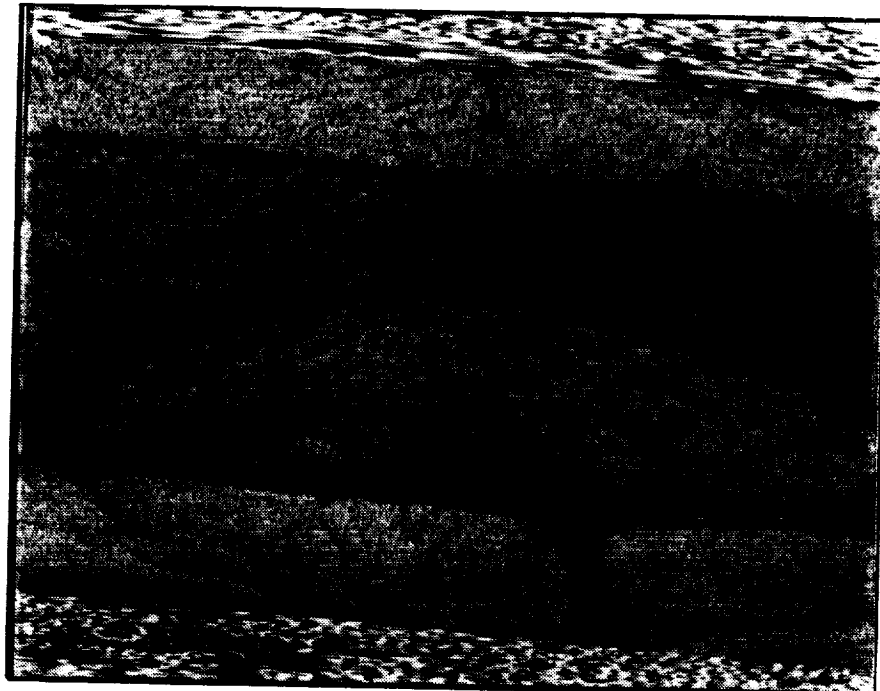
(RTM Panel 71190P1)                                    (40X)

**Ply Orientation**

90 °

+45°

0 °

-45°

90 °
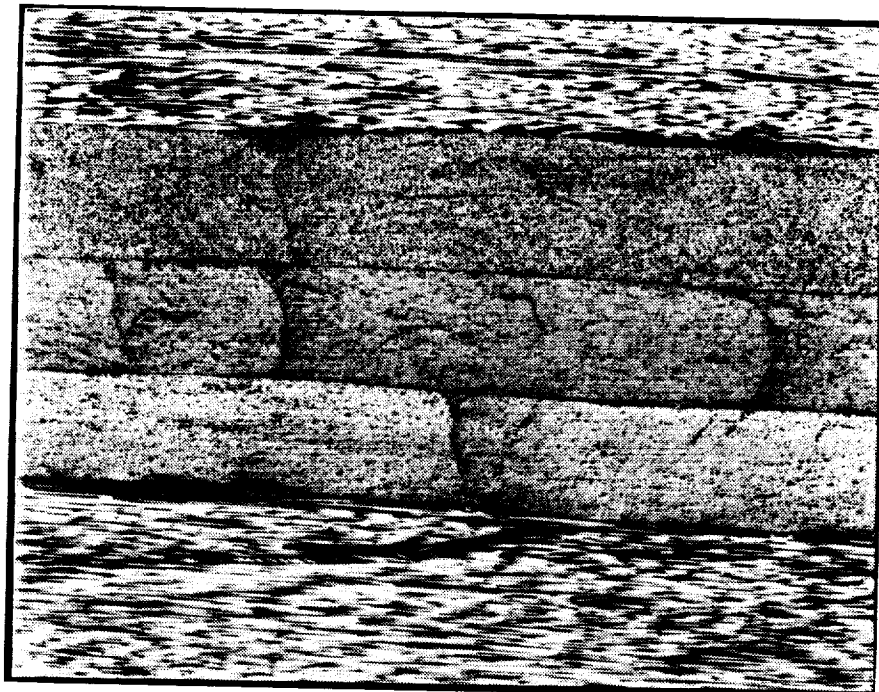
(RTM Panel 72390P1)                                    (40X)

*Figure 5.7.1  Photomicrographs of Hexcel Hi-Tech AS4 6k knitted*
*(+45°/0°/-45°/90°)ₐₛ/Hercules 3501-6 panels.*

Hexcel Hi-Tech Multiaxial Warp Knit Material Evaluation

C1  S1
    S2
C2  C3    S3
    C4  C5

**Test Specimen Cutting Diagram: 1/4 Scale**

C: SBC Specimen
S: Iosipescu Shear Specimen

90°

0°

**Ply Orientation**

Bottom FDEMS    C-Scan 1/2 Scale

32    **Signal Response**    2047

**RTM Panel 72390P1**

**Photomicrograph**    **(400X)**
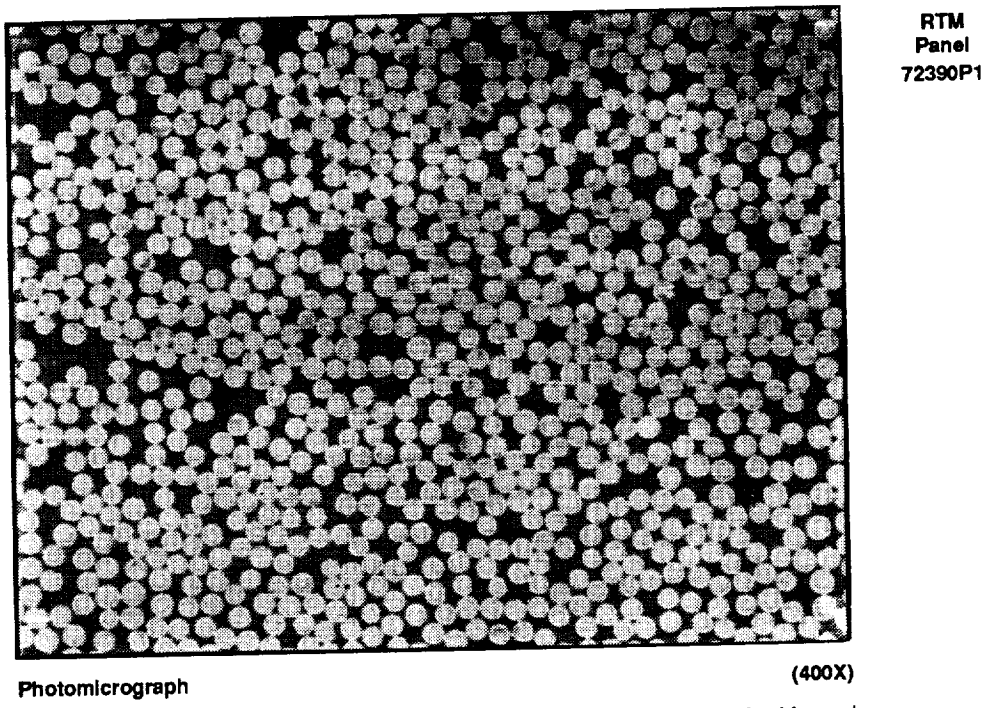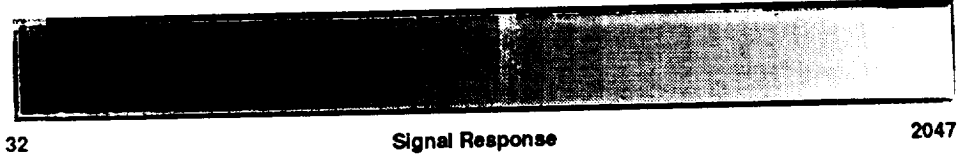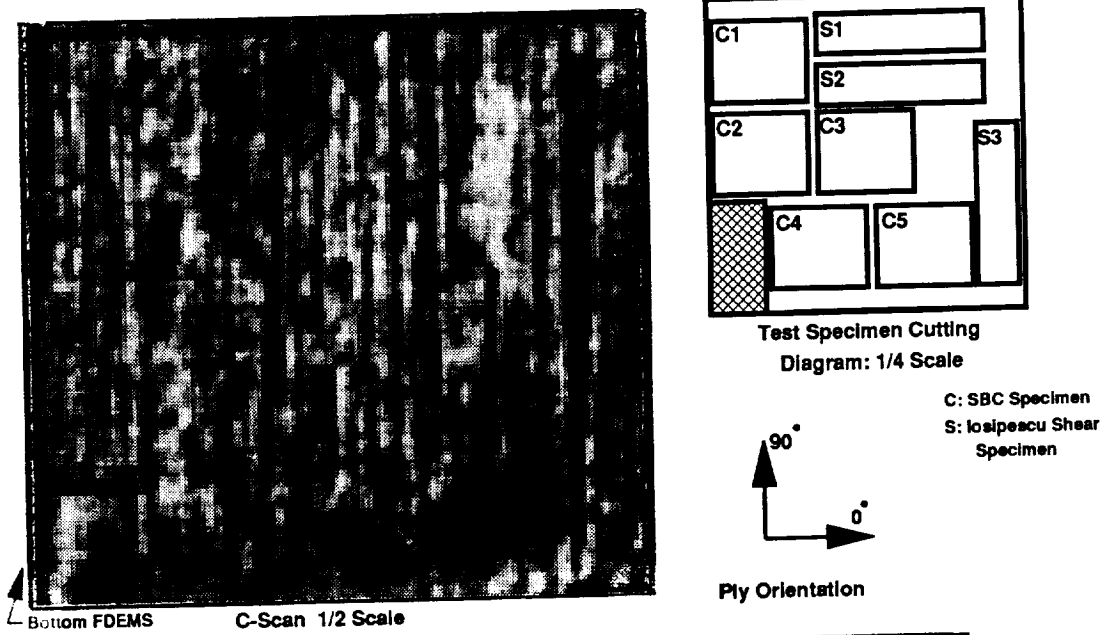
*Figure 5.7.2  C-scan, test specimen diagram, and photomicrograph of a Hexcel Hi-Tech AS4 6k knitted (+45°/0°/-45°/90°)$_{2s}$ /Hercules 3501-6 composite panel fabricated at 347.4 kPa with the manufacturer's cure cycle.*

Hexcel Hi-Tech Multiaxial Warp Knit Material Evaluation

**Ply Orientation**

0 °

-45°

90 °

90 °

-45°

0 °

(RTM Panel 71290P1)

Through-The-Thickness
Stitches

(40X)

**Ply Orientation**

0 °

-45°

90 °

+45°

0 °

(RTM Panel 72090P1)

(40X)
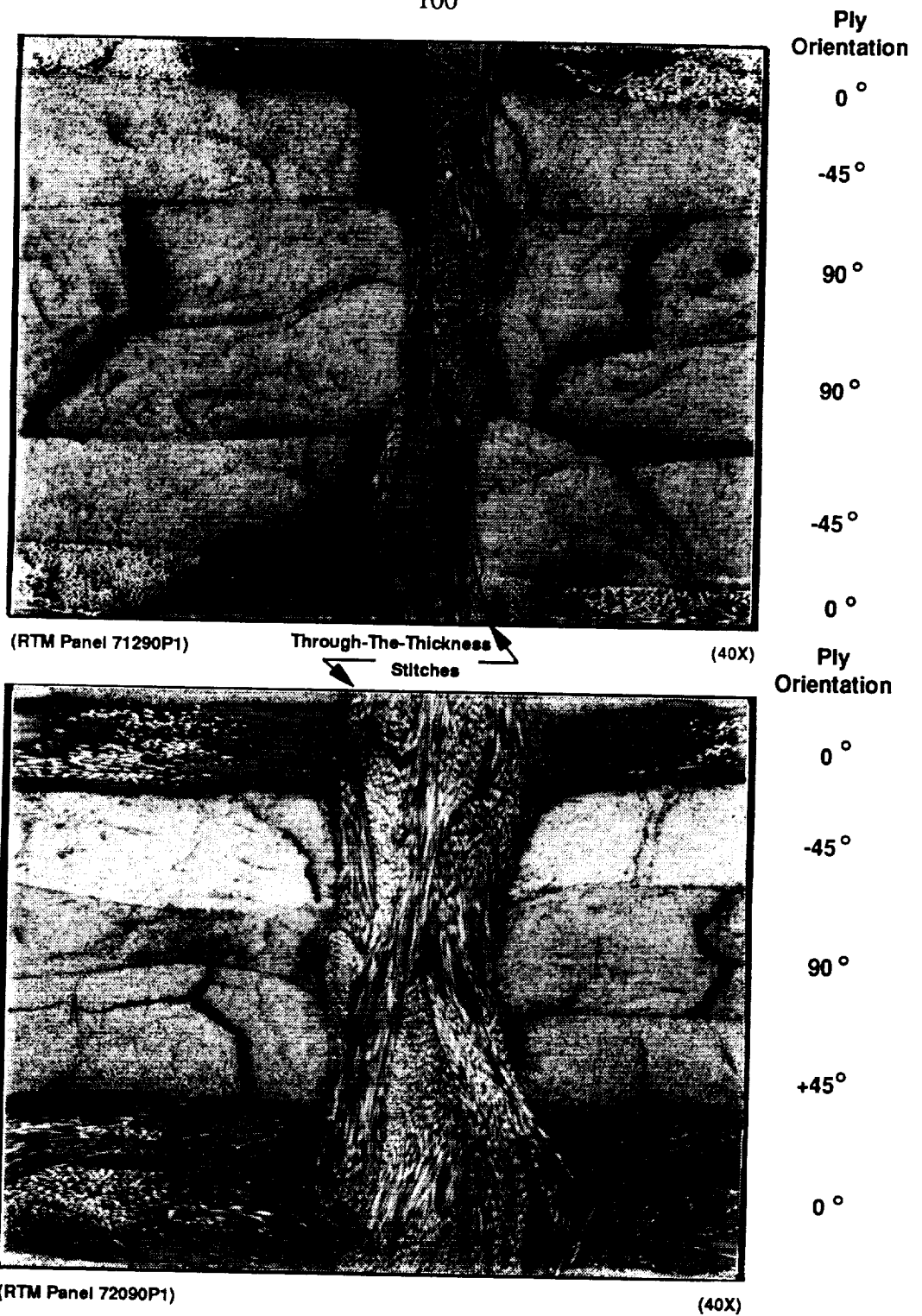
*Figure 5.7.3  Photomicrographs of Hexcel Hi-Tech AS4 6k knitted/stitched*
*(+45°/0°/-45°/90°)$_{2S}$/Hercules 3501-6 composite panels.*

Hexcel Hi-Tech Multiaxial Warp Knit Material Evaluation

panel processed at 705.5 kPa appeared to be well consolidated. A noticeable crimping of the carbon stitching tows was detected when high compaction pressures were utilized during fabrication (see bottom of Fig. 5.7.3). No apparent difference in quality was detected between knitted/stitched panels fabricated with the manufacturer's cure cycle and the rapid cure cycle at similar compaction pressures.

An ultrasonic C-scan, a mechanical test specimen cutting diagram, and a local photomicrograph (400X) for a knitted/stitched panel processed at 347.4 kPa with the manufacturer's cure cycle are presented on Fig. 5.7.4. The C-scan, test specimen cutting diagram, and photomicrograph (400X) for a knitted/stitched panel processed at 705.5 kPa with the rapid cure cycle are shown on Fig. 5.7.5. Both panels were found to have C-scans with geometrical distortions that match the stitching patterns. According to Long [33], the through-the-thickness carbon stitches distort the transducer signal of the C-scan by transmitting sound waves at a higher velocity than the surrounding medium thus creating a differential in the response signal. High porosity regions were evident at the location of the FDEMS sensors. All of the mechanical test specimens were obtained from laminate areas unaffected by the FDEMS. Both panels contained very little microporosity. The packing arrangement of fibers in the low pressure (347.4 kPa) panel (bottom of Fig. 5.7.4) was very irregular and identical to the packing observed in the knitted panels processed at a similar pressures (see bottom of Fig. 5.7.2). The high pressure (705.5 kPa) panel had densely packed fibers in both random and hexagonal packing arrangements (see bottom of Fig. 5.7.5). No difference in quality was detected between panels fabricated with different temperature cure cycles at similar compaction pressures.

No significant quantities of macroporosity and microporosity were detected from the photomicrographs of the knitted and knitted/stitched micrograph specimens. However, large resin pockets were detected near the stitching tows of the knitted/stitched specimens and microcracks were prevalent in all of the specimens examined. Microporsity may have resulted from air entrapment during fabrication. The compaction pressure applied during processing was found to affect the consolidation and the packing of the fiber bed. The temperature cure cycle had no discernable effect on the panel quality.
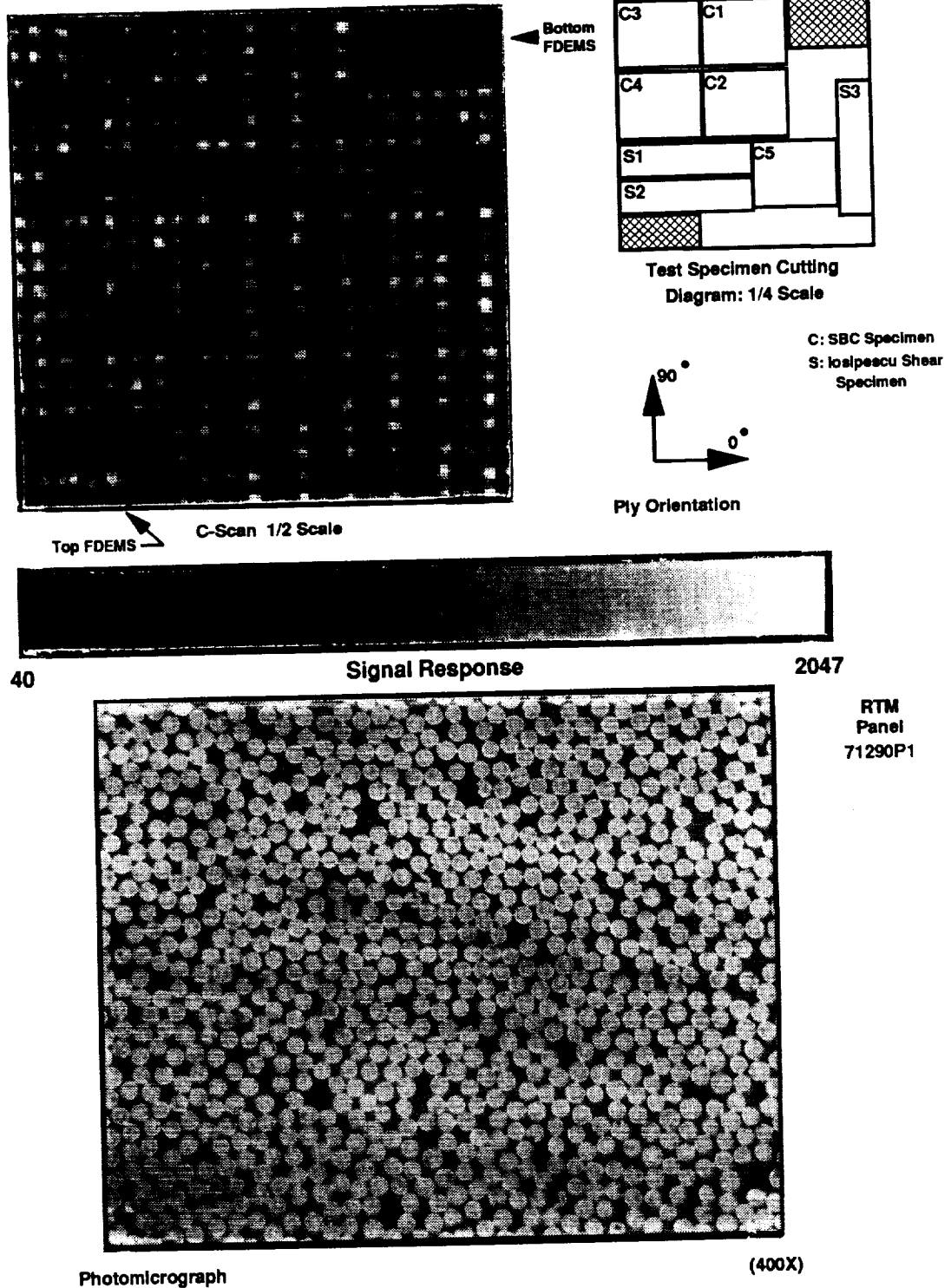
Figure 5.7.4  C-scan, test specimen diagram, and photomicrograph of a Hexcel
Hi-Tech AS4 6k knitted/stitched (+45°/0°/-45°/90°)$_{2s}$/Hercules 3501-6
composite panel fabricated at 347.4 kPa with the manufacturer's cure cycle.

Hexcel Hi-Tech Multiaxial Warp Knit Material Evaluation
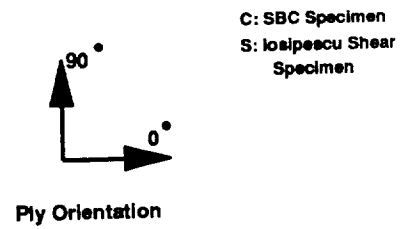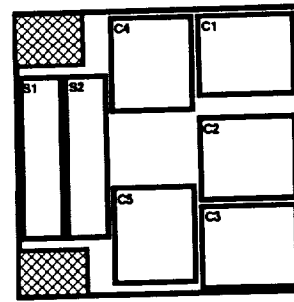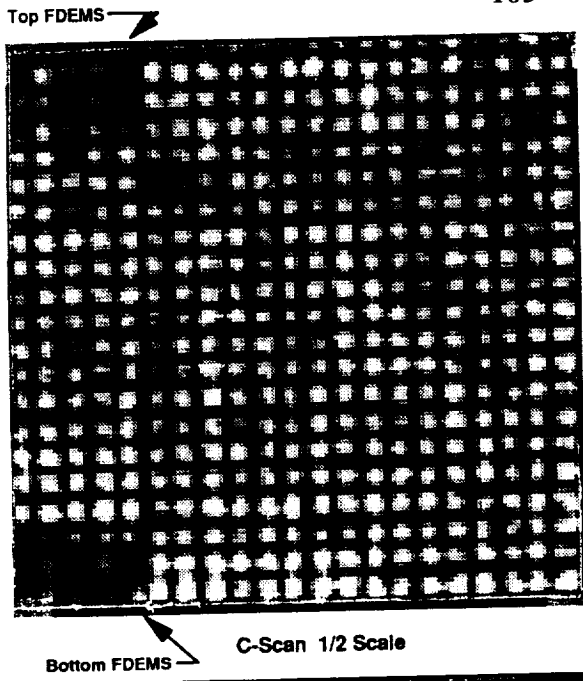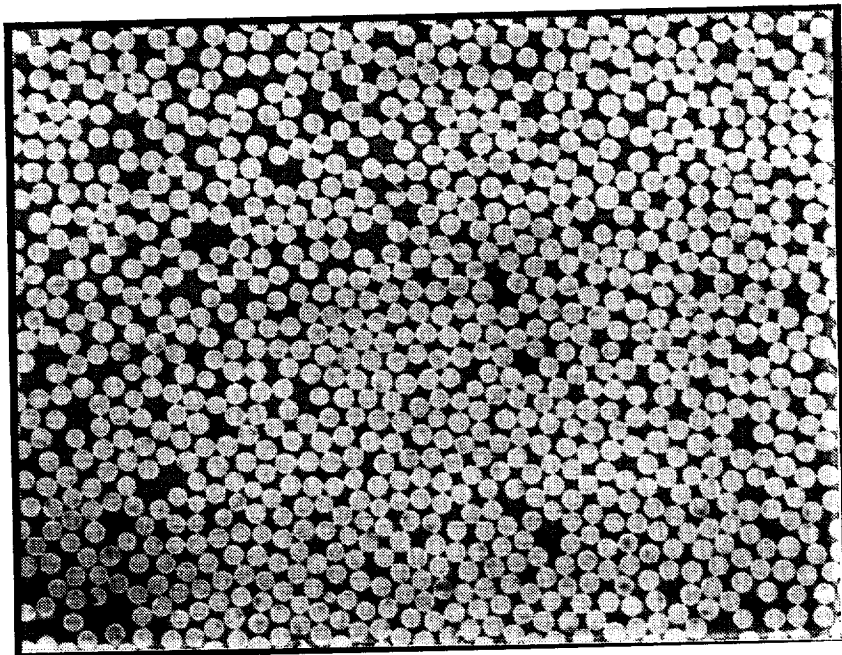
Figure 5.7.5  C-scan, test specimen diagram, and photomicrograph of a Hexcel
Hi-Tech AS4 6k knitted/stitched (+45°/0°/-45°/90°)$_{2s}$/Hercules 3501-6
composite panel fabricated at 705.5. kPa with the rapid cure cycle.

Hexcel Hi-Tech Multiaxial Warp Knit Material Evaluation

# 5.8 Destructive Evaluation: Short Block Compression

Five short block compression (SBC) specimens were cut from each of the Hexcel Hi-Tech/Hercules 3501-6 panels and individually loaded in compression to failure using the technique presented in Section 4.9. Specimens were loaded in compression along either the 0° or the 90° plies. The primary goal of the compression study is to determine the effect of the processing cycles on the compressive properties of the panels.

Upon examination of the failure surfaces of the Hexcel Hi-Tech SBC specimens, it was found that all of the specimens experienced a combination of transverse shear failure and extensive delamination. The failure paths across the surfaces of all of the knitted SBC specimens were very irregular (see top of Fig. 5.8.1). The Hexcel Hi-Tech knitted/stitched SBC specimens primarily experienced transverse shear failure. The through-the-thickness carbon stitches helped to control delamination and crack growth during failure (see bottom of Fig. 5.8.1). All of the stitched SBC specimens had irregular failure pathways along the width. The manufacturer's cure cycle SBC specimens and the rapid cure cycle SBC specimens had similar failure surfaces.

The compressive strength and ultimate longitudinal strain obtained from the Hexcel SBC specimens loaded in compression along the 0° degree plies are presented on the top and bottom of Fig. 5.8.2, respectively. The compression strength and ultimate longitudinal strain of specimens loaded in compression along the 90° plies are presented in a similar fashion in Fig. 5.8.3. The Young's modulus at 0.2% longitudinal strain and Poisson's ratio at 0.2% longitudinal strain obtained from the SBC specimens loaded in compression along the 0° and 90° plies are presented in Figs. 5.8.4 and 5.8.5, respectively. The compressive strength and Young's modulus at 0.2% longitudinal strain of AS4 $(+45_3°/0_3°/-45_3°/90_3°)_{2s}$ prepreg SBC specimens are presented in the respective figures, (no ultimate longitudinal strain or Poisson's ratio results were obtained). The compression strength, ultimate longitudinal strain, Poisson's ratio, and Young's modulus of the knitted and knitted/stitched SBC specimens are presented in Appendix D.1.

The compressive properties of the SBC specimens fabricated with the rapid cure cycle

(RTM Panel 71190P1) (7.5X)

**Hexcel Hi-Tech AS4 6k Knitted (+45°/0°/-45°/90°)$_{2s}$/Hercules 3501-6 SBC Specimen**



(RTM Panel 71290P1) (7.5X)

**Hexcel Hi-Tech AS4 6k Knitted/Stitched (+45°/0°/-45°/90°)$_{2s}$/Hercules 3501-6 SBC Specimen**

*Figure 5.8.1  Hexcel Hi-Tech multiaxial warp knit SBC failure surfaces.*

Hexcel Hi-Tech Multiaxial Warp Knit Material Evaluation

ORIGINAL PAGE
BLACK AND WHITE PHOTOGRAPH
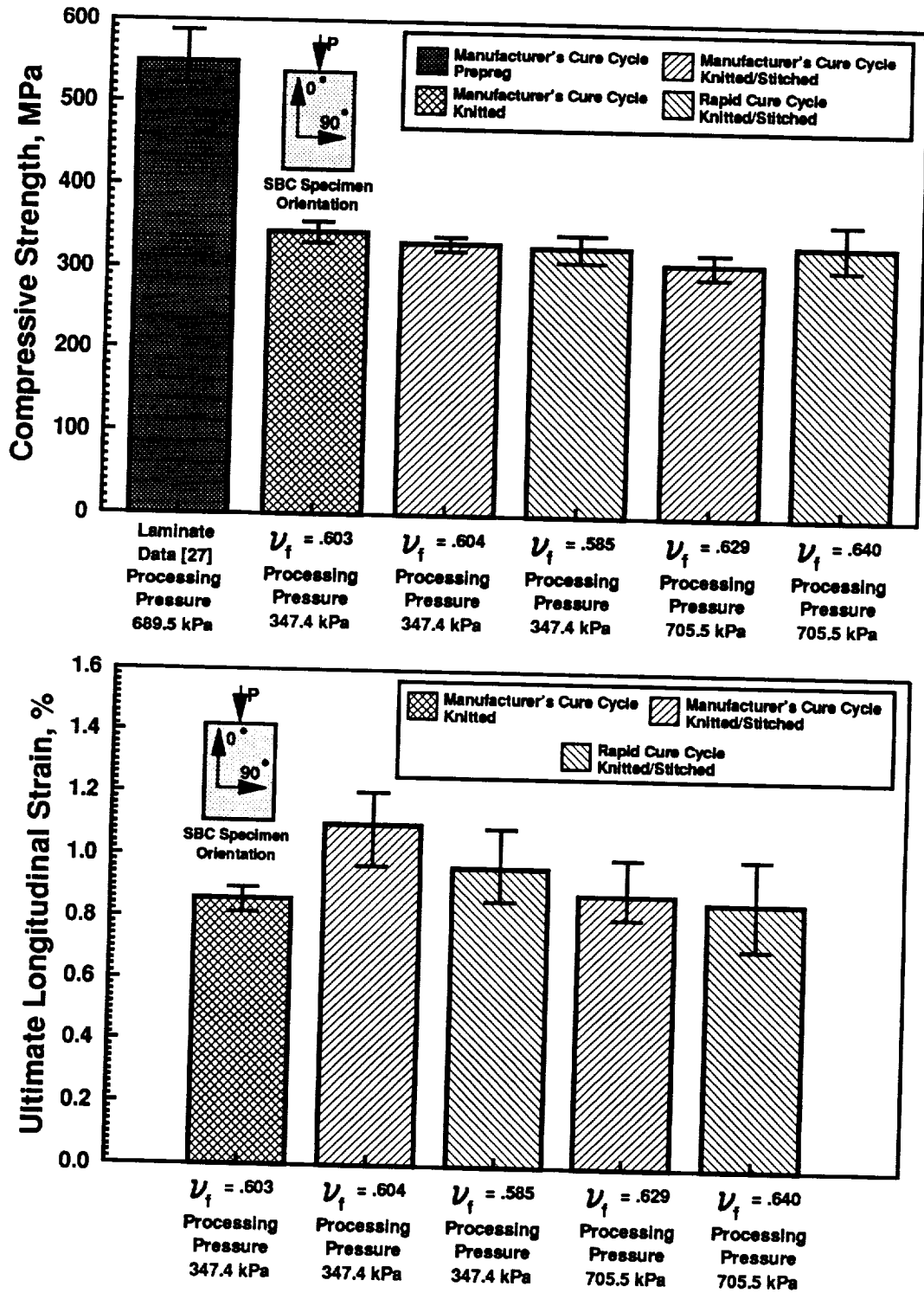
Figure 5.8.2 Compressive strength and ultimate longitudinal strain of Hexcel Hi-Tech AS4 6k (+45°/0°/-45°/90°)$_{2s}$/ Hercules 3501-6 SBC specimens loaded in compression along the 0° plies.

Hexcel Hi-Tech Multiaxial Warp Knit Material Evaluation
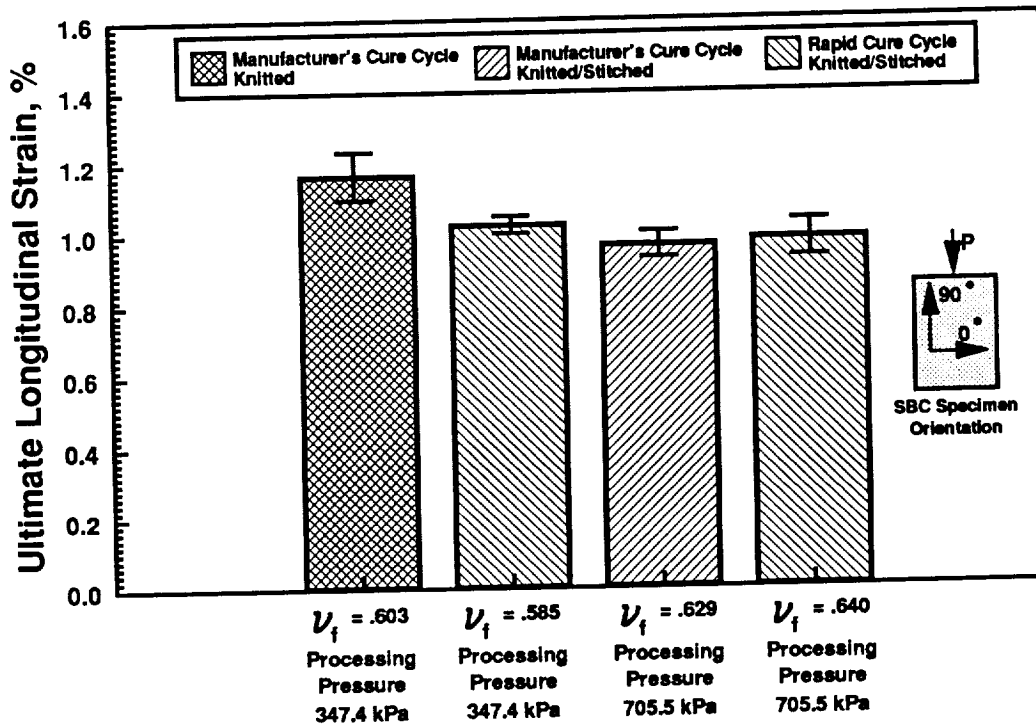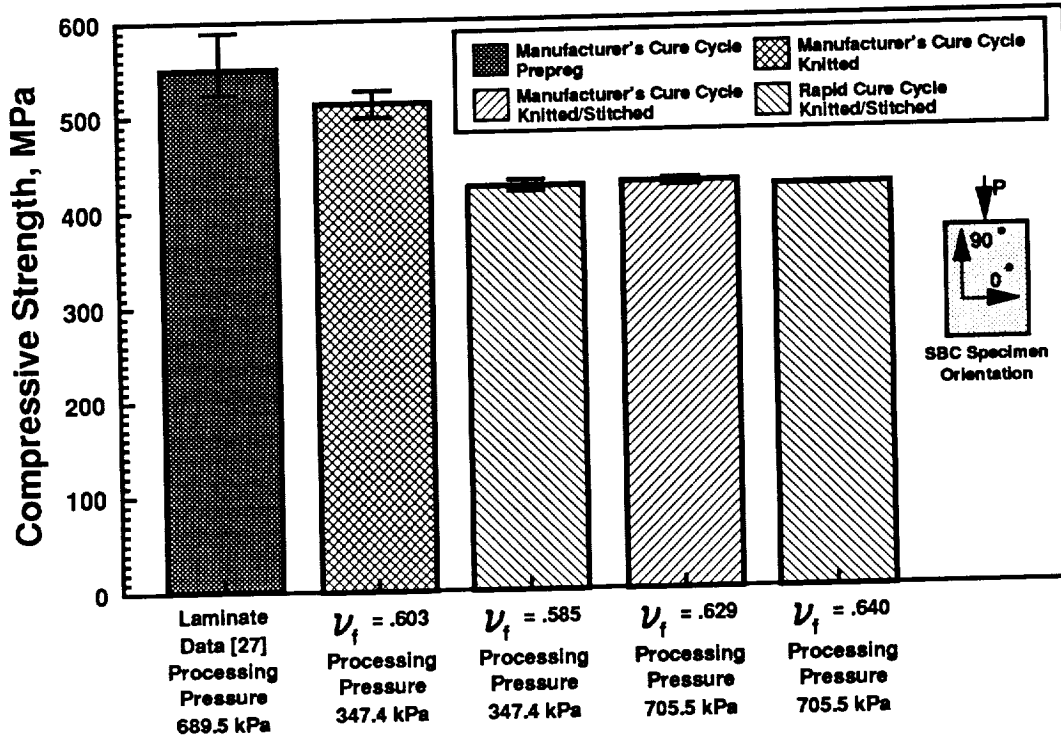
*Figure 5.8.3  Compressive strength and ultimate longitudinal strain of Hexcel Hi-Tech AS4 6k (+45°/0°/-45°/90°)$_{2s}$/ Hercules 3501-6 SBC specimens loaded in compression along the 90° plies.*

Hexcel Hi-Tech Multiaxial Warp Knit Material Evaluation
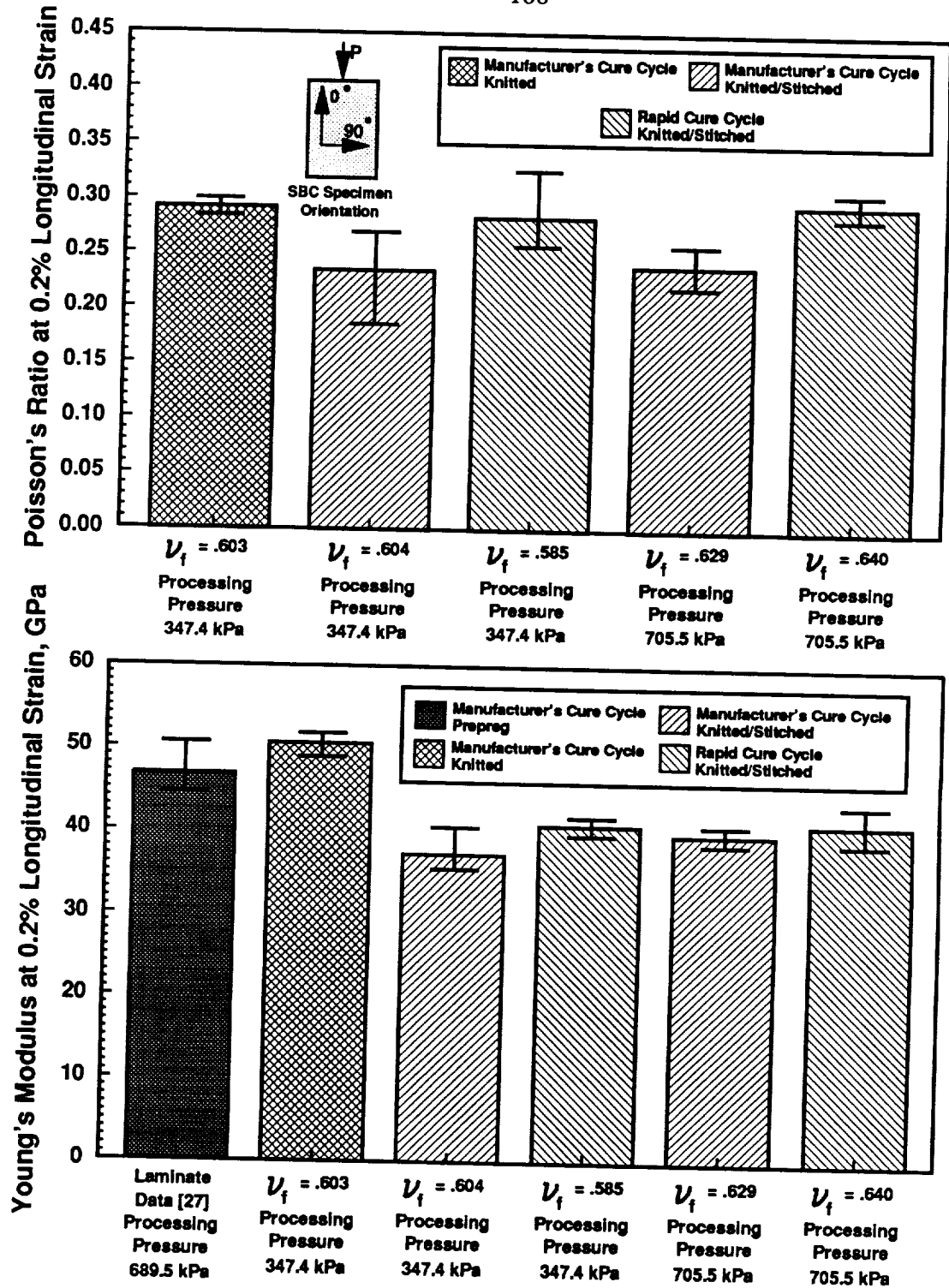
Figure 5.8.4  Poisson's ratio and Young's modulus at 0.2% longitudinal strain of Hexcel Hi-Tech AS4 6k (+45°/0°/-45°/90°)$_{2s}$/ Hercules 3501-6 SBC specimens loaded in compression along the 0° plies.

Hexcel Hi-Tech Multiaxial Warp Knit Material Evaluation
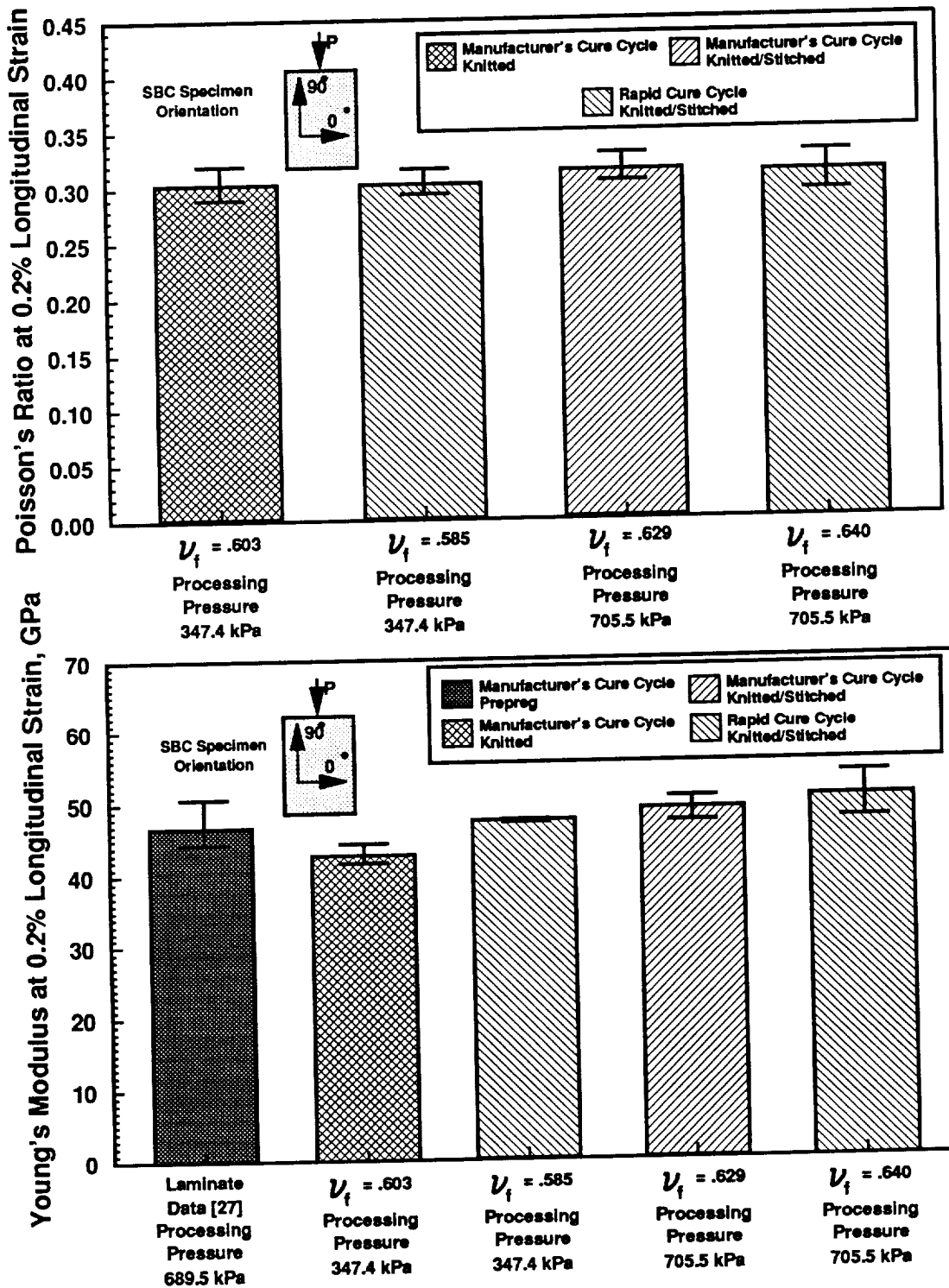
Figure 5.8.5   Poisson's ratio and Young's modulus at 0.2% longitudinal
strain of Hexcel Hi-Tech AS4 6k $(+45°/0°/-45°/90°)_{2s}/$
Hercules 3501-6 SBC specimens loaded in
compression along the 90° plies.

Hexcel Hi-Tech Multiaxial Warp Knit Material Evaluation

were found to be as good or better than SBC specimens fabricated with the manufacture's cure cycle. Rapid cure cycle SBC specimens loaded in compression along the 0° plies were found to have a 1.4% lower ultimate longitudinal strain, a 3% higher compressive strength, a 7.7% higher Young's modulus, and a 22% higher Poisson's ratio in comparison to the manufacturer's cure cycle specimens. Rapid cure cycle SBC specimens loaded in compression along the 90° plies were found to have a 3.6 % lower ultimate longitudinal strain, a 3.5 % higher Young's modulus, and a similar compressive strength and Poisson's ratio. Both the rapid and the manufacturer's cure cycle knitted/stitched SBC specimens had similar states of final cure (Table C.2.1). Therefore, the difference in mechanical properties may be attributed to errors in the experimental measurements or to the effects of localized microporosity and microcracks.

The effect of processing pressure and the resulting fiber volume fraction upon the compression properties was found to be small. The only evident trend was a decrease in ultimate longitudinal strain and an increase in the Young's modulus with increasing fiber volume fraction.

The effect of knitting and stitching on the compression properties were found to be significant. The knitted SBC specimens, loaded in compression along the 0° plies, were found to have a 38% lower compressive strength and a 22% lower Young's modulus in comparison to the prepreg SBC specimen properties. The knitted SBC specimens, loaded in compression along the 90° plies, were found to have a 5% lower compressive strength and a 7% lower Young's modulus in comparison to the prepreg SBC specimens. Knitted/ stitched SBC specimens loaded in compression along the 0° plies were found to have a 4% lower compressive strength, a 28% higher ultimate longitudinal strain, a 22% lower Young's modulus, and a 12% lower Poisson's ratio in comparison to the knitted SBC specimens. Knitted/stitched SBC specimens loaded in compression along the 90° plies were found to have a 17% lower compressive strength, a 12% lower ultimate longitudinal strain, a 3% higher Young's modulus, and a 6% lower Poisson's ratio in comparison to the knitted SBC specimens.

The lower compression properties obtained from the knitted and knitted/stitched SBC

specimens are probably due to the kinking and misalignment of the fiber bed by the stitching tows and knitting yarns (fabrication defects). Regions near the stitches also tended to be resin rich and contaminated with microvoids and microcracks.

## 5.9 Destructive Evaluation: Iosipescu Shear

The Iosipescu shear test (Section 4.9) was used to evaluate the shear properties of the Hexcel Hi-Tech/Hercules 3501-6 composite panels. Two to three Iosipescu shear specimens were obtained from each panel. The Iosipescu specimens were loaded in shear with either the 0° or 90° fiber orientations perpendicular to the direction of the applied load (Fig. D.2.1). The shear strength of each Iosipescu shear specimen was measured at failure. The primary goal of the Iosipescu shear test was to determine the effect of the processing pressure and temperature cure cycles on the shear strength of the Hexcel panels.

The failure surfaces of the Hexcel Hi-Tech knitted Iosipescu shear specimens were dominated by extensive delamination and cracks between the individual plies at the notch (see top of Fig. 5.9.1). Failure surfaces of a rapid cure cycle/low pressure (347.5 kPa) Iosipescu shear specimen and a manufacturer's cure cycle/high pressure (705.5 kPa) Iosipescu shear specimen are shown in the middle and bottom of Fig. 5.9.1, respectively. The failure surface of the Hexcel Hi-Tech knitted/stitched Iosipescu shear specimens had much less delamination and cracking between the individual plies. The through-the-thickness carbon stitches helped to significantly control delamination during failure. The failure surfaces of the knitted/stitched Iosipescu shear specimens fabricated using either the manufacturer's cure cycle of the rapid cure cycle were identical at both the high and low processing pressures.

The shear strengths obtained from the knitted and knitted/stitched Iosipescu shear specimens tested in the 0° and 90° orientations are shown in Fig. 5.9.2. The ultimate shear strength of each specimen is presented in Appendix D.2. No shear results were obtained from the AS4 prepreg laminates. All of the strain gauges used for the shear tests

(RTM Panel 72390P1)

(18X)

**Hexcel AS4 6k Knitted (+45°/0°/-45°/90°)₂ₛ/Hercules 3501-6 Iosipescu Shear Specimen**

Fiber Orientation

0°



(RTM Panel 71790P1)

(18X)

Through-The-Thickness Stitch

Fiber Orientation

0°

**Hexcel AS4 6k Knitted/Stitched (+45°/0°/-45°/90°)₂ₛ/Hercules 3501-6 Iosipescu Shear Specimen**

*Figure 5.9.1  Failure surfaces of Hexcel Hi-Tech multiaxial warp knit Iosipescu shear specimens, (at notch).*

Hexcel Hi-Tech Multiaxial Warp Knit Material Evaluation
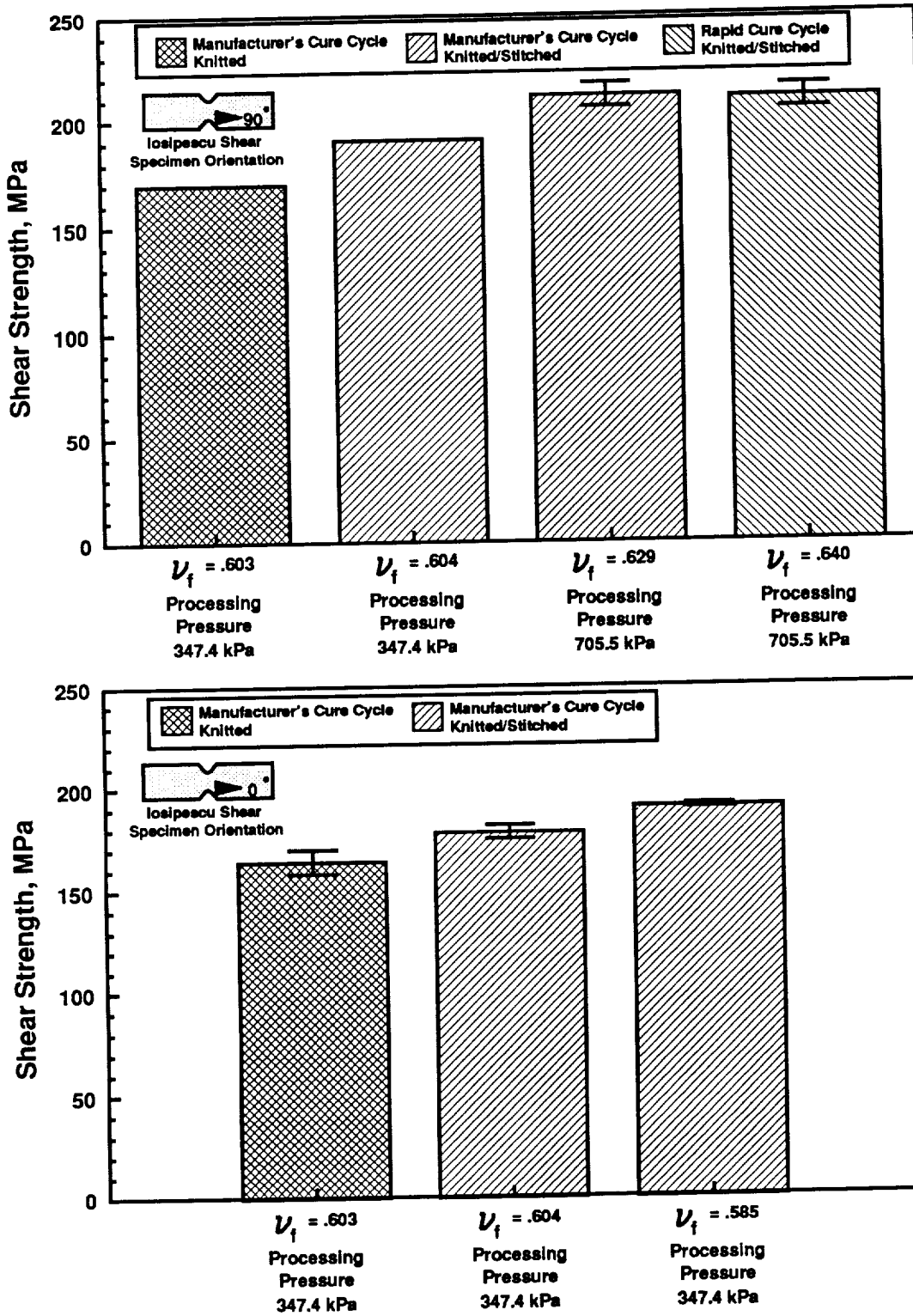
Figure 5.9.2    Shear strength of the Hexcel Hi-Tech AS4 6k
$(+45°/0°/-45°/90°)_{2s}$ /Hercules 3501-6 Iosipescu shear
specimens tested in the orientations shown.

Hexcel Hi-Tech Multiaxial Warp Knit Material Evaluation

failed prematurely and subsequently no ultimate shear strains were obtained.

The rapid cure cycle knitted/stitched Iosipescu shear specimens had as good or better shear properties compared with equivalent Iosipescu shear specimens fabricated with the manufacture's cure cycle. The rapid cure cycle/low pressure (347.5 kPa) Iosipescu shear specimens were found to have a 0.5% lower shear strength in comparison to the manufacturer's cure cycle/low pressure (347.5 kPa) Iosipescu shear specimens (0° orientation). The rapid cure cycle/high pressure (705.5 kPa) specimens were found to have a 8.6% higher shear strength in comparison to the manufacturer's cure cycle/high pressure specimens (90° orientation).

The high processing pressure Iosipescu shear specimens had greater shear strengths than the low processing pressure Iosipescu shear specimens.

As with the SBC specimens, the Iosipescu shear specimens were influenced by the through-the-thickness carbon stitches. The knitted/stitched Iosipescu shear specimens were found to have a 12% higher shear strength in the 0° orientation and a 10.6% higher shear strength in the 90° orientation in comparison to the knitted Iosipescu shear specimens. At similar fiber volume fractions, knitted Iosipescu shear specimens loaded in the 90° orientation were found to have a 7.4% higher ultimate shear strength in comparison to identical knitted Iosipescu shear specimens loaded in the 0° orientation. An 8.5% increase in shear strength was obtained from knitted/stitched Iosipescu shear specimens loaded in the 90° orientation in comparison to identical knitted/stitched Iosipescu shear specimens loaded in the 0° orientation.

# 6.0 TTI IM7/8HS Material Evaluation

The following chapter will present an evaluation of studies using TTI IM7/8HS fabric preforms. The compaction and permeability characteristics of the fabric preforms were determined experimentally and incorporated into the RTM simulation model. Textile composites composed of 16 ply TTI IM7/8HS fabric preforms and Hercules 3501-6 resin were fabricated with the RTM film infusion technique using several different temperature cure cycles and processing pressures. In-situ measurements were taken of the resin infiltration front position, the panel temperature, and the resin degree of cure and viscosity as a function of time. The experimental measurements were compared with the RTM simulation model results to evaluate the accuracy of the model. Non-destructive evaluation techniques and mechanical testing (compression and shear) were used to evaluate the effect of processing parameters on the quality and physical properties of the fabricated panels.

## 6.1 Areal Weight and Initial Thickness

The initial uncompacted thickness and areal weight of a single ply of TTI IM7/8HS are presented in Table 6.1.1. The experimental measurements were obtained by averaging the physical properties of three different 50.8 mm by 50.8 mm single ply test samples (see Section 4.3). The experimental measurements of the initial uncompacted thickness and areal weight were greater than the manufacturer's results by 1.9% and 10%, respectively.

## 6.2 Dry/Wet Compaction

The transverse deflection of 8 ply TTI IM7/8HS fabric preform test samples (171.2 mm by 152.4 mm) was measured experimentally and modeled using the techniques presented in Sections 4.4 and 4.4.1. Two dry test samples and one wet test sample were

Table 6.1.1. *Areal weight and initial uncompacted thickness of a single ply of TTI IM7/8HS obtained from experimental measurements and manufacturer's data.*

| TTI IM7/8HS (1 Ply) | Areal Weight, $g/m^2$ | Initial Thickness, mm |
|---|---|---|
| Measured | 430 | 0.75 |
| Manufacturer's Data | 422 | 0.68 |

**TTI IM7/8HS Material Evaluation**

compacted at fast deflection rates of 0.2 mm/min. Two fast dry compaction experiments were conducted to determine the repeatability of the compaction experiments. A slow (deflection rate of 0.02 mm/min) dry compaction experiment was not conducted. All of the test results were scaled by a factor of 1/8 to model the deflection of a single ply of TTI IM7/8HS. In this section, the fast dry and wet compaction model results will be presented.

A through-the-thickness permeability fixture, developed and fabricated by Claus and Loos [1], was used for the compaction experiments. (A description of the test fixture is provided in [1]). The deflection of the test fixture was modeled as a function of the applied compaction pressure (Eq. 4.4.2) and is given in Fig. B.1.1, Appendix B.1.

Compaction loads, ranging from 0 to 36 kN, were applied to 8 ply TTI IM7/8HS test samples test samples and the resulting deflections were measured. (A transverse compaction load of 36.5 kN applied to a 171.2 mm by 152.4 mm test sample results in a transverse compaction pressure of 1400 kPa). The deflection data obtained from the compaction experiments with the test samples were fit to a least squares polynomial (Eq. 4.4.3). The results were corrected for the deflection of the test fixture (Eq. 4.4.4) and scaled by a factor of 1/8. The coefficients of the fast wet and dry compaction models are given in Table 6.2.1 for a single ply of TTI IM7/8HS. The fabric preform deflections obtained from the compaction models are plotted as a function of applied compaction pressure in Fig. 6.2.1.

The deflection versus applied compaction pressure profiles obtained from the TTI IM7/8HS test samples were found to be very similar to the profiles obtained from Hexcel Hi-Tech AS4 6k knitted $(+45°/0°/-45°/90°)_{2s}$ test samples (Section 5.2). A nonlinear relationship was found to exist between the applied compaction pressure and the measured preform deflections for compaction pressures ranging from 0 to 500 kPa. A linear relationship existed between 500 kPa and 1400 kPa. The majority of the deflection of each test sample was obtained when the compaction pressure was increased from 0 to 300 kPa. The measured deflection of the two dry test samples differed by 0.0125 mm at compaction pressures greater than 250 kPa. The difference in deflection may be a result

Table 6.2.1 Dry/wet compaction model coefficients (Eq. 4.4.4) for a single ply
of TTI IM7/8HS.

| TTI IM7/8HS (1 Ply) | | | | | |
|---|---|---|---|---|---|
| Compaction Model | $a_0$ (mm) | $a_1$ (mm) | $a_2$ (mm) | $a_3$ (mm) | $a_4$ (mm) |
| Fast Dry #1. | -.06072 | -.04333 | .06755 | -.01216 | .00069 |
| Fast Dry #2. | -.03868 | -.06533 | .07070 | -.01161 | .00060 |
| Fast Wet | .85923 | -.87093 | .35060 | -.04062 | .00190 |
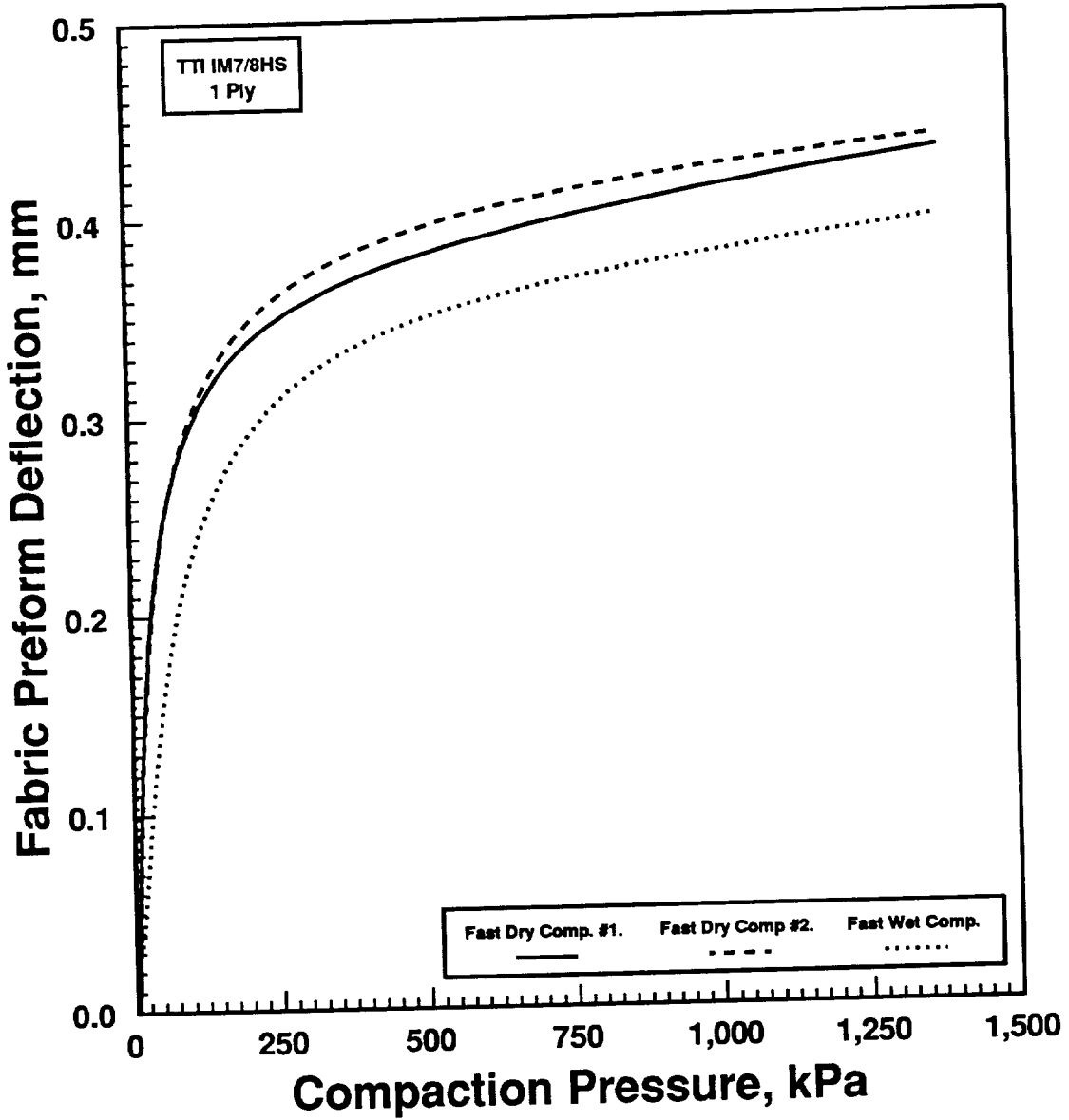
Figure 6.2.1 Wet and dry preform deflections as a function of applied compaction pressure for a single ply of TTI IM7/8HS.

of experimental error or different preform stiffnesses.

The two fast dry test samples had the greatest amount of deflection as a function of applied compaction pressure, while the fast wet test sample had the least. The greater stiffness of the wet test sample results from the entrapment of fluid within the fully saturated fabric preform during compaction. The fluid supports a portion of the applied pressure, leading to smaller deflections.

## 6.3 Through-The-Thickness Permeability

An experimental study was conducted to measure the through-the-thickness permeability of TTI IM7/8HS fabric preforms as a function of porosity. Test samples (50.8 mm by 50.8 mm) composed of either 6, 8, 12, or 20 plies of TTI IM7/8HS were examined to determine the influence of preform thickness upon the through-the-thickness permeability. The test samples were examined with the compaction/permeability test fixture (Section 4.2) using the experimental techniques presented in Section 4.5. All of the permeability experiments were conducted with fully saturated preforms using room temperature (17 °C) tap water (viscosity 0.001 Pa.s).

Flow experiments were initially conducted with the compaction/permeability test fixture to characterize the through-the-thickness pressure drop through the test section as a function of the flow rate. The test fixture flow characteristics and the flow meter calibration data are given in Appendix B.2.

Flow experiments were conducted with the TTI IM7/8HS fabric, measuring the through-the-thickness flow rate as a function of the pressure differential. The through-the-thickness pressure differentials were corrected for the pressure drop due to the test fixture. The permeability constant was obtained by fitting a linear least squares curve to the data (Eq. 4.5.4). The measured through-the-thickness flow rates are plotted as a function of the applied through-the-thickness pressure gradient in Fig. 6.3.1 for 8-ply and 20-ply TTI IM7/8HS test samples. The experimental results indicate that the flow resistance of the TTI IM7/8HS fabric preforms increases as the porosity decreases. The 8-ply test sample
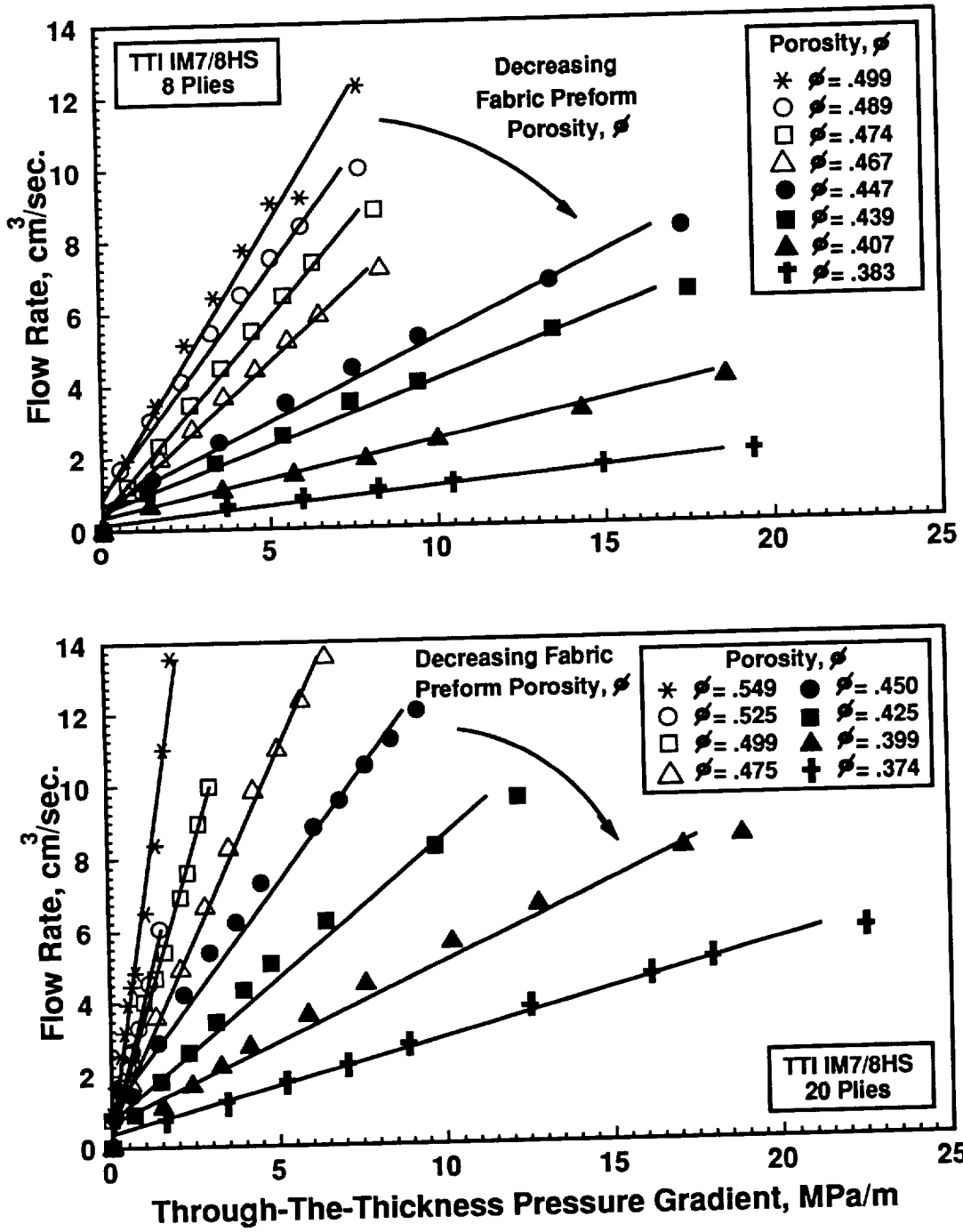
Figure 6.3.1 Flow rate as a function of the through-the-thickness pressure gradient for the TTI IM7/8HS fabric preforms.

was found to have a slightly greater resistance to flow than the 20-ply test sample (at similar porosities). Linear relationships between the applied through-the-thickness pressure gradient and the measured flow rate were established for all of the samples tested at porosities ranging from 0.30 to 0.55.

The permeability constants for the 6-, 8-, 12-, and 20-ply test samples are plotted as a function of the preform porosity in Fig. 6.3.2. The effect of test sample thickness (number of plies) on the through-the-thickness permeability of the TTI IM7/8HS test samples was found to be negligible. Consequently, the results from the different test samples were fit to the modified Gebart equation (Eq. 2.4.8) relating the through-the-thickness permeability to porosity. The modified Gebart relationship provided an excellent model to relate the through-the-thickness permeability of the TTI IM7/8HS test samples with the porosity. The TTI IM7/8HS test samples were found to have a minimum porosity of 0.283 and the constant S was 9.44. The results indicate that the TTI IM7/8HS fabric preforms contain geometrically or randomly packed fibers (Section 2.4.2).

The permeability characteristics of the TTI IM7/8HS test samples were very similar to the characteristics of the Hexcel Hi-Tech AS4 knitted $(+45°/0°/-45°/90°)_{2s}$ test samples (Section 5.3). Since both fabric preforms were composed solely of fibers perpendicular to the flow direction, the flow through the fiber beds was controlled by both the fiber bed packing arrangement and the gap distance between individual fibers, as predicted by the modified Gebart relationship.

# 6.4 Final Thickness/Fiber Volume Fraction/Resin Mass

The purpose of this section is to record the validity of the TTI IM7/8HS compaction models (Section 6.2) and to examine the effects of processing pressure on the physical properties of the TTI IM7/8HS fabric preforms. The TTI IM7/8HS compaction models and material properties (Section 6.1) were incorporated into the RTM simulation model. The RTM simulation model was then used to predict the final thickness (Eq. 2.1.2), the fiber volume fraction (Eq. 2.1.6), and the resin mass at full saturation (Eq. 2.1.8) as a
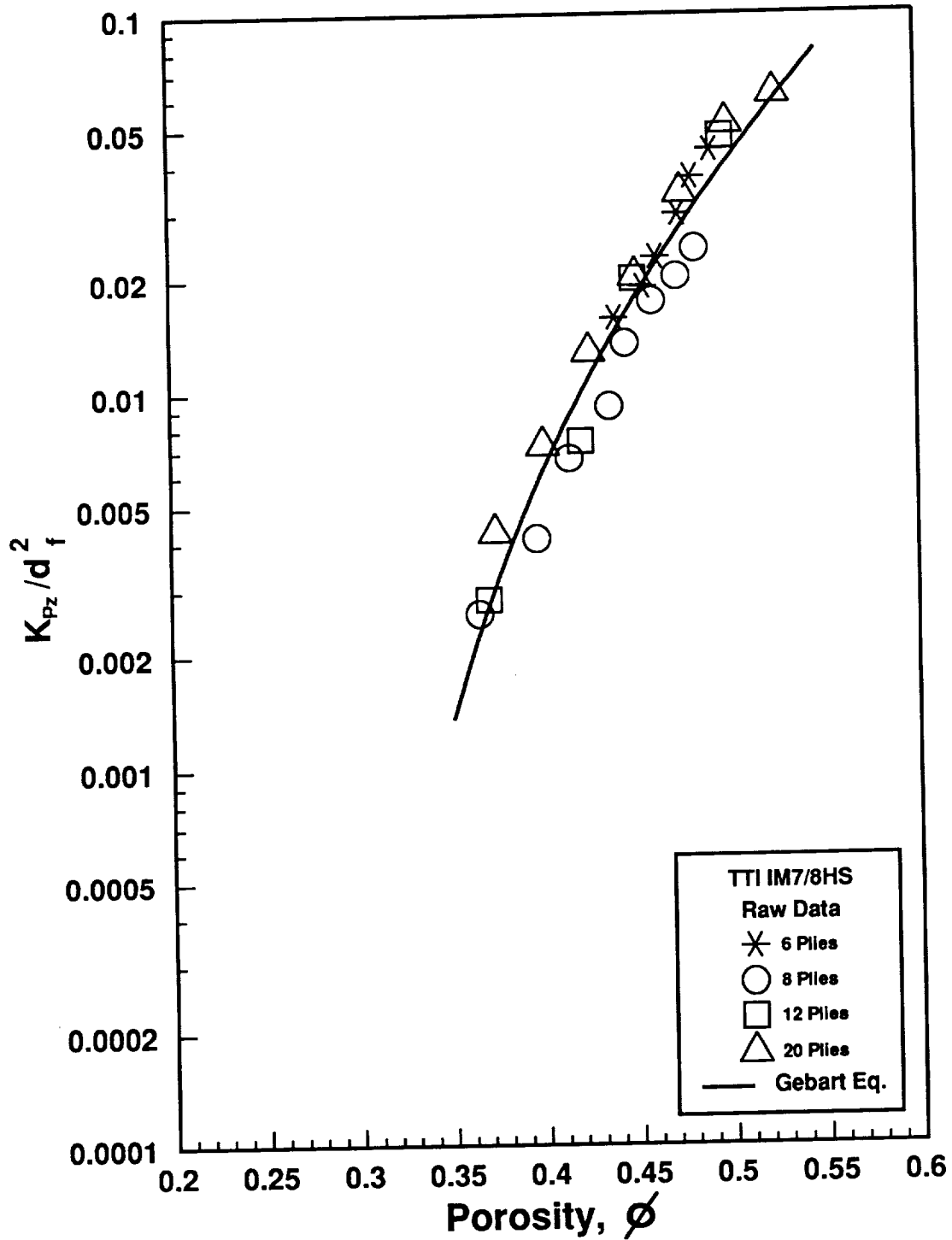
*Figure 6.3.2.  $K_{Pz}/d_f^2$  as a function of porosity for the TTI IM7/8HS fabric preforms.*

function of applied compaction pressure (0 to 1400 kPa). Panels were fabricated with the RTM film infusion technique using different temperature cure cycles and either a single-step or multiple-step compaction pressure application. Measurements of the final thickness, fiber volume fraction, and resin mass were taken (Section 4.8) for comparison to the model predictions .

The final thickness, fiber volume fraction, and resin mass at full saturation measured from 16 ply TTI IM7/8HS/Hercules 3501-6 composites and predicted by the RTM simulation model panels are plotted as a function of applied compaction pressure in Fig. 6.4.1. The cure cycles are presented in Table 4.6.1. The RTM simulation model predictions and panel results are presented in tabular form in Appendix C along with the corresponding processing conditions used during fabrication.

The final thickness, fiber volume fraction and resin mass of panels fabricated at different compaction pressures with either the manufacturer's cure cycle or a model generated advanced cure cycle were within 10% of the predictions obtained from the fast dry compaction model (#1.). The disagreement between the model results and the experimental measurements may have resulted from an incorrect measurement of the processing pressure during fabrication and/or different preform stiffnesses.

If a single step pressure is used during fabrication, the fast dry compaction model can be used to achieve relatively high fiber volume fraction panels at low compaction pressures if the exact resin mass (predicted by the model at a particular compaction pressure) is used.

## 6.5 Temperature Simulation

Composite panels composed of 16 plies of TTI IM7/8HS and Hercules 3501-6 resin were fabricated at different compaction pressures with either the manufacturer's cure cycle or one of the model generated cure cycles (Table 4.6.1). The purpose of this section is to determine the effects of different temperature cure cycles on the temperature distribution, resin viscosity, and resin degree of cure in the RTM layup. The RTM
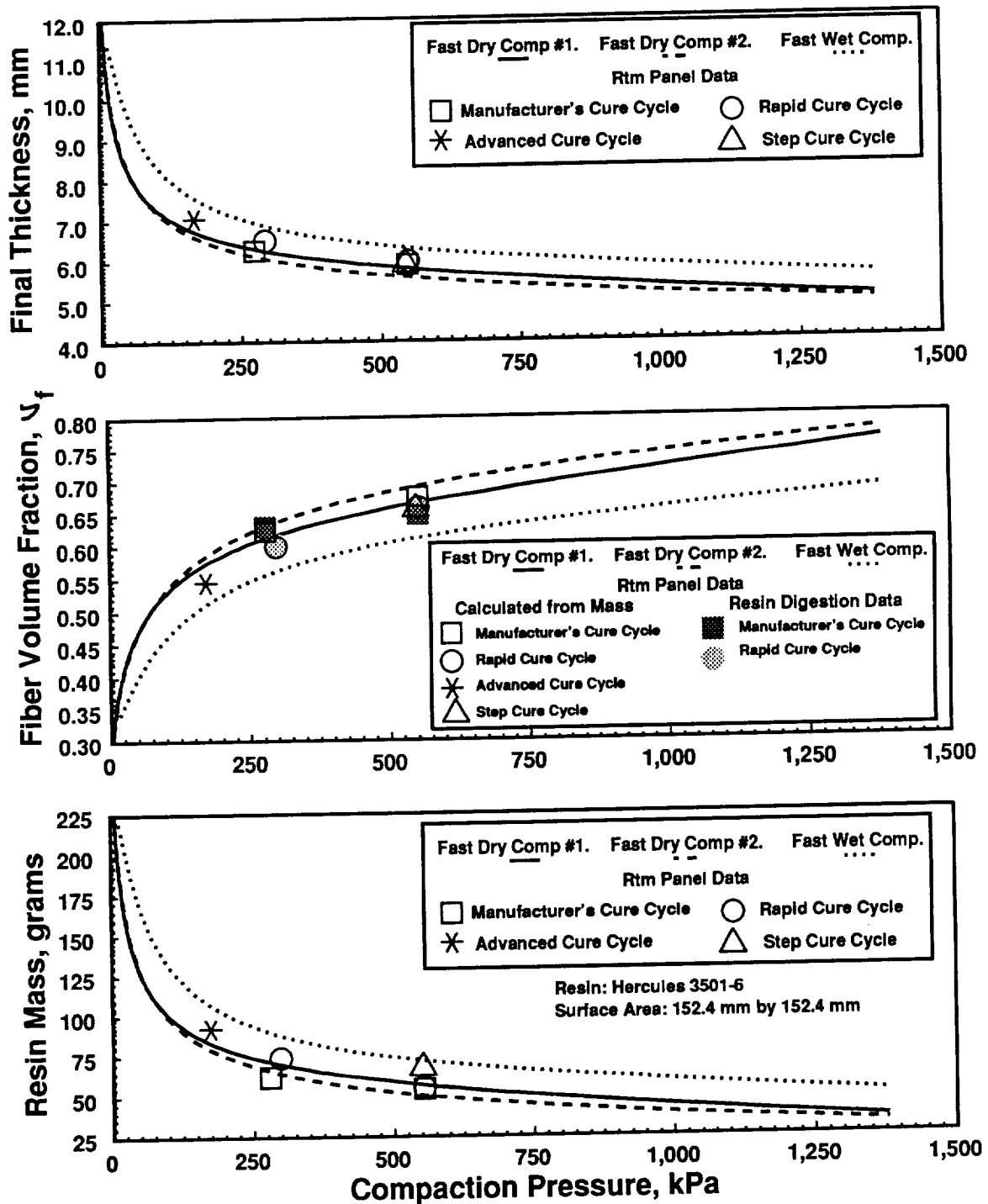
*Figure 6.4.1   Final thickness, fiber volume fraction, and resin mass as a function of applied compaction pressure for 16 ply TTI IM7/8HS/ Hercules 3501-6 composite panels.*

simulation model predictions of the temperature distribution and the resin viscosity and degree of cure are compared with experimental measurements obtained during fabrication.

In-situ measurements of the temperature distribution in the RTM layup were made with either J-type or K-type thermocouples located at the top and bottom of the composite panel and on the surfaces of the upper and lower hot press platens (Fig. A.1.2). A frequency dependent electromagnetic sensor (FDEMS) was placed at the bottom and top of the composite panel to measure the viscosity and resin degree of cure during processing. The temperature history of the upper and lower platens was incorporated into the RTM simulation model as the temperature boundary conditions at the upper and lower surfaces of the layup (Section 2.2.4). The kinetics/viscosity characteristics of the Hercules 3501-6 resin (Appendix A.2) were incorporated into the RTM simulation model (Chapter 3). The model was then used to calculate the temperature distribution in the RTM layup and the resin viscosity and degree of cure as a function of time.

The temperature distribution in the RTM layup and the resin viscosity and degree of cure were influenced primarily by the temperature cure cycle and unaffected by the processing pressure. Therefore, results will only be presented for selected panels fabricated with different temperature cure cycles.

The RTM simulation model predictions and experimental measurements of the temperature distribution in 16 ply TTI IM7/8HS/Hercules 3501-6 panels fabricated with the manufacturers's cure cycle and the rapid cure cycle are presented on the top and bottom of Fig. 6.5.1, respectively. Similar plots are presented on top and bottom of Fig. 6.5.2 for panels fabricated with the advanced cure cycle and the step cure cycle (Table 4.6.1).

The temperature differentials across the thickness of the panels fabricated with the manufacturer's cure cycle and the rapid cure cycle were found to be negligible (<2 °C). Panels fabricated with the advanced cure cycle and the step cure cycle had larger temperature differentials (10 °C). The RTM simulation model predictions of the temperatures in the panels fabricated with the manufacturer's cure cycle and the rapid cure cycle were within 5 °C of the experimentally measured temperatures. The RTM
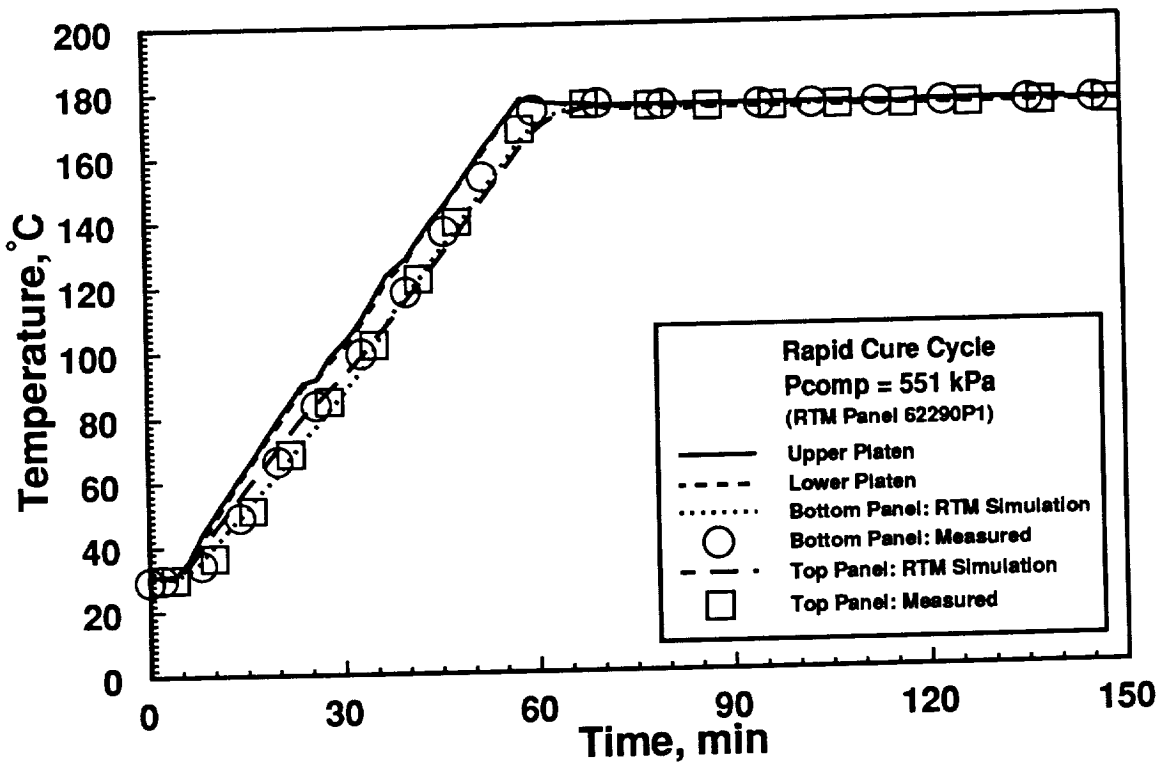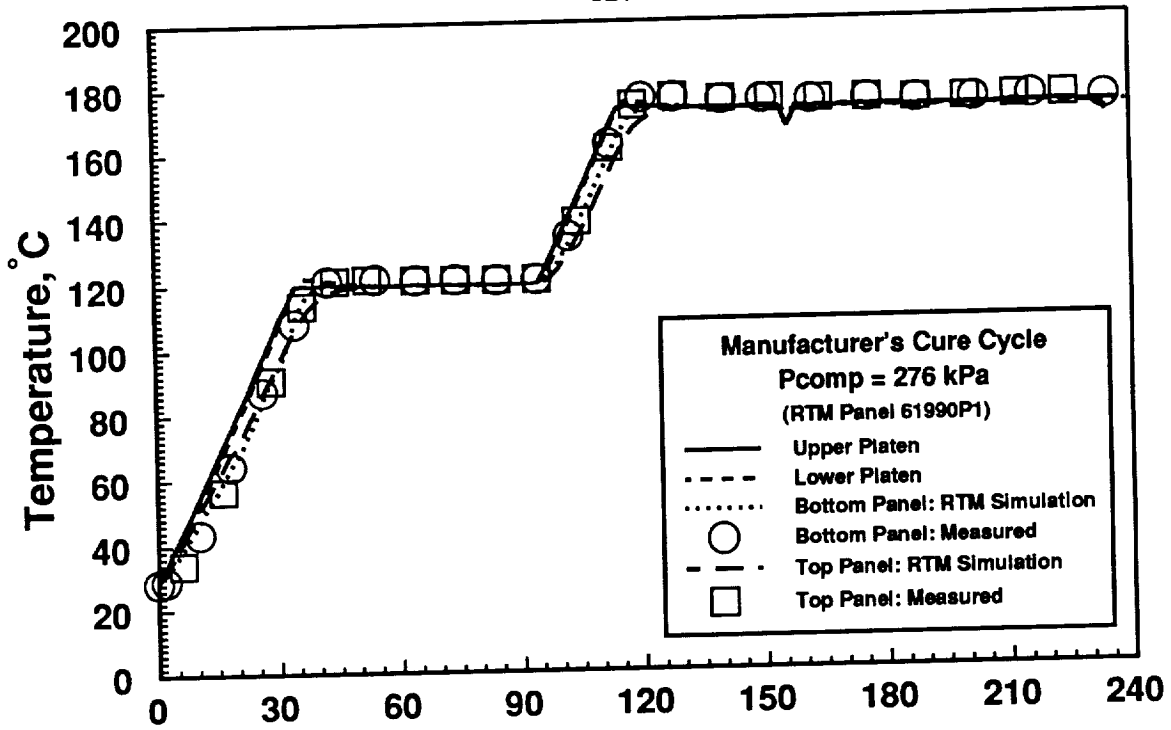
Figure 6.5.1  Temperature as a function of time at selected locations for 16 ply
TTI IM7/8HS/Hercules 3501-6 composite panels fabricated with the
temperature cure cycles shown.
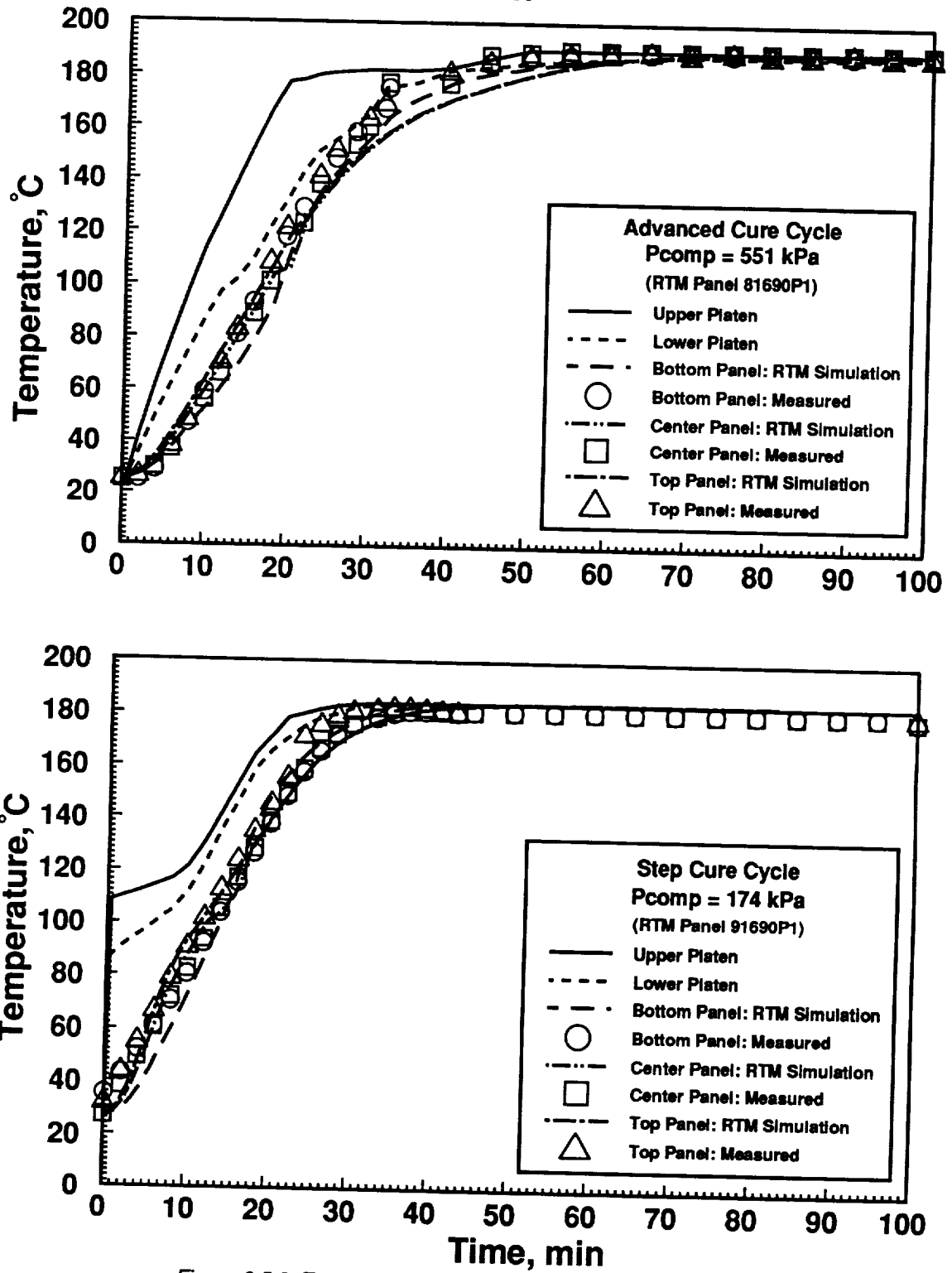
*Figure 6.5.2  Temperature as a function of time at selected locations for 16 ply TTI IM7/8HS/Hercules 3501-6 composite panels fabricated with RTM model generated temperature cure cycles.*

simulation model predictions of the temperatures in the panels fabricated with the advanced cure cycle and the step cure cycle were within 20 °C of the experimentally measured temperatures. The differences between the measured and calculated temperatures may be a result an incorrect measurement of the platen temperatures during fabrication, leading to an incorrect prediction of the temperature distribution by the RTM simulation model.

The resin viscosity and degree of cure at the bottom of a panel fabricated at 276 kPa with the manufacturer's cure cycle and a panel fabricated at 551 kPa with the rapid cure cycle are plotted as a function of time in Figs. 6.5.3-6.5.4, respectively. The model prediction of the temperature at the FDEMS location is plotted as a function of time in the respective figures. The model predictions of the resin degree of cure agree with the FDEMS measurements. However, the FDEMS measurements of the minimum viscosity (0.3 Pa.s) tended to be lower than the model predictions (0.8 Pa.s). The RTM simulation model also predicted longer flow windows (defined as the length of time at which the resin viscosity is less than 1000 Pa.s) and longer gelation times (defined as the time at which the resin achieves a viscosity greater than 1000 Pa.s). Disagreements between the RTM simulation model results and FDEMS measurements may be a result of an incorrect calibration of the sensors or an incorrect prediction of the resin degree of cure and viscosity by the RTM simulation model resulting from a poor measurement of the boundary temperatures.

The resin viscosity and degree of cure at the bottom of composite panels fabricated with the advanced cure cycle and the step cure cycle are plotted as a function of time in Figs. 6.5.5- 6.5.6, respectively. No FDEMS measurements were taken during the fabrication of the panels. The temperature at the bottom of the panels is plotted as a function of time in the respective figures.

The RTM model generated cure cycles significantly reduced the time required by the resin to gelate, and the time required to complete cure (degree of cure > 0.90). Panels fabricated with the manufacturer's cure cycle gelled in 132.5 minutes and cured in 240 minutes (Fig. 6.5.3). In comparison, the rapid cure cycle panels gelled in 76.5 minutes
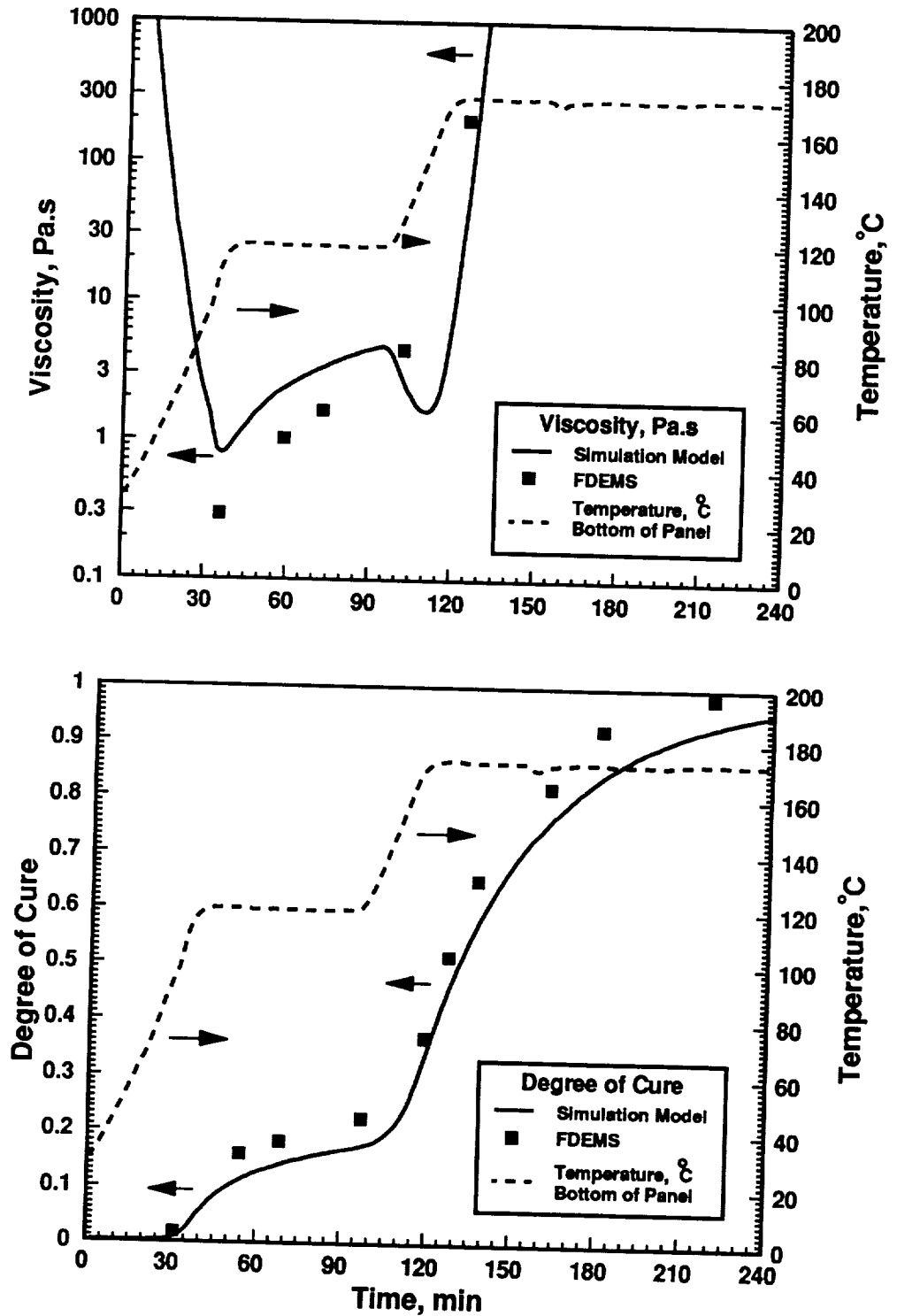
Figure 6.5.3   Resin viscosity and degree of cure as a function of time at the bottom of a 16 ply TTI IM7/8HS/Hercules 3501-6 composite panel fabricated at 276 kPa with the manufacturer's cure cycle.
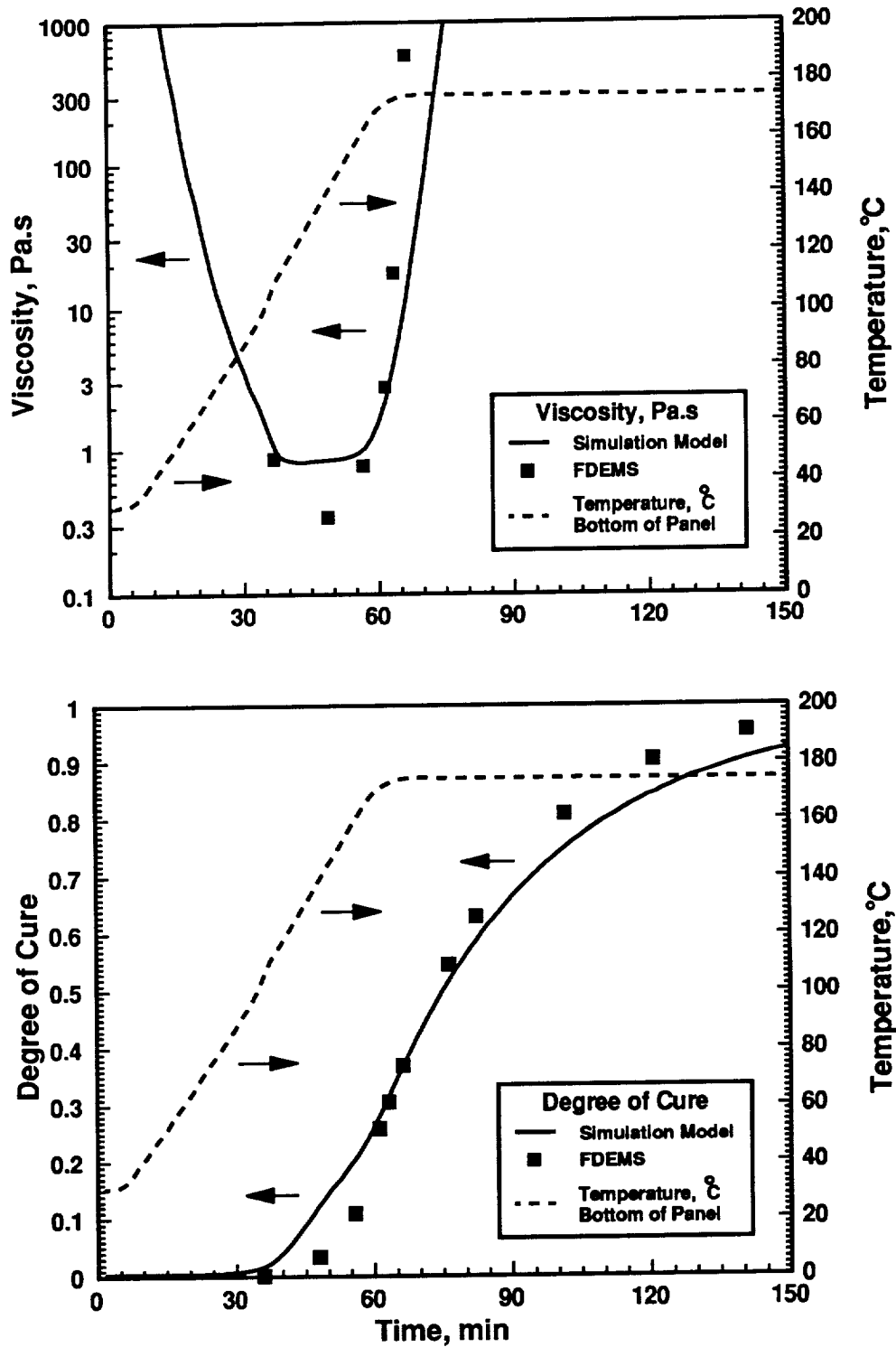
Figure 6.5.4 Resin viscosity and degree of cure as a function of time at the bottom of a 16 ply TTI IM7/8HS/Hercules 3501-6 composite panel fabricated at 551 kPa with the rapid cure cycle.

TTI IM7/8HS Material Evaluation
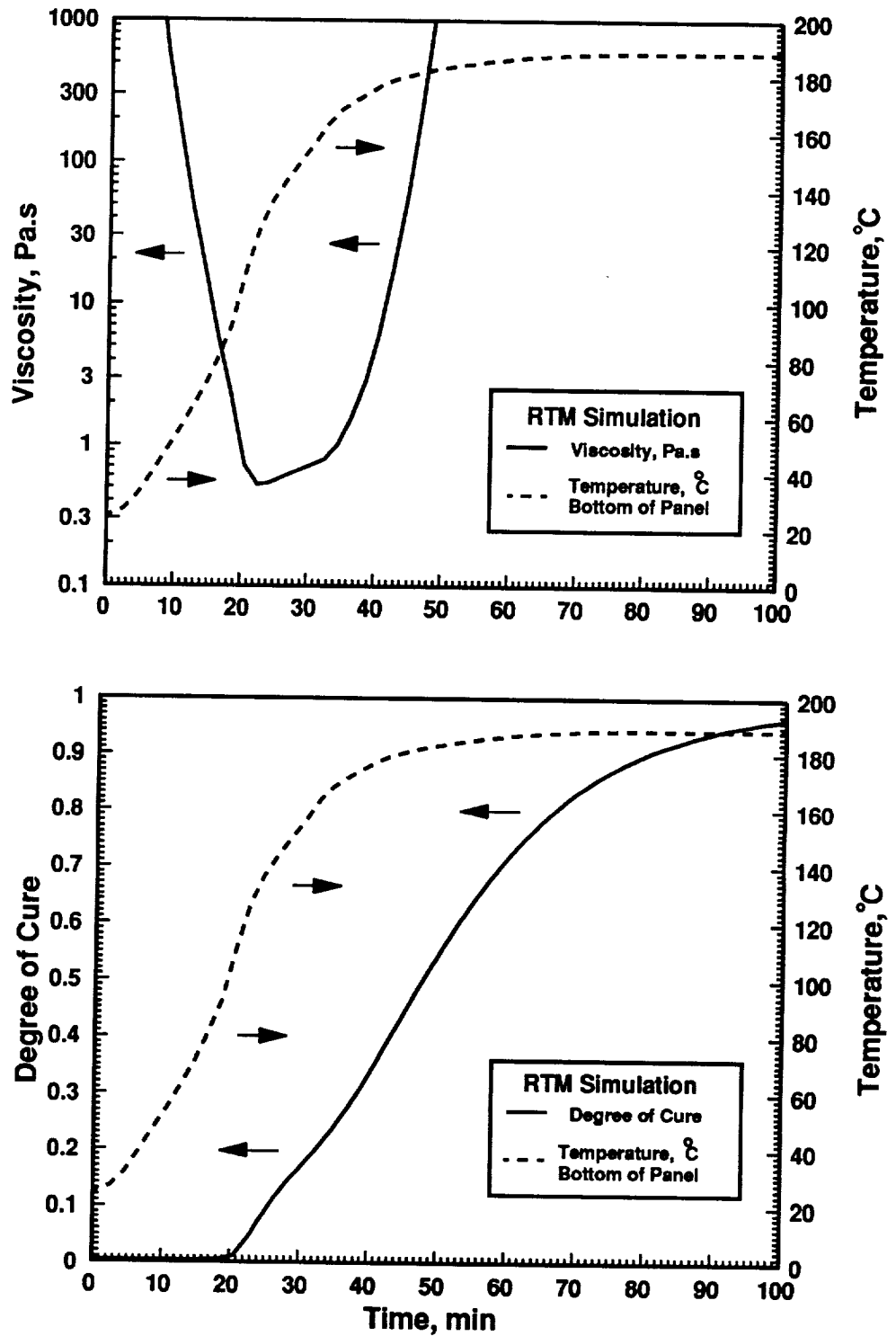
Figure 6.5.5  *Resin viscosity and degree of cure as a function of time at the bottom of a 16 ply TTI IM7/8HS/Hercules 3501-6 composite panel fabricated at 174 kPa with the advanced cure cycle.*
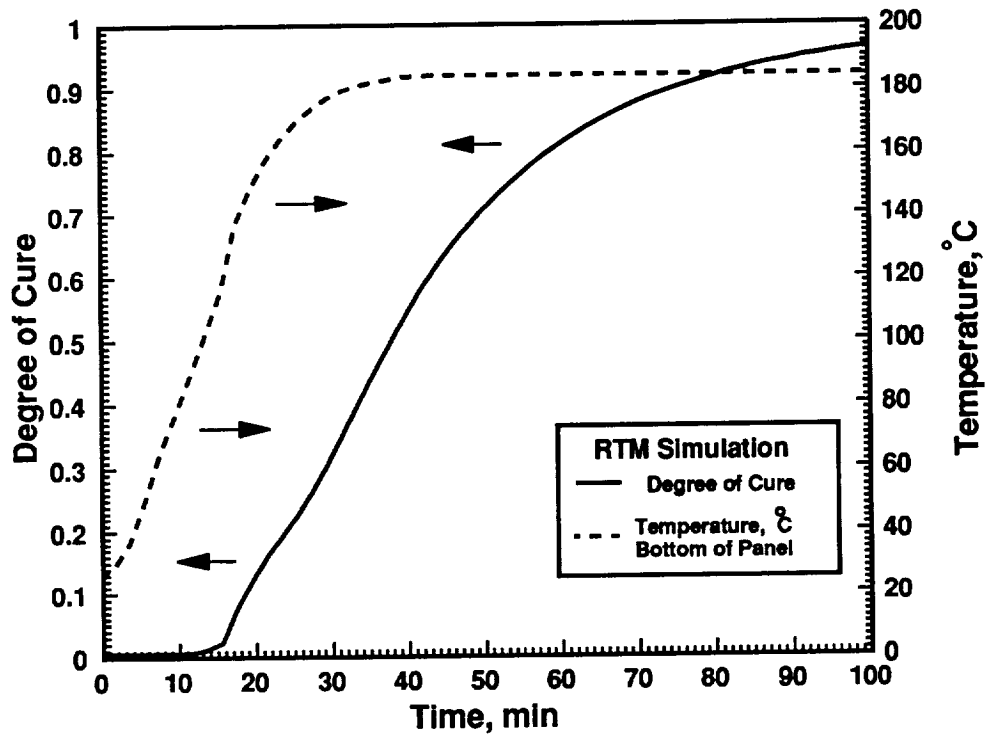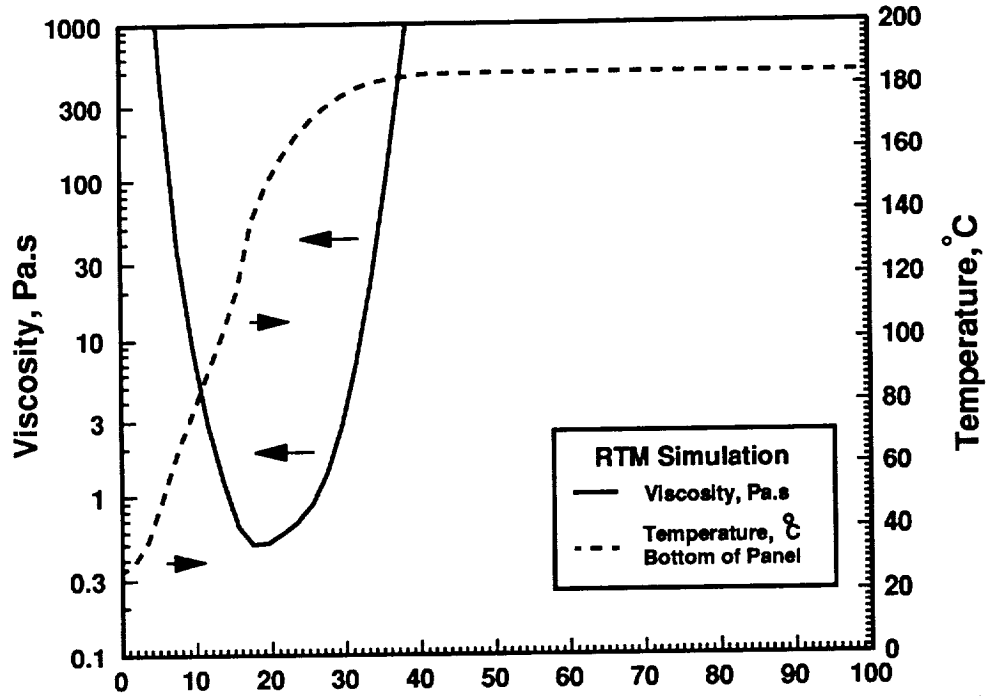
*Figure 6.5.6 Resin viscosity and degree of cure as a function of time at the
bottom of a 16 ply TTI IM7/8HS/Hercules 3501-6 composite panel
fabricated at 551 kPa with the step cure cycle.*

and cured in 155 minutes (Fig. 6.5.4), the advanced cure cycle panel (Fig. 6.5.5) gelled in 47.2 minutes and cured in 105 minutes, and the step cure cycle panel (Fig. 6.5.6) gelled in 39.5 minutes and cured in 95 minutes.

The length of the flow window also significantly decreased. The manufacturer's cure cycle panel had a flow window of 123.7 minutes, while the rapid cure cycle, advanced cure cycle, and step cure cycle panels had flow windows of 64.5, 41, and 35 minutes, respectively.

## 6.6 Infiltration Simulation

The effect of different temperature cure cycles and processing pressures on resin infiltration of 16 ply TTI IM7/8HS fabric preforms with Hercules 3501-6 resin was investigated. Experimental measurements of the flow front position as a function of time and the total infiltration time will be compared to RTM simulation model predictions to determine the validity of both the model and the fabric characterization study.

The RTM film infusion technique was used to fabricate 16 ply TTI IM7/8HS/Hercules 3501-6 panels with a single step compaction pressure application and either the manufacturer's cure cycle or a model generated advanced cure cycle (Table 4.6.1). During fabrication, the resin flow front position was measured as a function of time using the techniques presented in Section 4.7. The compaction and permeability characteristics of the TTI IM7/8HS fabric preform (Section 6.1-6.3) were incorporated into the model. The RTM simulation model was then used to simulate the nonisothermal infiltration of the panel and the results were compared to experimental data.

The normalized flow front position is plotted as a function of time for selected 16 ply TTI IM7/8HS/Hercules 3501-6 panels in Figs. 6.6.1 - 6.6.3. The model predicted resin viscosity at the flow front is plotted as a function of time on each of the respective figures. The model predictions of the normalized flow front position agrees well with the experimental measurements. Disagreements between the model predictions and experimental measurements may be caused by an incorrect measurement of the position
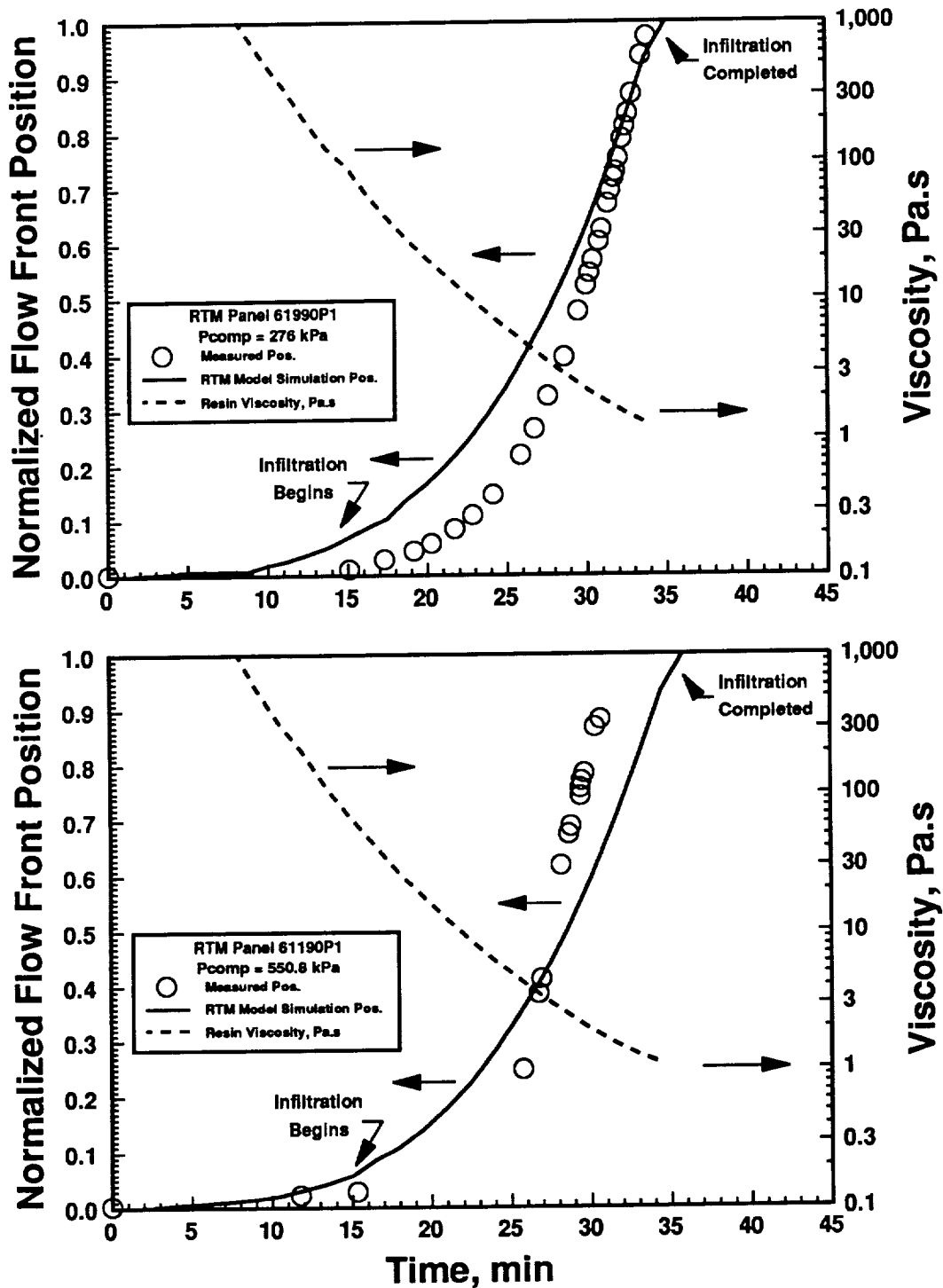
Figure 6.6.1 Normalized flow front position and resin viscosity as a function of time for 16 ply TTI IM7/8HS/Hercules 3501-6 composite panels fabricated at different compaction pressures with the manufacturer's cure cycle.
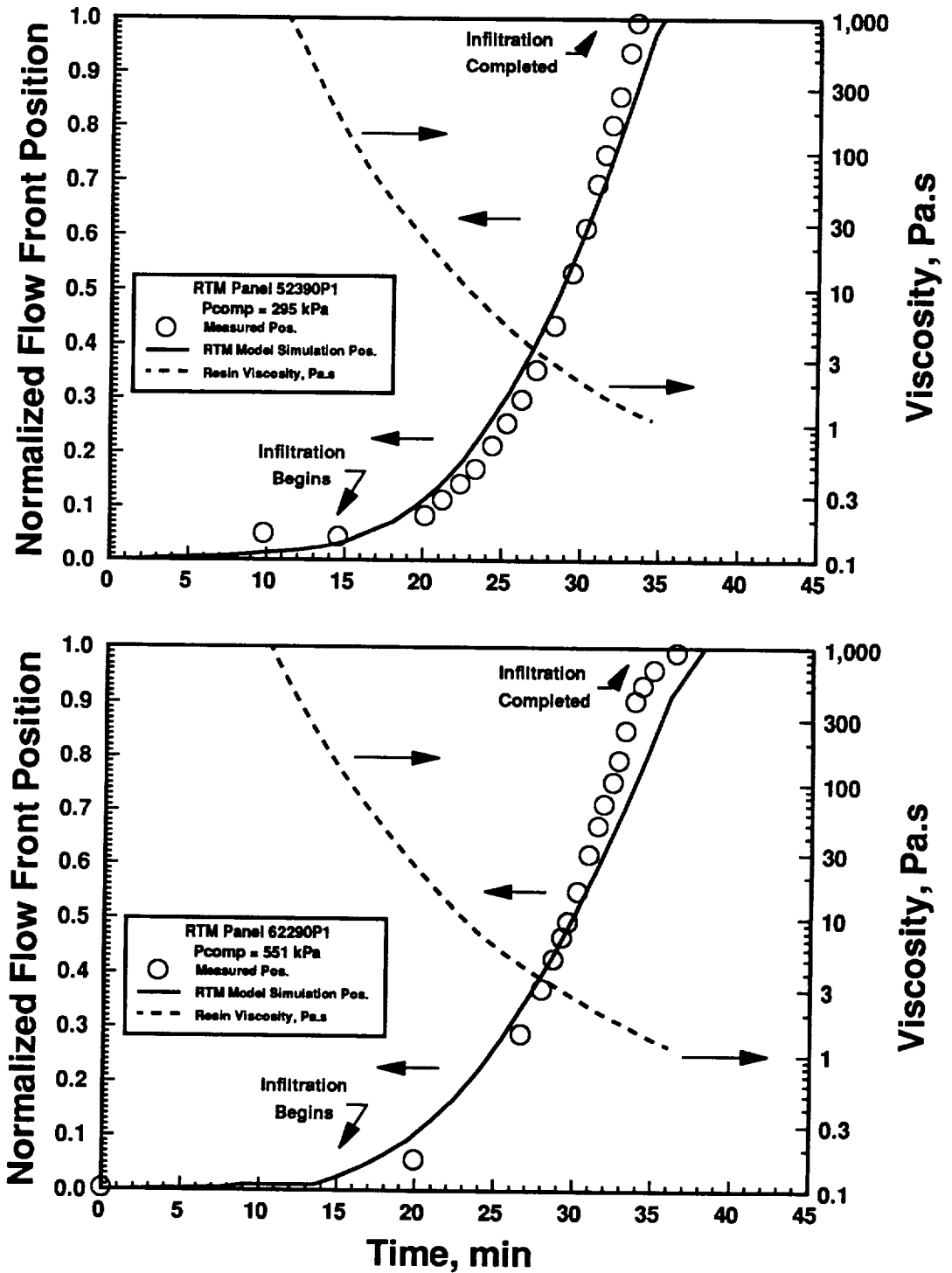
*Figure 6.6.2 Normalized flow front position and resin viscosity as a function of time for 16 ply TTI IM7/8HS/Hercules 3501-6 composite panels fabricated at different compaction pressures with the rapid cure cycle.*
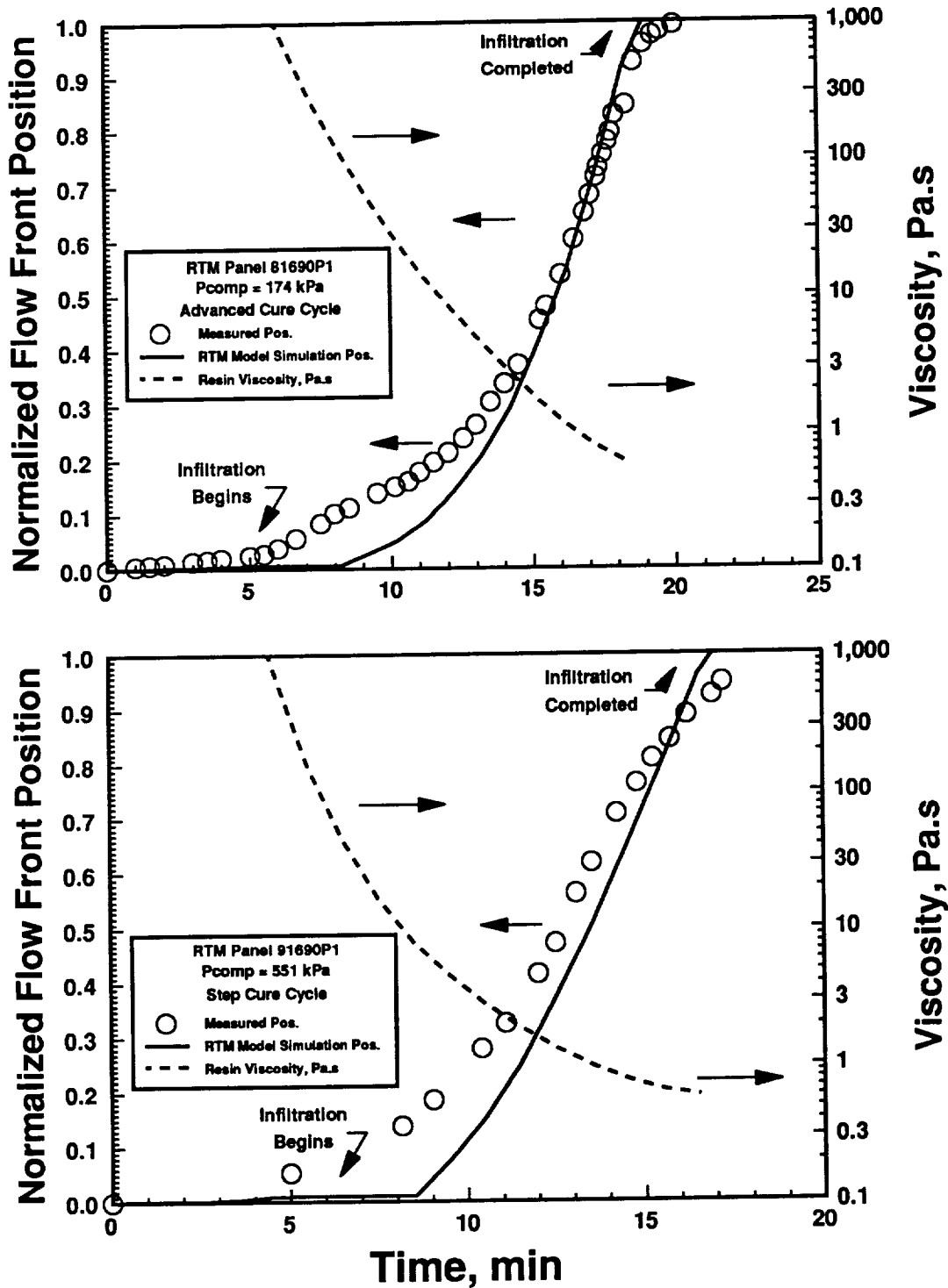
*Figure 6.6.3* *Normalized flow front position and resin viscosity as a function of time for 16 ply TTI IM7/8HS/Hercules 3501-6 composite panels fabricated at different compaction pressures with the cure cycles shown.*

of the flow front or an incorrect prediction of the resin viscosity, which greatly affects the model prediction of the flow front position. It is believed that the permeability constants utilized in the RTM simulations were correct since the model simulations of the flow front position matched the measured results for a number of panels.

The effect of the processing pressure on the rate of infiltration was investigated. Infiltration data obtained from panels fabricated with the manufacturer's cure cycle showed no significant change in the position of the infiltration as a function of time with increasing compaction pressure, (see Fig. 6.6.1). Results obtained from panels fabricated using the RTM model generated rapid cure cycle (Table A.3.1) indicate that the panel processed at 551 kPa has a greater resistance to flow (delayed flow front profile) in comparison to a panel fabricated at 295 kPa, (see Fig. 6.6.2). The infiltration of the low pressure (276 kPa and 295 kPa) panels initiated when the viscosity dropped below 1000 Pa.s (10 minutes into the cure cycle). Panels fabricated at 551 kPa were initially infiltrated 15 minutes into the cure cycle when the resin viscosity dropped below 300 Pa.s. The lower viscosities and longer times required for infiltration to initiate indicate a higher resistance to flow (relative to the applied compaction pressure). As with the Hexcel Hi-Tech panel infiltration results (Section 5.6), most of the infiltration of the 16 ply TTI IM7/8HS/Hercules 3501-6 panels occurred when the resin viscosity dropped below 10 Pa.s.

The effect of the heating rate on the infiltration was investigated through the use of the advanced cure cycle and step cure cycle, (see Table 4.6.1). The manufacture's cure cycle and the rapid cure cycle panels had the same heating rate (3 °C/min). Therefore, composite panels fabricated using these cycles have similar flow front profiles when identical compaction pressures were used. Results obtained from panels fabricated with higher temperature ramp rates (6-7 °C/min) are shown in Fig. 6.6.3. The higher temperature ramp rates decreased the time required for full infiltration by a factor of 2.

The total infiltration times for the 16 ply TTI IM7/8HS/Hercules 3501-6 composite panels are presented as a function of compaction pressure and processing conditions in Fig. 6.5.4. The RTM simulation model predictions of the total infiltration time were
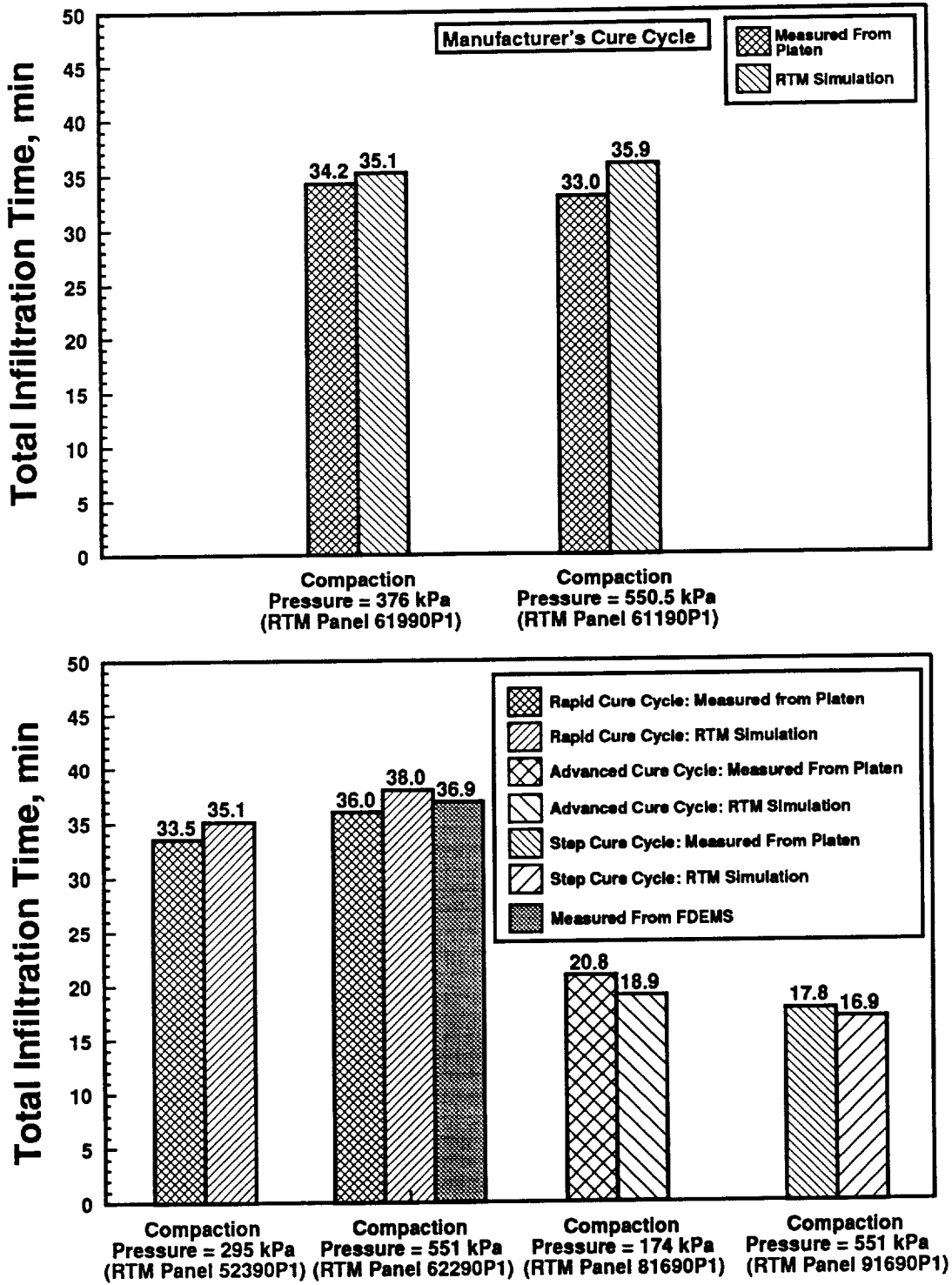
Figure 6.6.4 Total infiltration times for 16 ply TTI IM7/8HS/Hercules 3501-6
composite panels fabricated under the conditions shown.

TTI IM7/8HS Material Evaluation

within 9% of the experimental results. The temperature heating rate had the greatest overall effect on the time required for complete infiltration. The compaction pressure (for the ranges investigated) had a smaller effect on total infiltration time.

The higher heating rates decreased the overall infiltration time by decreasing the time for the resin viscosity to decrease to a minimum value. The effect of the applied compaction pressure on the infiltration process is negligible due to the relationship between the preform porosity and through-the-thickness permeability. When the preforms are compacted to lower porosities, the resistance to resin flow through the preform increases offsetting the corresponding gain in infiltration pressure.

## 6.7 Non Destructive Evaluation

TTI IM7/8HS/Hercules 3501-6 panels were evaluated by non-destructive methods. Photomicrographs were taken at 40X and 400X from specimens obtained from each panel (Fig. 4.9.1). The photomicrographs were analyzed to determine the effect of processing pressure on the composite microstructure and to detect the presence of porosity. Ultrasonic C-scans were taken at 10 MHz to detect the presence of porosity and non-uniform resin distributions in the panels. The effects of the temperature cure cycle and processing pressure on the microstructure of 16 ply TTI IM7/8HS/Hercules 3501-6 panels will be discussed.

The effect of processing pressure on consolidation of TTI IM7/8HS/Hercules 3501-6 panels fabricated using either the manufacturer's cure cycle or the rapid cure cycle was investigated. Cross-sectional photomicrographs (40X) of composite specimens fabricated at 276 kPa with the manufacturer's cure cycle (Table A.3.1, Appendix A) and at 551 kPa with the rapid cure cycle are presented on the top and bottom of Fig. 6.7.1, respectively. The photomicrographs show a clear relationship between the applied compaction pressure and fiber bed consolidation. As higher compaction pressures were applied, the thickness of the specimens decreased and the individual tows consolidated together and straightened out. The resin rich regions disappear at high compaction pressures (see bottom of Fig.

(RTM Panel 61990P1)   (40X)
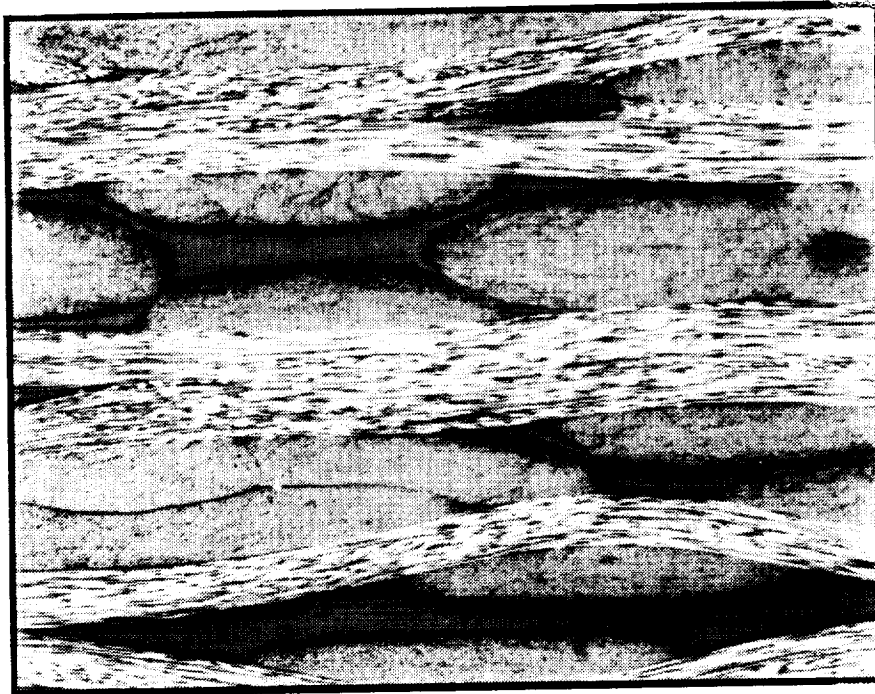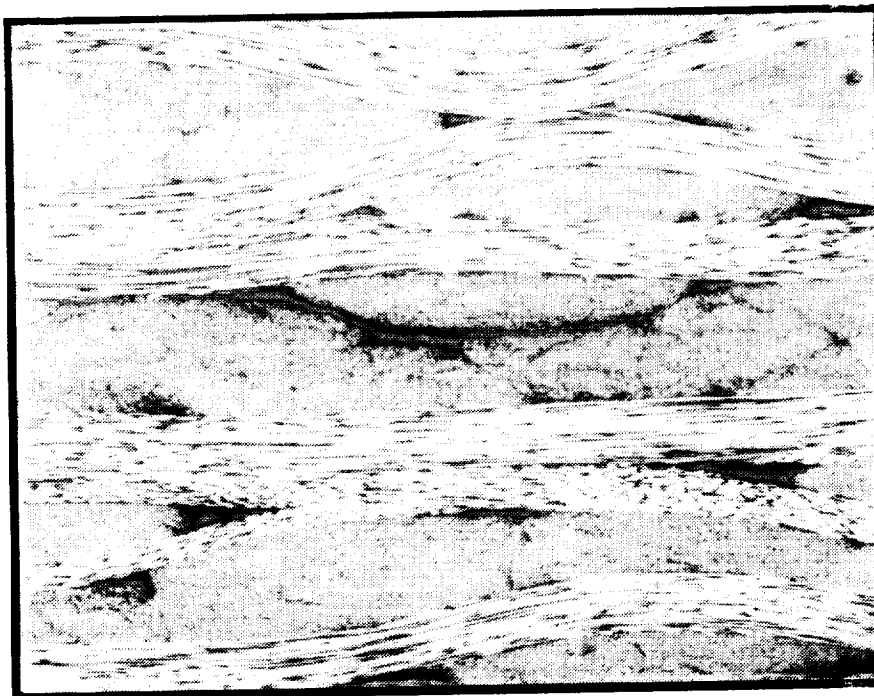
**Tow Orientation**

90 °

0 °



(RTM Panel 62290P1)   (40X)

**Tow Orientation**

90 °

0 °

*Figure 6.7.1  Photomicrographs of 16 Ply TTI IM7/8HS/Hercules 3501-6 composite panels.*

**TTI IM7/8HS Material Evaluation**

ORIGINAL PAGE
BLACK AND WHITE PHOTOGRAPH

5.7.1). All of the panels investigated were found to be free of porosity and the only visible difference in the microstructure of the panels resulted from use of different processing pressures.

Ultrasonic C-scans (with response scale), photomicrographs (400 X), and test specimen orientation diagrams of selected 16 ply TTI IM7/8HS/Hercules 3501-6 panels are shown in Figs. 6.7.2 and 6.7.3. The white regions of the C-scans correspond to void free, uniformly infiltrated areas. The three black dots under each C-scan were the support pins. Panels fabricated at similar processing pressures had identical test sample orientations for convenience.

The effect of the temperature cure cycle and processing pressure on the panel quality was determined by comparing the NDE results for a panel fabricated at 276 kPa with the manufacturer's cure cycle (Fig. 6.7.2) and a panel fabricated at 551.5 kPa with the rapid cure cycle (Fig. 6.7.3). Both panels had identical C-scans and were found to be generally free of major defects. The edges and FDEMS locations were found to have a great deal of microporosity, as seen by the dark region of the C-scans. Mechanical test specimens were obtained from the void free regions of each panels. The local photomicrographs revealed a void free, fully saturated fiber bed.

In summary, the manufacturer's and rapid cure cycle panels were found to have an excellent overall quality, regardless of the applied compaction pressure. The use of higher processing pressures was found to increase the consolidation of individual fiber bed tows and plies.

## 6.8 Destructive Evaluation: Short Block Compression

The goal of the mechanical experiments was to determine the effects of different temperature cure cycles and processing pressures on the compressive properties of 16 ply TTI IM7/8HS/Hercules 3501-6 panels fabricated with the RTM film infusion technique. Five short block compression (SBC) specimens (Section 4.9) were obtained from each panel and loaded in compression to failure along either the warp or fill direction. Each

143



Top and
Bottom
FDEMS

Test Specimen Cutting
Diagram: 1/4 Scale
C: SBC Specimen
S: Iosipescu Shear
Specimen

90°

0°

Ply Orientation

C-Scan 1/2 Scale

61                              Signal Response                              2047



RTM
Panel
61990P1
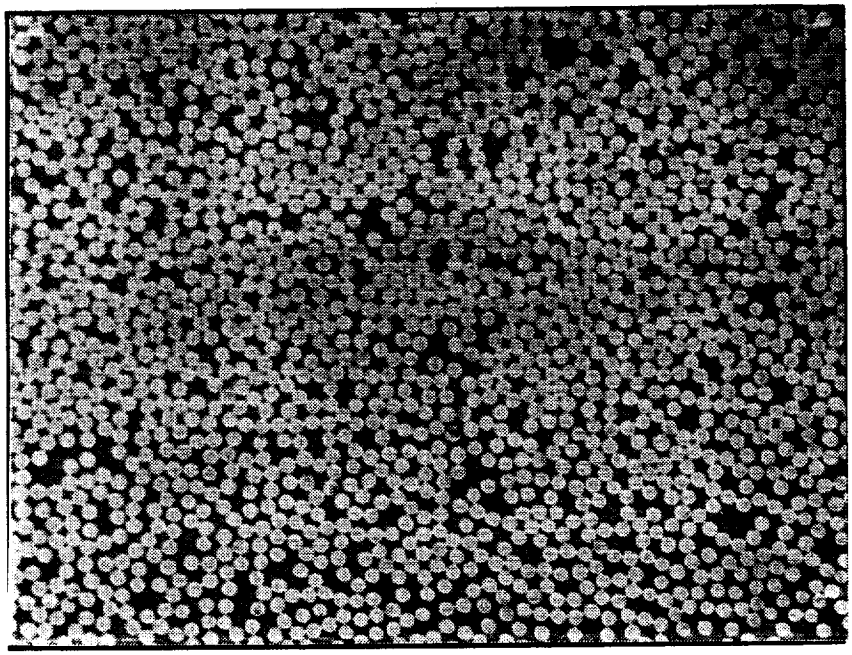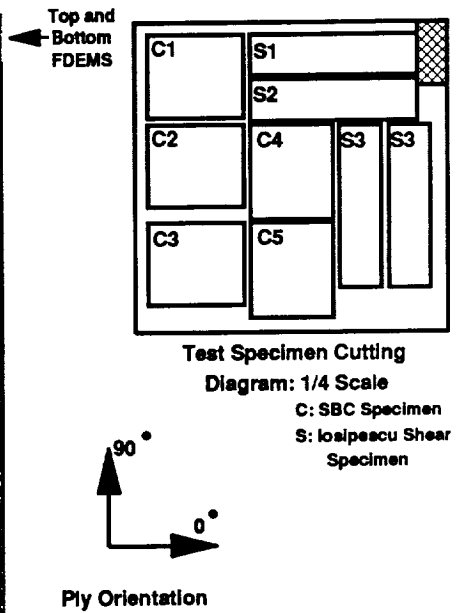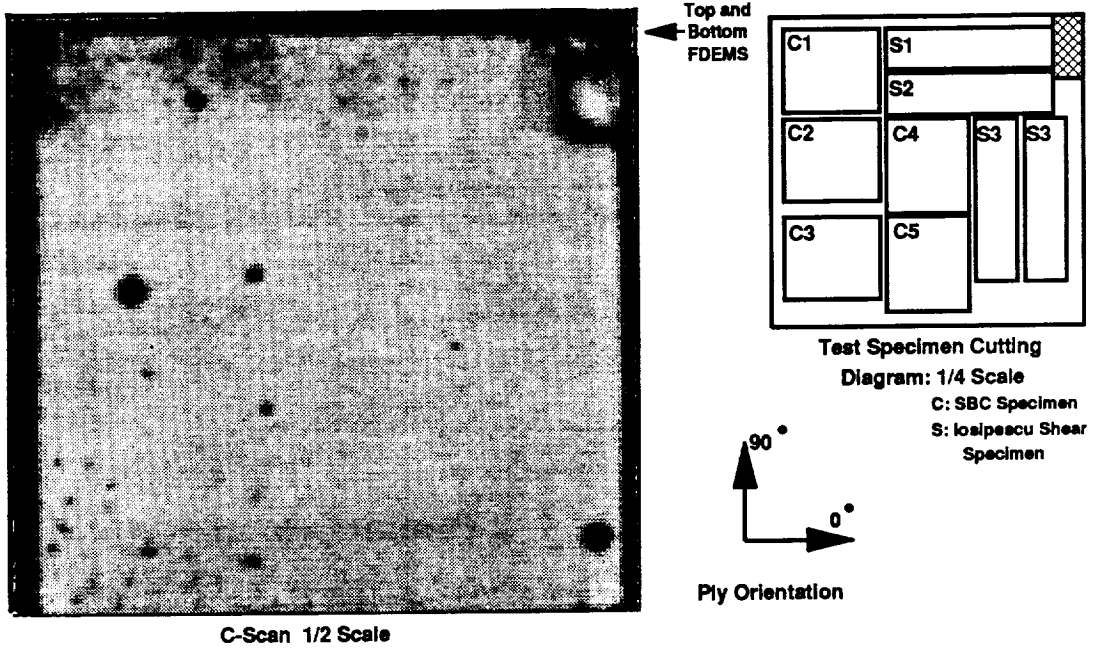
Photomicrograph                                                    (400X)

*Figure 6.7.2   C-scan, test specimen diagram, and photomicrograph of a
16 ply TTI IM7/8HS/Hercules 3501-6 composite panel
fabricated at 276 kPa with the manufacturer's cure cycle.*

**TTI IM7/8HS Material Evaluation**

C-Scan 1/2 Scale

Top and Bottom FDEMS —

Test Specimen Cutting
Diagram: 1/4 Scale
C: SBC Specimen
S: Iosipescu Shear
Specimen

90°

0°

Ply Orientation

62  **Signal Response**  2047

RTM
Panel
62290P1

**Photomicrograph**

**(400X)**
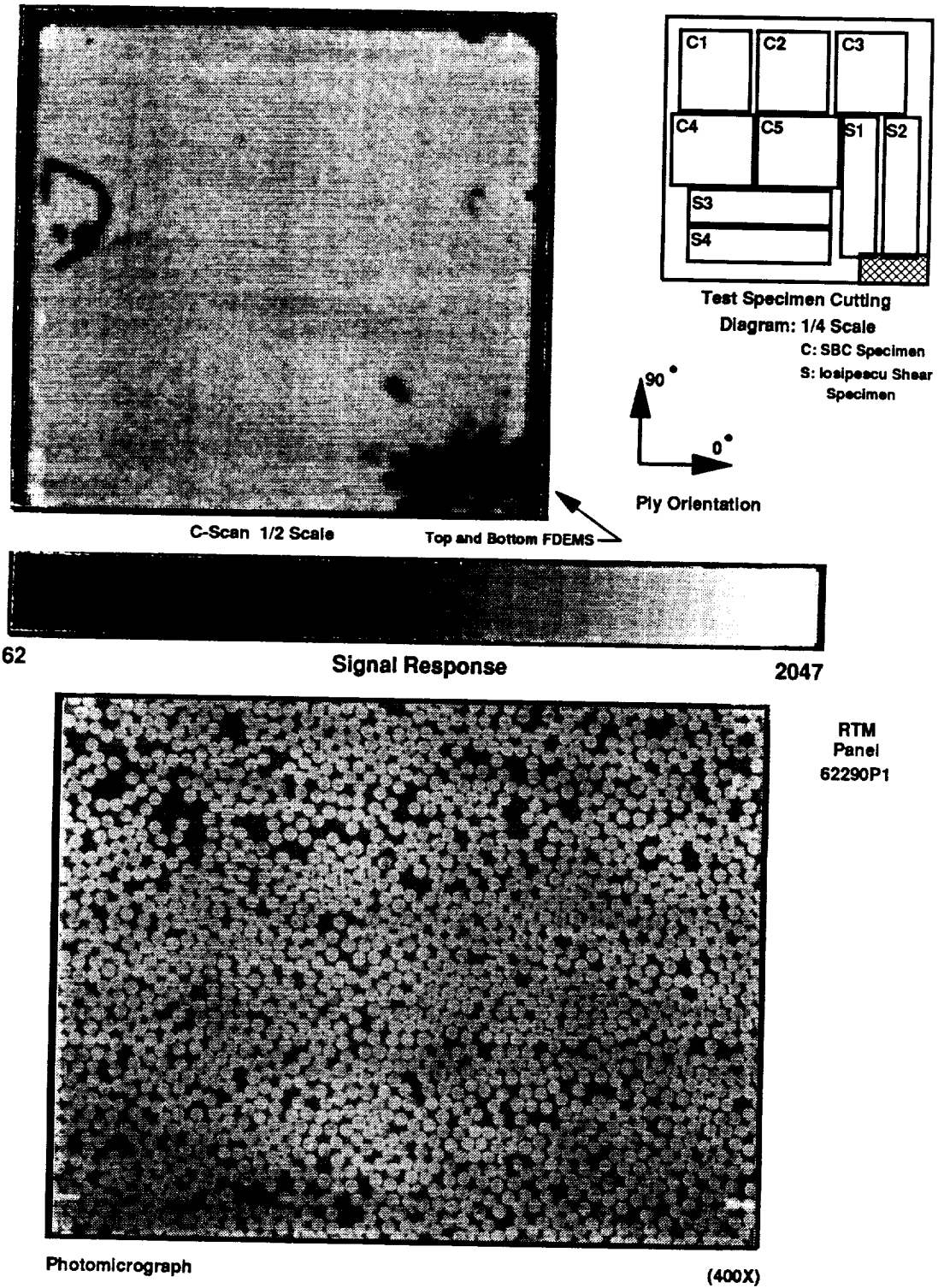
*Figure 6.7.3  C-scan, test specimen diagram, and photomicrograph of a
16 ply TTI IM7/8HS/Hercules 3501-6 composite panel
fabricated at 551 kPa with the rapid cure cycle.*

**TTI IM7/8HS Material Evaluation**

SBC specimen contained an equal number of filament tows in the $0°$ and $90°$ direction. The compressive strength, ultimate longitudinal strain, Poisson's ratio at 0.2% longitudinal strain, and Young's modulus at 0.2% longitudinal strain were obtained from each specimen using the techniques presented in Section 4.9. Results obtained from the SBC specimens evaluated in compression along the warp and fill directions were found to be identical, and were subsequently averaged together.

The failure surfaces of the 16 ply TTI IM7/8HS/Hercules 3501-6 SBC specimens were similar in appearance. A photomicrograph of a SBC specimen is given in Fig. 6.8.1. All of the SBC specimens experienced extensive delamination and transverse shear failure. The failure surfaces were located at the middle of the specimens away from the upper and lower grips of the compression fixture.

The compressive strength and ultimate longitudinal strain of the 16 ply TTI IM7/8HS/Hercules 3501-6 SBC specimens are presented as a function of fiber volume fraction and processing conditions in Fig. 6.8.2. The Poisson's ratio at 0.2% longitudinal strain and Young's modulus at 0.2% longitudinal strain obtained from the SBC specimens are presented on the top and bottom of Fig. 6.8.3, respectively. The compressive strength, ultimate longitudinal strain and Young's modulus of AS4/8HS/Hercules 3501-6 prepreg SBC specimens are presented on the respective figures. The compression strength, ultimate longitudinal strain, Poisson's ratio, and Young's modulus data from each SBC specimen are presented in tabular from in Appendix D.1.

The compressive properties of the 16 ply TTI IM7/8HS/Hercules 3501-6 SBC specimens fabricated with the rapid cure cycle were found to be almost identical to the properties obtained from SBC specimens with the manufacturer's cure cycle. The rapid cure cycle SBC specimens were found to have a 1.5% higher compressive strength, a 4% higher ultimate longitudinal strain, and a 4% lower Young's modulus when compared with the manufacturer's cure cycle SBC specimens.

The effect of the processing pressure on the compression properties was found to be significant. Panels fabricated at 279 kPa with the manufacturer's cure cycle were found to have a 4.5% lower compressive strength, a 11% lower ultimate longitudinal strain, and

ORIGINAL PAGE
BLACK AND WHITE PHOTOGRAPH



(RTM Panel 62290P1)

(7.5X)

*Figure 6.8.1  Failure surface of a 16 Ply TTI IM7/8HS/Hercules 3501-6
SBC specimen.*

**TTI IM7/8HS Material Evaluation**
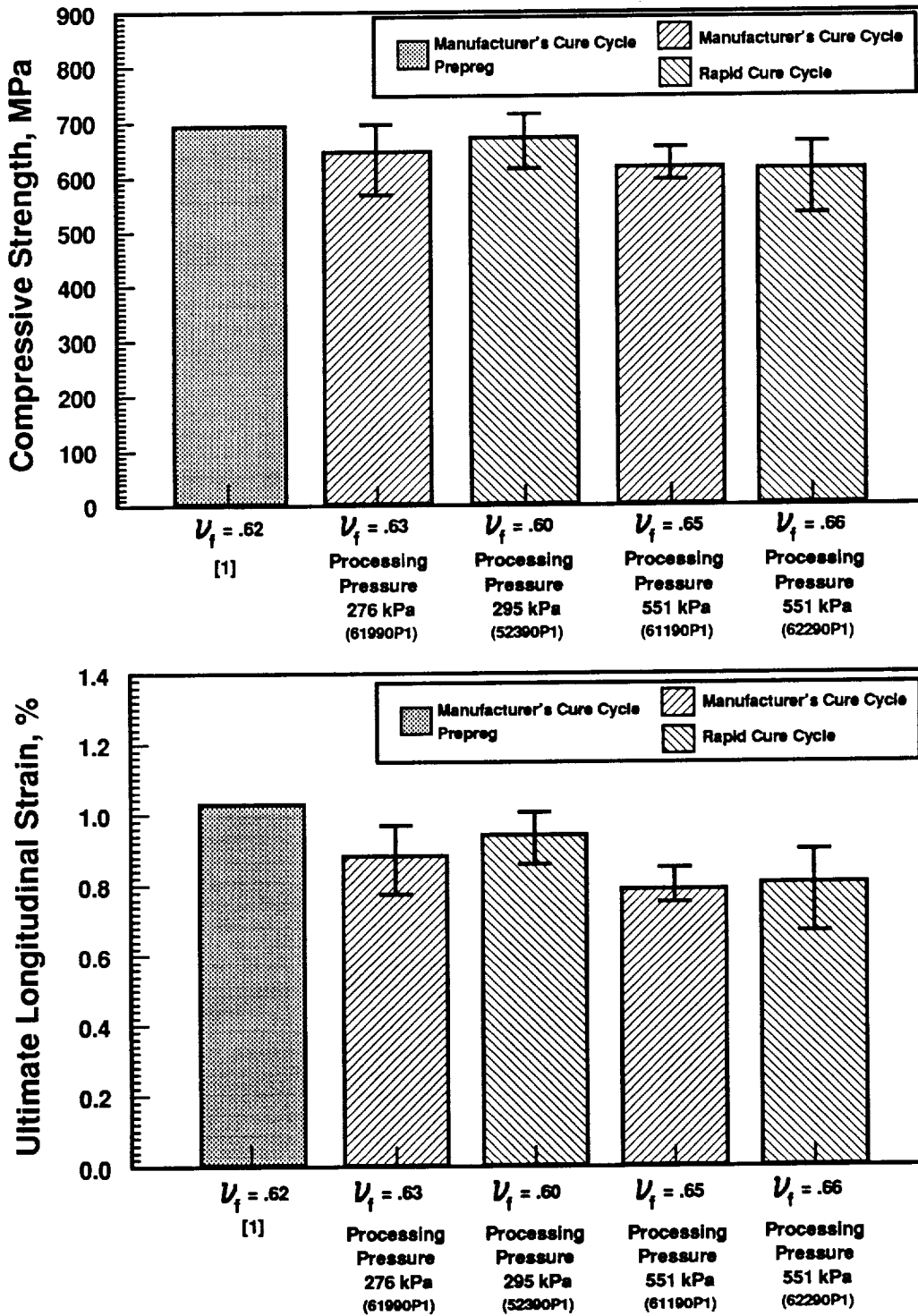
Figure 6.8.2    Compressive strength and ultimate longitudinal strain
of 16 ply TTI IM7/8HS/Hercules 3501-6 SBC specimens.
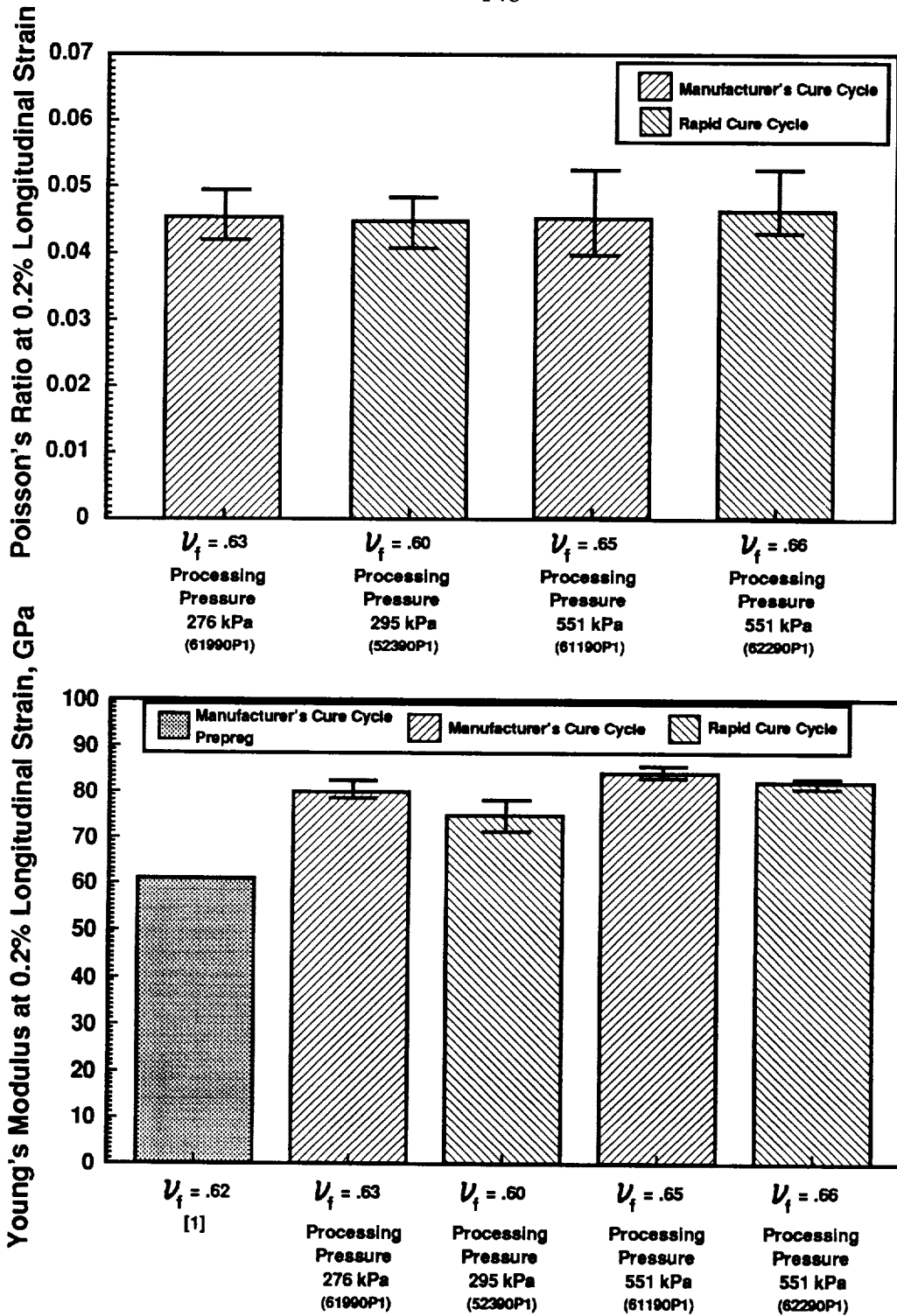
*Figure 6.8.3* Poisson's ratio and Young's modulus at 0.2% longitudinal strain
obtained from 16 ply TTI IM7/8HS/Hercules 3501-6 SBC specimens.

TTI IM7/8HS Material Evaluation

a 5% higher Young's modulus than similar SBC specimens fabricated at 551 kPa. It was apparent that the best compressive strength and ultimate longitudinal strain were obtained from SBC specimens fabricated at low pressures (276 kPa or 290 kPa) with either the manufacturer's cure cycle or the RTM model generated rapid cure cycle.

## 6.9 Destructive Evaluation: Iosipescu Shear

The Iosipescu shear test was used to evaluate the effects of temperature cure cycles and processing pressures on the shear properties of 16 ply TTI IM7/8HS/Hercules 3501-6 panels fabricated by RTM. Iosipescu shear test specimens (Section 4.9), taken from each panel, were tested in shear until failure. The specimens were evaluated with either the warp or fill tows perpendicular to the direction of the applied load (see Fig. D.2.1, Appendix D). The shear strength and the shear modulus at 0.2% shear strain were determined from each specimen using the techniques presented in Section 4.9. Iosipescu shear specimens tested in different orientations were found to have identical shear properties, and subsequently the results were averaged together.

The failure surfaces of the manufacturer's cure cycle specimens and the rapid cure cycle specimens were identical. All of the failed specimens had transverse delaminations at the 0°/90° tow interfaces as exemplified in the photomicrograph of an Iosipescu shear specimen fabricated at 276 kPa with the rapid cure shown in Fig. 6.9.1. All of the specimens experienced an increase in thickness at the notch location prior to failure.

The shear strengths and shear moduli at 0.2% shear strain of the 16 ply TTI IM7/8HS/Hercules 3501-6 Iosipescu shear specimens are presented in Fig. 6.9.2 as a function of fiber volume fraction and processing conditions. The shear strength and shear modulus (at 0.2% shear strain) data for each of the individual Iosipescu shear specimens are presented in tabular form in Appendix D.2. As with the Hexcel Hi-Tech Warp Knit/Hercules 3501-6 Iosipescu shear specimens (Section 5.9), all of the strain rosettes failed prior to the failure of the specimens.

The rapid cure cycle Iosipescu specimens were found to have a 2% higher ultimate

150



(RTM Panel 61990P1)        (18X)

*Figure 6.9.1 Failure surface of a 16 ply TTI IM7/8HS/Hercules 3501-6 Iosipescu shear specimen, (at notch).*

TTI IM7/8HS Material Evaluation
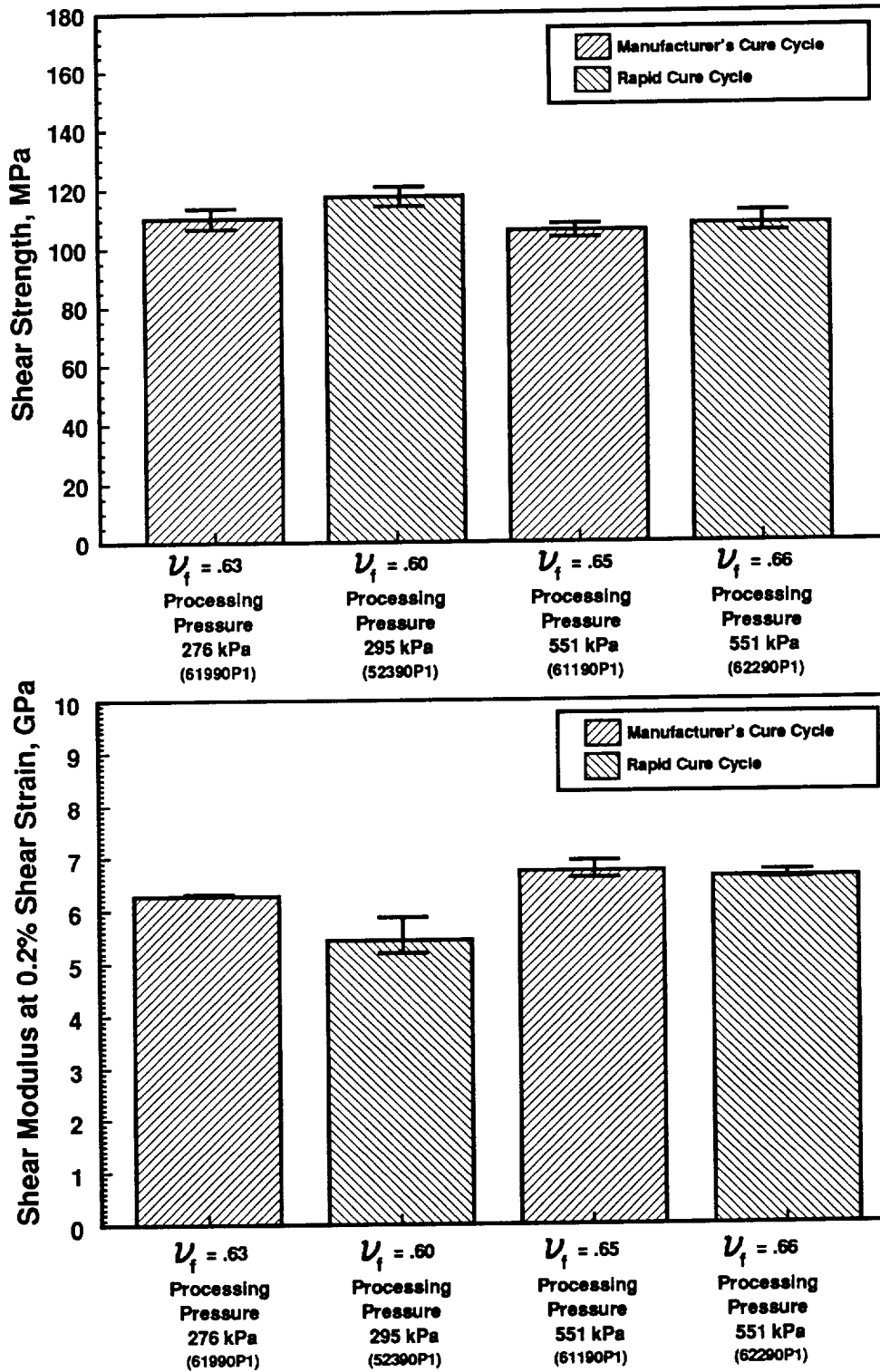
*Figure 6.9.2  Shear strengths and shear moduli of 16 ply TTI IM7/8HS/Hercules 3501-6 Iosipescu shear specimens fabricated with the conditions shown.*

shear strength and a 1.4% lower shear modulus when compared to the manufacturer's cure cycle specimens (similar fiber volume fractions). The high processing pressure (551 kPa) specimens were generally found to have a lower ultimate shear strength and shear modulus.

# 7.0 Conclusions and Future Work

The RTM film infusion technique was successfully developed and utilized to fabricate advanced textile composites from knitted, knitted/stitched, and 2-D woven preforms with a standard epoxy resin system.

Experiments were performed to characterize the compaction and permeability behavior of textile preforms. The deflection of dry preforms was found to be greater than the deflection of wet preforms. Preforms subjected to slow compaction rates acquired the greatest deflection. The fabric preform deflection as a function of applied compaction pressure was successfully modeled with a 4th order least squares polynomial. Relationships were then developed to model the fabric preform thickness, fiber volume fraction, and resin mass at full saturation as a function of the compaction pressure.

All of the test samples examined followed D'arcy's law for through-the-thickness flow. The modified Gebart equation was fit to the through-the-thickness permeability verses porosity data for the knitted and 2-D woven fabric preforms. The Kozeny-Carman relationship was fit to the through-the-thickness permeability verses porosity data of the knitted/stitched fabric preforms.

A model was developed to simulate the infiltration and cure of advanced textile composites fabricated with the RTM film infusion technique. The model was successfully used to predict the final thickness and fiber volume fraction of textile composites to within 7% of measured values and the resin mass within 11% of the measured values. The model prediction of the position of the infiltration front as a function of time correlated well with the experimental results. The total infiltration times obtained from the model were within 12% of the experimentally measured values. The measured and calculated temperature distributions in the RTM layup agreed well for the four different cure cycles. Finally, the model predictions of the resin viscosity and degree of cure correlated with the experimentally measured results obtained from frequency dependent electromagnetic sensors (FDEMS).

Temperature cure cycles, developed with the RTM simulation model, were used to

significantly reduce the cure cycle time and the total time for infiltration. The temperature cure cycle heating rate greatly influenced the rate of resin infiltration and total infiltration time. When the heating rate was increased from 3 °C/min to 7 °C/min, the total infiltration time was reduced by a factor of 2 for panels processed at similar pressures.

Non-destructive evaluation techniques consisting of ultrasonic C-scans and micrographs were utilized to evaluate the overall quality of the panels fabricated for this study. C-scans were able to evaluate the quality of knitted and 2-D woven composite panels. However, the C-scans were ineffective at evaluating the quality of knitted/stitched composite panels due to the distortion created by the through-the-thickness carbon stitches.

Micrographs revealed a large amount of microcracks in the knitted/stitched panels and resin pockets near the stitches. The knitted and 2-D woven panels contained very few microcracks. The consolidation and fiber packing arrangement in the three different types of fabric preforms evaluated for this study was directly visible.

Short block compression (SBC) and Iosipescu shear specimens were utilized to evaluate the compression and shear mechanical properties of the panels. SBC and Iosipescu shear specimens processed at similar pressures with different cure cycles to the same state of cure had nearly identical compression and shear mechanical properties. The high processing pressure (high fiber volume fraction) SBC and Iosipescu shear specimens obtained from the TTI IM7/8HS panels were found to have lower strengths and higher moduli when compared with specimens fabricated at low processing pressures (low fiber volume fraction). The compressive properties of the knitted/stitched SBC specimens appeared to be unaffected by the processing pressure and corresponding fiber volume fraction. The low processing pressure Iosipescu shear specimens were found to have the best shear mechanical properties. The knitting and stitching of the Hexcel fabric preforms led to a reduction in the compression strength but a corresponding increase in the shear strength.

**Conclusions and Future Work**

Possible future objectives for this study include the following:

1) Introduce new thermoset resins and cyclic thermoplastics into the study.

2) Use the RTM film infusion technique to manufacture complex shape textile composites and update the RTM simulation model to simulate the new processing techniques.

3) Analyze the compaction and permeability characteristics of 3-D woven or braided fabric preforms.

4) Investigate and analyze in-plane infiltration.

# Bibliography

[1] Claus, S.J. and Loos, A.C., "A Cure Process Model for Resin Transfer Molding of Advanced Composites," **CCMS-89-07**, April 1989, VPI & SU, Blacksburg, VA 24061.

[2] Gauvin, R., Chaibaini, M., and LaFontaine, P., "The Modeling of Pressure Distribution in Resin Transfer Molding," **41st Annual Conference Reinforced Plastics/Composites Institute**, The Society of The Plastics Industry, Inc., Jan. 27-31, 1986.

[3] Chapman, A.J., *Heat Transfer*, 4th ed., Macmillan Publishing Company, New York, 1984.

[4] Loos, A.C. and Springer, G.S., "Curing of Epoxy Matrix Composites," **Journal of Composite Materials**, Vol. 17, 1983, pp. 135-169.

[5] Springer, G.S. and Tsai, S.W., "Thermal Conductivities of Unidirectional Materials," **Journal of Composite Materials**, Vol. 1, 1967, pp. 166-173.

[6] Lee, W.I., Loos, A.C., and Springer, G.S., "Heat of Reaction, Degree of Cure, and Viscosity of Hercules 3501-6 Resin," **Journal of Composite Materials**, Vol. 16, Nov 1982, pp. 510-520.

[7] Hou, T.H. and Bai, J.M., "A Semi-Empirical Approach for The Chemoviscosity Modeling of Reactive Resin System," **SAMPE Journal**, Vol. 24, No. 6, Nov/Dec 1988 pp. 43-51.

[8] Chiou, P. and Letton, A., "Reaction Kinetics and Chemoviscosity of a Thermoset Exhibiting Complex Curing Behavior," **Processing of Polymers and Polymeric Composites MD-Vol. 19, The Winter Annual Meeting of the American Society of Mechanical Engineers**, Dallas, Texas, November 25-30, 1990, pp. 35-48.

[9] Coulter, J.P. and Guceri, S.I., "Resin Impregnation During Composite Manufacturing: Theory and Experimentation," **Composites in Science and Technology**, Vol. 35., 1989, pp. 317-330.

[10] Young, W.B., Rupel, K., Han, K., Lee, J.L., and Liou, M.J., "Analysis of Resin Injection Molding in Molds with Preplaced Fiber Mats. II: Numerical Simulation and Experiments of Mold Filling," **Polymer Composites**, Vol. 12, No. 1, February 1991, pp. 30-38.

[11] Milovich, D. and Nelson, R.H., "Aerospace Resin Transfer Molding, A Multidisplinary Approach," **Resin Transfer Molding for The Aerospace Industry: SME**, March 6-7, 1990, pp. 1-18.

[12] Um, M.K. and Lee, W.I., "Numerical Solution of Resin Transfer Molding Process Using Boundary Element Method," **35th International SAMPE Symposium**, April 2-5, 1990, pp. 1905-1917.

[13] Gutowski, T.G. and Cai, Z., "The Consolidation of Composites," **Manufacturing International ' 88 Proceedings Volume IV, The Manufacturing Science of Composites**, Atlanta, Georgia, April 17-20, 1988, pp. 13-15.

[14] White, F.M., *Viscous Fluid Flow*, McGraw Hill, 1974.

[15] Dave, R., "A Unified Approach to Modeling Resin Flow During Composite Processing," **Journal of Composite Materials**, Vol. 24, January 1990, pp. 22-41.

[16] Williams, J.G., Morris, C.E.M., and Ennis, B.C., "Liquid Flow Through Aligned Fiber Beds," **Polymer Engineering and Science**, Vol. 14, No. 6, June 1974, pp. 413-419.

[17] Ahn, K.J. and Seferis, J.C., "Autoclave Resin Infusion Process: Analysis and Prediction of Resin Content," **SAMPE Quarterly**, Volume 31, No. 2., January 1990, pp 3-10.

[18] Scheidegger, A.E., *The Physics of Flow Through Porous Media*, 3rd Edition, University of Toronto Press, 1974.

[19] Gebart, B.R., "Permeability of Unidirectional Reinforcements for RTM," **SCICOMP Technical Report 90-006**, August 1990.

[20] Gutowski, T.G., "A Resin Flow/Fiber Deformation Model for Composites," **SAMPE Quarterly**, Vol. 16, No. 4, July 1985.

[21] Lam, R.C. and Kardos, J.L., "The Permeability of Aligned and Cross-Plied Fiber Beds During Processing of Continuous Fiber Composites," **Proceedings of The American Society for Composites Third Technical Conference, Integrated Composites Technology**, Seattle, WA, Sept. 25-29, 1988, pp. 3-11.

[22] Kim, Y.R., McCarthy, S.P., Fanucci, J.I., Nolet, S.C., Koppernaes, C., "Resin Flow Through Fiber Preforms During Composite Processing," **SAMPE Quarterly**, Vol. 22, No. 3, April 1991, pp. 16-22.

[23] Cook, R.D., *Concepts and Applications of Finite Element Analysis*, 2nd Edition, John Wiley & Sons, Inc., 1981.

[24] Reddy, J.N., *An Introduction To The Finite Element Method*, 1st Edition, McGraw Hill, 1984.

[25] Lambart, J.D., *Computational Methods in Ordinary Differential Equations*.

[26] Hercules Advanced Materials & Systems Company, **Product Data**, Magna, UT, 1990.

[27] Dexter, H.B., Hasko, G.H., and Cano, R.J., "Characterization of Multiaxial Warp Kn Composites," **First NASA Advanced Composites Technology Conference**, Seattle, Washingtoi October 29-November 1, 1990, pp 589-619. n

[28] Kranbuehl, D., Delos, S., Hoff,M., and Haverty, P., "Use of Frequency Dependence of The Impedance to Monitor Viscosity During Cure," **Polymer Eng. & Sci.**, vol. 29, No. 5, Ma 1989, pp 285-289. y

[29] Kranbuehl, D., Delos, S., Hoff,M., Weller, L., Haverty, P., and Seeley, J., "Dynamic Dielectric Analysis: Monitoring The Chemistry and Rheology During Cure of Thermosets," **ACS Division of Polymeric Materials: Science and Engineering**, vol. 56, 1987 pp. 163-168.

[30] Kranbuehl, D., "Cure Monitoring," *Encyclopedia of Composites*, S.M. Lee, ed. VCH Publishers, 1989, pp. 531-543.

[31] ACEE Composites Project Office, Compiler, "NASA/Aircraft Industry Standard

# Appendix A.1: RTM Film Infusion Technique

The RTM film infusion fabrication procedure for a composite panel composed of 16 plies of TTI IM7/8HS and Hercules 3501-6 resin is presented in the following outline. A single compaction pressure of 689.5 kPa and the resin manufacturer's cure cycle is applied during processing. The RTM simulation model is utilized to predict the fabric preform thickness, the fiber volume fraction, the resin mass for full saturation, and the initial resin film thickness as a function of applied compaction pressure, based upon an empirical fabric preform characterization.

A) Fabric Preform Preparation

    1) A utility knife is utilized to cut the TTI IM7/8HS fabric to fit snugly into the cavity of a flat plate mold (using the mold plunger as a pattern). After 16 plies have been cut, the plies are assembled into a composite panel with an equal number of tows in the warp (0°) and fill (90°) direction. The fabric preform is then placed into a vacuum oven (at 100 °C) for 2 to 3 hours to allow for entrapped moisture to be evaporated from the fibers.

    2) The fabric preform is removed from the vacuum oven and allowed to cool to room temperature. The initial dry weight, length, width, and thickness of the fiber preform are measured and recorded.

B) Resin film Preparation (Letters in parentheses correspond to resin preparation materials in Figs. A.1.1.-A.1.2.).

    1) Hercules 3501-6 resin, encapsulated within a plastic storage bag, is removed from a freezer 5 minutes prior to preparation. The dry fabric compaction model (#1.) experiment results (single-step compaction pressure is utilized during processing) are utilized to determine the final thickness (top of Fig. A.1.3.), fiber volume fraction (bottom of Fig. A.1.3.), and resin mass (top of Fig. A.1.4.) of the composite panel for a single applied compaction pressure of 689.5 kPa (-96.5 kPa vacuum bag pressure plus 593 kPa applied platen pressure).

**Temp = 100 °C**
**Pvac = -96.5 KPa**
**Time = 10 min**
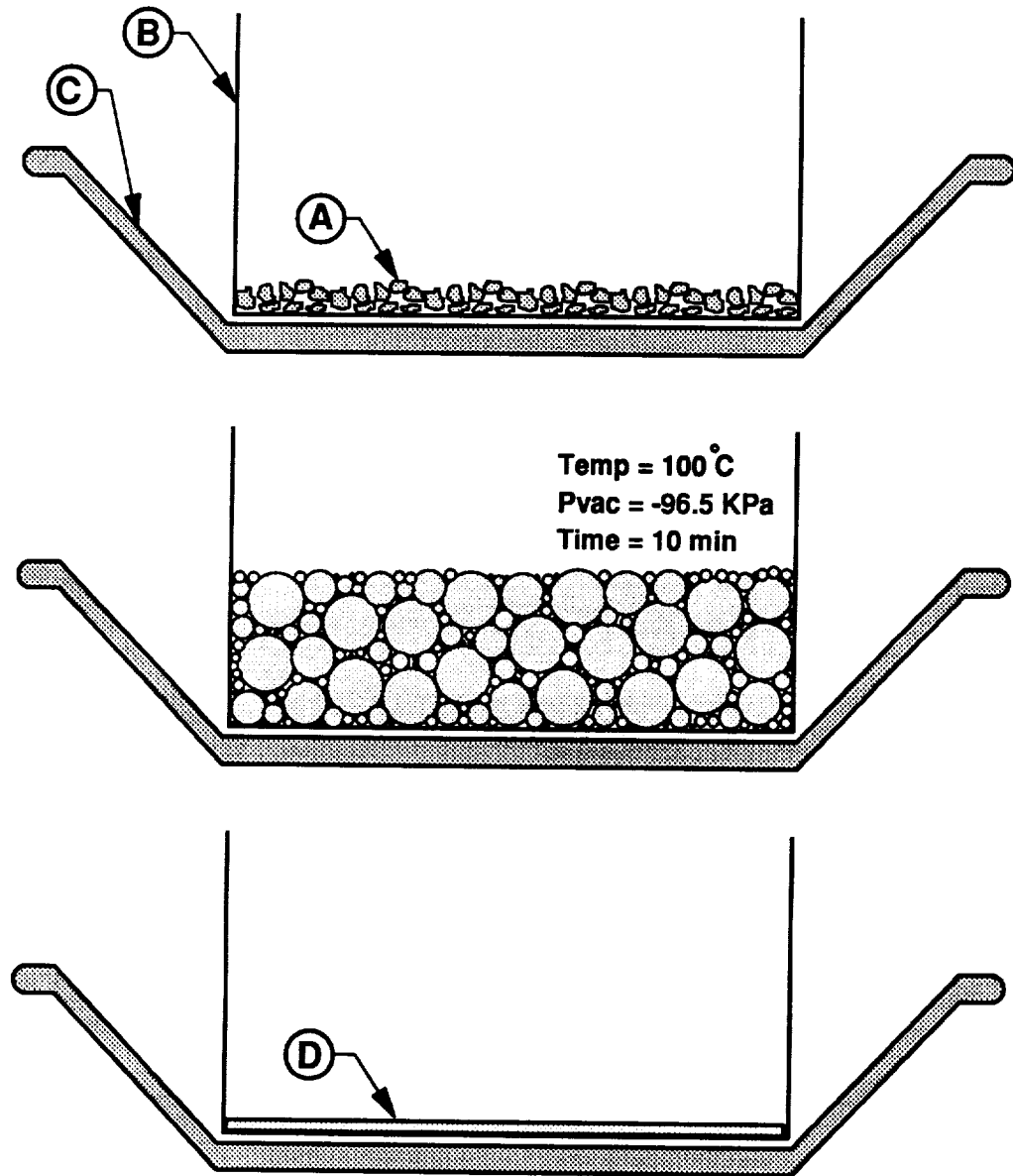
## Resin Film Preparation Materials

(A) Hercules 3501-6 Resin Particles    (B) Nonporous Release Film Bag

(C) Aluminum Container    (D) Degassed Resin Film

*Figure A.1.1 Placement of resin particles into container (top), expansion of resin under a full vacuum (middle), and the formation of the degassed resin panel after all of the entrapped air has been removed (bottom).*

**Appendix A.1: RTM Film Infusion Technique**

161

## Resin Film Pressing Materials

(D) Degassed Resin Film

(E) Porous Release Film

(F) Nonporous Release Film

\* Platens preheated to 38°C

Upper Platen\*

(E) — (D) (F)

Lower Platen\*

Load = 900 Kg

## PANEL LAYUP MATERIALS

(1) Plunger

(2) Mold Cavity

(3) Attachment Bolts

(4) J-Type or K-Type Thermocouples

1: Bottom Platen
$T_\#$  2: Top Platen
    3: Lower Panel
    4: Upper Panel

(5) Degassed Resin Film

(6) Fabric Preform

(7) FDEMS Sensors
    1: Lower Sensor
    2: Upper Sensor

(8) Nonporous Release Film

(9) Vacuum Sealant

(10) Porous Teflon Coated Fiberglass Bleeder

(11) N-10 Heavy Breather

(12) Thin Fiberglass Bleeder

(13) Vacuum Bag

(14) Vacuum Port

(15) Support Plate

*Figure A.1.2. Schematic of the assembly to press the degassed resin film to a desired thickness (top) and the general RTM layup assembly (bottom).*

**Appendix A.1: RTM Film Infusion Technique**
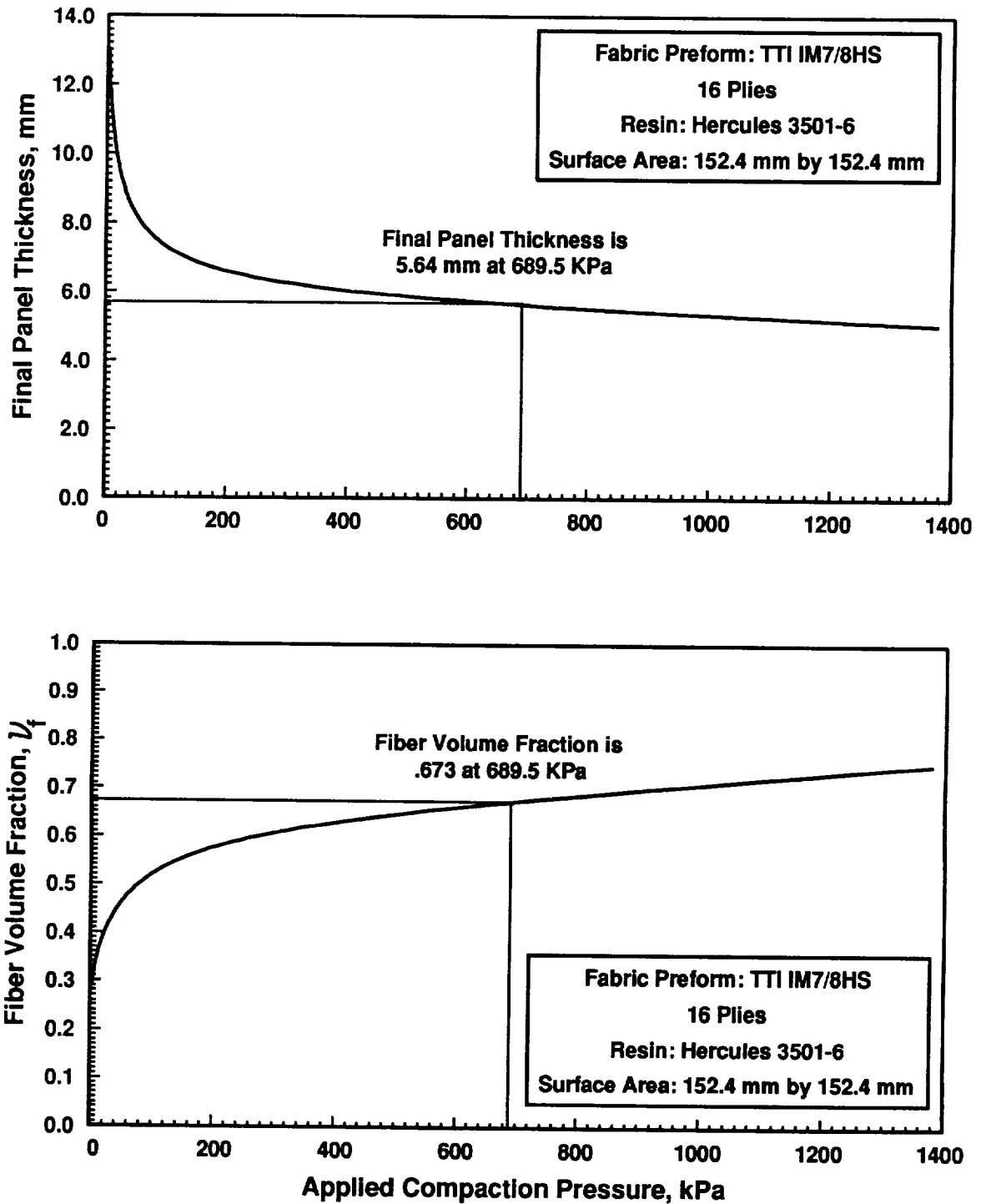
Figure A.1.3. Final panel thickness and fiber volume fraction as a function
of applied compaction pressure obtained from the TTI IM7/8HS
fast dry compaction model (#1).

Appendix A.1: RTM Film Infusion Technique
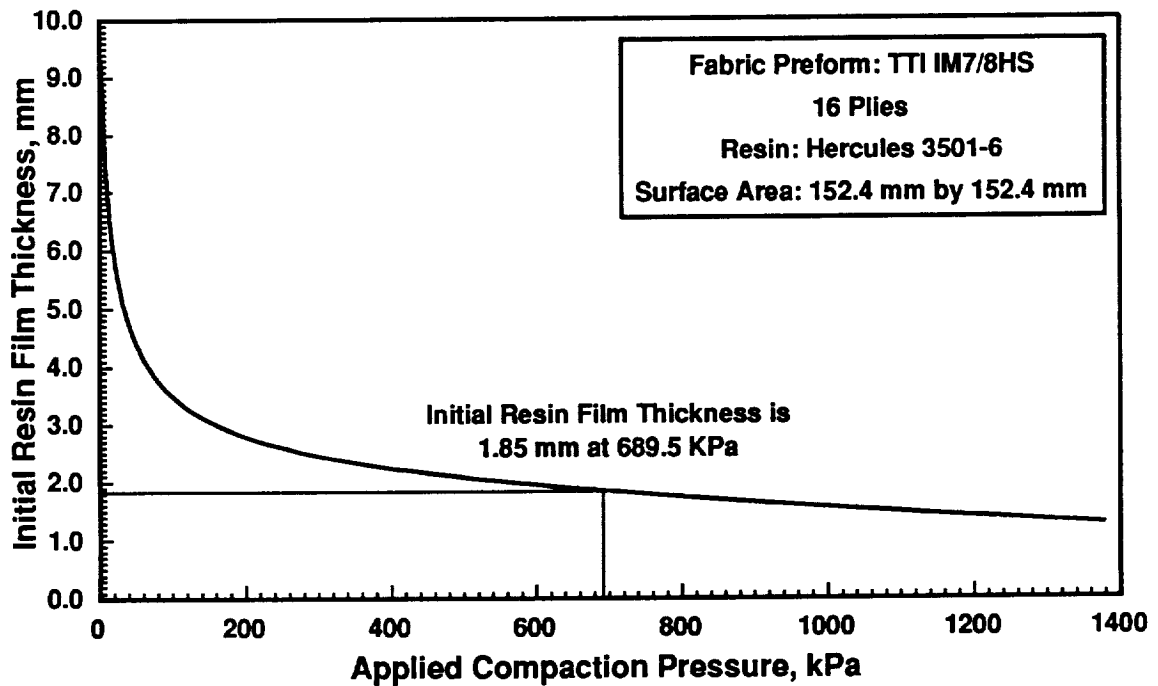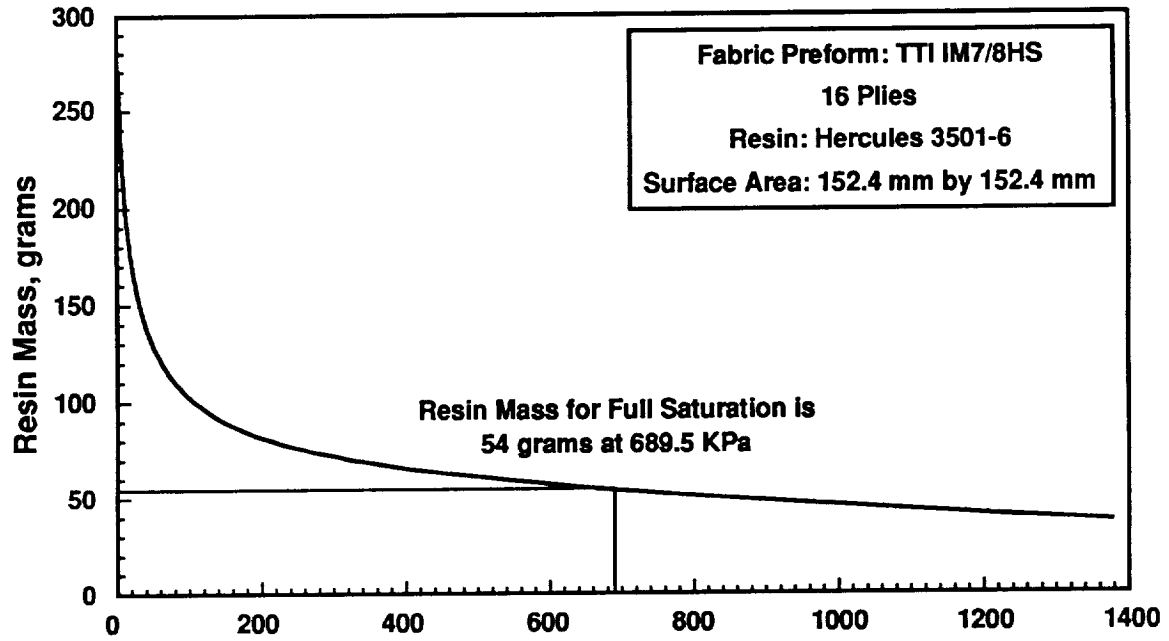
Figure A.1.4. Resin mass and initial resin film thickness as a function of
applied compaction pressure obtained from the TTI IM7/8HS
fast dry compaction model (#1).

a) For a 152.4 mm by 152.4 mm fabric preform (16 plies TTI IM7/8HS) under a transverse compaction pressure of 689.5 kPa, the required initial resin mass is 54 grams and the fiber volume fraction is 0.673 (the corresponding resin volume fraction or porosity is 0.327).

2) A quantity of resin, with a 20% greater mass (65 grams) than predicted by the RTM simulation model is removed from the storage bag and placed into a disposable plastic bag and weighed. The remaining resin is then returned to the freezer. (Excess resin is required for resin loss during preparation of the resin panel.) The resin is crushed within the bag with a blunt instrument until the average diameter of resin particles was less than 2.5 mm. The resin particles (A) are then transferred to a leak-proof bag constructed from non-porous release film (B), (top of Fig. A.1.1.), and spread evenly across the bottom surface of the bag (dimensions 152.4 mm by 152.4 mm by 60 mm). The release bag, with the resin particles inside, is placed into a large flat aluminum container (C). As a rule, for smaller amounts of resin, lower amounts of time are required for degassing.

3) The container of resin (C) is inserted into a vacuum oven preheated to 100 °C. A vacuum of -96.5 kPa is then applied to the oven and the resin was allowed to fully expand and degas for 10 minuets, (middle of Fig. A.1.1.). After degassing is completed, atmospheric pressure is restored to the vacuum oven. The resin film (D) should be very clear with no visible entrapped air bubbles, (bottom of Fig. A.1.1.) The resin film assembly is removed from the vacuum oven and allowed to cool to room temperature. The initial and final times and temperatures of the degassing procedure are recorded for the determination of the resin prestaging history by the RTM simulation model.

4) The degassed resin film (D) is removed from the container (C) and the release film (B), and placed between two sheets of porous Teflon-coated fiberglass release film (E). The resin film and release film assembly are placed between two sheets of nonporous release film (F) and inserted between the platens of a hot press (preheated to 38 °C) as shown on the top of Fig. A.1.2. The resin film assembly

Appendix A.1: RTM Film Infusion Technique

is compressed to a thickness predicted by the RTM simulation model (bottom of Fig. A.1.4.). (Use approximately 900 kg to press a 152.4 mm by 152.4 mm panel at 38 °C.) Calipers are utilized to measure the distance between the platens.

a) For the 152.4 mm by 152.4 mm panel to be manufactured using a compaction pressure of 689.4 kPa, the desired resin film thickness is 1.85 mm, assuming the density of the resin (Hercules 3501-6) to be 1,260 Kg/m$^3$.

5) Finally, the resin film and the attached release films (E,F) are cut to fit into the mold cavity by using the plunger of the flat plate mold as a pattern.

a) The initial weight, length, width, and thickness of the resin film are measured and recorded.

C) Mold Preparation and Preform Layup Procedure (Numbers in parentheses correspond to layup materials in bottom of Fig. A.1.2).

1) The flat plate mold plunger (1) and cavity assembly (2) are thoroughly coated with release agent. The bottom cavity is assembled by attaching the side pieces to the bottom plate and hand tightening the attachment bolts (3).

2) Two thermocouple wires (4) are inserted into the bottom half of the mold through a 1.27 mm diameter hole predrilled into one of the side pieces. One thermocouple is taped to the top surface of the bottom plate and the other thermocouple is taped to one of the side pieces near the top of the test section. Both thermocouples are located at the front right corner of the mold.

a) The thermocouples monitor the temperature at the top and bottom surfaces of the composite panel during processing. Temperature is recorded as a function of time with external devices and compared with the RTM simulation model results. The temperature history is also utilized to determine the state of cure and viscosity of the resin during processing.

3) Release films are then removed from the degassed resin film (5), and the resin film is attached to the bottom surface of the fabric preform (6).

4) A Frequency Dependent Electromagnetic Sensor(s) (FDEMS) (7), enclosed within a protective glass filter, is attached (face up) to the bottom surface of the degassed

**Appendix A.1: RTM Film Infusion Technique**

resin film (5) at the front right corner. A second FDEMS assembly is attached (face down) to the top surface of the fabric preform (6) at the same corner as the other sensor.

    a) FDEMS are utilized to measure the capacitance and conductance of the resin during processing and the total infiltration time (wetout of top sensor). Experimental measurements are then correlated with DSC and viscometer results to determine the state of cure and viscosity of the resin during processing.

5) The resin film/fabric preform/thermocouple/FDEMS assembly is placed (resin film on bottom) onto a large sheet of nonporous release film (8) with a surface area greater than the test section surface area. Wires leading from the FDEMS (7) are taped to the release film.

6) The composite assembly is inserted (nonporous release film (8) on bottom) into the mold cavity (2) and the nonporous film is pulled up around the inner walls of the cavity and over the upper surface of the side pieces, (top of Fig. A.1.5).

7) A strip of vacuum sealant (9) is stretched to circumnavigate the lower edge of the plunger (1) (see top of Fig. A.1.5), and pressed to the lower corner by hand.

8) A large single ply of porous Teflon coated fiberglass bleeder (10) with a surface area equal to the nonporous release film (8) is secured to the bottom of the steel plunger (1) and vacuum sealant (9), and pulled up around the sides.

9) The plunger (1)/bleeder ply assembly (10) is inserted into the cavity (2) and allowed to rest on top of the fiber preform (6). The sides of the mold cavity are tightened against the porous Teflon-coated fiberglass bleeder (10) and the release film (8) exiting the inner layup, (see bottom of Fig. A.1.5). The clearance between the sides of an empty cavity and the plunger, after tightening the attachment bolts, should range from 0.0245 mm to 0.0762 mm. This creates a controlled pathway for the evacuation of air from the inner layup, while preventing the loss of resin from

**Appendix A.1: RTM Film Infusion Technique**
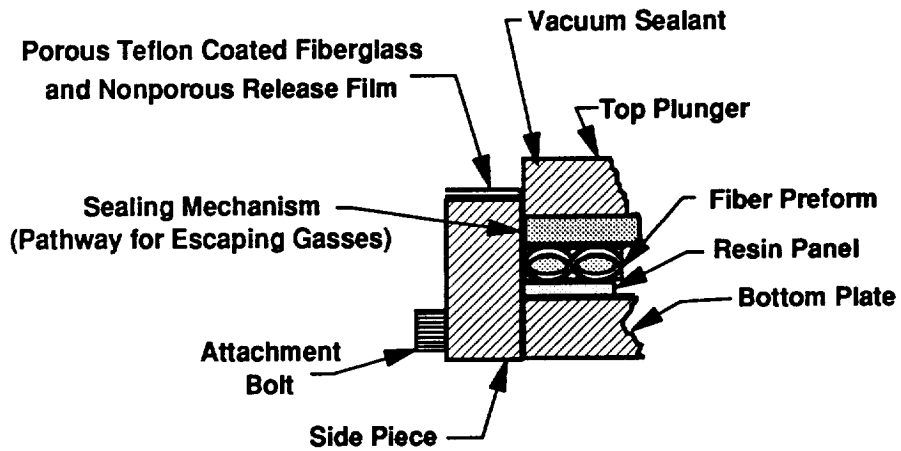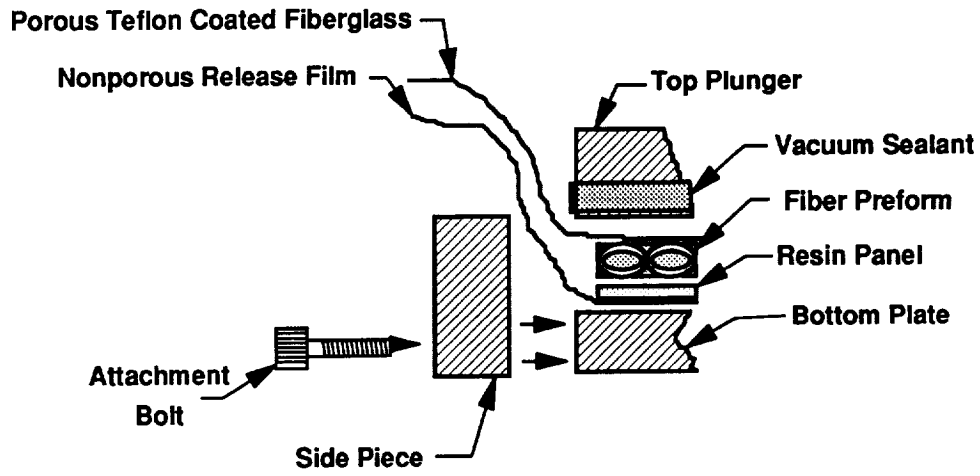
Figure A.1.5. Attachment of side peices to close the gap between the mold plunger and the mold cavity (top) and the closure of the gap to restrict resin flow (bottom).

Appendix A.1: RTM Film Infusion Technique

the inner cavity, and maintaining a high hydrostatic resin pressure after full resin saturation occurs.

10) A large sheet of heavy breather (11) is utilized to provide a pathway for evacuating air from the inner layup with a vacuum. A single ply of N-10 breather, with a section cut out for the mold, is placed around the assembled mold (1) and (2) and two layers of thin fiberglass bleeder (12) are placed over the top of the mold to prevent rupture of the outer vacuum bag (13) on the sharp edges of the mold plunger. Finally, the mold assembly and the breather are placed onto a 400 mm by 400 mm by 6 mm support plate (14) and the assembly is placed into a vacuum bag. The entire assembly was then placed between the platens of the hot press.

a) Wires for the thermocouples (4) and the FDEMS (7) are brought through the internal seal of the vacuum bag (13) and connected to data acquisition systems. A vacuum port (15), connected to a vacuum pump with a vacuum line, is inserted into the bag and sealed. The vacuum bag is then sealed and a full vacuum -96.5 kPa was initiated. Typically, a full vacuum is applied to the layup for 45 minutes prior to cure cycle to ensure full evacuation of air from the preform for a 152.4 mm by 152.4 mm composite panel (the vacuum is maintained for the entire process).

11) After the inner layup has been completely evacuated, a platen compaction pressure of 593 kPa is applied to the mold test section, and the manufacturer's recommended cure cycle (top of Table A.2.1.) is applied by the hot press.

a) The deflection rate of the lower plunger as a function of time during the production of the panel is recorded with a stop watch and either a Linear Voltage Displacement Transducer (LVDT) or a dial gauge and a stop watch. The deflection data are utilized to estimate the position of the resin infiltration front as a function of time and are utilized for comparison with RTM simulation model and FDEMS generated data.

12) Finally, after the cure cycle, with cool down, has been completed, the mold is

Appendix A.1: RTM Film Infusion Technique

taken out of the hot press, disassembled, and the composite panel is removed.

a) The final weight, width, length, and thickness (along with the platen deflection data), are then measured, recorded, and compared with the RTM simulation model predictions.

Appendix A.1: RTM Film Infusion Technique

# Appendix A.2: Hercules 3501-6 Cure Kinetics/Viscosity Model

A Hercules 3501-6 cure kinetics and viscosity model, developed by Chiou and Letton [8], was chosen for this study.

The overall rate of cure was modeled as an summation of three separate consecutive curing reactions which take place during the curing of Hercules 3501-6 resin. Each separate reaction was characterized by the Arrhenius rate equation which is written as

$$\frac{\partial \alpha_i}{\partial t} = A_i \exp(\frac{E_i}{RT})(1 - \alpha_i)^{n_i} \, , \, i=1,3 \tag{A.2.1}$$

where the subscript i is order of the reaction, $E_i$ are the Arrhenius activation energies, $A_i$ are the Arrhenius pre-exponential factors, $n_i$ are the reaction order constants, and R is the universal gas constant. Each separate reaction obtained from Eq. A.2.1 is integrated with Eq. 2.3.3 to obtain the degree of resin cure of each individual reaction at a particular time t.

The full degree of resin cure at any time t is determined by summing the contributions of the individual reactions

$$\alpha_{total} = \sum_{i=1}^{3} g_i \alpha_i \tag{A.2.2}$$

where $g_i$ are the ratios of the total heat of generation produced by an individual reaction to the total heat of generation generated by all three reactions. Consequently, the total heat of generation at any time t, $\dot{H}(T,t)_{total}$, is given as,

$$\dot{H}(T,t)_{total} = \sum_{i=1}^{3} \frac{\partial \alpha_i}{\partial t} H_i g_i \tag{A.2.3}$$

All of the constants for Eqs. A.2.1-A.2.3 are presented in Table A.2.1.

A modified WLF equation was utilized for the viscosity characterization and is written as,

$$\ln\left[\frac{\mu(T,\alpha)}{\mu(T_g,\alpha)}\right] - \frac{-C_1(T - T_g(\alpha)}{C_2 + (T - T_g(\alpha))} \tag{A.2.4}$$

where $C_1$ and $C_2$ are the WLF equation constants, $T_g$ is the glass transition temperature, and $\mu(T_g,\alpha)$ is the viscosity of the resin at $T_g$.

Empirical measurements of the glass transition temperature, $T_g$, as a function of the degree of resin cure, where fitted to an 5th order polynomial written as,

$$T_g(\alpha) - \sum_{i=0}^{5} c_i \alpha^i \tag{A.2.5}$$

where the $c_i$ are the model coefficients.

The resin viscosity at $T_g$, $\mu(T_g(\alpha))$, was also dependent upon the degree of resin cure and empirical data were fit to an 3rd order polynomial written as,

$$\mu(T_g(\alpha)) - \exp\left\{\sum_{i=0}^{3} d_i \alpha^i\right\} \tag{A.2.6}$$

where $d_i$ are the model coefficients.

The coefficients for Eqs. A.2.4-A.2.6 are presented in Table A.2.1.

*Table A.2.1. Coefficients for Hercules 3501-6 cure kinetics and viscosity model obtained from Chiou/Letton [8].*

| Hercules 3501-6 Cure Kinetics Parameters | | | | | |
|---|---|---|---|---|---|
| i | $A_i$, 1/sec | $E_i$, J/mol | $n_i$ | $g_i$ | $H_i$, J/g |
| 1 | 3.496996E+07 | 93,283 | 1.06 | 0.850 | 427.8 |
| 2 | 2.094509E+08 | 85,219 | 1.17 | 0.095 | 50.0 |
| 3 | 1.183289E+20 | 171,019 | 3.05 | 0.055 | 27.4 |

| Glass Transition Temperature, $T_g$, Coefficients | | | | | |
|---|---|---|---|---|---|
| $C_0$ | $C_1$ | $C_2$ | $C_3$ | $C_4$ | $C_5$ |
| 283.4 | 196.5 | -925.4 | 3,435.0 | -4,715.0 | 2,197.0 |

| $\mu$ ($T_g$) Coefficients | | | |
|---|---|---|---|
| $d_0$ | $d_1$ | $d_2$ | $d_3$ |
| 20.72 | 8.51 | -9.69 | 41.17 |

| WLF Parameters | |
|---|---|
| $C_1$ | $C_2$ |
| 29.67 | 36.93 |

**Appendix A.2: Hercules 3501-6 Cure Kinetics/Viscosity Model**

# Appendix A.3: Thermal Coefficients of Layup Materials

*Table A.3.1 Thermal and physical properties of the RTM layup materials.*

| Material | Density, kg/m$^3$ | Thermal Conductivity W/(m$^2$K) | Specific Heat, J/(kg $^\bullet$K) |
|---|---|---|---|
| Vacuum Bag [3] | 2,200 | 4.00 | 1,548 |
| S Glass [34] | 2,400 | 3.03 | 711 |
| Steel [3] | 7,865 | 52.00 | 452 |
| Teflon Fiberglass | 2,380 | 0.71 | 1,096 |
| AS4/IM7 Fiber [4] | 1,780/1,800 | 25.97 | 712 |
| Hercules 3501-6 [4] | 1,260 | 0.17 | 1,256 |
| Release Film [3] | 2,200 | 0.34 | 1,548 |
| Aluminum [3] | 2,659 | 164.00 | 896 |

# Appendix B.1: Test Fixture Deflection



**Compaction/Permeability Test Fixture**
**Test Section: 50.8 mm by 50.8 mm**

**Deflection Eq. 4.4.2**

$$d_{fix} = .106061 - .122484^*\ln(Pcomp) + .046866^*(\ln(Pcomp))^2 - .006471^*(\ln(Pcomp))^3 + .000349^*(\ln(Pcomp))^4$$

**Large Permeability Test Fixture [1]**
**Test Section: 171.2 mm by 152.4 mm**

**Deflection Eq. 4.4.2**

$$d_{fix} = -.374391 + .301137^*\ln(Pcomp) + -.040962^*(\ln(Pcomp))^2 + .003258^*(\ln(Pcomp))^3 + .000158^*(\ln(Pcomp))^4$$
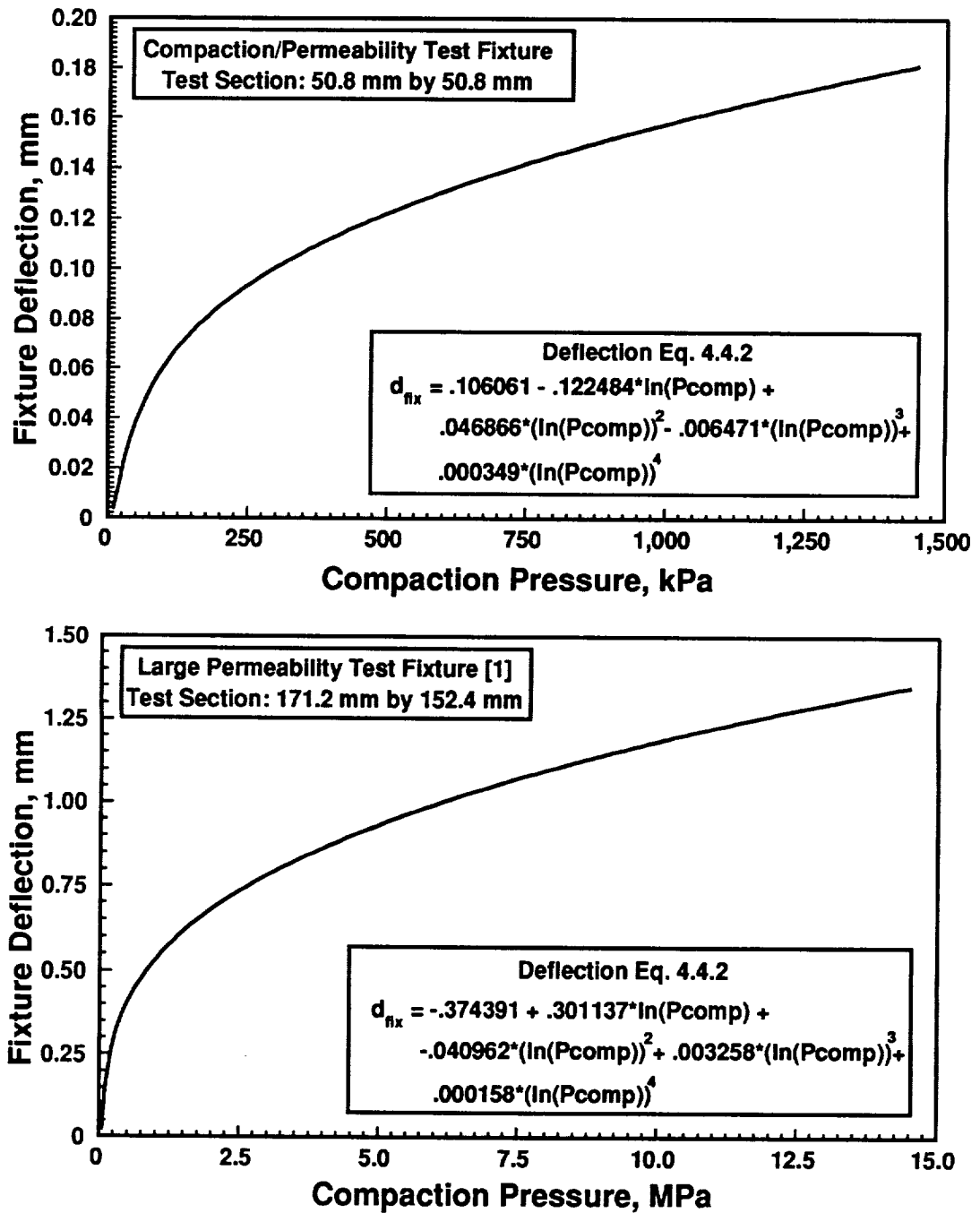
Figure B.1.1  Deflection of the test fixtures as a function of
applied compaction pressure

# Appendix B.2: Flow Meter Calibration/
# Test Fixture Pressure Drop

**Flow Meter Calibration Eq. 4.5.1**

$$Q_z = -.03965 + .39335*s + .36583*s^2 -.05848*s^3 + .00422*s^4 - .00010*s^5$$

Flow Rate*$10^{-6}$, m$^3$/sec.

Flow Meter Setting, s

**Through-The-Thickness Pressure Drop Eq. 4.5.2**

$$\Delta P(Q)_{fix} = -2.4596 + 21.0734*Q_z - 7.9239*Q_z^2 + 2.2259*Q_z^3 - .1629*Q_z^4 + .0049*Q_z^5 - .00006*Q_z^6$$

Compaction/Permeability Test Fixture
Text Section: 50.8 mm by 50.8 mm

Pressure Drop, Pa

Flow Rate*$10^{-6}$m$^3$/sec
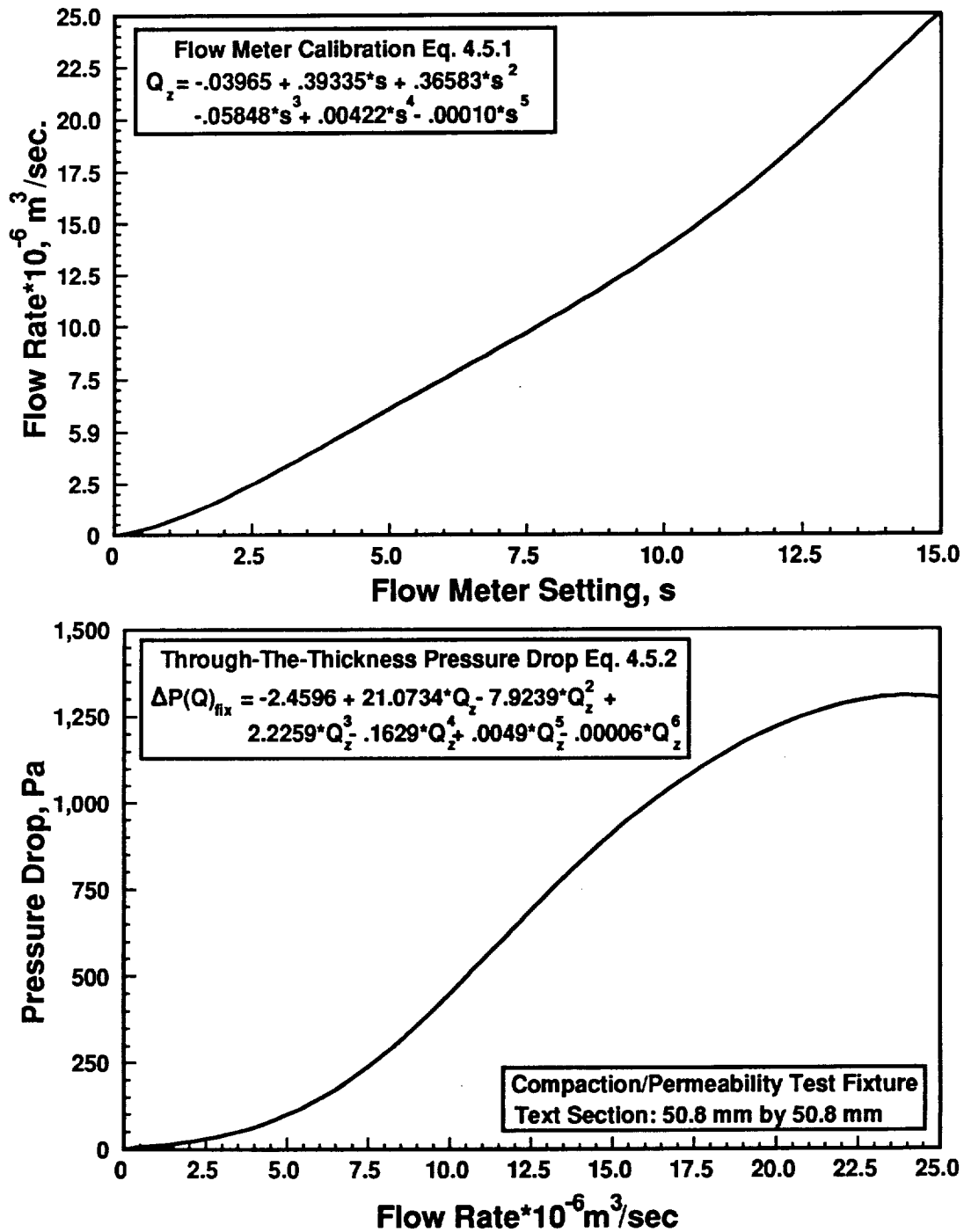
*Figure B.2.1  Flow rate as a function of the flow meter setting (top) and the through-the-thickness pressure drop as a function of flow rate (bottom).*

# Appendix C.1: Processing Parameters for the Composite Panels

Table C.1.1  Processing parameters for the Hexcel Hi-Tech AS4 6k knitted $(+45^\circ/0^\circ/-45^\circ/90^\circ)_{2s}$/Hercules 3501-6 composite panels.

| Processing Parameters | Hexcel Hi-Tech knitted Composite Panel | |
|---|---|---|
| | 71190P1 | 72390P1 |
| Applied Compaction Pressure | 347.4 kPa | 347.4 kPa |
| Full Vacuum ? | Yes | Yes |
| Temperature Cycle | Manuf. | Manuf. |
| Temp Ramp During Infiltration Phase | 3.1°C/min | 2.9°C/min |
| FDEMS ? | Yes | Yes |
| Infiltration Time | | |
| Measured, min | 33.9 min | 35 min |
| Model Simulation | 34.2 min | 33 min |
| % Error | +0.9 | -5.7 |
| Start of Infiltration | | |
| Time | 15 min | 13.5 min |
| Resin Viscosity | 912 Pa.s | 770.7 Pa.s |
| Gelation | | |
| Time | 133.5 min | 132 min |
| Degree of Cure | .512 | .516 |
| Length of Flow Window | 118.5 min | 118.5 min |
| Final Degree of Cure | .963 | .965 |
| Final Quality | | |
| C-Scan Quality | None Taken | Good |
| Micrograph Quality | Excellent | Good |
| Destructive Eval. | | |
| SBC ? | Yes | Yes |
| Iosipescu Shear | No | Yes |

Table C.1.2 Processing parameters for the Hexcel Hi-Tech AS4 6k knitted/stitched
$(+45^\circ/0^\circ/-45^\circ/90^\circ)_{2s}$/Hercules 3501-6 composite panels.

| Processing Parameters | Hexcel Hi-Tech Knitted/Stitched Composite Panel | | | |
|---|---|---|---|---|
| | 71290P1 | 71790P1 | 71990P1 | 72090P1 |
| Applied Compaction Pressure | 347.4 kPa | 347.4 kPa | 705.5 kPa | 705.5 kPa |
| Full Vacuum ? | Yes | Yes | Yes | Yes |
| Temperature Cycle | Manuf. | Rapid | Manuf. | Rapid |
| Temp Ramp During Infiltration Phase | 2.9 C/min | 3.1 C/min | 2.9 C/min | 3.1 C/min |
| FDEMS ? | Yes | Yes | Yes | Yes |
| Infiltration Time | | | | |
| Measured, min | 30.5 min | 31.2 min | 27.5 min | 28.5 min |
| Model Simulation | 29.4 min | 28.5 min | 27.7 min | 25 min |
| % Error | -6.9 | +0.7 | -8.6 | -12.2 |
| Start of Infiltration | | | | |
| Time | 13.5 min | 12.24 min | 13.5 min | 10.9 min |
| Resin Viscosity | 456 Pa.s | 684 Pa.s | 695 Pa.s | 911 Pa.s |
| Gelation | | | | |
| Time | 133.5 min | 77.3 min | 132 min | 66.4 min |
| Degree of Cure | .510 | .501 | .509 | .506 |
| Length of Flow Window | 120 min | 60 min | 118.5 min | 55.5 min |
| Final Degree of Cure | .945 | .901 | .955 | .948 |
| Final Quality | | | | |
| C-Scan Quality | Good | Good | Good | Good/Excel. |
| Micrograph Quality | Good | Good | Good | Good/Excel. |
| Destructive Eval. | | | | |
| SBC ? | Yes | Yes | Yes | Yes |
| Iosipescu Shear | Yes | Yes | Yes | Yes |

Appendix C.1: Processing Parameters for
the Composite Panels

*Table C.1.3  Processing parameters for the 16 ply TTI IM7/8HS/Hercules 3501-6 composite panels.*

| Processing Conditions | TTI IM7/8HS  Composite Panels | | | | | |
|---|---|---|---|---|---|---|
| | 61990P1 | 52390P1 | 61190P1 | 62290P1 | 81690P1 | 91690P1 |
| Applied Compaction Pressure | 276.3 kpa | 295.4 kPa | 550.8 kPa | 551.6 kPa | 174.2 kPa | 551.6 kPa |
| Full Vacuum ? | Yes | Yes | Yes | Yes | Yes | Yes |
| Temperature Cycle | Manuf. | Rapid | Manuf. | Rapid | Advanced | Step |
| Temp Ramp During Infiltration Phase | 2.6°C/min | 3.0°C/min | 2.6°C/min | 2.6°C/min | 6.0°C/min | 7.0°C/min |
| FDEMS ? | Yes | Yes | Yes | Yes | Yes | Yes |
| Infiltration Time | | | | | | |
| Measured, min | 34.2 min | 33.5 min | 33 min | 36 min | 20.5 min | 17.8 min |
| Model Simulation | 35.1 min | 35.1 min | 35.9 min | 36.9 min | 18.9 min | 16.9 min |
| % Error | +2.6 | +4.8 | +8.8 | +2.5 | -7.8 | -5.0 |
| Start of Infiltratio | | | | | | |
| Time | 8.7 min | 12 min | 8.7 min | 10.5 min | 6.2 min | 4.5 min |
| Resin Viscosity | 829 Pa.s | 654 Pa.s | 829 Pa.s | 965 Pa.s | 770 Pa.s | 922 Pa.s |
| Gelation | | | | | | |
| Time | 132.5 min | 66 min | 132.5 min | 76.5 min | 47.2 min | 39.5 min |
| Degree of Cure | .509 | .529 | .509 | .520 | .524 | .537 |
| Length of Flow Window | 123.7 min | 54 min | 123.7 min | 64.5 min | 41 min | 35 min |
| Final Degree of Cure | .955 | .984 | .955 | .926 | .968 | .949 |
| Final Quality | | | | | | |
| C-Scan Quality | Excellent | Excellent | Excellent | Excellent | None Taken | None Taken |
| Micrograph Quality | Excellent | Excellent | Excellent | Excellent | Good | Good |
| Destructive Eval. | | | | | | |
| SBC ? | Yes | Yes | Yes | Yes | No | No |
| Ioslpescu Shear | Yes | Yes | Yes | Yes | No | No |

Appendix C.1: Processing Parameters for
the Composite Panels

# Appendix C.2: Physical Properties of the Composite Panels

Table C.2.1  Physical Properties of Hexcel Hi-Tech AS4 6k knitted ($+45°/0°/-45°/90°)_{2S}$/Hercules 3501-6 composite panels.

| Physical Properties | | Hexcel Hi-Tech Knitted Composite Panels | |
|---|---|---|---|
| | | 71190P1 | 72390P1 |
| Applied Compaction Pressure, kPa | | 347.4 | 347.4 |
| Consolidation ? | | No | No |
| Measured Final Thickness, mm | | 6.64 | 6.62 |
| Predicted From Compaction Models | 1 | 6.60 | 6.60 |
| | 2 | 6.67 | 6.67 |
| % Error of Compaction Models | 1 | 0.59 | 0.29 |
| | 2 | -0.42 | -0.73 |
| Fiber Volume Fraction | | | |
| Predicted From Compaction Models | 1 | 0.585 | 0.585 |
| | 2 | 0.579 | 0.579 |
| Measured From Mass | | 0.590 | 0.590 |
| % Error of Compaction Models | 1 | -0.75 | -1.84 |
| | 2 | 1.75 | -0.81 |
| Measured by Resin Digestion Techniques | | 0.603 | 0.603 |
| % Error of Compaction Models | 1 | 2.88 | -0.10 |
| | 2 | 3.86 | 0.91 |
| Measured Resin Mass, grams | | 77.2 | 77.2 |
| Predicted From Compaction Models | 1 | 80.1 | 80.1 |
| | 2 | 82.0 | 82.0 |
| % Error of Compaction Models | 1 | -3.70 | -1.46 |
| | 2 | -6.24 | -3.95 |

1: Fast Dry Compaction Model   2: Slow Dry Compaction Model

*C -3*

Table C.2.2 Physical properties of Hexcel Hi-Tech AS4 6k knitted/stitched $(+45°/0°/-45°/90°)_{2S}$/Hercules 3501-6 composite panels.

| Physical Properties | | Hexcel Hi-Tech Knitted/Stitched Panels | | | |
| --- | --- | --- | --- | --- | --- |
| | | 71290P1 | 71790P1 | 71990P1 | 72090P1 |
| Applied Compaction Pressure, kPa | | 347.4 | 347.4 | 705.5 | 705.5 |
| Consolidation ? | | No | No | No | No |
| Measured Final Thickness, mm | | 7.00 | 7.08 | 6.37 | 6.51 |
| Predicted From Compaction Models | 1 | 6.89 | 6.89 | 6.67 | 6.67 |
| | 2 | 6.84 | 6.84 | 6.47 | 6.47 |
| | 3 | 6.98 | 6.98 | 6.72 | 6.72 |
| % Error of Compaction Models | 1 | 1.51 | 2.62 | -4.72 | -2.46 |
| | 2 | 2.18 | 3.28 | -1.62 | 0.56 |
| | 3 | 0.29 | 1.41 | -5.54 | -3.27 |
| Fiber Volume Fraction | | | | | |
| Predicted From Compaction Models | 1 | .590 | .590 | .610 | .61 |
| | 2 | .594 | .594 | .628 | .628 |
| | 3 | .583 | .583 | .605 | .605 |
| Measured From Mass | | .58 | .59 | .65 | .63 |
| % Error of Compaction Models | 1 | -1.78 | -0.06 | 6.13 | 3.14 |
| | 2 | -2.48 | -0.75 | 3.27 | 0.19 |
| | 3 | -0.55 | 1.159 | 6.86 | 3.91 |
| Measured by Resin Digestion Techniques | | .604 | .585 | .629 | .640 |
| % Error of Compaction Models | 1 | 2.25 | -0.92 | 2.99 | 4.66 |
| | 2 | 1.58 | -1.61 | 0.04 | 1.75 |
| | 3 | 3.48 | 0.31 | 3.75 | 5.41 |
| Measured Resin Mass, grams | | 82.3 | 84.0 | 63.3 | 66.5 |
| Predicted From Compaction Models | 1 | 82.6 | 82.6 | 76.1 | 76.0 |
| | 2 | 81.3 | 81.3 | 76.3 | 70.3 |
| | 3 | 85.1 | 85.1 | 77.6 | 77.6 |
| % Error of Compaction Models | 1 | -0.42 | 1.61 | -20.2 | -14.4 |
| | 2 | 1.25 | 3.25 | -11.1 | -5.75 |
| | 3 | -3.45 | -1.36 | -22.6 | -16.75 |

1: Fast Dry Compaction model   2: Slow Dry Compaction Model
3: Fast Wet Compaction Model

Appendix C.2: Physical Properties of
the Composite Panels

Table C.2.3  Physical properties of 16 ply TTI IM7/8HS/Hercules 3501-6 composite panels.

| Physical Properties | | TTI IM7/8HS Composite Panels | | | | | |
|---|---|---|---|---|---|---|---|
| | | 61990P1 | 52390P1 | 61190P1 | 62290P2 | 81690P1 | 91690P1 |
| Applied Compaction Pressure, kPa | | 276.3 | 295.4 | 550.8 | 551.58 | 174.2 | 551.58 |
| Consolidation ? | | No | No | No | No | No | No |
| Measured Final Thickness, mm | | 6.25 | 6.50 | 5.89 | 5.97 | 7.13 | 6.07 |
| Predicted From Compaction Models | 1 | 6.31 | 6.26 | 5.80 | 5.80 | 6.71 | 6.35 |
| | 2 | 6.12 | 6.06 | 5.58 | 5.58 | 6.57 | 6.30 |
| | 3 | 6.94 | 6.87 | 6.31 | 6.31 | 7.50 | 7.29 |
| % Error of Compaction Models | 1 | 0.97 | -3.72 | -1.51 | -2.84 | -5.91 | 4.72 |
| | 2 | -2.08 | -6.75 | -5.25 | -6.54 | -7.84 | 3.83 |
| | 3 | 11.10 | 5.73 | 7.18 | 5.73 | 5.15 | 20.14 |
| Fiber Volume Fraction | | | | | | | |
| Predicted From Compaction Models | 1 | 0.61 | 0.62 | 0.67 | 0.67 | 0.67 | 0.53 |
| | 2 | 0.63 | 0.64 | 0.69 | 0.69 | 0.69 | 0.54 |
| | 3 | 0.56 | 0.56 | 0.61 | 0.61 | 0.61 | 0.46 |
| Measured From Mass | | 0.62 | 0.60 | 0.68 | 0.67 | 0.55 | |
| % Error of Compaction Models | 1 | -1.61 | 3.20 | -1.47 | 0.0 | 5.23 | |
| | 2 | 1.61 | 6.67 | 1.47 | 2.98 | 7.43 | |
| | 3 | -9.60 | -6.67 | -10.29 | -8.95 | -5.84 | |
| Measured by Resin Digestion Techniques | | 0.63 | 0.60 | 0.65 | 0.66 | | 0.66 |
| % Error of Compaction Models | 1 | -3.18 | 2.16 | 2.56 | 1.18 | | 1.18 |
| | 2 | -0.16 | 5.47 | 6.62 | 5.18 | | 5.18 |
| | 3 | -12.01 | -6.97 | 0.61 | -7.03 | | -7.03 |
| Measured Resin Mass, grams | | 63.20 | 75.0 | 55.0 | 56.0 | 94.0 | 69.0 |
| Predicted From Compaction Models | 1 | 71.66 | 71.13 | 56.77 | 56.74 | 83.31 | 56.74 |
| | 2 | 66.09 | 64.38 | 50.31 | 50.28 | 79.29 | 50.28 |
| | 3 | 90.21 | 88.11 | 71.75 | 71.57 | 106.39 | 71.72 |
| % Error of Compaction Models | 1 | 13.4 | -6.6 | 3.21 | 1.32 | -11.37 | -17.77 |
| | 2 | 4.57 | -14.2 | -8.53 | -10.21 | -15.64 | -27.13 |
| | 3 | 42.7 | 17.5 | 30.45 | 28.1 | 13.18 | 3.94 |

1: Fast Dry Compaction Model #1.  2: Fast Dry Compaction Model #2.
3: Fast Wet Compaction Model

**Appendix C.2: Physical Properties of the Composite Panels**

# Appendix D.1: Short Block Compression Data
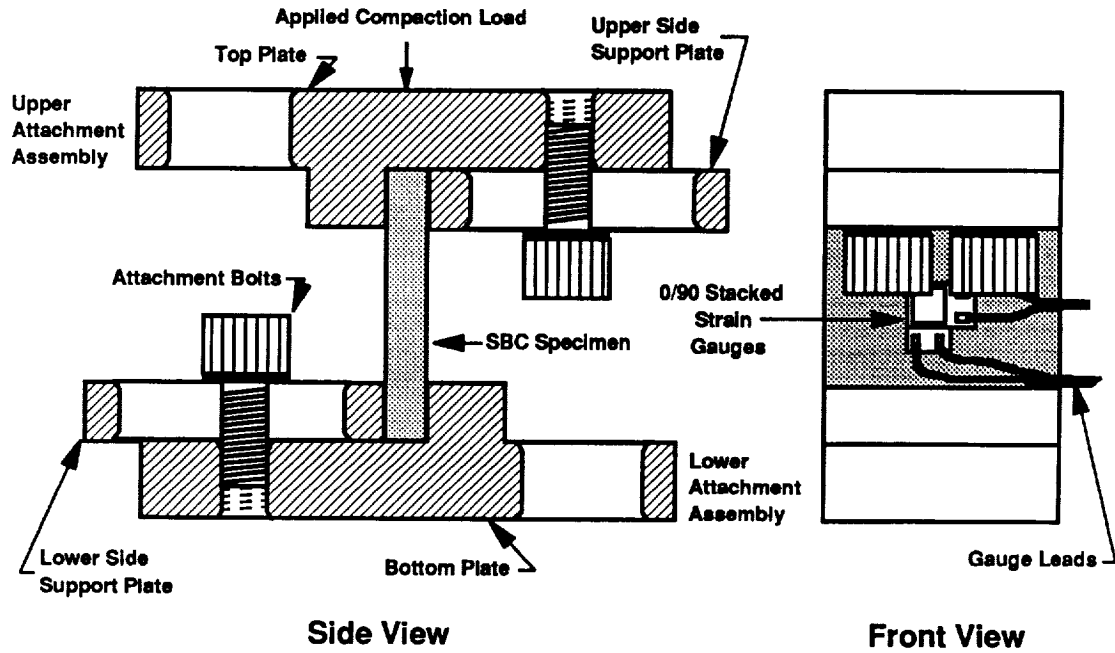


**Short Block Compression Test Fixture**

Compressive Strength

$$\sigma_{max} = \frac{Load}{L*W}$$

Ultimate Longitudinal Strain, %

$$\epsilon_{max_{long}} = \frac{(\epsilon_{max_{front}} + \epsilon_{max_{back}})}{2} \ long$$

Poisson's Ratio at
0.2% Longitudinal Strain

$$\nu_{.2\%} = \frac{(\epsilon_{.2\%_{front}} + \epsilon_{.2\%_{back}})_{long}}{(\epsilon_{.2\%_{front}} + \epsilon_{.2\%_{back}})_{lat}}$$

Young's Modulus at
0.2% Longitudinal Strain

$$E_{.2\%} = \frac{2\,\sigma_{max}}{(\epsilon_{.2\%_{front}} + \epsilon_{.2\%_{back}})_{long}}$$

*Figure D.1.1. Short block compression test fixture (top) and the equations utilized to reduce the SBC experimental data (bottom).*

*Table D.1.1. SBC results obtained from the Hexcel Hi-Tech AS4 6k knitted*
*(+45°/0°/-45°/90°)$_{2S}$/Hercules 3501-6 SBC specimens.*

| RTM Panel | SBC Specimen | Loading Orientation | Compressive Strength, MPa | Ultimate Longitudinal Strain, % | Poisson's Ratio at 0.2% Strain | Young's Modulus, GPa at 0.2% Strain |
|---|---|---|---|---|---|---|
| 71190P1 | C1 | 0° | 505.06 | 1.147 | 0.2922 | 50.47 |
| | C2 | 0° | 526.37 | 1.229 | 0.2929 | 48.77 |
| | C3 | 0° | 518.53 | 1.183 | 0.2871 | 50.99 |
| | C4 | 0° | 518.51 | 1.176 | 0.2901 | 51.70 |
| | C5 | 0° | 506.05 | 1.128 | 0.2995 | 50.62 |
| | C6 | 0° | 515.36 | 1.171 | 0.2840 | 50.64 |
| | C7 | 0° | 497.48 | 1.093 | 0.2958 | 50.43 |
| | Ave. | 0° | 512.48 | 1.161 | 0.2917 | 50.52 |
| | STD | 0° | 9.22 | 0.040 | 0.0048 | 0.82 |
| 72390P1 | C1 | 90° | 339.78 | 0.852 | 0.2930 | 42.26 |
| | C2 | 90° | 349.37 | 0.877 | 0.2877 | 42.17 |
| | C3 | 90° | 355.37 | 0.898 | 0.2940 | 42.89 |
| | C4 | 90° | 338.99 | 0.818 | 0.3181 | 44.24 |
| | C5 | 90° | 329.88 | 0.850 | 0.3121 | 41.71 |
| | Ave. | 90° | 342.68 | 0.859 | 0.3010 | 42.65 |
| | STD | 90° | 8.85 | 0.027 | 0.0119 | 0.88 |

**Appendix D.1: Short Block Compression Data**

Table D.1.2 SBC results obtained from the Hexcel Hi-Tech AS4 6k knitted/stitched
(+45°/0°/-45°/90°)₂ₛ/Hercules 3501-6 SBC specimens.

| RTM Panel | SBC Specimen | Loading Orientation | Compressive Strength, MPa | Ultimate Longitudinal Strain, % | Poisson's Ratio at 0.2% Strain | Young's Modulus, GPa at 0.2% Strain |
|---|---|---|---|---|---|---|
| 71290P1 | C1 | 0° | 339.10 | 1.117 | 0.2295 | 35.80 |
| | C2 | 0° | 336.88 | 1.202 | 0.2487 | 35.54 |
| | C3 | 0° | 321.14 | 1.186 | 0.2692 | 40.58 |
| | C4 | 0° | 327.05 | 0.969 | 0.2395 | 37.07 |
| | C5 | 0° | 325.60 | 1.018 | 0.1854 | 37.25 |
| | Ave. | 0° | 329.96 | 1.098 | 0.2345 | 37.25 |
| | STD | 0° | 6.88 | 0.092 | 0.0278 | 1.80 |
| 71790P1 | C1 | 0° | 309.64 | 0.950 | 0.2662 | 41.08 |
| | C2 | 0° | 342.99 | 0.861 | 0.2566 | 41.74 |
| | C3 | 0° | 329.16 | 1.091 | 0.3258 | 39.48 |
| | Ave. | 0° | 327.26 | 0.967 | 0.2829 | 40.77 |
| | STD | 0° | 13.68 | 0.095 | 0.0306 | 0.95 |
| | C4 | 90° | 429.77 | 1.044 | 0.3129 | 47.33 |
| | C5 | 90° | 418.20 | 0.996 | 0.2889 | 46.96 |
| | Ave. | 90° | 423.98 | 1.020 | 0.3009 | 47.15 |
| | STD | 90° | 5.78 | 0.024 | 0.0120 | 0.18 |
| 71990P1 | C1 | 0° | 322.91 | 0.998 | 0.2403 | 39.64 |
| | C2 | 0° | 309.34 | 0.843 | 0.2572 | 40.76 |
| | C3 | 0° | 292.22 | 0.806 | 0.2207 | 38.53 |
| | Ave. | 0° | 308.16 | 0.882 | 0.2394 | 39.64 |
| | STD | 0° | 12.56 | 0.083 | 0.0149 | 0.91 |
| | C4 | 90° | 418.68 | 0.927 | 0.2989 | 50.51 |
| | C5 | 90° | 426.68 | 0.999 | 0.3248 | 46.92 |
| | Ave. | 90° | 522.48 | 0.963 | 0.3119 | 48.72 |
| | STD | 90° | 3.80 | 0.036 | 0.0130 | 1.80 |
| 71990P1 | C1 | 0° | 303.46 | 0.713 | 0.2957 | 43.11 |
| | C2 | 0° | 329.91 | 0.863 | 0.2842 | 38.69 |
| | C3 | 0° | 358.91 | 1.000 | 0.3060 | 44.22 |
| | Ave. | 0° | 330.76 | 0.859 | 0.2953 | 42.01 |
| | STD | 0° | 22.65 | 0.117 | 0.0089 | 2.39 |
| | C4 | 90° | 421.42 | 0.979 | 0.2944 | 47.27 |
| | C5 | 90° | 418.73 | 0.877 | 0.3284 | 53.56 |
| | Ave. | 90° | 420.07 | 0.928 | 0.3114 | 50.42 |
| | STD | 90° | 1.35 | 0.051 | 0.0170 | 3.14 |

Appendix D.1: Short Block
Compression Data

*Table D.1.3. SBC results obtained from the 16 ply TTI IM7/8HS/Hercules 3501-6 SBC specimens.*

| RTM Panel | SBC Specimen | Compressive Strength, MPa | Ultimate Longitudinal Strain, % | Poisson's Ratio at 0.2% Strain | Young's Modulus, GPa at 0.2% Strain |
|---|---|---|---|---|---|
| 61990P1 | C1 | 692.21 | 0.956 | 0.0496 | 79.20 |
| | C2 | 661.21 | 0.904 | 0.0439 | 78.70 |
| | C3 | 664.70 | 0.911 | 0.0420 | 80.00 |
| | C4 | 564.55 | 0.764 | 0.0458 | 78.50 |
| | C5 | 628.01 | 0.829 | 0.0463 | 82.60 |
| | Ave. | 642.14 | 0.873 | 0.0455 | 79.80 |
| | STD | 43.82 | 0.068 | 0.0025 | 1.50 |
| 52390P1 | C1 | 708.09 | 0.994 | 0.0423 | 71.26 |
| | C2 | 647.32 | 0.896 | 0.0484 | 72.26 |
| | C4 | 611.39 | 0.846 | 0.0482 | 78.02 |
| | C5 | 695.70 | 0.985 | 0.0408 | 78.02 |
| | Ave. | 665.63 | 0.930 | 0.0449 | 74.89 |
| | STD | 38.68 | 0.062 | 0.0034 | 3.15 |
| 61190P1 | C1 | 602.49 | 0.757 | 0.0394 | 84.80 |
| | C2 | 588.20 | 0.742 | 0.0401 | 83.40 |
| | C3 | 647.80 | 0.828 | 0.0439 | 83.10 |
| | C4 | 597.96 | 0.767 | 0.0522 | 83.20 |
| | C5 | 629.25 | 0.786 | 0.0491 | 85.60 |
| | Ave. | 613.14 | 0.778 | 0.0450 | 84.00 |
| | STD | 22.03 | 0.034 | 0.0050 | 1.00 |
| 62290P1 | C1 | 665.20 | 0.821 | 0.0439 | 83.10 |
| | C2 | 618.85 | 0.801 | 0.0471 | 82.70 |
| | C3 | 526.00 | 0.359 | 0.0444 | 82.90 |
| | C4 | 658.46 | 0.886 | 0.0428 | 80.80 |
| | C5 | 622.34 | 0.807 | 0.0522 | 82.10 |
| | Ave. | 618.17 | 0.795 | 0.0461 | 82.30 |
| | STD | 49.70 | 0.074 | 0.0034 | 0.80 |

**Appendix D.1: Short Block Compression Data**

# Appendix D.2: Iosipescu Shear Data



**Iosipescu Shear Test Fixture**
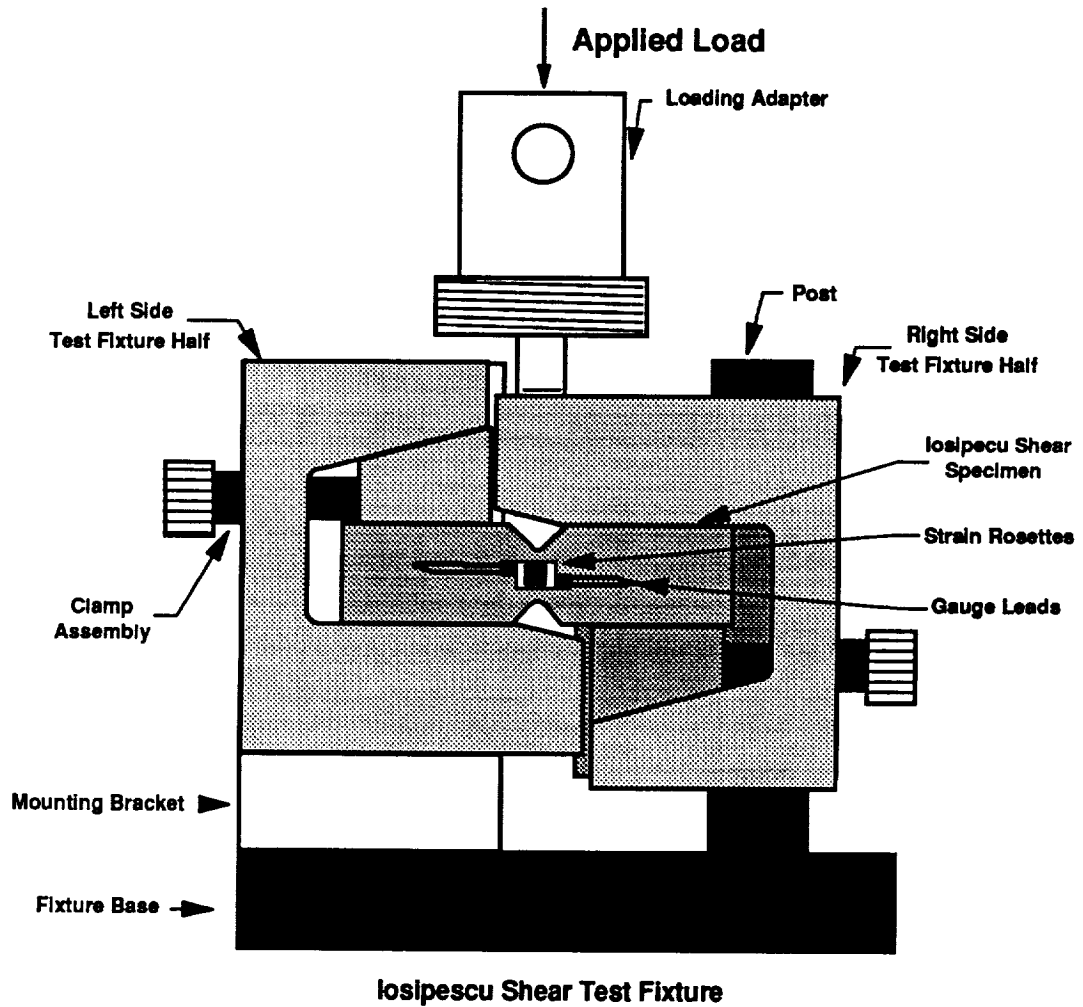
Shear Strength

$$\tau_{max} = \frac{L_{max}}{(t*w)_{notch}}$$

Shear Modulus at 0.2% Shear Strain

$$G_{2\%\gamma} = \frac{2\tau}{(\gamma_{2\%_{45}} - \gamma_{2\%_{-45}})_{ave}}$$

*Figure D.2.1 Iosipescu shear fixture (top) and the equations utilized to reduce experimental data (bottom).*

Table D.2.1. Iosipescu shear results for the Hexcel Hi-Tech AS4 6k
$(+45°/0°/-45°/90°)_{2S}$/Hercules 3501-6 knitted (top) and
knitted/stitched (bottom) Iosipescu shear specimens.

| RTM Panel | Iosipescu Shear Specimen | Loading Orientation | Shear Strength, Mpa |
|---|---|---|---|
| 72390P1 | S1 | 90° | 152.30 |
| | S2 | 90° | 164.40 |
| | Ave. | 90° | 158.35 |
| | STD | 90° | 6.05 |
| | S3 | 0° | 170.10 |

| RTM Panel | Iosipescu Shear Specimen | Loading Orientation | Shear Strength, Mpa |
|---|---|---|---|
| 71290P1 | S1 | 90° | 178.60 |
| | S2 | 90° | 171.70 |
| | Ave. | 90° | 175.15 |
| | STD | 90° | 3.45 |
| | S3 | 0° | 190.60 |
| 71790P1 | S1 | 90° | 191.10 |
| | S2 | 90° | 189.30 |
| | Ave. | 90° | 190.20 |
| | STD | 90° | 0.90 |
| 71990P1 | S1 | 0° | 200.10 |
| | S2 | 0° | 211.50 |
| | Ave. | 0° | 205.80 |
| | STD | 0° | 5.70 |
| 72090P1 | S1 | 0° | 199.20 |
| | S2 | 0° | 210.10 |
| | Ave. | 0° | 204.70 |
| | STD | 0° | 5.50 |

Appendix D.2: Iosipescu Shear Data

*Table D.2.2. Iosipescu shear results for the 16 ply TTI IM7/8HS/ Hercules 3501-6 Iosipescu shear specimens.*

| RTM Panel | Iosipescu Shear Specimen | Shear Strength, Mpa | Shear Modulus at 0.2% Shear Strain GPa |
|---|---|---|---|
| 61990P1 | S1 | 110.00 | 6.31 |
| | S2 | 106.60 | 6.26 |
| | S3 | 110.00 | 6.27 |
| | S4 | 113.40 | 6.25 |
| | Ave. | 110.00 | 6.27 |
| | STD | 2.40 | 0.02 |
| 52390P1 | S1 | 120.10 | 5.86 |
| | S2 | 117.90 | 5.21 |
| | S3 | 113.80 | 5.28 |
| | Ave. | 117.30 | 5.45 |
| | STD | 2.60 | 0.29 |
| 61190P1 | S1 | 103.10 | 6.59 |
| | S2 | 105.40 | 6.59 |
| | S3 | 107.80 | 6.93 |
| | S4 | 105.80 | 6.78 |
| | Ave. | 105.50 | 6.72 |
| | STD | 1.70 | 0.14 |
| 62290P1 | S1 | 104.70 | 6.56 |
| | S2 | 107.40 | 6.73 |
| | S3 | 111.80 | 6.58 |
| | S4 | 107.40 | |
| | Ave. | 107.80 | 6.62 |
| | STD | 2.60 | 0.08 |

Appendix D.2: Iosipescu Shear Data

| BIBLIOGRAPHIC DATA SHEET | 1. Report No. VPI-E-92-05; CCMS-92-05 | 2. | 3. Recipient's Accession No. |
|---|---|---|---|

**4. Title and Subtitle**

An Infiltration/Cure Model for Manufacture of Fabric Composites by the Resin Infusion Process

**5. Report Date**

February 1992

**6.**

**7. Author(s)**

M.H. Weideman, A.C. Loos, H.B. Dexter and G.H. Hasko

**8. Performing Organization Rept. No.**

VPI-E-92-05

**9. Performing Organization Name and Address**

Virginia Polytechnic Institute and State University
Department of Engineering Science and Mechanics
Blacksburg, VA 24061-0219

**10. Project/Task/Work Unit No.**

**11. Contract/Grant No.**
NAG-1-343      NASA-Va.
Tech Composites Prog.

**12. Sponsoring Organization Name and Address**

Applied Materials Branch
National Aeronautics and Space Administration
Langley Research Center
Hampton, VA 23665-5225

**13. Type of Report & Period Covered**

Interim Report 89
8/89-10/91

**14.**

**15. Supplementary Notes**

**16. Abstract**

A one-dimensional infiltration/cure model was developed to simulate fabrication of advanced textile composites by the resin film infusion process. The simulation model relates the applied temperature and pressure processing cycles, along with the experimentally measured compaction and permeability characteristics of the fabric preforms, to the temperature distribution, the resin degree of cure and viscosity, and the infiltration flow front position as a function of time. The model also predicts the final panel thickness, fiber volume fraction, and resin mass for full saturation as a function of compaction pressure. The infiltration model is based on D'arcy's law for flow through porous media.

Composite panels were fabricated using the RTM film infusion technique from knitted, knitted/stitched, and 2-D woven carbon preforms and Hercules 3501-6 resin. Prior to fabrication, the deflection and permeability of the preforms were measured as a function of compaction pressure. Measurements of the temperature distribution, the resin viscosity and degree of cure, and the infiltration flow front position were compared with the RTM simulation model results. The model predictions were within 12% of the experimental results.

Fabric composites were fabricated at different compaction pressures and temperature cycles to determine the effects of the processing on the properties. The composites were C-scanned and micrographed to determine the quality of each panel. Composite panels fabricated using different temperature cycles to the same state of cure and similar compaction pressures were found to have similar compressive and shear properties.

Advanced cure cycles, developed from the RTM simulation model, were utilized to reduce the total cure cycle times by a factor of 3 and the total infiltration times by a factor of 2.

**17. Key Words and Document Analysis.     17a. Descriptors**
Resin transfer molding, composites, modeling, manufacture, graphite fiber, epoxy resin

**17b. Identifiers/Open-Ended Terms**

**17c. COSATI Field/Group**

| 18. Availability Statement | 19. Security Class (This Report) UNCLASSIFIED | 21. No. of Pages 205 |
|---|---|---|
| | 20. Security Class (This Page UNCLASSIFIED | 22. Price |

# VIRGINIA TECH CENTER FOR
# COMPOSITE MATERIALS AND STRUCTURES

The Center for Composite Materials and Structures is a coordinating organization for research and educational activity at Virginia Tech. The Center was formed in 1982 to encourage and promote continued advances in composite materials and composite structures. Those advances will be made from the base of individual accomplishments of the sixty-five full and associate members who represent eleven different departments in three colleges.

The Center functions through an Administrative Board which is elected yearly and a Director who is elected for a three-year term. The general purposes of the Center include:

- collection and dissemination of information about composites activities at Virginia Tech,
- contact point for other organizations and individuals,
- mechanism for collective educational and research pursuits,
- forum and agency for internal interactions at Virginia Tech.

The Center for Composite Materials and Structures is supported by a vigorous program of activity at Virginia Tech that has developed since 1963. During 1988-89 and 1989-90 fiscal years sponsored research project expenditures for investigation of composite materials and structures have totalled approximately five million dollars annually.

Various Center faculty are internationally recognized for their leadership in composite materials and composite structures through books, lectures, workshops, professional society activities, and research papers.

Research is conducted in a wide variety of areas including design and analysis of composite materials and composite structures, chemistry of materials and surfaces, characterization of material properties, development of new material systems, and relations between damage and response of composites. Extensive laboratories are available for mechanical testing, nondestructive testing and evaluation, stress analysis, polymer synthesis and characterization, material surface characterization, component fabrication, and other specialties.
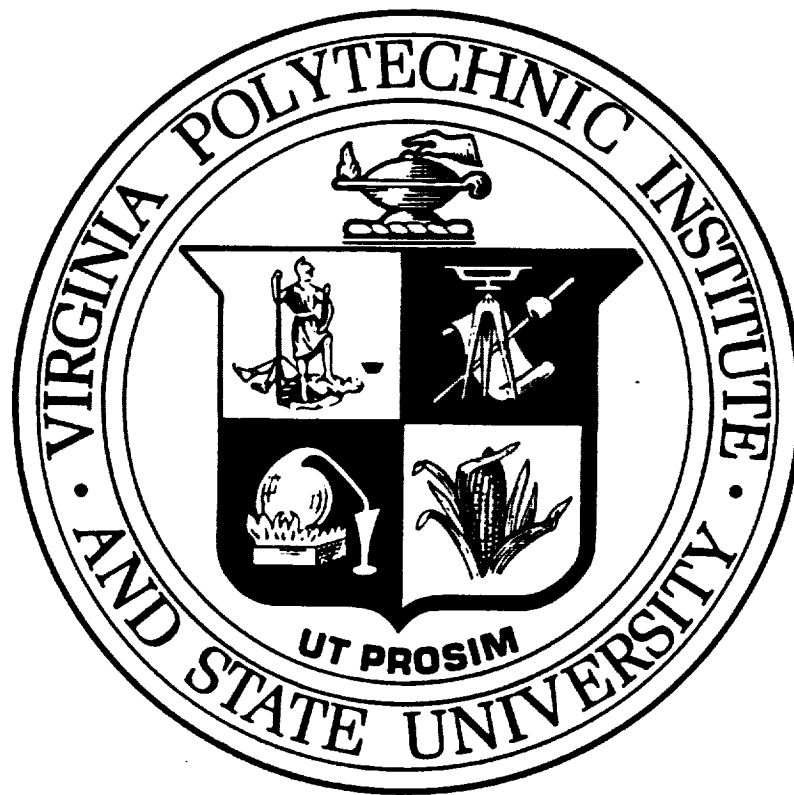
Educational activities include ten formal courses offered at the undergraduate and graduate levels dealing with the physics, chemistry, mechanics, and design of composite materials and structures. As of 1991, 129 Doctoral and 172 Master's students have completed graduate programs and are now active in industry, government, and education in the United States and abroad. The Center averaged 125 active student members during 1989-90 and 1990-91. Many Bachelor-level students have been trained in various aspects of composite materials and structures.

The Center has invested in the development of an administrative database (now fully operational for Center members) and a composite material properties database (now ready for data entry).

In addition to the CCMS Report Series, the Center sponsers a bi-monthly Seminar Series attended by faculty, staff, and students and the Center jointly sponsors a sesqui-annual Technical Review with the Center for Adhesive and Sealant Science which is well attended by government and corporate contacts.

## MEMBERS OF THE CENTER

| Aerospace and Ocean Engineering | Electrical Engineering | Industrial and Systems Engineering |
|---|---|---|
| Raphael T. Haftka | Ioannis M. Besieris | Joel A. Nachlas |
| Eric R. Johnson | Richard O. Claus | |
| Rakesh K. Kapania | Douglas K. Lindner | **Materials Engineering** |
| | | Jesse J. Brown, Jr. |
| **Chemical Engineering** | **Engineering Science and Mechanics** | Seshu B. Desu |
| | | Ronald S. Gordon |
| Donald G. Baird | Robert Czarnek | D. P. H. Hasselman |
| Garth L. Wilkes | David A. Dillard | Robert W. Hendricks |
| | Normal E. Dowling | Ronald G. Kander |
| | John C. Duke, Jr. | |
| **Chemistry** | Daniel Frederick | |
| | O. Hayden Griffin, Jr. | **Mathematics** |
| John G. Dillard | Zafer Gurdal | |
| Harry W. Gibson | Robert A. Heller | Werner E. Kohler |
| James E. McGrath | Edmund G. Henneke, II | |
| Thomas C. Ward | Michael W. Hyer | |
| James P. Wightman | Robert M. Jones | **Mechanical Engineering** |
| | Ronald D. Kriz | |
| | Liviu Librescu | Charles E. Knight |
| | Alfred C. Loos | Craig A. Rogers |
| **Civil Engineering** | Don H. Morris | Curtis H. Stern |
| | John Morton | |
| Richard M. Barker | Ali H. Nayfeh | |
| Richard E. Weyers | Daniel Post | |
| | J. N. Reddy | |
| | Kenneth L. Reifsnider | |
| **Clothing and Textiles** | C. W. Smith | |
| | Wayne W. Stinchcomb | |
| Jeanette M. Cardamone | Surot Thangjitham | |

Inquiries should be directed to:
Center for Composite Materials and Structures
Virginia Tech
Blacksburg, VA 24061-0257
Phone: (703) 231-4969
Fax: (703) 231-9452